SURFACE FUNCTIONALIZED CELLULOSE NANOCRYSTALS FOR SYNTHETIC LATEX PROPERTY MODIFICATION

SURFACE FUNCTIONALIZED CELLULOSE NANOCRYSTALS FOR SYNTHETIC LATEX PROPERTY MODIFICATION

A Thesis

Submitted to the School of Graduate Studies

in Partial Fulfillment of the Requirements

for the Degree

Doctor of Philosophy

McMaster University

DOCTOR OF PHILOSOPHY (2017) McMaster University

(Chemical Engineering) Hamilton, Ontario

TITLE: SURFACE FUNCTIONALIZED CELLULOSE NANOCRYSTALS FOR SYNTHETIC LATEX PROPERTY MODIFICATION

AUTHOR: Stephanie A. Kedzior
B.A.Sc. (University of Waterloo)

SUPERVISOR: Professor Emily D. Cranston

NUMBER OF PAGES: ix, 157

Abstract

The objective of this thesis is to incorporate cellulose nanocrystals (CNCs) into polymer latexes prepared using various emulsion polymerization methods. CNCs are a promising new class of renewable materials with unique properties including nanoscale dimensions, a high aspect ratio, low density, and high strength. They show significant promise to enhance the properties of existing materials, but challenges often arise due to incompatibility and processing difficulties. This work investigates novel surface modification routes to improve the compatibility of CNCs with emulsion polymerization components, and aims to control the location and function of CNCs in latex systems in order to modify latex properties.

Three approaches to incorporate CNCs into polymer latexes are presented: (1) exploiting CNC-surfactant interactions in order to promote CNCs as Pickering stabilizers or as "passive" additives in the water phase, (2) enhancing the surface activity of CNCs by adsorbing the surface active biopolymer methyl cellulose (MC) to act as Pickering co-stabilizers, or (3) hydrophobic modification of CNCs through polymer grafting in order to provide improved compatibility between CNCs and the monomer/polymer phase to incorporate CNCs into the latex core.

First, the interactions between CNCs and surfactants were studied in suspension and at surfaces and the CNC-surfactant combinations were used to stabilize miniemulsion polymerization of methyl methacrylate (MMA), a model system used in this work. Oppositely charged CNCs and surfactants showed improved stability as Pickering stabilizers and the ability to co-stabilize the monomer/polymer-water interface. When like-charged CNCs and surfactants were used, the poly(methyl methacrylate) (PMMA) polymer particles were stabilized by surfactant only, while the CNCs remained in the water phase. Next, in order to avoid the use of surfactants, CNCs were coated with MC to provide improved surface activity. MC-coated CNCs were effectively used as Pickering stabilizers in the microsuspension polymerization of MMA, where a double morphology of PMMA particles was observed, and the morphology could be tuned based on the ratio of CNC to MC used. Finally, CNCs were modified with hydrophobic polymer via two different "grafting from" methods: free radical polymerization and atom transfer radical polymerization (ATRP). Free radical polymer grafting from CNCs resulted in polymer-grafted CNCs but the method lacked control over polymer graft length and graft density. To overcome this, CNCs were modified via surface initiated ATRP where considerably higher amounts of polymer were grafted from the CNCs in short reaction times and with simple purification steps. Furthermore, polymer-grafted CNCs were added to the monomer phase of the miniemulsion polymerization of MMA and latexes with CNCs inside the hydrophobic polymer particle core were prepared. Given the difficulties in characterizing polymer grafted CNCs, a novel solution state NMR method was used, whereby the modified CNCs were dissolved in ionic liquids and the polymer grafts were cleaved and collected to determine graft length and graft density.

Overall, this work provides three approaches for the preparation of nanocomposite latexes with CNCs using PMMA as a model system. The results presented here may expand the use of CNCs in latex products such as adhesives, paints, coatings, and cosmetics.

Lay Abstract

This research aims to prepare polymer latexes with tailorable properties using renewably-sourced particles and nanotechnology. Latexes are polymer particles dispersed in water, typically on the order of a few hundred to thousand nanometers (where a “nanometer” is one billionth of a meter), and are used in products such as adhesives, paints, and coatings. The field of nanotechnology takes advantage of nanomaterials where unique properties stem from the small size and high surface-area-to-volume ratio. In this work, we use cellulose, the most abundant natural polymer on earth, in the form of cellulose nanocrystals (CNCs). These nanoparticles are extracted from pulp, cotton, and other natural resources to yield nanometer-sized rigid rod-like particles. CNCs have recently gained attention in research and the media because of their new industrial production and “safe nanomaterial” designation in Canada. In this work, CNCs were chemically modified by the attachment of new molecules or by coating them with polymers and were subsequently added during the synthesis of the polymer latex. Incorporating CNCs imparted new properties and the ability to control latex size, shape, and surface topography. CNCs are also expected to improve the overall mechanical strength of the latex, and may enhance the stickiness of adhesive latexes in particular, leading to products that are more environmentally friendly and that show improved performance.

Acknowledgements

First, I would like to express my deepest and sincerest thank you to my supervisor Dr. Emily Cranston. Thank you for letting me pursue the areas of research I found most interesting, for sharing your love for Sweden with me (and facilitating mine!) and for your constant support and guidance. I cannot express my gratitude for having you as my supervisor and role model. Your work ethic, compassion, and leadership are qualities that are truly admirable.

My sincere thanks is extended to my collaborators, in particular the kind and talented researchers I was able to work with at KTH in Stockholm. Drs. Anna Carlmark, Eva Malmström, and Fiona Hatton; thank you for welcoming me into the lab and teaching me all I know about ATRP. Without you this thesis would be so incomplete.

Lab life would not have been the same without my labmates. To all past and current members of the Cranston Research Group, thank you for always making each day fun. I am truly honoured to have worked with such bright and talented people.

Finally, I must thank the most important people in my life. To my parents; thank you for your unconditional love and support, for providing me someone to talk to at the end of a long day, a washing machine to do my laundry on Sundays and a homecooked Sunday dinner that caught the attention of my lunch companions. I love you and I wouldn't be here today without your support. To my brother Patrick, thank you for always sending me pick me ups, giving me money advice, and keeping me grounded. And finally, thank you to my two loves: Graeme and Oreo. To my fiancé Graeme, you've shown me how to stay calm in the most stressful of times, and although we've been 3500 km apart, I know you've constantly been by my side. Thank you for cooking for me, giving me trips to look forward to, and always pushing me to work hard. I love you and can't wait to see where life takes us. And to our Oreo, thanks for always waiting at the door for me when I got home, for sitting beside me as I worked, and for bringing me happiness every day. I feel truly blessed for the support I have received from my close friends and family.

Table of Contents

Chapter 1

Chapter 2

Chapter 3

Chapter 4

Chapter 5

Chapter 6

Chapter 7

Chapter 8

Chapter 9

Abbreviations

AFM	atomic force microscopy
ATRP	atom transfer radical polymerization
BA	butyl acrylate
BNCs	bacterial nanocellulose
BPO	benzoyl peroxide
CAN	ceric ammonium nitrate
Cat-CNCs	cationic cellulose nanocrystals
CIF	crystal information file
CNCs	cellulose nanocrystals
CNFs	cellulose nanofibrils
CNTs	carbon nanotubes
CTAB	cetyltrimethylammonium bromide
Cu	copper
CuBr	copper I bromide
$CuBr_2$	copper II bromide
Đ	dispersity
DLS	dynamic light scattering
DMF	dimethylformamide
DMSO	dimethyl sulfoxide
DP	degree of polymerization
DSC	differential scanning calorimetry
EPTMAC	2,3-epoxypropyltrimethylammonium chloride
GPC	gel permeation chromatography
H-CNCs	acid form CNCs
HCl-CNCs	cellulose nanocrystals hydrolyzed with hydrochloric acid
HEC	hydroxyethyl cellulose
KPS	potassium persulfate
LODP	level-off degree of polymerization
MC	methyl cellulose
Me_6TREN	tris(2-(dimethylamino)ethyl)amine
MFC	microfibrillated cellulose
MW	molecular weight
Na-CNCs	sodium form CNCs
NCC	nanocrystalline cellulose
NFC	nanofibrillated cellulose
NMP	nitroxide mediated polymerization
NMR	nuclear magnetic resonance
O/w	oil-in-water
P-CNCs	cellulose nanocrystals hydrolyzed with phosphoric acid
P4VP	poly(4-vinyl pyridine)
PA	poly(acrylamide)
PAA	poly(acrylic acid)
PCL	poly(caprolactone)
PDI	polydispersity index
PEG	poly(ethylene glycol)

PEO	poly(ethylene oxide)
PLA	poly(lactic acid)
PMA	poly(methyl acrylate)
PMMA	poly(methyl methacrylate)
PNIPAm	poly(N-isopropylacrylamide)
PP	poly(propylene)
PS	poly(styrene)
PSAs	pressure sensitive adhesives
RDRP	reversible deactivation radical polymerization
ROP	ring opening polymerization
SDS	sodium dodecyl sulfate
SEC	size exclusion chromatography
SEM	scanning electron microscopy
SI-ATRP	surface initiated atom transfer radical polymerization
TC	terminal complex
TEM	transmission electron microscopy
TEMPO	2,2,6,6-tetramethylpiperidine 1-oxyl
T_g	glass transition temperature
TGA	thermogravimetric analysis
THF	tetrahydrofuran
TTAB	tetradecyltrimethylammonium bromide
W/o	water-in-oil
XPS	X-ray photoelectron spectroscopy
XRD	X-ray diffraction

Chapter 1 Introduction and Objectives

1.1 Introduction

Since the 12 principles of green chemistry were first proposed by Paul Anastas and John C. Warner in the late 1990s,[1] scientists and engineers have broadened their efforts in the search for sustainable materials to replace toxic and petroleum-derived chemicals. This drive towards environmentally-friendly and safe chemistries has mandated improved efficiency of reactions and products, a reduction in both the use of organic solvents and waste produced, and the development of more benign synthetic pathways.[1] In more recent years, nanotechnology has offered solutions to many of these challenges.[2] In particular, nanoparticles from renewable resources, such as cellulose nanocrystals (CNCs) have the potential to address several of the 12 principles, while additionally imparting new properties and functionality to existing materials. CNCs have gained popularity in both the patent[3] and academic literature[4–6] and furthermore have the potential to be used in a number of industrial applications.[7–9]

CNCs were first discovered by Nickerson and Habrle in the 1940s,[10] but the widespread interest in their use was spurred by a series of papers published by Derek Gray and coworkers in the 1990s.[11] Potential applications for CNCs include coatings, composites, packaging, food additives, cosmetic stabilizers, and pharmaceutical excipients[5,6] and recently their use in commercial products (e.g. wood adhesives and inks) and oil & gas extraction processes has been demonstrated. CNCs are isolated from natural cellulose sources such as wood and cotton via an acid hydrolysis procedure that degrades the disordered cellulose regions into sugars, while the crystalline regions remain intact.[12] The hydrolysis yields rigid rod-shaped nanoparticles that are strong and lightweight. Typically, sulfuric acid is used, yielding sulfate half ester groups on the surface of the CNCs which impart an anionic charge and colloidal stability in water.[13] The acid hydrolysis process is relatively straightforward and has been scaled up for commercial production.[14] CelluForce Inc., in Windsor, Quebec, is currently the largest industrial producer of CNCs worldwide with ton-per-day production capacity. CelluForce Inc. uses a sulfuric acid hydrolysis procedure whereby the sulfuric acid is recycled and the degraded sugars are collected and can be fermented for use in biofuels. The industrial production of CNCs thus follows the tenets of green chemistry whereby the starting material is renewable and the waste production is minimized throughout the entire process.

For many envisioned applications, CNCs need to be functionalized in order to improve their compatibility with hydrophobic polymers and non-polar solvents. The abundance of hydroxyl groups on their surface results in a relatively hydrophilic nanoparticle yet provides opportunities for a wide variety of surface modification routes via well-known carbohydrate chemistries.[15] The packing of cellulose chains within each CNC also results in an amphiphilic nanoparticle.[16] Furthermore, the anionic sulfate half ester groups provide the option for non-covalent surface modification via electrostatic interactions.[15] Many sophisticated surface modification methods, such as controlled polymer grafting, have been demonstrated in the literature,[15] however, an important consideration when performing these reactions is the need to avoid irreversible nanoparticle aggregation. Thorough characterization of modified CNCs, including the degree of functionalization, wettability, particle dimensions, crystallinity and stability, is important to properly predict CNC performance and target suitable applications. The first objective of this thesis work is to develop new surface modification routes for CNCs and methods to characterize them.

In recent years, other anisotropic nanoparticles such as carbon nanotubes (CNTs) and clays have shown potential as reinforcing agents, stabilizers and rheological modifiers due to their unique properties. CNTs are stiff, strong and conductive.[17] However, they lack the renewability aspect and remain expensive to produce uniformly, limiting their widespread use in high volume applications. Clays are a cheaper substitute, and have similar properties to high aspect ratio CNTs.[18] The pitfalls of clays are their tendency to aggregate and the high energy required to fully separate them into individual platelets which is necessary to take full advantage of their "nano" properties. Fortunately, CNCs have the benefits of both CNTs and clays, as they are relatively inexpensive, industrially produced in large quantities and easy to disperse in aqueous media.[19] For these reasons (and since they can be surface modified to suit a wide variety of applications), CNCs have the potential to be used as property modifiers in hydrophilic or hydrophobic polymer matrices, especially in latex polymer systems where both polar (water) and non-polar (monomer/polymer) phases are present.

Polymer nanocomposites are prepared by adding a nanofiller to a polymer matrix, with the hope of obtaining a hybrid material with improved properties.[20] Polymer nanocomposites containing CNCs are an exciting and emerging topic in the literature since CNCs have high strength and stiffness. However, CNC polymer nanocomposites typically require processes that are not industrially feasible, such as solvent casting, or require melt processing at high temperatures which results in CNC aggregation and thermal degradation. One method to overcome these issues is to prepare latex nanocomposites whereby CNCs are incorporated into synthetic latexes to provide improved properties.

Synthetic latexes are commonly used in paints, adhesives and coatings and are produced by emulsion polymerization which is a water-based, heterogeneous polymerization method that produces polymer particles dispersed in water. The second objective of this thesis is to modify the properties of latex systems using CNCs. While poly(methyl methacrylate) (PMMA) is used here as a model latex system, we are ultimately interested in latex-based pressure sensitive adhesives (PSAs). We propose that CNCs can be used to replace toxic/undesirable components of the latex, provide mechanical reinforcement to the polymer, control latex morphology, improve adhesive properties, and/or impart new functionality. In general, latex-based PSAs have been shown to underperform compared to their solvent-based counterparts and we believe that incorporating nanoparticles to improve their adhesive and mechanical properties may allow for industry to adopt the "greener" emulsion polymerization method of producing PSAs.

In this thesis we present three approaches for incorporating CNCs into polymer latexes: (1) the addition of CNCs to the water phase of the emulsion polymerization by simple mixing, (2) to exploit the amphiphilic nature of CNCs for their use as stabilizers (or enhance their surface activity through non-covalent surface modification), or (3) hydrophobically modify CNCs via covalent polymer grafting in order to incorporate CNCs inside the polymer particle core. All existing work regarding nanocomposite latexes with CNCs has been done via simple mixing where the CNCs remain in the water phase and play no active role in the polymerization of the latex.[21–23] This previous work has produced latex films with improved mechanical and adhesive properties,[24,25] and therefore by controlling the CNC location within the latex, we aim to achieve even greater tunability over latex properties.

1.2 Thesis Objectives

CNCs show significant promise to enhance the properties of existing materials, but challenges often arise due to incompatibility and processing difficulties. This thesis sets out to modify CNCs following new, useful, water-based/green methods and to control surface functionalization such that the location of CNCs within a polymer latex can be tailored. Both covalent and non-covalent surface modification routes are explored. Importantly, this research aims to improve the current understanding of the governing interactions between CNCs, modified CNCs, and emulsion polymerization components, and how these interactions affect latex properties. The main objectives of this thesis are as follows:

1. To investigate novel surface modification routes to improve the compatibility of CNCs with hydrophobic materials. This work provides new methods which will allow CNCs to be incorporated into organic solvents, nanocomposites, and various polymer-based products.

2. To control the location and function of CNCs in latex polymer systems to modify latex properties. This objective is broken down into three sub-goals including:

a. To elucidate the role that CNCs can play during latex polymerization when surfactants are present. The results can provide industry with generic "design rules" for formulating surfactant-based products with CNCs.

b. To optimize CNCs as Pickering stabilizers (to replace surfactants) in various emulsion polymerization systems such as miniemulsion and microsuspension polymerization. This may extend the use of CNCs in polymer latex products, including pressure sensitive adhesives.

c. To incorporate CNCs into the core of the latex particles by compatibilizing them with the monomer phase using surface grafted polymers. The findings will allow for an understanding of surface modification required in order to compatibilize CNCs with hydrophobic polymers and will be used to prepare novel nanocomposite latexes for applications such as paints, adhesives, and coatings.

1.3 Thesis Outline

Chapter 1 *Introduction.*
This chapter introduces the main themes, objectives, and outline of this thesis.

Chapter 2 *Background and Literature Review.*
This chapter presents a thorough review of the current literature and concepts relevant to the work presented in this thesis.

Chapter 3 *Poly(methyl methacrylate)-Grafted Cellulose Nanocrystals: One-step Synthesis, Nanocomposite Preparation, and Characterization.*
This chapter presents the first account of a one pot, water-based method to graft PMMA from CNCs. Ceric-ion initiation allowed for polymer grafting directly from the cellulose backbone in one step and CNC aggregation was avoided by sonicating throughout the polymerization reaction. Extensive characterization demonstrated that hydrophobic CNCs that retained the favourable properties of unmodified CNCs were produced and could be used to reinforce PMMA nanocomposites. This chapter has been published in *The Canadian Journal of Chemical Engineering*.[25]

Chapter 4 *Grafting-from Cellulose Nanocrystals via Photoinduced Cu-mediated Reversible-deactivation Radical Polymerization.*
This chapter describes a novel method for controlled grafting of poly(methyl acrylate) from CNCs using a photoinduced Cu-mediated RDRP polymerization method and minimal copper catalyst. This method allowed for a known polymer graft density and graft length due to the preparation of initiator-modified CNCs and the controlled nature of the polymerization. This method is highly versatile for the modification of CNCs with hydrophobic polymers, where considerably high amounts of grafted polymer were achieved in short reaction times with simple purification. The work was a collaboration with KTH Royal Institute of Technology in Stockholm, Sweden. This chapter has been published in *Carbohydrate Polymers*.[26]

Chapter 5 *Liquids NMR Toolbox for the Analysis of Chemically Modified Nanocelluloses.*
This chapter reports the development of a new quantitative NMR-based technique to analyze polymer-grafted CNCs. An ionic liquid was used to dissolve the modified CNCs followed by methanolysis to cleave the polymer grafts, allowing for both graft length and graft density to be determined. No other characterization techniques can provide this information for modified CNCs and the method was corroborated by testing polymer-grafted cellulose filter paper polymerized in the presence of sacrificial initiator. The work is a collaboration with the University of Helsinki in Finland. This chapter will be submitted to the *Journal of the American Chemical Society* for publication.

Chapter 6 *Tailoring Cellulose Nanocrystal and Surfactant Behavior in Miniemulsion Polymerization.*
This chapter presents a comprehensive study of the behavior of CNCs in miniemulsion polymerization with surfactants. The binding between anionic and cationic CNCs with anionic and cationic surfactants in suspension was investigated and surfactant structuring on CNC films was measured using colloid probe atomic force microscopy. The surfactant-CNC combinations were then used as stabilizers in the miniemulsion polymerization of methyl methacrylate, where PMMA *micro*particles were produced using oppositely charged CNCs and surfactants, and PMMA *nano*particles were produced when like-charged CNCs and surfactants were used. This chapter has been published in *Macromolecules.*[27]

Chapter 7 *Cellulose Nanocrystals and Methyl Cellulose as Co-stabilizers for Nanocomposite Latexes with Double Morphology.*
This chapter evaluates the use of methyl cellulose-coated CNCs as Pickering stabilizers for the microsuspension polymerization of methyl methacrylate. The resulting PMMA latex particle size, surface roughness, and morphology were characterized and it was demonstrated that the hierarchical double morphology achieved was highly tunable. This chapter has been submitted to *ACS Sustainable Chemistry & Engineering* for publication.

Chapter 8 *Polymer-grafted Cellulose Nanocrystals for Incorporation into the Core of Latex Polymer Particles.*
This chapter reports the covalent modification of CNCs with hydrophobic polymers poly(butyl acrylate) and poly(methyl methacrylate) using surface initiated atom transfer radical polymerization. The modified CNCs were characterized and incorporated into the hydrophobic monomer phase of a series of miniemulsion polymerization reactions. The effect of polymer graft length and grafted polymer type on the final latex properties was studied and polymer-grafted CNCs were successfully incorporated into the core of polymer latex particles. This chapter is in preparation for publication.

Chapter 9 *Concluding Remarks.*
This chapter summarizes the major contributions from this thesis and presents suggestions for future work.

1.4 Other Contributions

Other published contributions to date (not included in this thesis):

Reid, M. S.; Kedzior, S. A.; Villalobos, M.; Cranston, E. D. Effect of Ionic Strength and Surface Charge Density on the Kinetics of Cellulose Nanocrystal Thin Film Swelling, *Langmuir*, **2017**, DOI: 10.1021/acs.langmuir.7b01740.

Abitbol, T.; Marway, H. S.; Kedzior, S. A.; Yang, X.; Franey, A.; Gray, D. G.; Cranston, E.D. Hybrid Fluorescent Nanoparticles from Quantum Dots Coupled to Cellulose Nanocrystals. *Cellulose*, **2017**, 24 (3), 1287-1293.

Prosperi-Porta, G.; Kedzior, S.; Muirhead, B.; Sheardown, H. Phenylboronic Acid Based Polymeric Micelles for Mucoadhesive Anterior Segment Ocular Drug Delivery. *Biomacromolecules,* **2016,** 17 (4), 1449-1547.

Klemm, D.; Cranston, E. D.; Fischer, D.; Gama, F. M. P.; Kedzior, S. A.; Kondo, T.; Kralisch, D.; Kramer, F.; Lindström, T.; Neitzsche, S.; Rachfuβ, F. Nanocelluloses as Natural Sources for Groundbreaking Novel Applications in Materials Science: Today's State. *Submitted to Materials Today,* **2017.**

References

(1) Anastas, P. T.; Warner, J. C. *Green Chemistry: Theory and Practice*; Oxford University Press: New York, 1998.

(2) Stark, W. J.; Stoessel, P. R.; Wohlleben, W.; Hafner, A. Industrial applications of nanoparticles. *Chem. Soc. Rev.* **2015**, *44* (16), 5793–5805.

(3) Charreau, H.; L. Foresti, M.; Vazquez, A. Nanocellulose Patents Trends: A Comprehensive Review on Patents on Cellulose Nanocrystals, Microfibrillated and Bacterial Cellulose. *Recent Pat. Nanotechnol.* **2012**, *7* (1), 56–80.

(4) Reid, M. S.; Villalobos, M.; Cranston, E. D. The role of hydrogen bonding in non-ionic polymer adsorption to cellulose nanocrystals and silica colloids. *Curr. Opin. Colloid Interface Sci.* **2017**, *29*, 76–82.

(5) Habibi, Y.; Lucia, L. A.; Rojas, O. J. Cellulose Nanocrystals: Chemistry, Self-Assembly, and Applications. *Chem. Rev.* **2010**, *110* (6), 3479–3500.

(6) Klemm, D.; Kramer, F.; Moritz, S.; Lindström, T.; Ankerfors, M.; Gray, D.; Dorris, A. Nanocelluloses: A New Family of Nature-Based Materials. *Angew. Chemie Int. Ed.* **2011**, *50* (24), 5438–5466.

(7) *The Global Market for Nanocellulose to 2020*; 2013.

(8) Shatkin, J.; Wegner, T.; Bilek, E. M. T.; Cowie, J. Market Projections of Cellulose Nanomaterial-enabled Products - Part 1: Applications. *TAPPI J.* **2014**, *13* (5), 9–16.

(9) Cowie, J.; Bilek, E. M. T.; Wegner, T. H.; Shatkin, J. Market Projections of Cellulose Nanomaterial-enabled Products - Part 2: Volume Estimates. *TAPPI J.* **2014**, *13* (6), 57–69.

(10) Nickerson, R. F.; Habrle, J. A. Cellulose Intercrystalline Structure. *Ind. Eng. Chem.* **1947**, *39* (11), 1507–1512.

(11) Revol, J. F.; Bradford, H.; Giasson, J.; Marchessault, R. H.; Gray, D. G. Helicoidal self-ordering of cellulose microfibrils in aqueous suspension. *Int. J. Biol. Macromol.* **1992**, *14* (3), 170–172.

(12) Moon, R. J.; Martini, A.; Nairn, J.; Simonsen, J.; Youngblood, J. Cellulose Nanomaterials Review: Structure, Properties and Nanocomposites. *Chem. Soc. Rev.* **2011**, *40* (7), 3941.

(13) Beck-Candanedo, S.; Roman, M.; Gray, D. Effect of Conditions on the Properties Behavior of Wood Cellulose Nanocrystals Suspensions. *Biomacromolecules* **2005**, *6*, 1048–1054.

(14) Reid, M. S.; Villalobos, M.; Cranston, E. D. Benchmarking Cellulose Nanocrystals: From the Laboratory to Industrial Production. *Langmuir* **2017**, *33* (7), 1583–1598.

(15) Habibi, Y. Key Advances in the Chemical Modification of Nanocelluloses. *Chem. Soc. Rev.* **2014**, *43* (5), 1519–1542.

(16) Kalashnikova, I.; Bizot, H.; Cathala, B.; Capron, I. Modulation of Cellulose Nanocrystals Amphiphilic Properties to Stabilize Oil/Water Interface. *Biomacromolecules* **2012**, *13* (1), 267–275.

(17) Baughman, R. H. Carbon Nanotubes - The Route Toward Applications. *Science* **2002**, *297*, 787–792.

(18) Lebaron, P. C.; Wang, Z.; Pinnavaia, T. J. Polymer-layered silicate nanocomposites: An overview. *Appl. Clay Sci.* **1999**, *15* (1–2), 11–29.

(19) Beck, S.; Bouchard, J.; Berry, R. Dispersibility in Water of Dried Nanocrystalline Cellulose. *Biomacromolecules* **2012**, *13* (5), 1486–1494.

(20) Oksman, K.; Aitomäki, Y.; Mathew, A. P.; Siqueira, G.; Zhou, Q.; Butylina, S.; Tanpichai, S.; Zhou, X.; Hooshmand, S. Review of the Recent Developments in Cellulose Nanocomposite Processing. *Compos. Part A Appl. Sci. Manuf.* **2016**, *83*, 2–18.

(21) Elmabrouk, A. Ben; Thielemans, W.; Dufresne, A.; Boufi, S. Preparation of Poly(styrene-co-hexylacrylate)/Cellulose Whiskers Nanocomposites via Miniemulsion Polymerization. *J. Appl. Polym. Sci.* **2009**, *114* (5), 2946–2955.

(22) Mabrouk, A. Ben; Vilar, M. R.; Magnin, A.; Belgacem, M. N.; Boufi, S. Synthesis and Characterization of Cellulose Whiskers/Polymer Nanocomposite Dispersion by Mini-Emulsion Polymerization. *J. Colloid Interface Sci.* **2011**, *363* (1), 129–136.

(23) Mabrouk, A. Ben; Kaddami, H.; Magnin, A.; Belgacem, M. N.; Dufresne, A.; Boufi, S. Preparation of Nanocomposite Dispersions Based on Cellulose Whiskers and Acrylic Copolymer by Miniemulsion Polymerization: Effect of the Silane Content. *Polym. Eng. Sci.* **2011**, *51* (1), 62–70.

(24) Dastjerdi, Z.; Cranston, E. D.; Dubé, M. A. Synthesis of Poly(n-butyl acrylate/methyl methacrylate)/CNC Latex Nanocomposites via In Situ Emulsion Polymerization. *Macromol. React. Eng.* **2017**, *201700013*, 1700013.

(25) Dastjerdi, Z.; Cranston, E. D.; Dubé, M. A. Adhesive Property Modification using Cellulose Nanocrystals. *Int. J. Adhes. Adhes.* **2017**, submitted.

(26) Hatton, F. L.; Kedzior, S. A.; Cranston, E. D.; Carlmark, A. Grafting-from Cellulose Nanocrystals via Photoinduced Cu-mediated Reversible-deactivation Radical Polymerization. *Carbohydr. Polym.* **2017**, *157*, 1033–1040.

(27) Kedzior, S. A.; Marway, H. S.; Cranston, E. D. Tailoring Cellulose Nanocrystal and Surfactant Behavior in Miniemulsion Polymerization. *Macromolecules* **2017**, *50* (7), 2645–2655.

Chapter 2 Background and Literature Review

2.1 Cellulose

With trends in literature and industrial research shifting towards sustainable and renewable materials, cellulose shows much promise as an alternative to petroleum derived chemicals. Cellulose is the most abundant natural polymer, with annual production estimated to be over 10^{11} tons.[1] Cellulose is widely distributed in higher plants, in several marine animals (e.g. tunicates) and to a lesser degree in algae, fungi, and bacteria. It is a fibrous, tough, water-insoluble substance that plays a critical role in maintaining the structure of plant cell walls.[2]

Cellulose is characterized as a high molecular weight homopolymer of β-1,4-linked anhydro-D-glucose units where every unit is corkscrewed 180° with respect to its neighbours.[2] Figure 2.1 shows the structure of cellulose with repeating glucose dimers, known as cellobiose. Each cellulose chain has two different end groups: one has a chemically reducing functionality (a hemiacetal unit), and the other has a pendant hydroxyl group and is the nominal nonreducing end (Figure 2.1). The number of glucose units or the degree of polymerization (DP) can be up to 20 000, but depends on the cellulose source.[2] A selection of cellulose sources and their respective DP values are listed in Table 2.1.

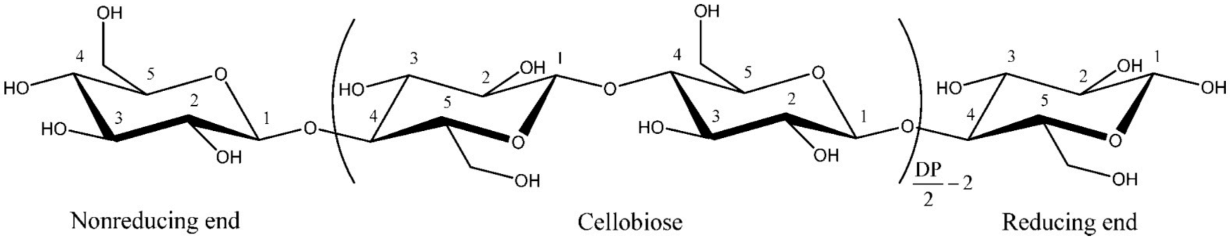

Figure 2.1 Chemical structure of cellulose chains, where DP represents the degree of polymerization. Figure reproduced from reference 2.

Table 2.1 Cellulose sources and their corresponding degree of polymerization. Adapted from reference 3.

Cellulose Source	Degree of Polymerization (DP)
Wood	6000 – 10 000
Pulp	500 – 2000
Sulfate pulp	950 – 13 000
Cotton	10 000 – 15 000
Bacterial cellulose	4000 – 6000

The chair conformation of the glucose rings lead to the hydroxyl groups being positioned in the ring (equatorial plane), while the hydrogen atoms are in the vertical (axial) position.[2] This results in cellulose chains having a hydrophobic plane and significant amphiphilicity.[4] Furthermore, this conformation allows for both inter- and intramolecular hydrogen bonding between adjacent cellulose chains, and because of this, in nature cellulose is never found as individual chains, but rather as microfibril bundles of 36 closely packed cellulose chains. These microfibrils typically assemble into larger units known as elementary fibrils which pack into even larger units called cellulose fibers (which furthermore contain other hemicellulose and lignin components). Biosynthesis conditions dictate cellulose packing, and therefore variations are found between sources.

Cellulose biosynthesis in plants is orchestrated by specific enzymatic terminal complexes (TCs) located in the plasma membrane. The synthesis process is not fully understood, but the structure of cellulose microfibrils implies that their synthesis and assembly involve the coordination of 36 active sites.[5] TCs assemble in the Golgi apparatus where they are inactive, but move through the plasma membrane when they become activated. During cellulose synthesis, TCs move through the plasma membrane in directions that coincide with the orientation of the microtubules which have been shown to exert a direct influence on the orientation of cellulose deposition.[6] During biosynthesis, cellulose chains are aggregated in microfibrils with cross sectional dimensions ranging from 2 to 20 nm, depending on the cellulose source.[2] The aggregation occurs via van der Waals forces and intra- and inter-molecular hydrogen bonding. If the TCs are not perturbed, they can generate a limitless supply of microfibrils with a small number of defects or amorphous domains.[7] Many studies have been performed in order to propose the nature of the supramolecular structure of cellulose including the crystal structure and dimensions as well as defects and amorphous domains, with much debate remaining to this day. A common view is that the amorphous regions are distributed as chain dislocations on segments along the elementary fibril where the microfibrils are distorted by internal strain in the fiber and proceed to tilt and twist.[8]

While the degree of crystallinity and distribution of crystalline regions in cellulose in nature (i.e., before processing) is still being deliberated, it is well known that the hydrogen bonding between chains results in three polymorphic forms: cellulose I, II, and III. All native cellulose is cellulose I. Cellulose I exists in two different forms, Iα and Iβ which are present in different ratios depending on cellulose source. Iα is predominant in cellulose derived from bacteria and algae, while Iβ is predominant in cellulose derived from plants.[9] The hydrogen bonding and van der Waals interactions between chains also contribute to the fact that cellulose is entirely insoluble in water as well as most other common solvents.[10]

Traditionally, cellulose has been used in the form of wood and plant fibers for energy sources, building materials, and clothing.[11] The use of cellulose has also expanded to include applications such as cosmetics, food, coatings, adhesives, and membranes. More recently, nanocellulose, or cellulose materials with dimensions on the nanometer scale, have gained increasing interest in both academic and industrial applications.

2.2 Nanocellulose

The term nanocellulose is used to define a wide variety of cellulosic materials including cellulose nanofibrils (CNFs), bacterial nanocellulose (BNC), and cellulose nanocrystals (CNCs). All types of nanocellulose are ribbon-like or rod shaped nanoparticles with varying lengths and widths depending on the isolation method and the starting cellulose source. CNFs are produced through the mechanical disintegration of plant fibers, BNC are produced via a "bottom up" approach by specific bacteria, while CNCs may be produced from many sources (such as plants, bacteria, and algae) via chemical methods. An overview of the various nomenclature/acronyms, cellulose sources, production methods, sizes, and select anticipated applications for each type of nanocellulose is provided in Table 2.2, with representative electron micrographs shown in Figure 2.2.

Table 2.2 Different types of nanocelluloses, their typical sources, averages sizes, and applications. Adapted from reference 12.

Type of nanocellulose	Synonyms	Typical sources	Production method and average size	Common research directions and applications
Cellulose nanofibrils (CNFs)	Microfibrillated cellulose (MFC) Nanofibrillated cellulose (NFC) Nanofibrils Microfibrils	Wood, sugar beet, hemp, flax	High pressure homogenization (often with chemical or enzymatic pre-treatment) Width = 5-60 nm[13] Length = up to several µm[14]	Hydrogels,[15] packaging and barrier coatings,[16] composites[17]
Bacterial nanocellulose (BNC)	Bacterial cellulose	Low molecular weight sugars and alcohols	Bacterial synthesis Width = 20-100 nm[18] Different types of nanofiber networks[19]	Hydrogels and wound healing,[20,21] films,[22] food thickeners[23]
Cellulose nanocrystals (CNCs)	Nanocrystalline cellulose (NCC) Cellulose nanowhiskers	Wood, cotton, hemp, flax, wheat straw, ramie, tunicin, algae, bacterial cellulose	Acid hydrolysis Width = 5-70 nm[2] Length = 100-250 nm (from plant sources), 100 nm-several µm (from tunicate, algae, bacteria)[2]	Hydrogels and aerogels,[24–26] coatings,[27] chiral nematic films/templates,[28] emulsions,[29] drug delivery,[30,31] energy storage,[32,33] water treatment,[34] composites[35,36]

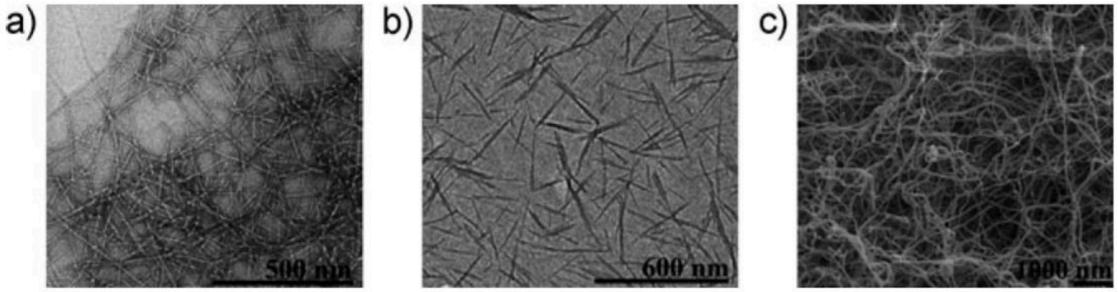

Figure 2.2 Transmission electron micrographs of (a) CNFs, and (b) CNCs, and a scanning electron micrograph of (c) BNC. Figure reproduced from reference 12.

The isolation, characterization, and applications of nanocellulose is currently a widely studied topic,[37] and each class of nanocellulose finds applications based on its favourable properties (i.e., length, flexibility, self-assembly behaviour, or mechanical strength). While cellulose nanocrystals are the focus of this work, many reports have used either CNFs or BNC for similar applications. CNFs are isolated from plant sources whereby shearing is used to tear apart large fibers into nano-scale fibers. Because of this preparation method, CNFs contain both crystalline and disordered cellulose regions. Their amorphous regions and high aspect ratio allow for them to entangle, forming gels at lower concentrations than those reported for CNCs. This entanglement makes CNFs excellent candidates for applications such as hydrogel materials and as reinforcement in flexible packaging (Table 2.2). Mechanical disintegration requires high amounts of energy, over 25 000 kWh per tonne as a result of multiple passes through the homogenizers.[38,39] In order to reduce the energy required, pre-treatments such as acid hydrolysis, enzymatic degradation, and the introduction of charged groups through carboxymethylation or 2,2,6,6-tetramethyl-1-piperidinyloxy (TEMPO)-mediated oxidation have been used to facilitate the homogenization process.[13,14,40–42] These surface groups also impart improved stability for use in water-based applications.

In contrast to the mechanical disintegration used to isolate CNFs, BNC is produced by certain bacteria strains in response to specific environmental conditions.[43,44] The bacteria are cultured in aqueous nutrient media with low molecular weight carbon and nitrogen sources and form highly porous networks of nanofibers, with individual nanofibers having diameters of 20-100 nm. BNC has an identical structure to cellulose from plant sources but is highly crystalline with a high degree of polymerization (Table 2.1) and good mechanical properties.[45–47] Common applications for BNC are in the medical field,[12] in products such as wound dressings and as thickening agents in foods.

2.3 Cellulose Nanocrystals

The production of cellulose nanocrystals via acid hydrolysis was first reported in 1947 by Nickerson and Habrle,[48] and later in 1949 by Rånby.[49] It is now well known that acid hydrolysis produces crystalline cellulose nanoparticles because the disordered regions are hydrolyzed first and the crystalline regions have a higher resistance to acid, therefore remaining intact.[50,51] These sustainable nanoparticles are being used in both academic research and industrial applications due to their unique properties: they are non-toxic and biodegradable and are approved as the first safe nanomaterial in Canada; they have a large specific Young's modulus, similar to that of Kevlar and steel; and due to their amphiphilicity and high aspect ratio they show promise as reinforcing agents, rheological modifiers, and interface stabilizers.[2]

During acid hydrolysis, rod-like cellulose nanocrystals are produced along with degraded sugars, oligosaccharides and residual acid. The byproducts and acid are removed by centrifugation and extensive dialysis. Sonication is then used to "unhinge" the nanocrystals and disperse them, forming a stable colloidal suspension in water.[12] The aspect ratio of the cellulose nanocrystals depends mostly on the source but also on the hydrolysis conditions such as hydrolysis time and acid concentration.[52] In general, acid hydrolysis results in a rapid decrease of the DP, to a value called the level-off DP (LODP). The DP then decreases much slower, even during prolonged hydrolysis times.[53–55] The value of the LODP is therefore dependent on the cellulose source, and a high polydispersity in particle size is typically seen.

The type of acid used for hydrolysis directly effects the properties of the resulting CNCs. Hydrolysis with sulfuric acid grafts sulfate half ester groups on the surface of the CNCs (Figure 2.3), typically in the range of 0.6-1.1 %S by mass, corresponding to 0.3-0.6 charges/nm^2, or 1 sulfate half ester for every 2-3 surface anhydroglucose units.[56] These sulfate half ester groups impart a negative surface charge on the CNCs and allow for colloidal stability in water. The dispersibility of CNCs in water is strongly dependent on electrostatic repulsion between the nanocrystals that arises from their surface charge.[57–60] Although providing colloidal stability, sulfate half ester groups may hinder CNC packing at an interface, and desulfation reactions are often required to remove some or all of the sulfate groups. Concentrated hydrochloric acid[29,61] or sodium hydroxide[62,63] have been used to desulfate CNCs in order to remove some or all of the sulfate half ester groups. Extensive purification is required in both cases in order to remove residual acid or base and to ensure a pure CNC material.

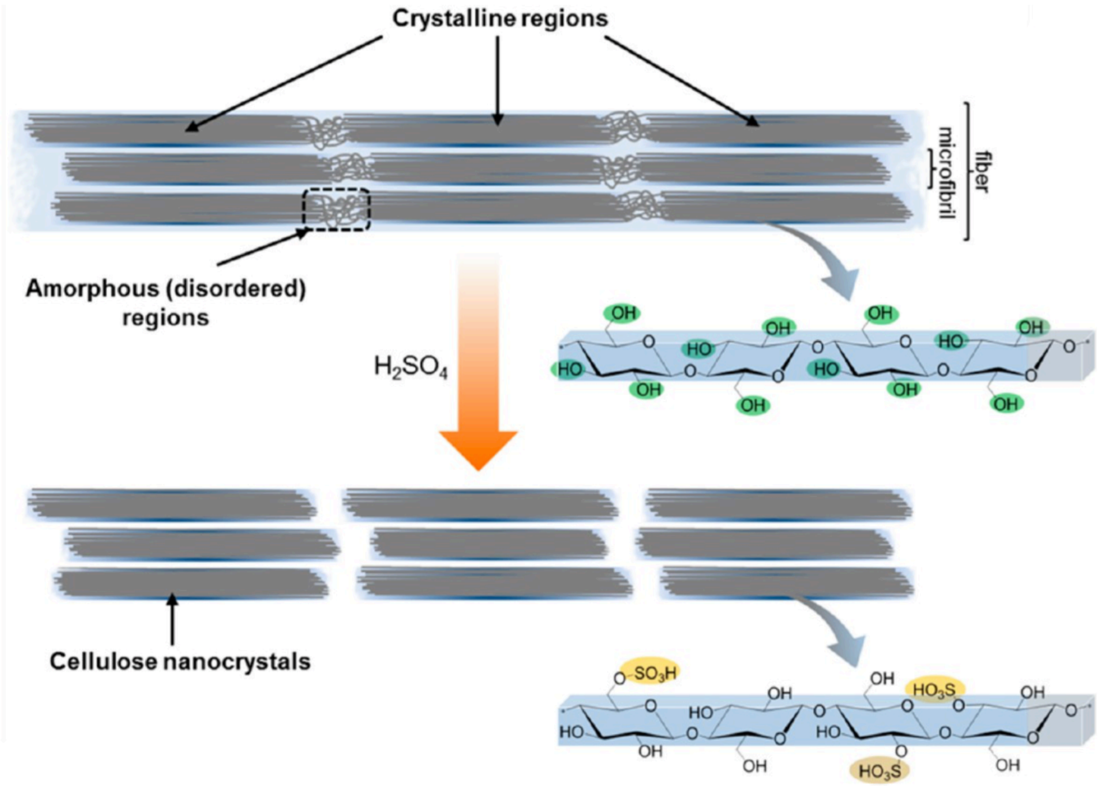

Figure 2.3 Schematic of the sulfuric acid hydrolysis of cellulose fibers which imparts sulfate half ester groups (yellow) on the surface of the cellulose nanocrystals. Reproduced from reference 64.

For long term storage and transport of CNCs, it is often necessary to dry suspensions via spray or freeze drying. In order for CNCs to be dried and redispersed, the proton of the sulfate half ester group must be replaced by a Na^+ counterion, whereby acid-form CNCs (H-CNCs) are titrated to sodium-form CNCs (Na-CNCs). This step, which is essentially a neutralization step and raises the pH from ~3 to ~7, limits CNC-CNC hydrogen bonding during drying. This allows either spray or freeze dried CNCs to be redispersed in water with sonication.[57] Furthermore, if CNCs are to be stored in the wet state, Na-CNCs are less prone to slow hydrolysis leading to auto-desulfation and have been shown to have improved shelf life.[65] We have recently observed differences in surfactant binding between H-CNCs and Na-CNCs,[66] further confirming the importance of the counterion for CNCs in various applications.

Other acids such as phosphoric[67,68] and hydrochloric[69] acid may be used to produce CNCs with different surface chemistry. Hydrolysis with phosphoric acid imparts phosphate half ester groups on the CNC surface, though with a much lower charge density than in the case of sulfuric acid. Phosphoric acid hydrolyzed CNCs (P-CNCs) are less colloidally stable than typical sulfuric acid hydrolyzed CNCs, but more colloidally stable than CNCs hydrolyzed using hydrochloric acid (HCl-CNCs). HCl-CNCs have no surface charge groups and are therefore aggregated and tend to settle out in water. Differences in thermal stability of CNCs produced from sulfuric, phosphoric, and hydrochloric acid have also been reported. Sulfuric acid CNCs tend to thermally degrade at lower temperatures than P-CNCs, with HCl-CNCs having the highest thermal stability.[67] Thermal stability of CNCs plays an important role in applications where high temperatures are required such as melt compounding to produce composites or oil and gas extraction.

The CNC aspect ratio is dependent on the cellulose source and directly impacts properties such as rheological behavior,[70] packing density,[71] and mechanical reinforcement.[72] Aspect ratio is calculated as the ratio of the length to width of the nanocrystals. Typically, cotton cellulose has the lowest aspect ratio, while bacterial/tunicate cellulose sources result in CNCs with higher aspect ratios.[71] The dimensions of CNCs produced from common sources are shown in Table 2.3.

Table 2.3 Dimensions of sulfuric acid hydrolyzed cellulose nanocrystals from various sources. Adapted from reference 52.

Cellulose source	Length	Cross section
Algal (*Valonia*)[73,74]	> 1000 nm	10 – 20 nm
Tunicate[75,76]	100 nm – several μm	10 – 20 nm
Bacterial[77,78]	100 nm – several μm	5 – 10 nm by 30 – 50 nm
Cotton[79]	200 – 350 nm	5 nm
Wood[69,79]	100 – 300 nm	3 – 5 nm diameter

With the goal of facilitating the use of CNCs in high volume applications, CNC production has been scaled up using different hydrolysis conditions and a variety of cellulose sources. *CelluForce Inc,* located in Windsor, Quebec currently operates the largest production facility with the capacity to produce ton per day quantities of CNCs via the sulfuric acid hydrolysis of bleached Kraft pulp. *Alberta Innovates Technology Futures* (recently renamed *InnoTech Alberta*), and the *USDA Forest Products Lab* are also producing CNCs at a kg per day capacity and tens of kg per day, respectively, using wood and cotton sources. These industrially produced CNCs have properties comparable to those made via lab scale processes.[56] With an expanding variety of producers and sources, it becomes critical to properly characterize CNC starting materials in order to ensure proper dispersion and the desired properties in a given application.

2.3.1 Characterization of Cellulose Nanocrystals

The physicochemical properties and dimensions of cellulose nanocrystals may be studied either in the wet state (in suspension) or in the dry state. The term "suspension" is used in recognition of the fact that CNCs are not soluble in water or other common solvents, and are rather dispersed or suspended. CNCs form stable suspensions in water due to colloidal stability, most of which is lost in organic solvents. Polar solvents such as dimethyl sulfoxide (DMSO) and dimethylformamide (DMF) have been shown to be the most suitable organic solvents for the redispersion of CNCs.[80] Therefore, characterization of CNCs is primarily performed in water or on dried material. CNC size, surface charge, and sulfate content are measured in aqueous suspensions via dynamic light scattering (DLS), zeta potential, and conductometric titrations, respectively. In the dry state, CNCs are commonly characterized by atomic force microscopy (AFM), transmission electron microscopy (TEM), X-ray diffraction (XRD), X-ray photoelectron spectroscopy (XPS), thermogravimetric analysis (TGA), differential scanning calorimetry (DSC), and solid state nuclear magnetic resonance (NMR). These techniques are discussed in detail in further chapters but are mentioned briefly below.

2.3.1.1 Characterization of CNCs in Suspension

Dynamic light scattering (DLS) is used to measure the apparent size of CNCs in suspension. The term "apparent" is used to denote the fact that DLS measures the hydrodynamic radius of spherical particles, whereas CNCs are rod-shaped.[81] DLS measurements are made at dilute concentrations in order to avoid particle agglomeration. Apparent size by DLS is commonly reported in CNC literature but should only be used as an internal check in order to ensure good dispersion. Other techniques such as AFM or TEM are more accurate in their determination of CNC particle size.

The zeta potential of a CNC suspension is related to the CNC surface charge and colloidal stability. Zeta potential of CNCs is measured by assuming Smoluchowski behavior.[81] The addition of salt is required in order to produce a consistent and small double layer around the charged CNC surface. Typical CNC suspensions prepared for zeta potential measurements are in 10 mM NaCl. A suspension of anionic CNCs made via a sulfuric acid hydrolysis should have a zeta potential below -30 mV, significantly less than -20 mV which is typically assumed to be the maximum required for moderate colloidal stability of anionic particles.[81]

The CNC sulfate half-ester content (and indirectly the surface charge density) is measured by conductometric titrations following existing literature protocols.[58,82] For this step, it is necessary for the CNCs to be in the acid form, since the titration is essentially an ion exchange where the proton counterions are replaced with Na^+ counterions from the NaOH used to titrate. The sulfate half-ester content can be confirmed via other characterization methods such as elemental analysis in the dry state.

2.3.1.2 Characterization of Dried CNCs

In the dry state, CNCs are characterized in order to determine their size, chemical composition, and crystallinity. AFM is a common technique to determine the size and shape of CNCs. AFM samples are prepared by spin coating dilute suspensions of CNCs onto clean silica wafers that are coated with a cationic polymer layer. A typical AFM height image of a spin coated film of CNCs is shown in Figure 2.4 whereby rod-shaped CNCs are observed. In less concentrated films, individual CNCs can be imaged and their length and cross section can be measured. TEM is another useful technique for measuring CNC size, however the sample preparation of drop casting dilute CNCs suspensions onto Formvar grids often results in CNC aggregation, making it more difficult to accurately measure the size of individual particles. TEM is often used complimentary to AFM in order to fully characterize CNC dimensions.[74,83]

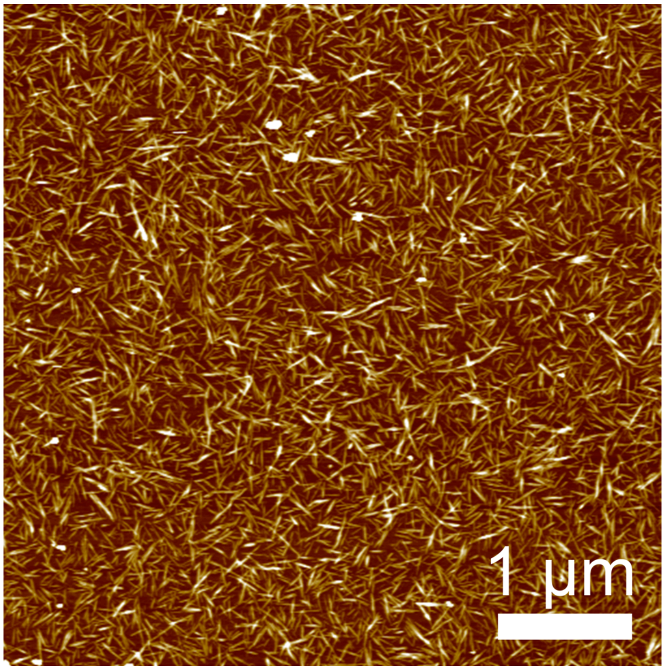

Figure 2.4 AFM height image of a spin coated film of unmodified CNCS.

XRD is used to determine the crystallinity of a CNC sample. While other techniques (NMR, Raman spectroscopy, etc.) may be used to measure crystallinity,[84] XRD is most commonly reported in literature. The percent crystallinity can be measured using several methods, the details of which are beyond the scope of this work. The Rietveld refinement method is commonly considered to be the most accurate method.[85] Ahvenainen et al. have recently shown a good correlation with the five most common XRD fitting methods and the two dimensional Rietveld method, and highlighted the difficulties in comparing values between laboratories.[86] Crystallinity values for unmodified CNCs are typically reported as >85%.

Techniques such as elemental analysis, FTIR, XPS, TGA and DSC are used to determine the chemical composition of CNCs. Elemental analysis is useful in determining sulfur content in order to confirm results by conductometric titration and can also be used to detect surface modifications that impart new elements to CNCs (as opposed to C and O). FTIR, XPS, TGA, and DSC are typically used to characterize modified CNCs and will be discussed in further detail in section 2.5.

2.4 Surface Modification of Cellulose Nanocrystals

Surface modifications are typically used to impart new functionality to CNCs, to improve compatibility between CNCs and a given matrix/environment, or to allow for improved dispersion in organic solvents.[87] Methods including non-covalent surface modifications (i.e., adsorption of polymers), or covalent surface modifications such as small molecule attachment or polymer grafting may be used to impart these new properties. A general overview of common surface modification reactions for CNCs is shown in Figure 2.5. The most relevant modification routes for this thesis work are discussed further below.

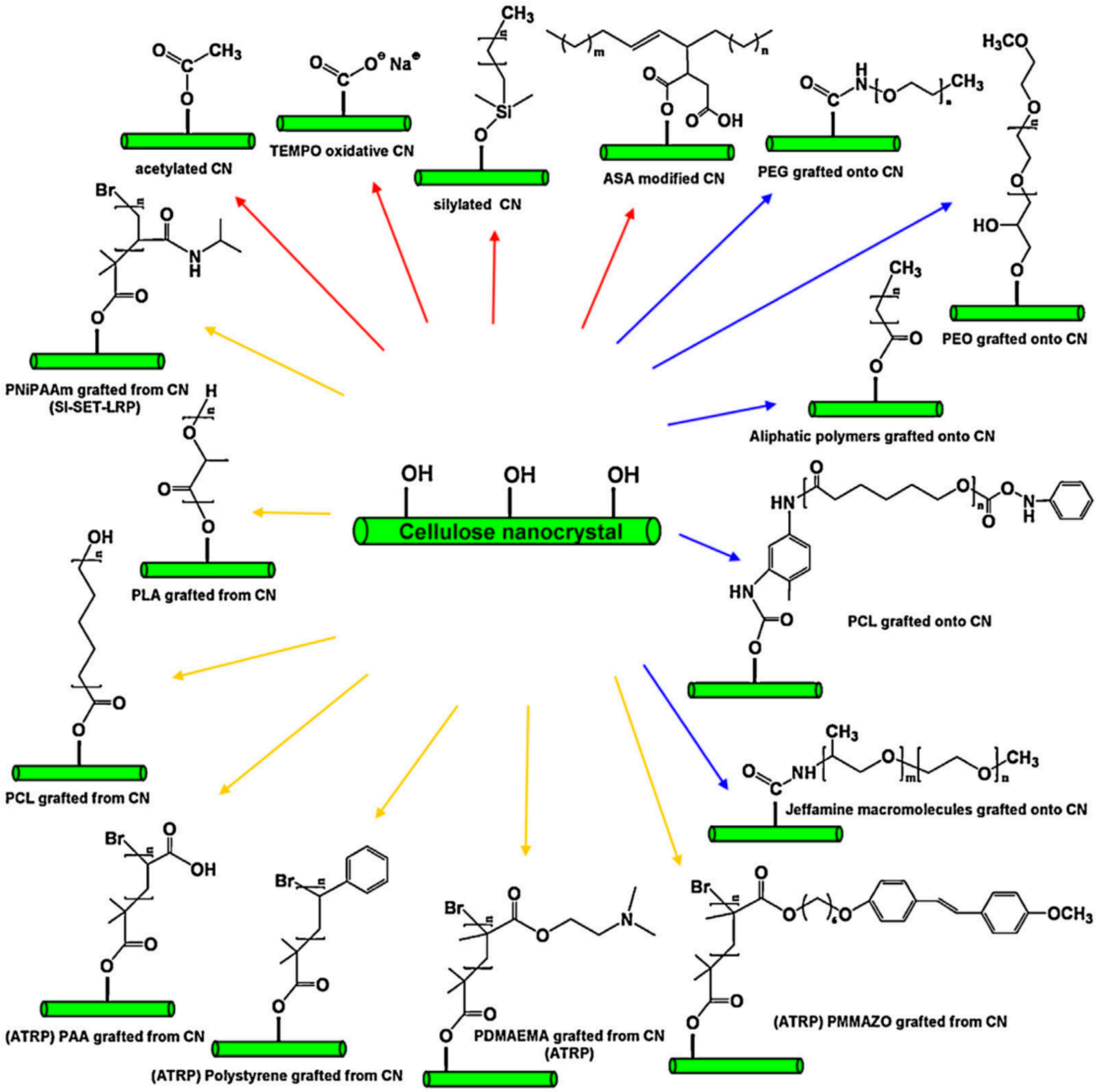

Figure 2.5 Schematic showing common surface modification reactions of cellulose nanocrystals (CN). Reproduced from reference 88.

2.4.1 Non-covalent Surface Modification of Cellulose Nanocrystals

Non-covalent surface modification of CNCs is typically achieved via adsorption by electrostatic interactions, hydrogen bonding, hydrophilic affinity, or hydrophobic interactions.[87] The negative surface charge on the CNCs allows for the adsorption of cationic surfactants and polymers, while the abundant hydroxyl groups on the CNC surface allow for hydrogen bonding. The first report of non-covalent surface modification of CNCs was through surfactant binding, as demonstrated by Heux et al.[84] They used an anionic surfactant to coat the CNC surface in order to improve the dispersibility of the CNCs in non-polar solvents.[84] The surfactant-modified CNCs also showed good dispersion in a polypropylene matrix.[90] Using a similar approach, Bondeson and Oksman[91] used CNCs modified with an anionic surfactant to improve CNC dispersion in polylactic acid. Kim et al.[92] and Rojas et al.[93] used nonionic surfactants in order to disperse CNCs in polystyrene composites. In all of these cases, the interaction between CNCs and the surfactants was expected to arise from hydrophobic interactions and it is somewhat surprising that anionic CNCs and some specific anionic/non-ionic surfactants can bind without the inherent electrostatic repulsion interfering.

Recently, many reports of CNC surface modification have taken advantage of electrostatic attraction to modify anionic CNCs with cationic surfactants. Habibi et al. first exploited this electrostatic interaction to prepare Langmuir-Schaefer model films whereby the cationic surfactant was used to attract CNCs to the water-air interface in a Langmuir trough.[94] Since then, many reports studying the governing parameters for adsorption have emerged. Dhar et al.[95] investigated the adsorption of cationic tetradecyltrimethylammonium bromide (TTAB) with anionic CNCs by isothermal titration calorimetry and showed that the formation of CNC-TTAB complexes was electrostatically driven, followed by hydrophobically driven micellization of TTAB on the CNC surface. This work was expanded upon by Brinatti et al.[96] who studied the interactions between C_nTAB (n = 12, 14, and 16) and anionic CNCs. They identified the same driving forces for surfactant adsorption and micellization as Dhar et al. and furthermore showed that when the surfactant concentration was increased, charge neutralization and association of the surfactant-coated CNCs led to flocculation.[96]

In other work with CNCs and cationic surfactants, Salajková et al.[97] used quaternary ammonium surfactants to hydrophobically modify TEMPO-oxidized CNCs with a high charge density of surface carboxyl groups. This study was intended as a facile surface modification route for CNCs and was similarly demonstrated using sulfuric acid hydrolyzed CNCs with cetyltrimethylammonium bromide (CTAB).[98,99] This modification is essentially an ion exchange reaction where the CNC counterion is exchanged for a bulky amphiphilic salt. Since these pioneering studies, cationic surfactant-modified CNCs have been used in the preparation of a range of materials including semiconducting nanoparticles,[100] poly(lactic acid) composites,[101,102] poly(lactic acid)-poly(hydroxybutyrate) blends,[103,104] metal nanoparticles,[105] nanoclay/epoxy composites,[106] drug delivery vehicles,[107] coatings,[108] and films.[109] Cationic surfactant-modified CNCs have also been shown to provide improved stability in Pickering oil-in-water emulsions stabilized by CNCs.[110] Furthermore, we have recently used CNC-surfactant combinations to stabilize poly(methyl methacrylate) particles via miniemulsion polymerization[66] which is described in detail in Chapter 6.

Electrostatic interactions can also be used to adsorb cationic polyelectrolytes to CNCs. This is mainly done via layer-by-layer deposition whereby a substrate is coated with a cationic polymer, and sequential layers of anionic CNCs and cationic polyelectrolytes are adsorbed to the surface via a dip or spin coating layer-by-layer fabrication.[111–114] This layer-by-layer approach to film formation has recently been exploited to determine the elastic modulus of biomimetic nanobiocomposite films to better understand multicomponent thin films as well as the plant cell wall structure.[115]

Polymer adsorption to CNCs can also be facilitated through entropically driven adsorption, where structured water is released and the polymer/CNC interactions occur via hydrogen bonding, co-crystallization and/or hydrophobic interactions.[87] Zhou et al.[116] mimicked the natural lignin-carbohydrate copolymers and adsorbed xyloglucan oligosaccharide-poly(ethylene glycol)-polystyrene triblock copolymers onto the surface of CNCs. The polymer-adsorbed CNCs showed improved dispersion in non-polar solvents. Lee et al.[117] used a bio-derived PLA-carbohydrate copolymer to surface modify CNCs from bacterial cellulose in order to better compatibilize the CNCs with PLA. In their work, the carbohydrate polymer block was shown to interact strongly with the CNCs through hydrogen bonding. Other polysaccharides such as hydroxyethyl cellulose have been used to coat the surface of CNCs in order to improve or change their functionality.[118,119] Similarly, synthetic triblock copolymers of poly(ethylene oxide)-poly(propylene)-poly(ethylene oxide) were adsorbed to CNCs in order to better compatibilize them with polyethylene.[120] Our group has also demonstrated that the biopolymer methyl cellulose adsorbs to CNCs and provides improved surface activity for foam and emulsion stabilization.[121,122] In this thesis work, CNCs coated with methyl cellulose were used as Pickering stabilizers for microsuspension polymerization[123] as described further in Chapter 7.

2.4.2 Small Molecule Surface Modification of Cellulose Nanocrystals

CNC functionality can be tuned by the grafting of small molecules. Many modification routes exist, but in this work we focus on tuning the surface charge of the CNCs and aim to give a general overview on the available methods to impart new anionic charge groups or cationic charge groups.

In order to impart anionic carboxylic acid groups on the CNC surface, TEMPO-mediated oxidation may be used. TEMPO-mediated oxidation of CNCs was first performed on CNCs prepared via a hydrochloric acid hydrolysis by Araki et al.[124] TEMPO-CNCs have also been shown to have improved dispersibility in organic solvents such as dimethylacetamide, dimethylformamide, 1,3-dimethyl-2-imidazolidinone, and N-methyl-2-pyrrolidone.[125] Furthermore, carboxylic acid groups may be used as sites for other modifications such as coupling via carbodiimide chemistry.[126]

CNCs can also be rendered cationic via surface cationization using (2,3-epoxypropyl)trimethylammonium chloride (EPTMAC) through a nucleophilic addition of the alkali-activated hydroxyl groups on the CNC surface to the epoxy moiety of EPTMAC, shown in Figure 2.6.[62] This reaction yields cellulose nanocrystals with cationic hydroxypropyltrimethylammonium chloride substituents on the surface. This functionalization typically requires the removal of all or some of the sulfate half ester groups, and has been shown to result in an overall net cationic charge on the CNCs. Uses for this type of surface modification are discussed further in Chapter 6.

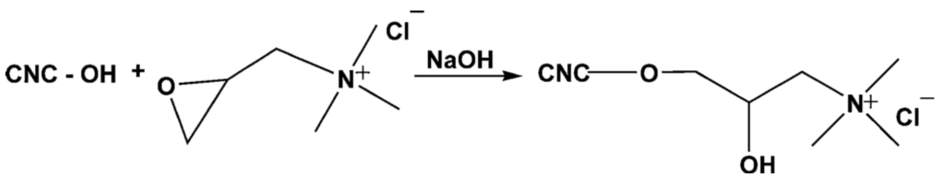

Figure 2.6 Grafting of epoxypropyltrimethylammonium chloride to the CNC surface. Reproduced from reference 62.

2.4.3 Polymer Grafting to and from Cellulose Nanocrystals

Cellulose nanocrystals can be surface modified with polymer chains following two methods: "grafting to" where pre-formed polymer is attached to the surface of the CNCs, or "grafting from" where the polymerization is initiated from the CNC surface (Figure 2.7). Polymer "grafting to" is beneficial since the polymer can be carefully synthesized and thoroughly characterized before it is grafted to the CNCs, however steric hindrance limits the density of polymers that can be grafted to a single nanoparticle. In comparison, "grafting from" allows for a higher graft density, as many initiating sites are available on the CNC surface, but characterizing the polymer chain length and polymerization kinetics can be challenging.[127]

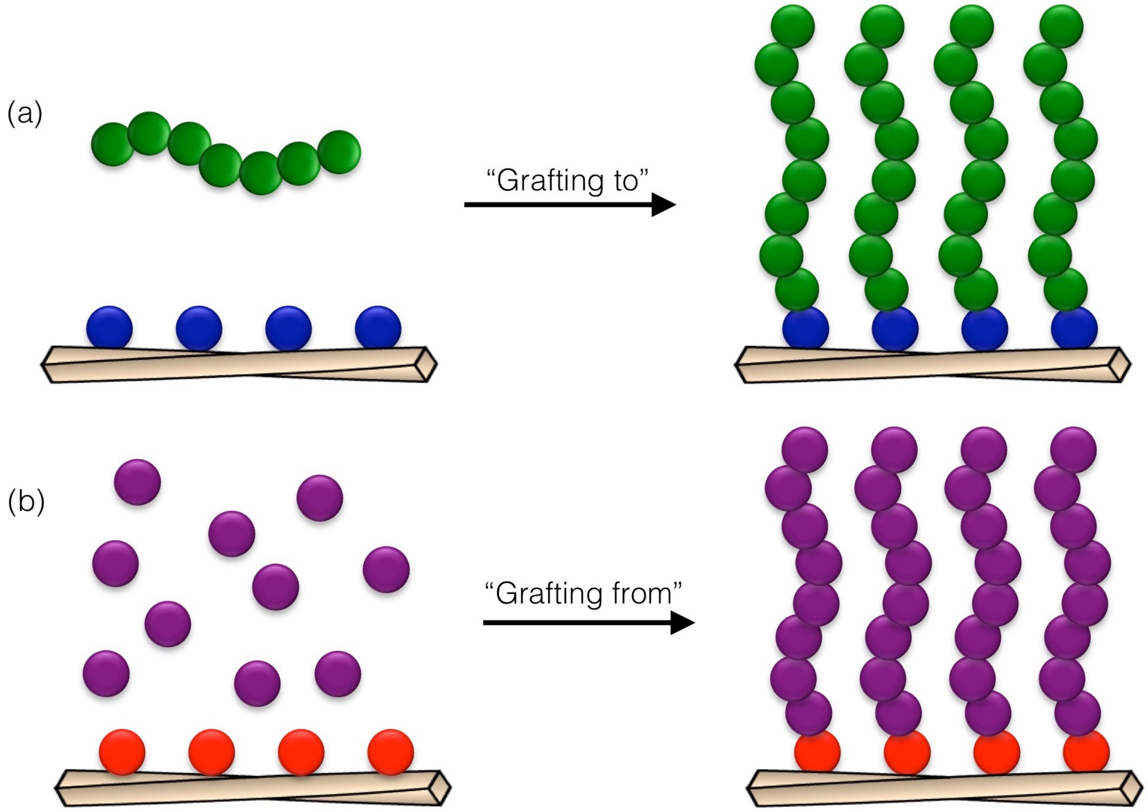

Figure 2.7 Schematic of (a) "grafting to" CNCs with a given reactive group (blue) and a pre-formed polymer (green) and (b) "grafting-from" CNCs with inherent or added

initiating groups (red). Individual purple circles represent monomers and chains of circles are polymers.

The "grafting to" method generally takes advantage of the abundance of reactive hydroxyl groups on the CNC surface and can occur via esterification[128] or by a nucleophilic addition of the alkali-activated cellulose hydroxyl groups to an epoxy terminated polymer.[129,130] Furthermore, carbodiimide-catalyzed amidation (using carboxylic acid groups after TEMPO-oxidation)[124] has been used to couple poly(ethylene glycol) to CNCs. In work by Habibi et al., poly(caprolactone) (PCL) was grafted to CNCs using isocyanate-mediated coupling, and in this work the graft density was high enough such that the PCL chains were able to crystallize at the surface of the CNCs, as shown by enhanced mechanical properties.[131] However, to reach such a high graft density the reaction was carried out over a period of one week with continuous addition of the coupling agent. More recently, UV-light induced thiol-ene click chemistry was used to prepare CNCs prefunctionalized with mono-unsaturated hydrocarbon brushes crosslinked with polybutadiene by using a dithiol crosslinker.[132] High loading was achieved, however the modification was a multi-step process which is less ideal when considering the scale-up required for high volumes of modified CNCs.

"Grafting from" cellulose nanocrystals provides a modification route where high grafting densities (hundreds to thousands of polymer chains per CNC) may be achieved, and tends to be more popular in literature, with reports of both hydrophilic and hydrophobic polymers grafted from CNCs.[133,134] The following discussion highlights the pioneering and most recent and relevant work for the purpose of this thesis and can be divided into four "grafting from" categories: free radical polymerization, ring opening polymerization (ROP), nitroxide mediated polymerization (NMP), and Cu-mediated reversible deactivation radical polymerization (RDRP).

2.4.3.1 Free Radical Polymer Grafting from Cellulose Nanocrystals

Free radical polymer grafting from CNCs is typically carried out in an aqueous environment using a water soluble initiator. This is a favourable reaction since CNCs are most colloidally stable in water, and when performing surface modifications on CNCs it is important to maintain a proper dispersion such that the modification occurs on individual nanoparticles as opposed to aggregates. Free radical polymer grafting from CNCs with ceric ammonium nitrate (CAN), a water soluble initiator, was first demonstrated by our group, although many examples using CAN and other types of cellulose have also been reported.[135–144] We first used CAN to graft CNCs with the hydrophilic, pH responsive polymer poly(4-vinylpyridine) (P4VP). Grafting P4VP from CNCs resulted in pH responsive CNCs which showed the potential for use as reversible flocculants.[145] In order to extend this method to hydrophobic polymers, the work presented in Chapter 3 describes using CAN to graft poly(methyl methacrylate) from CNCs in a one-pot, water based polymerization. The polymer grafted CNCs were thoroughly characterized via solid state NMR, XPS, FTIR, contact angle, thermogravimetric analysis, XRD, and AFM.[146]

Another method of free radical polymerization from CNCs is via potassium persulfate (KPS) initiated free radical polymerization which has been used to graft poly(acrylamide) [147,148] and poly(acrylic acid)[149] in water. The pitfalls of these free radical polymerization methods are the inability to control both the grafted polymer length and the graft density, leading to a heterogeneous modification that is typically difficult to characterize. Additionally, a significant amount of free homopolymer (not grafted to the CNCs) is also produced as a side reaction during free radical polymerization which can be difficult to separate from the modified CNCs, leading to impure products. For some applications (e.g. if the grafted CNCs are to be added to a bulk polymer to produce nanocomposites), producing "side" homopolymer may not be detrimental, however, the yield of the polymer grafting reaction is low and we have estimated that 95% of the starting monomer is likely not grafted to the CNCs.

2.4.3.2 Ring Opening Polymerization from Cellulose Nanocrystals

Ring opening polymerization (ROP) is a method used to polymerize cyclic monomers, mainly lactones. ROP was first used to graft polymer from CNCs by Habibi et al.[150] who grafted PCL from the surface of CNCs using stannous octoate as the catalyst. The reaction was conducted in toluene and the PCL-grafted CNCs (PCL-*g*-CNCs) were shown to maintain their morphology and crystalline structure and the graft density was high enough such that the PCL-*g*-CNCs were successfully added to masterbatches by melt blending with a homopolymer of PCL.[151] Since this pioneering work, Chen et al.[152] and Lin et al.[153] performed the same grafting reactions without solvent and under microwave irradiation in order to enhance the grafting efficiency. To avoid the use of metal-based catalysts, Labet and Thielemans[154] used citric acid as a catalyst in order to facilitate a greener modification of CNCs. Additionally, Goffin et al.[155] have modified CNCs with poly(lactide) (PLA) using ROP and showed improved compatibilization in a PLA matrix. Braun et al.[156] have used partially acetylated CNCs (obtained via Fisher esterification) to provide control of the graft density using ROP from CNCs. In general, ROP provides a facile method for polymerizing cyclic monomers from CNCs with relatively good control over graft density and polymer graft lengths.

2.4.3.3 Nitroxide Mediated Polymerization from Cellulose Nanocrystals

Nitroxide mediated polymerization (NMP) is a form of reversible deactivation radical polymerization (RDRP) that relies on a reversible termination equilibrium between growing propagating macroradicals and the nitroxide moieties that act as control agents. This allows for the synthesis of well-defined polymeric structures from a variety of monomers such as styrene, acrylates, and methacrylates.[157,158] NMP is a simple polymerization method as it does not involve reversible redox processes or chain transfer reactions and is convenient to use in grafting from CNCs as the purification does not require the removal of transition metals. The major disadvantage is the typically lower polymerization rates, higher temperatures needed, and monomer limitations compared to other RDRP methods. Roeder and coworkers were the first to use NMP from CNCs to produce CNC-*g*-PMMA and CNC-*g*-PMA.[159] The polymer-grafted CNCs showed improved dispersion in organic solvents and the potential for the NMP technique to be used to graft other polymers from CNCs.

2.4.3.4 Cu-mediated Reversible Deactivation Radical Polymerization from Cellulose Nanocrystals

Cu-mediated atom transfer radical polymerization (ATRP, a type of RDRP) was first reported by Wang and Matyjaszewski.[160] In ATRP, control is achieved by the equilibrium between propagating radicals (R•) and dormant species (R-X), shown in the schematic in Figure 2.8. Growing radical polymer chains are activated by the reaction between the dormant species and the transition metal complexes in their lower oxidation state (M_t^n/L). Chains are deactivated by the reaction with transition metal complexes in their higher oxidation state. The equilibrium is strongly shifted towards the deactivation state so that there is only a small number of growing chains at any time.[161,162] Control of the reaction is further determined by the rate constants: k_{act} (activation), k_{deact} (deactivation), and k_p (propagation) which can be controlled by the choice of temperature, monomer, and solvent as well as the halide/ligand (M_t^n/L) catalyst system. If the initiation proceeds at a high rate and a fast deactivation occurs, the polymer chains will grow concurrently. However, if deactivation is slow, the number of terminated species will increase, thus leading to a loss of control.[161]

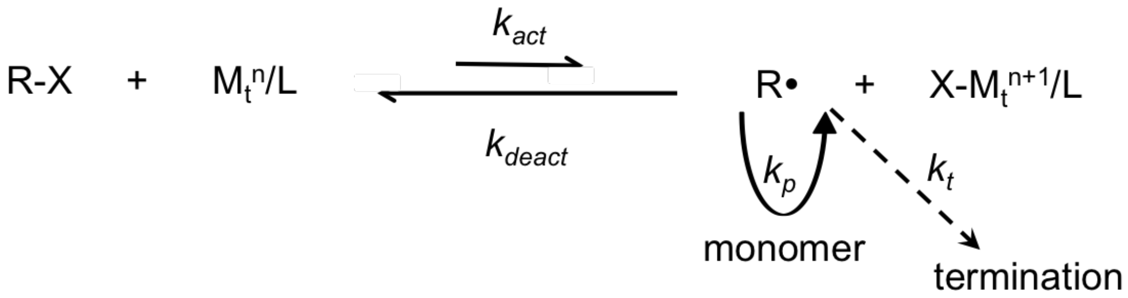

Figure 2.8 ATRP reaction scheme. Adapted from reference 163.

ATRP is a multicomponent system that consists of a monomer, an initiator with a transferable halogen, a ligand and a catalyst composed of a transition metal species.[163] ATRP has been successfully used to polymerize styrenes, (meth)acrylates, (meth)acrylamides, and acrylonitrile which contain substituents that can stabilize the propagating radicals.[161,162] The initiator used in our work is either bound to the surface of the CNCs, or free in solution and referred to as a sacrificial initiator. The amount of initiator determines the number of growing polymer chains, therefore the degree of polymerization in ATRP can be controlled based on the molar ratio of initiator:monomer used.[163] We chose a relatively common ligand and Cu catalyst for our systems in Chapters 4 and 8, however the residual Cu after the polymerization is relatively difficult to remove and requires extensive purification via centrifugation and separations with an EDTA/water solution.

The mechanism for the formation of radicals in ATRP remains debated. Halogen atom transfer from the alkyl halide to the Cu^I complex can occur via either the outer-sphere electron transfer (OSET) or the inner-sphere electron transfer (ISET). Polymerization by OSET is a single electron transfer mechanism, and OSET is also named single electron transfer living radical polymerization (SET-LRP), first derived by Percec and coworkers.[164] The ISET occurs by the mechanism described above, whereby activation occurs through Cu^I. The detailed mechanisms are important for understanding ATRP kinetics and control but are not the focus of this work.

Recently, Yagci and coworkers reported a temporal photoinduced Cu-mediated RDRP procedure for the polymerization of methyl methacrylate.[165] Anastasaki et al.[166] then utilized this technique for the homopolymerization of acrylates using low amounts of copper catalyst ($CuBr_2$) and ligand (Me_6TREN) in a UV box ($\lambda_{max} \approx 360$ nm) commonly used in nail salons. Since this work, this polymerization route has been further expanded by Anastasaki, Haddleton, and coworkers to include various functional monomers,[167] sequence control,[168,169] and has been performed in ionic liquids.[170] Due to the short reaction time (90 min), mild conditions, and small amount of catalyst/ligand required, this UV-initiation presents itself as an ideal morphology for the surface initiated (SI)-photoinduced RDRP from CNCs as demonstrated in detail in Chapter 4.[171]

Cu-mediated controlled radical polymerization provides a method for grafting polymers from CNCs with excellent control over both graft length and graft density. The first report of using ATRP from a cellulose substrate was by Malmström and Carlmark,[172] and since then, many examples of using surface initiated ATRP (SI-ATRP) from CNCs have been demonstrated. In order to perform SI-ATRP from CNCs, an initiator grafting step is necessary in order to convert the CNC surface into a macroinitiator. This is typically done by the introduction of alkyl initiators (usually bromide moieties) to the surface hydroxyl groups of the CNCs in an intermediate step via an esterification reaction (Figure 2.9). The ratio of reactive groups to hydroxyl groups can be varied in order to prepare CNCs with different amounts of initiating surface groups (and therefore different graft densities).

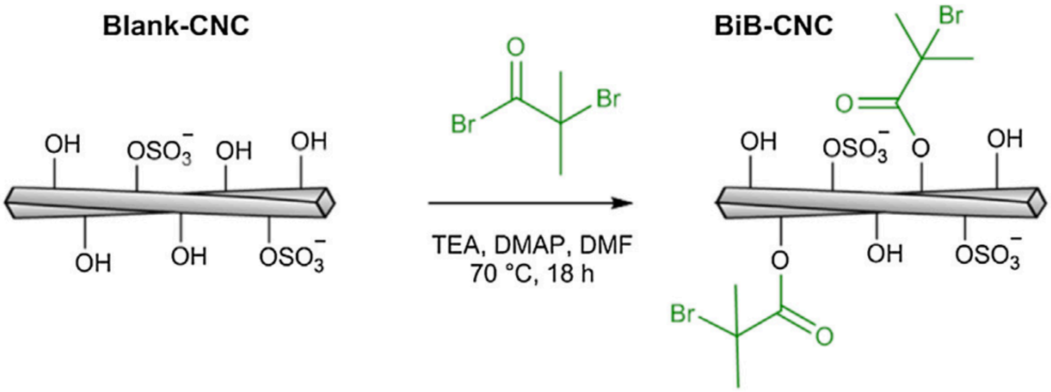

Figure 2.9 Immobilization of ATRP initiating groups on the surface of CNCs. The reaction is carried out in DMF, using triethylamine (TEA) as an organic base and 4-(dimethylamino)pyridine (DMAP) as a catalyst to attach α-bromoisobutyryl bromide (BiB) to the CNC surface, resulting in BiB-CNCs. Adapted from reference 171.

SI-ATRP from CNCs was first reported by Yi et al.[173] who grafted polystyrene (PS) from CNCs. Morandi et al.[133] also grafted PS from CNCs and showed a series of PS-*g*-CNCs with varying graft densities. In their work, the grafted polymer was cleaved from the surface and characterized to show that good control of the SI-ATRP was achieved.[127] If a non-cleavable ATRP initiator is used, as in most cases, a sacrificial initiator (that is a free initiator in solution with similar properties to the initiating groups on the CNC surface) is added to the reaction in order to polymerize free polymer which is collected and characterized to measure the molecular weight (MW) and dispersity (PDI) of the grafted polymer. Although discrepancies between free polymer and polymer grafted from the CNC are likely, this remains the most accurate method of determining the MW and PDI of polymer grafted from the CNC surface, and Morandi et al.[127] showed that the MW and PDI of grafted polymer cleaved from the CNC surface was similar to that of homopolymer polymerized from sacrificial initiator.

Since these first reports, various functional polymers have been grafted from CNCs via Cu-mediated SI-ATRP including PS,[173,133,174] poly(methacrylate) (PMA),[171,175] poly(methyl methacrylate) (PMMA),[176] poly(dimethylaminoethyl methacrylate),[177–179] poly(N-isopropylacrylamide) (PNIPAm),[134,180,181] PNIPAm fluorescent copolymers,[182] poly(N,N-dimethylacrylamide),[183] poly(2-aminoethylmethacrylate) and poly(2-aminoethylmethacrylamide),[184] poly(acrylic acid) through hydrolysis of poly(tert-butyl acrylate),[185] poly(6-(4-(4-methoxyphenylazo)phenoxy)hexyl methacrylate),[186] copolymers of poly(MMA-co-butyl acrylate),[187] poly(diethylaminoethyl methacrylate),[179] poly(ethylene glycol methylacrylate),[188] poly([(2-methacryloyloxy)ethyl] trimethylammonium chloride),[181] and poly(sodium 4-vinylbenzenesulfonate).[181] In most of this work, the SI-ATRP occurred in organic solvents, sacrificing some of the colloidal stability of the CNCs, and furthermore the purification of the reaction must be rather exhaustive to remove the Cu catalyst. A method to overcome this was shown by Wang et al.[175] who used Cu(0) (copper wire) as the catalyst. This allowed for a simple purification with only a few centrifugation steps. In our recent work, described in Chapter 4, we have used a photo-induced Cu-mediated RDRP method to graft hydrophobic polymer from CNCs, with a very low amount of Cu and a straightforward purification method.[171]

A significant pitfall of traditional SI-ATRP from CNCs is the multiple steps required to first attach initiating groups on the CNC surface followed by purification prior to polymer grafting. In order to overcome this, Boujemaoui et al.[176] used a functional acid (2-bromopropionic acid) during the hydrolysis of CNCs in order to prepare functionalized CNCs with SI-ATRP initiating groups, all in one step. This is an improvement if controlled polymer grafting of CNCs is expected to ever be used at an industrial scale.

2.5 Purification and Characterization of Modified Cellulose Nanocrystals

Modified CNCs must be thoroughly purified before characterization in order to avoid characterizing excess reagents that may be leftover or adsorbed to the CNC surface. Purification is typically done through centrifugation (where the modified CNCs are collected in the pellet and washed with solvent), dialysis to remove unreacted small molecules, or stirred cell ultrafiltration. These techniques become critical in the case of polymer grafting where homopolymer is present, since most characterization techniques cannot distinguish between covalently bound and adsorbed/trapped polymer. Furthermore, characterization difficulties arise when trying to distinguish between organic polymers and cellulose as they often have similar chemical compositions.[189]

The most common characterization techniques for modified CNCs are elemental analysis, FTIR, XPS, XRD, TGA, and DSC, all of which are used in the subsequent chapters of this thesis. Their advantages and pitfalls are described briefly below.

In order to probe the chemical composition of modified CNCs, elemental analysis, FTIR, and XPS are often used. Elemental analysis is a useful technique when the CNC modification contains an element different than carbon, hydrogen, or oxygen, which are found in unmodified CNCs. For example, in the cationic modification of CNCs, nitrogen is present in the surface modification such that elemental analysis to determine nitrogen content can be used to calculate the degree of substitution, or the number of cationic groups per CNC. Similarly, if new chemical bonds are introduced, FTIR can play a useful role in identifying the presence of these new bonds.[133] For example, when grafting acrylate monomers from CNCs, the presence of a carbonyl peak implies that polymer is present. XPS is another technique that can be used to confirm the presence of new elements, and furthermore can be used to collect high resolution carbon (C1s) spectra which measures the binding energy of carbon. C1s spectra can differentiate between four types of carbon: C1 (C-C, carbon bonded to only carbon), C2 (C-O-C, carbon bonded to one oxygen), C3 (O-C-O, carbon bonded to two oxygen), and C4 (O-C=O, carbon with three bonds to oxygen) which have different binding energies. Unmodified CNCs should only contain C2 and C3 (though C1 is always present due to contamination, so samples should be as pure as possible[190,191]), therefore the presence of C4 or an increase in C1 is often used to quantitatively determine the amount of polymer present.[146]

XRD can be used to determine changes in crystallinity upon modification of CNCs. When CNCs are grafted with amorphous polymer, the % crystallinity is expected to decrease for polymer-grafted CNCs, which has been shown in literature.[171] The maintenance of the characteristic cellulose I peaks confirms that the CNC crystalline structure is retained during the modification reaction[133,134] and that the decrease in crystallinity is due to the presence of amorphous polymer.

Modified CNCs often display differences in thermal stability which can be measured by TGA and DSC. TGA measures sample mass as a function of temperature and is used to determine the temperature at which a sample thermally degrades. Unmodified CNCs display a significant mass loss (and therefore thermal degradation) around 300°C.[192] A shift in thermal degradation temperature can be correlated to the presence of polymer or other small molecules. For example, after the attachment of ATRP initiators, the thermal degradation temperature of the CNCs decreases. This is attributed to the presence of the Br groups which may accelerate the degradation of the CNCs.[171,176] However, upon grafting polymer, the samples exhibit a secondary degradation curve which is shifted towards the onset of thermal degradation of pure homopolymer, confirming the presence of polymer.[134,185] TGA can be used to determine the weight percent of polymer grafted based on the ratio of the secondary degradation curve attributed to the grafted polymer.[171]

DSC is often used to determine the glass transition temperature (T_g) of amorphous polymers, so in the case of polymer-grafted CNCs, DSC is a way to characterize the polymer but not the CNC itself. The T_g is the temperature above which a hard polymer transitions into a soft or rubbery polymer as the polymer chains have increased mobility.[193] An increase in the T_g implies a reduced mobility of the polymer, and in the case of polymer grafting, this implies that the polymer chains have been tethered to a surface. As such, an increase in the T_g of the polymer has been used to support the covalent binding of polymers to the CNC surface.[171,134,194] Although DSC is beneficial in confirming the polymer is grafted to the CNC surface, it is qualitative and cannot determine the amount of grafted polymer or its molecular weight.

While NMR is the conventional "workhorse" of the synthetic and polymer chemist, challenges arise when trying to analyze the chemical composition of CNCs and their derivatives. As CNCs cannot be dissolved in traditional NMR solvents (such as deuterated DMSO and deuterated chloroform), to the best of our knowledge there are currently no reports of solution NMR used to characterize modified CNCs. Solid state NMR such as ^{13}C-cross polarization magic angle spinning (CP-MAS) NMR shows potential for quantitative characterization of polymer-grafted CNCs and is performed on dried samples. In the 1980s, ^{13}C CP-MAS NMR was first used to determine the structure and crystallinity of native cellulose I,[195,196] and in the 1990s, Heux et al. used the technique to study CNC structural aspects[197] and lateral dimensions.[198] It has recently been used to determine the degree of substitution of CNC modifications such as TEMPO oxidation,[199] esterification,[200] and polymer grafting,[201,202] among others. In Chapter 3 we use solid state NMR to determine the presence of PMMA grafted from CNCs via a free radical polymerization. The presence of PMMA was confirmed, but due to the low amount of polymer grafted, the signal-to-noise ratio was too low to quantitatively measure the amount of PMMA, even after 3000 scans.[146] NMR is limited for characterizing polymer-grafted CNCs due to the issues stated above as well as the large signal of cellulose (which can swamp the normally smaller signal from the added surface moieties) and the broad peaks that are often seen for CNCs in solid state NMR. Our current collaboration with NMR experts at the University of Helsinki aims to provide a method of dissolving polymer-grafted CNCs in ionic liquids in order to use solution state NMR to quantitatively determine the amount and distribution of polymer grafted from CNCs, even when the polymer is expected to be in small quantities. This work is presented in further detail in Chapter 5.

2.6 Pickering Emulsions

Emulsions are obtained by dispersing a fluid into another immiscible fluid via high energy shearing that results in a dispersion of droplets in a continuous phase.[203] The droplet interface is typically stabilized by small molecule surfactants. Surfactants are surface active molecules that readily partition at interfaces to lower the surface tension.

An interface is a boundary between two immiscible phases. Surfactants partition at the interface due to their amphiphilic nature, whereby they have one hydrophilic/polar end (typically the surfactant "head"), and a hydrophobic/non-polar end (typically the surfactant "tail(s)"). Emulsions may be oil-in-water (o/w), where the oil is the dispersed phase and water is the continuous phase, or water-in-oil (w/o), where water is dispersed in the continuous oil phase. Emulsions are used in applications such as cosmetics, foods, adhesives, coatings, toners, and many other liquid-formulated products.

Pickering emulsions are a type of emulsion that use solid particles to stabilize the oil-water interface, as opposed to surfactants. Pickering emulsions were first reported by Ramsden in 1903,[204] but they received their name after a report by Pickering in 1907.[205] Particle stabilized emulsions show greater resistance to droplet coalescence.[206] The energy required to remove a small particle from the interface is several orders of magnitude greater than the thermal energy, hence the particles are considered to be irreversibly adsorbed or "stuck" at the interface which leads to enhanced stability.[207] Particles that stabilize emulsions (called Pickering stabilizers) do not have to be amphiphilic to adsorb at the oil-water interface,[206,208] but must have partial wettability in both immiscible liquid phases. While conventional surfactants are typically used to lower oil-water interfacial tension, Pickering emulsions with micrometer sized droplets are often formed with relatively small reduction of the interfacial tension.[209–211]

In the case of Pickering stabilizers, the relevant parameter for determining the emulsion type (o/w or w/o) is the three phase contact angle θ measured in the aqueous phase; the emulsion type is then dictated by this contact angle according to the Bancroft rule.[206] For relatively hydrophilic particles (like cellulose nanocrystals), θ measured into the aqueous phase is $< 90°$ and a larger fraction of the particle resides in the water phase compared to the oil phase. For hydrophobic particles, θ is generally $> 90°$ and the particles reside more in oil phase. The particles will orient such that the larger area of the particle surface remains on the external side, giving rise to o/w emulsions when $\theta < 90°$ and w/o emulsions when $\theta > 90°$ (Figure 2.10).

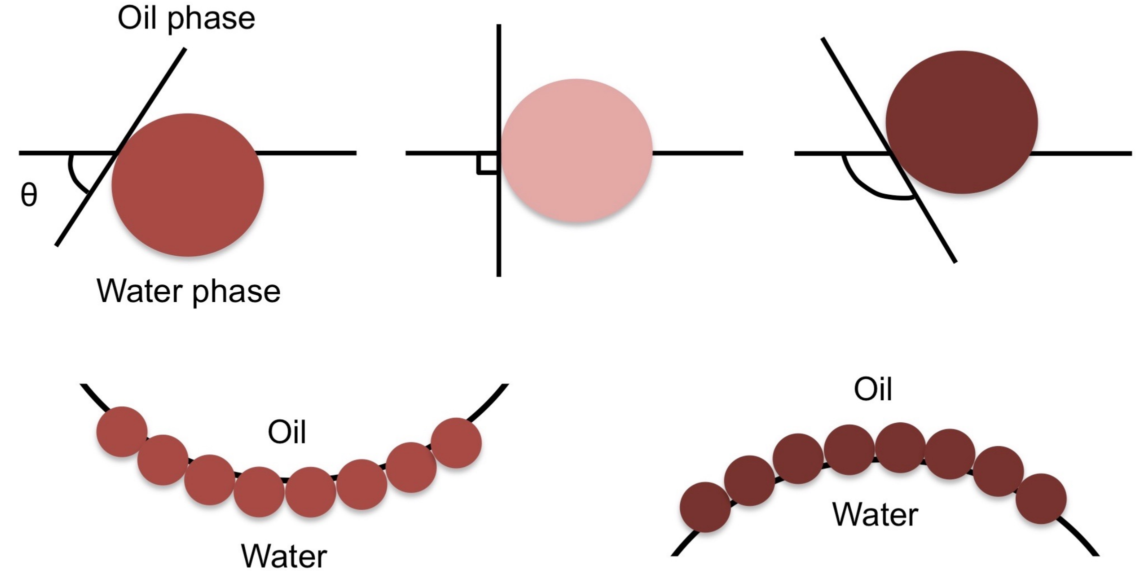

Figure 2.10 Three phase contact angle schematic where θ < 90° (upper left), θ = 90° (upper middle) and θ > 90° (upper right), as well as the probable positioning of particles at an oil-water interface (lower left for θ < 90° and lower right for θ > 90°. Adapted from reference 206.

In order to understand why Pickering stabilizers are strongly attached to oil-water interfaces, Binks[206] considered a spherical particle *s* of radius *r* which is initially in the water phase and is subsequently adsorbed to the oil-water interface. The energy of attachment of a particle to the oil-water interface is related not only to the contact angle but also to the surface tension of the contact interface $\gamma_{\text{oil-water}}$. Assuming the particle is small enough (less than a few microns in diameter) so that the effect of gravity is negligible, the energy (*E*) required to remove the particle from the interface is given by Equation 1.[206]

$$E = \pi r^2 \gamma_{oil-water}(1 \pm cos\theta)^2 \qquad (1)$$

The ± sign inside the brackets is negative for removal of particles into the water phase and positive for removal into the oil phase. For θ < 90°, the particle is more easily removed into the water and for θ > 90° the particle is more easily removed into the oil phase. The high energy of attachment of particles to interfaces means that the particles are thought to be irreversibly adsorbed, in comparison to surfactant molecules that are known to adsorb and desorb on a fast timescale. Since *E* depends on the square root of the particle radius, we see that for very small particles (i.e., <0.5 nm) we calculate energies comparable to that of surfactants. Therefore, the size of the stabilizing particles as well as the hydrophilicity play an important role in the stabilization of Pickering emulsions.

Another important property of Pickering stabilizers is their shape. Most Pickering stabilizers reported in literature are spherical; examples include silica nanoparticles,[208,212,213] polystyrene latexes,[214] iron nanoparticles,[215] and polymer microgels,[216] among many others. However, more recently, anisotropic nanoparticles such as clays,[217] graphene oxide,[218] chitin nanocrystals,[219] and cellulose nanocrystals[220] have been reported as Pickering stabilizers. Differences in Pickering stabilizer shape has been shown to effect the packing density and orientation at the interface.[221]

2.6.1 Cellulose Nanocrystals in Pickering Emulsions

CNCs produced via HCl hydrolysis of bacterial cellulose were the first CNCs reported as Pickering stabilizers.[220] In this pioneering work by Capron and coworkers in 2011, stable hexadecane oil droplets with diameters of 4 µm were prepared. The CNCs were good Pickering stabilizers since they had no surface charge groups to repel each other and they could pack in an ordered manner at the oil-water interface. Furthermore, the distribution of CNCs at the interface was imaged by SEM by substituting the liquid oil phase with styrene and polymerizing PS particles. This was done since liquid oil-water emulsions could not be introduced into the vacuum chamber required for SEM imaging.[220] Building on this work, Capron and coworkers showed that CNCs possess a hydrophobic plane that is oriented towards the oil phase when CNCs are at the oil-water interface.[29] They tuned the amphiphilicity of the CNCs based on the surface charge density, where a low surface charge density (<0.03 e/nm^2) was required in order to stabilize oil-water interfaces, but a higher surface charge density could be screened with the addition of 50 mM NaCl in order to promote more efficient CNC packing at the interface.

CNCs have been shown to partition at the oil-water interface via interfacial tension measurements which also supports their use as Pickering stabilizers.[121] CNCs alone lowered the interfacial tension of a dodecane-water interface, though at a much slower rate compared to surface active polymers or surfactants.[121] This slow partitioning to interfaces is likely due to their large hydrodynamic size.[222] However, as Pickering stabilizers, once the CNCs have partitioned to the interface they are irreversibly adsorbed and show improved emulsion stability compared to surface active polymers or surfactants.

The density of CNC packing (and therefore surface coverage) at the oil-water interface has been shown to be directly influenced by the CNC aspect ratio.[71] Capron and coworkers studied small aspect ratio CNCs from cotton (c-CNCs), medium aspect ratio CNCs from bacterial cellulose (b-CNCs), and high aspect ratio CNCs from *Cladophora* (Cla-CNCs) to stabilize hexadecane oil-in-water emulsions. All three types of CNCs were irreversibly adsorbed at the oil-water interface and formed ultrastable emulsions. Droplet diameters of the emulsions stabilized by all three types of CNCs were similar, showing similar wetting properties regardless of the cellulose source. However, the aspect ratio directly influenced the surface coverage. Short CNCs from cotton showed a dense organization at the interface, with coverage > 80%, while medium aspect ratio CNCs from bacteria resulted in 60% surface coverage, and the high aspect ratio CNCs from *Cladophora* required only 40% surface coverage. The surface of the droplets imaged by SEM can be seen in Figure 2.11, where the higher aspect ratio CNCs seem to form an entangled network between the polymer particles, whereas the cotton CNCs are much more densely packed and able to stabilize individual polymer particles. This work led to a better understanding of the adsorption of rod-like CNCs at interfaces and showed the versatility of CNCs as Pickering stabilizers.

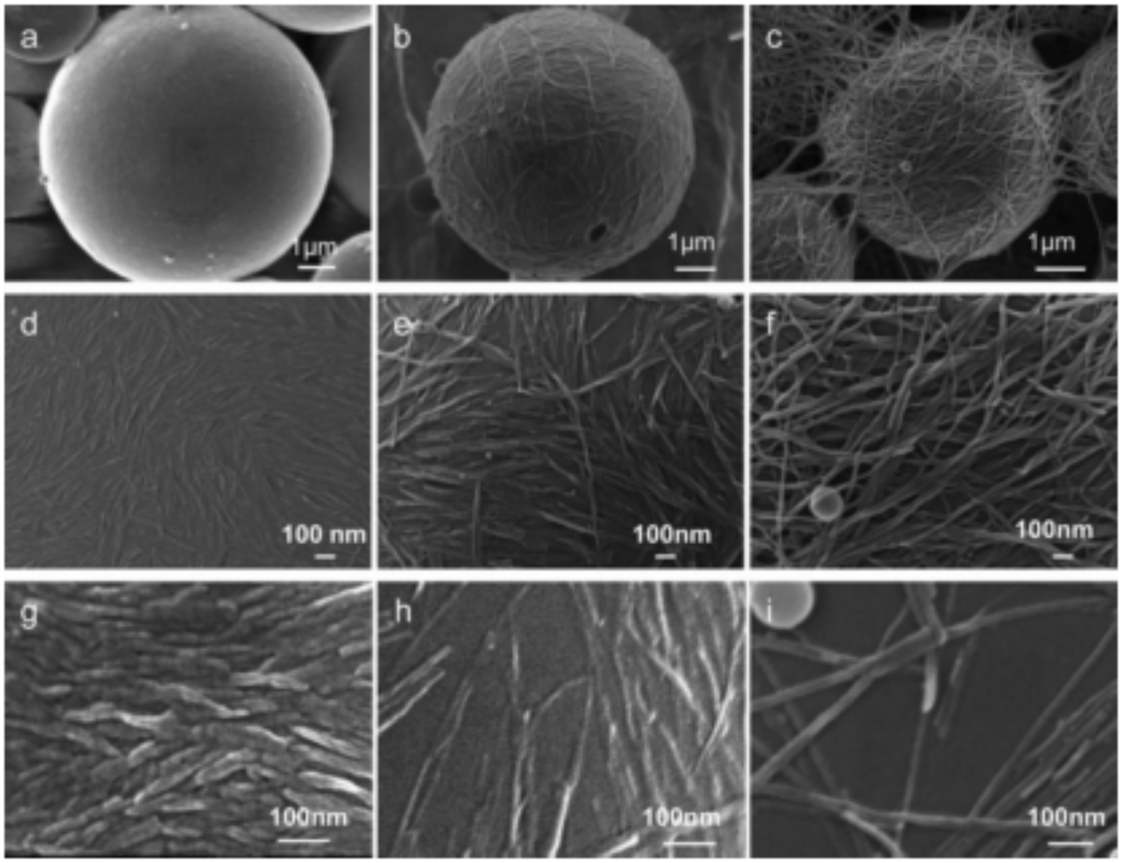

Figure 2.11 SEM images of PS particles stabilized by c-CNCs (a, d, g), b-CNCs (b, e, h), and Cla-CNCs (c, f, i) showing the surface coverage and packing of the CNCs at the particle interface. Reproduced from reference 71.

In 2013, the Capron group patented the use of CNCs as Pickering emulsifiers.[223] In that same year, they also showed the use of CNCs to stabilize high internal phase emulsions where the oil phase was > 74% of the emulsion by volume.[224] More recently, Capron et al. have used CNCs to stabilize water-in-water emulsions, where two incompatible water soluble polymer solutions were stabilized with CNCs.[225] Furthermore, they have shown that the thickness of the CNC layer at the oil-water interface is dependent on the CNC surface charge.[226] If fully desulfated CNCs are used as Pickering stabilizers, they form a layer 18 nm thick, whereas sulfated CNCs with the addition of salt form a 7 nm thick layer at the interface. This fundamental study is important in order to optimize the use of CNCs as Pickering stabilizers.[226]

Since this pioneering work by the Capron group, the field of CNC Pickering emulsions has grown tremendously, as evidenced by over 300 citations to their original papers in the past five years. The ability to modify CNC surface chemistry can lead to even more interesting systems and Pickering emulsions with tailorable properties, making this topic the next wave in CNC emulsion research. For example, stimuli responsive Pickering emulsions have been prepared by grafting stimuli responsive polymers from CNCs prior to their use as stabilizers. Zoppe et al.[227] grafted the thermoresponsive polymer poly(NIPAM) from CNCs and determined that the Pickering emulsion could be broken upon heating above the lower critical solution temperature of poly(NIPAM). Furthermore, Tang et al. prepared dual responsive Pickering emulsions by grafting poly[2-(dimethylamino)ethyl methacrylate] which is both temperature and pH responsive.[228] They further showed the use of these stimuli responsive Pickering emulsions for oil harvesting.[229] Nypelö et al. used magneto-responsive CNCs to prepare microbeads and hollow microcapsules,[230] while Low et al. prepared pH responsive CNC Pickering emulsions using Fe_3O_4-CNCs.[231] The ability to prepare stimuli responsive Pickering emulsions may extend the applications of these emulsions to areas such as oil recovery or biomedical applications.

CNCs have also been grafted with small molecules in order to prepare Pickering emulsions with new properties. Visanko et al. prepared dialdehyde and amino functionalized CNCs and used them to stabilize oil-in-water emulsions,[232] while Cunha and coworkers combined both CNFs and CNCs modified with C12 chains in order to prepare double Pickering emulsions.[233] They showed an increase in emulsion stability corresponding to an increase in nanofiber length. Svagan et al. also used a combination of CNFs and CNCs that were covalently crosslinked in order to prepare CNF/CNC reinforced capsules via Pickering emulsions.[234] Furthermore, CNCs have been modified via TEMPO oxidation and with quaternary ammonium salts to produce inverse emulsions[235] and with carboxylic and *n*-butylamino groups in order to be used as stabilizers for marine diesel oil-in-water emulsions.[236] This past work highlights the functionality of CNC Pickering emulsions due to the wide variety of surface modifications that may be performed on CNCs prior to their use as stabilizers.

In order to take advantage of CNC modification via adsorption (i.e., non-covalent surface modification), our group has previously prepared CNC Pickering emulsions enhanced with cationic surfactants that showed improved resistance to coalescence compared to those stabilized by CNCs alone.[110] In that work, the CNCs were simply mixed with cationic surfactants prior to emulsification with dodecane oil and the hydrophobicity of the surfactant allowed for the emulsion type (o/w or w/o) to be tailored. In order to avoid the use of surfactants all together, CNCs coated with surface active polymers were also used to prepare emulsions with improved stability (and the smallest oil droplets seen to date in CNC systems),[121] as well as dried oil powders.[122] The CNCs coated with surface active polymers (hydroxyethyl cellulose and methyl cellulose) proved to be better Picking stabilizers than either polymers or CNCs alone, and the facile modification route showed potential to be scaled up easily. The combination of CNCs and the surface active polymer methyl cellulose in particular has been the motivation for some of this thesis work using methyl cellulose-coated CNCs as stabilizers for microsuspension polymerization. This work is discussed in detail in Chapter 7.

2.7 Polymer Latexes

Polymer latexes are suspensions of synthetic polymer particles, typically on the order of nanometers or micrometers. Polymer latexes are used in a wide variety of every day products and have provided a platform to combine a variety of polymer properties.[237] Most polymer latexes are cast as films in order to provide coatings such as paints or adhesives. They are desirable since they are water-based and avoid the use of volatile organic solvents.[238] Polymer latexes can be prepared via emulsion polymerization, miniemulsion polymerization, or microsuspension polymerization. The differences in polymerization methods are described briefly in subsequent sections.

2.7.1 Emulsion Polymerization

Emulsion polymerization is considered an environmentally friendly process as it avoids the use of volatile organic solvents and is instead performed in an aqueous environment. Emulsion polymerization is used to produce nanoscale polymer latex particles used for water-based coatings such as adhesives and paints. It is a heterogeneous free radical polymerization process whereby a relatively hydrophobic monomer is emulsified by a surfactant. The polymerization is then initiated in the water phase via a water soluble initiator such as sodium persulfate.[239] Typical monomers for emulsion polymerization have a slight water solubility in order to facilitate diffusion between a large monomer droplet and growing polymer particles. An extremely large oil-water interfacial area is generated as the particle nuclei form and grow in size as the polymerization progresses. Therefore an effective stabilizer such as sodium dodecyl sulfate (SDS, an anionic surfactant) or cationic CTAB should be used to prevent the latex particles from coagulating via electrostatic stabilization.[240]

Emulsion polymerization is a rather complex process because nucleation, growth, and stabilization of polymer particles are controlled by the free radical polymerization mechanisms in combination with various colloidal phenomena. The emulsion polymerization method is shown schematically in Figure 2.12. In the initial emulsification, large monomer droplets are formed along with surfactant micelles. The slightly water soluble monomer is able to diffuse through the water phase where it is initiated via free radical water soluble initiators. As the oligomer grows in the water phase it reaches a point where it is no longer soluble in the water phase and diffuses into a surfactant micelle. Once in the micelle, the polymer grows by polymerizing monomer that has diffused from the large monomer reservoir. This process allows for the polymerization of discrete polymer particles with controllable size and composition.

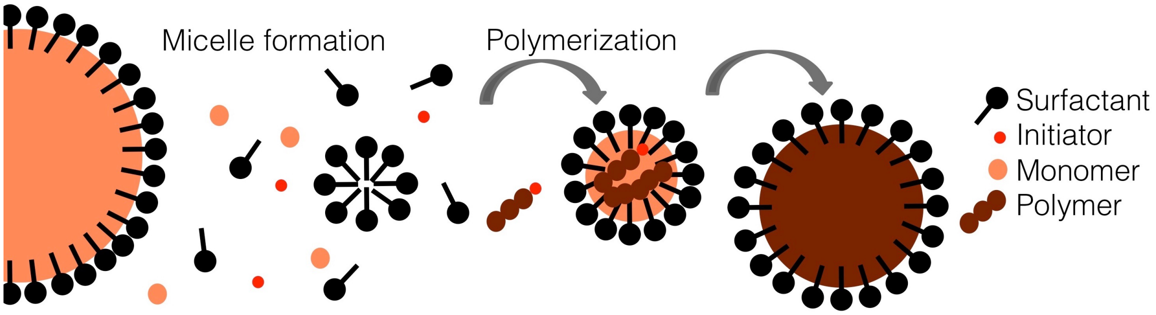

Figure 2.12 Emulsion polymerization schematic showing the process of polymer initiating in the water phase and chain growth in surfactant micelles. Not drawn to scale.

2.7.2 Miniemulsion Polymerization

Miniemulsion polymerization is a type of emulsion polymerization with different kinetics. In miniemulsion polymerization, monomer droplets are prepared via high shear emulsification (typically by sonication) to produce compartmentalized “nanoreactors” that are stabilized by a surfactant. These monomer droplets also contain oil soluble initiators which lead to the polymerization of monomer droplets into particle polymers with limited monomer diffusion between droplets, essentially following bulk polymerization kinetics within each nanoreactor.[241] The prevention of monomer diffusion between droplets typically requires a hydrophobe that is a monomer soluble molecule which may be polymerized into the particles or may act as a secondary stabilizer in order to maintain individual droplets and minimize monomer diffusion. Miniemulsion polymerization is discussed in further detail in Chapter 6.

2.7.3 Microsuspension Polymerization

Microsuspension polymerization is a type of suspension polymerization that is used to synthesize particles with sizes above those made by emulsion polymerization (hundreds of nm) yet below those made using conventional suspension polymerization (20-3000 µm).[242] In this polymerization method, a water insoluble monomer with an oil soluble initiator is dispersed in the continuous phase (i.e., water phase) using a small amount of stabilizer. This results in micron-sized monomer droplets that are converted to polymer particles in a similar method as miniemulsion polymerization. Advantages of using microsuspension polymerization are low dispersion viscosity, low separation costs, and a final product in the particle form.[243] Emulsion, miniemulsion, and microsuspension polymerization methods all produce suspensions of latex particles that may be cast as films for coating applications such as pressure sensitive adhesives.

2.8 Pressure Sensitive Adhesives

One latex system of particular interest is pressure sensitive adhesives (PSAs). PSAs are a class of adhesives that instantaneously form a bond upon the application of light pressure but that are reversible and do not leave behind adhesive residue. Tapes, labels, and protective films are common pressure sensitive adhesive products that find application in the automotive, aerospace, and electronic industry, among many others.[244] The PSA sector is among the fastest growing in the adhesive market, making the search for new pressure sensitive products and applications highly competitive.[245]

The basis for a PSA is a polymer with a low T_g, typically an alkyl acrylate such as poly(butyl acrylate) or poly(2-ethylhexyl acrylate). These polymers are inherently soft, with a T_g of -52 and -70°C, respectively, however they alone do not possess adequate shear strength. PSAs require a balanced combination of tack, peel strength, and shear strength. To meet these requirements, copolymers are necessary. Adding a co-monomer such as an alkyl methacrylate (for example methyl methacrylate, MMA), vinyl esters (such as vinyl acetate) or vinyl aromatics (for example styrene and its derivatives) with T_gs above 0°C is common. Additionally, monomers with acrylic or methacrylic acid functional groups provide potential crosslinking sites which can further improve the shear and peel strength of the PSA, which can consequently also reduce the tack. To counteract this, the presence of other components such as tackifiers can be used.

Solvent-based PSAs have been in use since the 19th century, while emulsion-based PSAs have only been widely used since the 1970s. The shift towards emulsion-based PSAs was largely due to the need to replace solvent-based formulations with other high-performance alternatives as a result of increased health and environmental concerns about using volatile solvents.[245] Initially it was expected that emulsion-based PSAs could not meet the performance standards of solvent-based PSAs. However, novel, flexible and versatile high performance emulsion-based PSAs are having an impact on today's market, with both academic and industrial research focused on preparing emulsion-based PSAs with improved properties. One method of improving PSA properties is by reinforcement with inorganic nanoparticles such as silica nanoparticles,[246] clays,[247] nanoplatelets,[247] and layered silicate.[248] The goal of incorporation is typically to provide reinforcement and improved mechanical properties. A few studies (by our collaborators) have used CNCs in PSA latexes and will be discussed in further detail in Section 2.9.

While this thesis work focuses on a model system of PMMA latexes (which are straightforward to characterize and image) and controlling the location of CNCs in the latex, it is part of a larger effort to improve commercial latex polymer properties. In our collaboration with the University of Ottawa we are producing a copolymer PSA by emulsion polymerization of butyl acrylate (the "soft" monomer) and methyl methacrylate (the "hard" monomer). A simple PSA is composed of water, surfactant, monomer, and initiator. In order to understand the role that CNCs can play in an emulsion-based PSAs, we have studied the interactions of CNCs and surfactants to be used as emulsion stabilizers (Chapter 6), and have improved the CNC surface activity through adsorption with methyl cellulose (Chapter 7) with the goal of replacing surfactants in emulsion polymerization with methyl cellulose-coated CNCs. Furthermore, by tuning the surface chemistry and modifying CNCs with grafted polymers (Chapters 3 and 4), we anticipate the ability to incorporate CNCs into emulsion-based latexes in order to provide enhanced mechanical and adhesive properties (Chapter 8).

2.9 CNC Latex Nanocomposites

Polymer nanocomposites are hybrid materials where a nanoparticle filler is added to a polymer matrix. The nanoparticle typically provides enhanced properties such as mechanical reinforcement, resulting in a polymer material with increased strength. Polymer nanocomposites containing CNCs have received much attention as CNCs have high strength, stiffness and a large aspect ratio. However, CNC polymer nanocomposites are typically made via processes that are not industrial feasible (i.e., solvent casting), or by melt processing at high temperatures which result in CNC aggregation and thermal degradation. Furthermore, the incompatibility of CNCs with most hydrophobic polymers is limiting. One method to overcome these issues is the preparation of latex nanocomposites, whereby the CNCs are added to a latex suspension. We envision three possible approaches to incorporate CNCs into synthetic latexes.

The first approach to preparing CNC latex nanocomposites is by blending a CNC suspension with a pre-formed latex suspension. In this case, the CNCs have no driving force to interact with the latex particles and are considered free in suspension (Figure 2.13a). This may also be accomplished by adding CNCs to an emulsion polymerization reaction *in situ*, where the CNCs are present during the latex polymerization but play a passive role. For example, this occurs when anionic CNCs are added to an (mini)emulsion polymerization stabilized using anionic SDS. CNCs can also be used as Pickering stabilizers in the polymerization of the latex, resulting in larger particles with a CNC "shell" on the surface (Figure 2.13b). Additionally, CNCs can be hydrophobically modified to improve their compatibility with the hydrophobic core of the polymer latex (Figure 2.13c). This thesis aims to tune the location of the CNCs within the latex nanocomposite in order to provide improved latex properties via all three proposed approaches.

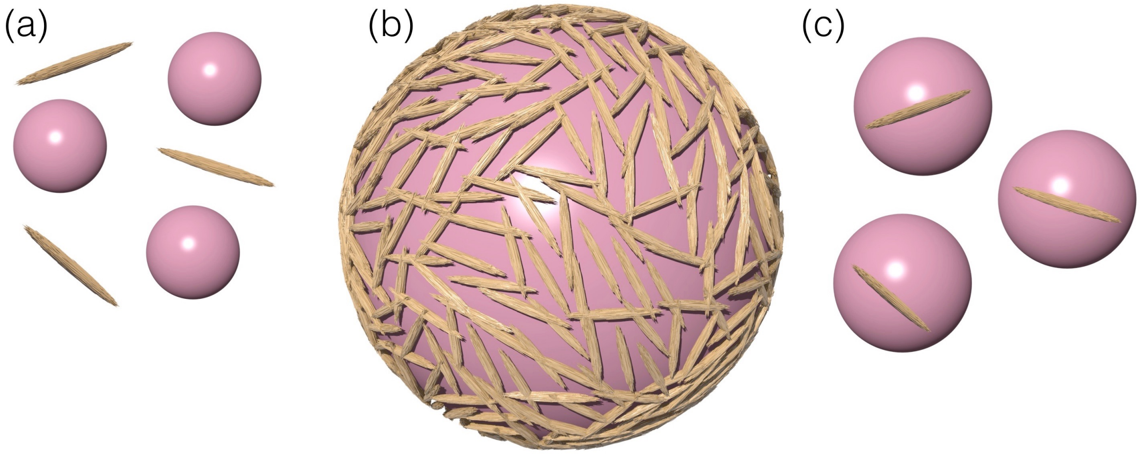

Figure 2.13 Schematic showing three approaches to incorporate CNCs into polymer latex nanocomposites: (a) blending a CNC suspension with a latex or *in situ* polymerization (but CNCs play a relatively passive role), (b) using CNCs as Pickering stabilizers, (c) hydrophobically modifying CNCs to be incorporated inside the latex particle core.

The initial reports of using CNCs in polymer latexes were by Favier and Chanzy in the mid 1990s.[75,249] In this work, CNCs were blended with low T_g polymer latexes in order to prepare nanocomposite films. TEM showed a good distribution of CNCs within the polymer film, and the nanocomposite film exhibited superior mechanical properties compared to polymer alone. More recently, Elmabrouk and coworkers used unmodified CNCs in order to improve the properties of a final polymer coating prepared by miniemulsion polymerization.[250] In their work, the CNCs were added to the water phase in the miniemulsion polymerization of poly(styrene-co-hexyl acrylate) to produce a final latex with a solids content of 20 wt.%, with 1-5 wt.% of CNCs added based on polymer content. Upon imaging the films with TEM, the CNCs were seen between the latex particles and did not play an active role in stabilizing the polymerization. The same authors then prepared poly(butyl methacrylate) latexes by miniemulsion polymerization in the presence of CNCs,[251] where unmodified CNCs were added to the water phase with a cationic surfactant as the stabilizer, and a solids content of 25 wt.% was achieved, with up to 5 wt.% of CNCs based on polymer content.[251] Due to the negative surface charges on the CNCs, when imaged by TEM the CNCs tended to appear anchored around the cationic latex particles, and this was the first report of using CNCs and a cationic surfactant in miniemulsion polymerization. Furthermore, Elmabrouk et al. studied the preparation of poly(styrene-co-2-ethyl hexylacrylate) latexes using a reactive silane (methacryloxypropyl triethoxysilane) in order to stabilize the dispersion and to promote the anchoring of CNCs on the polymer particles via hydrogen bonding between the silanol groups and the hydroxyl groups on the CNC surface. This provided improved mechanical properties in the resulting film, but the CNCs were not the main stabilizers in the polymerization and their main role was as reinforcing agents in the casted film.

Recently, Geng et al.[252] and Pracella et al.[253] used CNCs to improve the mechanical properties in a poly(vinyl acetate) latex whereby *in situ* addition of CNCs during polymerization gave better properties than the CNC-latex blend and further mixing of the nanocomposite latex within another bulk polymer also led to improved dispersibility of CNCs. CNCs played a passive role and provide mechanical reinforcement as opposed to particle stability within the latex.

Our collaborators have recently published work describing the addition of unmodified CNCs *in situ* during the emulsion polymerization of poly(n-butylacrylate-co-methyl methacrylate).[254,255] They showed that the gel content, viscosity, elasticity, tack, shear strength and peel strength of the resulting pressure sensitive adhesive films increased with increasing CNC content. In order to build upon this work, we aim to add CNCs into the emulsion polymerization system where they will play an active role either as latex particle stabilizers (in miniemulsion or microsuspension polymerization) or as hydrophobically modified CNCs that will remain in the monomer/polymer phase and act as reinforcing agents inside the core of individual polymer particles.

References

(1) Kaplan, D. L. *Biopolymers from Renewable Resources*; Springer: Berlin, 1998.
(2) Habibi, Y.; Lucia, L. A.; Rojas, O. J. Cellulose Nanocrystals: Chemistry, Self-Assembly, and Applications. *Chem. Rev.* **2010**, *110* (6), 3479–3500.
(3) Zugenmaier, P. *Crystalline cellulose and cellulose derivatives*; Timell, T. E., Wimmer, R., Eds.; Springer: Berlin, 2008.
(4) Medronho, B.; Romano, A.; Miguel, M. G.; Stigsson, L.; Lindman, B. Rationalizing cellulose (in)solubility: Reviewing basic physicochemical aspects and role of hydrophobic interactions. *Cellulose* **2012**, *19* (3), 581–587.
(5) Vincent, J. F. V. Survival of the cheapest. *Mater. Today* **2002**, *5* (12), 28–41.
(6) Somerville, C. Cellulose Synthesis in Higher Plants. *Annu. Rev. Cell Dev. Biol.* **2006**, *22* (1), 53–78.
(7) Brown, R. M. Cellulose Structure and Biosynthesis: What is in Store for the 21st Century? *J. Polym. Sci. Part A Polym. Chem.* **2004**, *42* (3), 487–495.
(8) Rowland, S. P.; Roberts, E. J. The nature of accessible surfaces in the microstructure of cotton cellulose. *J. Polym. Sci. Part A-1 Polym. Chem.* **1972**, *10* (8), 2447–2461.
(9) Delmer, D. P. Cellulose biosynthesis: exciting times for a difficult field of study. *Annu. Rev. Plant Physiol. Plant Mol. Biol.* **1999**, *50* (1), 245–276.
(10) Wang, H.; Gurau, G.; Rogers, R. D. Ionic liquid processing of cellulose. *Chem. Soc. Rev.* **2012**, *41* (4), 1519.
(11) Klemm, D.; Heublein, B.; Fink, H. P.; Bohn, A. Cellulose: Fascinating biopolymer and sustainable raw material. *Angew. Chemie - Int. Ed.* **2005**, *44* (22), 3358–3393.
(12) Klemm, D.; Kramer, F.; Moritz, S.; Lindström, T.; Ankerfors, M.; Gray, D.; Dorris, A. Nanocelluloses: A New Family of Nature-Based Materials. *Angew. Chemie Int. Ed.* **2011**, *50* (24), 5438–5466.
(13) Pääkkö, M.; Ankerfors, M.; Kosonen, H.; Nykänen, A.; Ahola, S.; Österberg, M.; Ruokolainen, J.; Laine, J.; Larsson, P. T.; Ikkala, O.; et al. Enzymatic Hydrolysis Combined with Mechanical Shearing and High-Pressure Homogenization for Nanoscale Cellulose Fibrils and Strong Gels. *Biomacromolecules* **2007**, *8* (6), 1934–1941.
(14) Wågberg, L.; Decher, G.; Norgren, M.; Lindström, T.; Ankerfors, M.; Axnäs, K. The buildrs of microfibrillated cellulose and cationic polyelectr-up of polyelectrolyte multilayeolytes. *Langmuir* **2008**, *24* (3), 784–795.
(15) Moon, R. J.; Martini, A.; Nairn, J.; Simonsen, J.; Youngblood, J. Cellulose Nanomaterials Review: Structure, Properties and Nanocomposites. *Chem. Soc. Rev.* **2011**, *40* (7), 3941.
(16) Carpenter, A. W.; De Lannoy, C. F.; Wiesner, M. R. Cellulose nanomaterials in water treatment technologies. *Environ. Sci. Technol.* **2015**, *49* (9), 5277–5287.
(17) Abitbol, T.; Rivkin, A.; Cao, Y.; Nevo, Y.; Abraham, E.; Ben-Shalom, T.; Lapidot, S.; Shoseyov, O. Nanocellulose, a tiny fiber with huge applications. *Curr. Opin. Biotechnol.* **2016**, *39* (I), 76–88.
(18) Sani, A.; Dahman, Y. Improvements in the production of bacterial synthesized biocellulose nanofibres using different culture methods. *J. Chem. Technol. Biotechnol.* **2010**, *85* (2), 151–164.

(19) Klemm, D.; Schumann, D.; Kramer, F.; Hebler, N.; Koth, D.; Sultanova, B. Nanocellulose materials - Different cellulose, different functionality. *Macromol. Symp.* **2009**, *280* (1), 60–71.

(20) Kalia, S.; Dufresne, A.; Cherian, B. M.; Kaith, B. S.; Avérous, L.; Njuguna, J.; Nassiopoulos, E. Cellulose-based bio- and nanocomposites: A review. *Int. J. Polym. Sci.* **2011**, 1–35.

(21) Petersen, N.; Gatenholm, P. Bacterial cellulose-based materials and medical devices: Current state and perspectives. *Appl. Microbiol. Biotechnol.* **2011**, *91* (5), 1277–1286.

(22) Eichhorn, S. J.; Dufresne, A.; Aranguren, M.; Marcovich, N. E.; Capadona, J. R.; Rowan, S. J.; Weder, C.; Thielemans, W.; Roman, M.; Renneckar, S.; et al. Review: current international research into cellulose nanofibres and nanocomposites. *J. Mater. Sci.* **2010**, *45* (1), 1–33.

(23) Iguchi, M.; Yamanaka, S.; Budhiono, A. Bacterial cellulose — a masterpiece of nature's arts. *J. Mater. Sci.* **2000**, *35*, 261–270.

(24) Yang, X.; Cranston, E. D. Chemically Cross-Linked Cellulose Nanocrystal Aerogels with Shape Recovery and Superabsorbent Properties. *Chem. Mater.* **2014**, *26* (20), 6016–6025.

(25) Yang, X.; Bakaic, E.; Hoare, T.; Cranston, E. D. Injectable polysaccharide hydrogels reinforced with cellulose nanocrystals: Morphology, rheology, degradation, and cytotoxicity. *Biomacromolecules* **2013**, *14* (12), 4447–4455.

(26) De France, K. J.; Chan, K. J. W.; Cranston, E. D.; Hoare, T. Enhanced Mechanical Properties in Cellulose Nanocrystal-Poly(oligoethylene glycol methacrylate) Injectable Nanocomposite Hydrogels through Control of Physical and Chemical Cross-Linking. *Biomacromolecules* **2016**, *17* (2), 649–660.

(27) Hubbe, M. A.; Rojas, O. J.; Lucia, L. A.; Sain, M. Cellulosic Nanocomposites: A Review. *BioResources* **2008**, *3* (3), 929–980.

(28) Shopsowitz, K. E.; Stahl, A.; Hamad, W. Y.; MacLachlan, M. J. Hard Templating of Nanocrystalline Titanium Dioxide with Chiral Nematic Ordering. *Angew. Chemie Int. Ed.* **2012**, *51* (28), 6886–6890.

(29) Kalashnikova, I.; Bizot, H.; Cathala, B.; Capron, I. Modulation of Cellulose Nanocrystals Amphiphilic Properties to Stabilize Oil/Water Interface. *Biomacromolecules* **2012**, *13* (1), 267–275.

(30) Mohanta, V.; Madras, G.; Patil, S. Layer-by-layer assembled thin films and microcapsules of nanocrystalline cellulose for hydrophobic drug delivery. *ACS Appl. Mater. Interfaces* **2014**, *6* (22), 20093–20101.

(31) Jorfi, M.; Foster, E. J. Recent advances in nanocellulose for biomedical applications. *J. Appl. Polym. Sci.* **2015**, *132* (14), 1–19.

(32) Jabbour, L.; Bongiovanni, R.; Chaussy, D.; Gerbaldi, C.; Beneventi, D. Cellulose-based Li-ion batteries: A review. *Cellulose* **2013**, *20* (4), 1523–1545.

(33) Yang, X.; Shi, K.; Zhitomirsky, I.; Cranston, E. D. Cellulose Nanocrystal Aerogels as Universal 3D Lightweight Substrates for Supercapacitor Materials. *Adv. Mater.* **2015**, *27* (40), 6104–6109.

(34) Belbekhouche, S.; Bras, J.; Siqueira, G.; Chappey, C.; Lebrun, L.; Khelifi, B.; Marais, S.; Dufresne, A. Water sorption behavior and gas barrier properties of cellulose whiskers and microfibrils films. *Carbohydr. Polym.* **2011**, *83* (4), 1740–

1748.

(35) Goetz, L.; Mathew, A.; Oksman, K.; Gatenholm, P.; Ragauskas, A. J. A novel nanocomposite film prepared from crosslinked cellulosic whiskers. *Carbohydr. Polym.* **2009**, *75* (1), 85–89.

(36) Kedzior, S. A.; Graham, L.; Moorlag, C.; Dooley, B. M.; Cranston, E. D. Poly(methyl methacrylate)-Grafted Cellulose Nanocrystals: One-step Synthesis, Nanocomposite Preparation, and Characterization. *Can. J. Chem. Eng.* **2016**, *94* (5), 811–822.

(37) Milanez, D. H.; Amaral, R. M. do; Faria, L. I. L. de; Gregolin, J. A. R. Assessing nanocellulose developments using science and technology indicators. *Mater. Res.* **2013**, *16* (3), 635–641.

(38) Zimmermann, T.; Bordeanu, N.; Strub, E. Properties of nanofibrillated cellulose from different raw materials and its reinforcement potential. *Carbohydr. Polym.* **2010**, *79* (4), 1086–1093.

(39) Nakagaito, A. N.; Yano, H. The effect of morphological changes from pulp fiber towards nano-scale fibrillated cellulose on the mechanical properties of high-strength plant fiber based composites. *Appl. Phys. A Mater. Sci. Process.* **2004**, *78* (4), 547–552.

(40) Boldizar, A.; Klason, C.; Kubát, J.; Näslund, P.; Sáha, P. Prehydrolyzed Cellulose as Reinforcing Filler for Thermoplastics. *Int. J. Polym. Mater.* **1987**, *11* (4), 229–262.

(41) Henriksson, M.; Henriksson, G.; Berglund, L. A.; Lindström, T. An environmentally friendly method for enzyme-assisted preparation of microfibrillated cellulose (MFC) nanofibers. *Eur. Polym. J.* **2007**, *43* (8), 3434–3441.

(42) Isogai, A.; Saito, T.; Fukuzumi, H. TEMPO-oxidized cellulose nanofibers. *Nanoscale* **2011**, *3* (1), 71–85.

(43) Son, H.-J.; Heo, M.-S.; Kim, Y.-G.; Lee, S.-J. Optimization of fermentation conditions for the production of bacterial cellulose by a newly isolated Acetobacter sp.A9 in shaking cultures. *Biotechnol. Appl. Biochem.* **2001**, *33* (1), 1.

(44) Ross, P.; Mayer, R.; Benziman, M. Cellulose Biosynthesis and Function in Bacteria. *Microbiol. Rev.* **1991**, *55* (1), 35–58.

(45) Mohite, B. V.; Patil, S. V. A novel biomaterial: bacterial cellulose and its new era applications. *Biotechnol. Appl. Biochem.* **2014**, *61* (2), 101–110.

(46) Huang, Y.; Zhu, C.; Yang, J.; Nie, Y.; Chen, C.; Sun, D. Recent advances in bacterial cellulose. *Cellulose* **2014**, *21* (1), 1–30.

(47) Lin, S. P.; Loira Calvar, I.; Catchmark, J. M.; Liu, J. R.; Demirci, A.; Cheng, K. C. Biosynthesis, production and applications of bacterial cellulose. *Cellulose* **2013**, *20* (5), 2191–2219.

(48) Nickerson, R. F.; Habrle, J. A. Cellulose Intercrystalline Structure. *Ind. Eng. Chem.* **1947**, *39* (11), 1507–1512.

(49) Rånby, B. G.; Banderet, A.; Sillén, L. G. Aqueous Colloidal Solutions of Cellulose Micelles. *Acta Chemica Scandinavica*. 1949, pp 649–650.

(50) Angle, M. N.; Dufresne, A. Plasticized Starch / Tunicin Whiskers Nanocomposite Materials. 2. Mechanical Behavior. *Macromolecules* **2001**, *34* (9), 2921–2931.

(51) Matos Ruiz, M.; Cavaillé, J. Y.; Dufresne, A.; Gérard, J. F.; Graillat, C. Processing

and characterization of new thermoset nanocomposites based on cellulose whiskers. *Compos. Interfaces* **2000**, *7* (2), 117–131.

(52) Beck-Candanedo, S.; Roman, M.; Gray, D. Effect of Conditions on the Properties Behavior of Wood Cellulose Nanocrystals Suspensions. *Biomacromolecules* **2005**, *6*, 1048–1054.

(53) Battista, O. A.; Coppick, S.; Howsmon, J. A.; Morehead, F. F.; Sisson, W. A. Level-Off Degree of Polymerization. *Ind. Eng. Chem.* **1956**, *48* (2), 333–335.

(54) Sharples, A. The hydrolysis of cellulose and its relation to structure. *Trans. Faraday Soc.* **1957**, *53*, 913–917.

(55) Håkansson, H.; Ahlgren, P. Acid hydrolysis of some industrial pulps: Effect of hydrolysis conditions and raw material. *Cellulose* **2005**, *12* (2), 177–183.

(56) Reid, M. S.; Villalobos, M.; Cranston, E. D. Benchmarking Cellulose Nanocrystals: From the Laboratory to Industrial Production. *Langmuir* **2017**, *33* (7), 1583–1598.

(57) Beck, S.; Bouchard, J.; Berry, R. Dispersibility in Water of Dried Nanocrystalline Cellulose. *Biomacromolecules* **2012**, *13* (5), 1486–1494.

(58) Beck, S.; Methot, M.; Bouchard, J. General procedure for determining cellulose nanocrystal sulfate half-ester content by conductometric titration. *Cellulose* **2015**, *22* (1), 101–116.

(59) Zhong, L.; Fu, S.; Peng, X.; Zhan, H.; Sun, R. Colloidal stability of negatively charged cellulose nanocrystalline in aqueous systems. *Carbohydr. Polym.* **2012**, *90* (1), 644–649.

(60) Araki, J. Electrostatic or steric? – preparations and characterizations of well-dispersed systems containing rod-like nanowhiskers of crystalline polysaccharides. *Soft Matter* **2013**, *9* (16), 4125.

(61) Jiang, F.; Esker, A. R.; Roman, M. Acid-catalyzed and solvolytic desulfation of H2SO 4-hydrolyzed cellulose nanocrystals. *Langmuir* **2010**, *26* (23), 17919–17925.

(62) Hasani, M.; Cranston, E. D.; Westman, G.; Gray, D. G. Cationic Surface Functionalization of Cellulose Nanocrystals. *Soft Matter* **2008**, *4* (11), 2238–2244.

(63) Kloser, E.; Gray, D. G. Surface Grafting of Cellulose Nanocrystals with Poly(ethylene oxide) in Aqueous Media. *Langmuir* **2010**, *26* (16), 13450–13456.

(64) Domingues, R. M. A.; Gomes, M. E.; Reis, R. L. The Potential of Cellulose Nanocrystals in Tissue Engineering Strategies. *Biomacromolecules* **2014**, *15* (7), 2327–2346.

(65) Beck, S.; Bouchard, J. Auto-catalyzed acidic desulfation of cellulose nanocrystals. *Nord. Pulp Pap. Res. J.* **2014**, *29* (1), 6–14.

(66) Kedzior, S. A.; Marway, H. S.; Cranston, E. D. Tailoring Cellulose Nanocrystal and Surfactant Behavior in Miniemulsion Polymerization. *Macromolecules* **2017**, *50* (7), 2645–2655.

(67) Camarero Espinosa, S.; Kuhnt, T.; Foster, E. J.; Weder, C. Isolation of Thermally Stable Cellulose Nanocrystals by Phosphoric Acid Hydrolysis. *Biomacromolecules* **2013**, *14* (4), 1223–1230.

(68) Lemke, C. H.; Dong, R. Y.; Michal, C. A.; Hamad, W. Y. New insights into nano-crystalline cellulose structure and morphology based on solid-state NMR. *Cellulose* **2012**, *19* (5), 1619–1629.

(69) Araki, J.; Wada, M.; Kuga, S.; Okano, T. Flow properties of microcrystalline

cellulose suspension prepared by acid treatment of native cellulose. *Colloids Surfaces A Physicochem. Eng. Asp.* **1998**, *142* (1), 75–82.

(70) Wu, Q.; Meng, Y.; Wang, S.; Li, Y.; Fu, S.; Ma, L.; Harper, D. Rheological behavior of cellulose nanocrystal suspension: Influence of concentration and aspect ratio. *J. Appl. Polym. Sci.* **2014**, *131* (15), 1–8.

(71) Kalashnikova, I.; Bizot, H.; Bertoncini, P.; Cathala, B.; Capron, I. Cellulosic Nanorods of Various Aspect Ratios for Oil in Water Pickering Emulsions. *Soft Matter* **2013**, *9* (3), 952–959.

(72) Rusli, R.; Shanmuganathan, K.; Rowan, S. J.; Weder, C.; Eichhorn, S. J. Stress transfer in cellulose nanowhisker composites - influence of whisker aspect ratio and surface charge. *Biomacromolecules* **2011**, *12* (4), 1363–1369.

(73) Revol, J. F. On the cross-sectional shape of cellulose crystallites in Valonia ventricosa. *Carbohydr. Polym.* **1982**, *2* (2), 123–134.

(74) Hanley, S. J.; Giasson, J.; Revol, J.; Gray, D. G. Atomic force microscopy of cellulose microfibrils: comparison with transmission electron microscopy. *Polymer (Guildf).* **1992**, *33* (21), 4639–4642.

(75) Favier, V.; Chanzy, H.; Cavaillé, J. Y. Polymer Nanocomposites Reinforced by Cellulose Whiskers. *Macromolecules* **1995**, *28* (18), 6365–6367.

(76) Terech, P.; Chazeau, L.; Cavaille, J. Y. Small-angle scattering study of cellulose whiskers in aqueous suspensions. *Macromolecules* **1999**, *32* (6), 1872–1875.

(77) Tokoh, C.; Takabe, K.; Fujita, M.; Saiki, H. Cellulose synthesized by Acetobacter xylinum in the presence of acetyl glucomannan. *Cellulose* **1998**, *5*, 249–261.

(78) Grunert, M.; Winter, W. T. Nanocomposites of cellulose acetate butyrate reinforced with cellulose nanocrystals. *J. Polym. Environ.* **2002**, *10* (1–2), 27–30.

(79) Fengel, D.; Wegener, G. *Wood: Chemistry, Ultrastructure, Reactions*; Water de Gruyter: New York, 1983.

(80) Viet, D.; Beck-Candanedo, S.; Gray, D. G. Dispersion of Cellulose Nanocrystals in Polar Organic Solvents. *Cellulose* **2007**, *14* (2), 109–113.

(81) Bhattacharjee, S. DLS and Zeta Potential - What They Are and What They Are Not? *J. Control. Release* **2016**, *235*, 337–351.

(82) Abitbol, T.; Kloser, E.; Gray, D. G. Estimation of the surface sulfur content of cellulose nanocrystals prepared by sulfuric acid hydrolysis. *Cellulose* **2013**, *20* (2), 785–794.

(83) Elazzouzi-Hafraoui, S.; Nishiyama, Y.; Putaux, J.; Heux, L.; Dubreuil, F.; Rochas, C. The Shape and Size Distribution of Crystalline Nanoparticles Prepared by Acid Hydrolysis of Native Cellulose. *Biomacromolecules* **2008**, *9* (1), 57–65.

(84) Agarwal, U. P.; Reiner, R. S.; Ralph, S. A. Cellulose I crystallinity determination using FT-Raman spectroscopy: Univariate and multivariate methods. *Cellulose* **2010**, *17* (4), 721–733.

(85) Driemeier, C.; Calligaris, G. A. Theoretical and experimental developments for accurate determination of crystallinity of cellulose I materials. *J. Appl. Crystallogr.* **2011**, *44* (1), 184–192.

(86) Ahvenainen, P.; Kontro, I.; Svedström, K. Comparison of sample crystallinity determination methods by X-ray diffraction for challenging cellulose I materials. *Cellulose* **2016**, *23* (2), 1073–1086.

(87) Habibi, Y. Key Advances in the Chemical Modification of Nanocelluloses. *Chem.*

Soc. Rev. **2014**, *43* (5), 1519–1542.

(88) Lin, N.; Huang, J.; Dufresne, A. Preparation, properties and applications of polysaccharide nanocrystals in advanced functional nanomaterials: a review. *Nanoscale* **2012**, *4* (11), 3274.

(89) Heux, L.; Chauve, G.; Bonini, C. Nonflocculating and chiral-nematic self-ordering of cellulose microcrystals suspensions in nonpolar solvents. *Langmuir* **2000**, *16* (21), 8210–8212.

(90) Bonini, C.; Heux, L.; Cavaillé, J. Y.; Lindner, P.; Dewhurst, C.; Terech, P. Rodlike cellulose whiskers coated with surfactant: A small-angle neutron scattering characterization. *Langmuir* **2002**, *18* (8), 3311–3314.

(91) Bondeson, D.; Oksman, K. Dispersion and characteristics of surfactant modified cellulose whiskers nanocomposites. *Compos. Interfaces* **2007**, *14* (7–9), 617–630.

(92) Kim, J.; Montero, G.; Habibi, Y.; Hinestroza, J. P.; Genzer, J.; Argyropoulos, D. S.; Rojas, O. J. Dispersion of cellulose crystallites by nonionic surfactants in a hydrophobic polymer matrix. *Polym. Eng. Sci.* **2009**, *49* (10), 2054–2061.

(93) Rojas, O. J.; Montero, G. A.; Habibi, Y. Electrospun nanocomposites from polystyrene loaded with cellulose nanowhiskers. *J. Appl. Polym. Sci.* **2009**, *113* (2), 927–935.

(94) Habibi, Y.; Hoeger, I.; Kelley, S. S.; Rojas, O. J. Development of Langmuir-Schaeffer Cellulose Nanocrystal Monolayers and Their Interfacial Behaviors. *Langmuir* **2010**, *26* (2), 990–1001.

(95) Dhar, N.; Au, D.; Berry, R. C.; Tam, K. C. Interactions of Nanocrystalline Cellulose with an Oppositely Charged Surfactant in Aqueous Medium. *Colloids Surfaces A Physicochem. Eng. Asp.* **2012**, *415*, 310–319.

(96) Brinatti, C.; Huang, J.; Berry, R. M.; Tam, K. C.; Loh, W. Structural and Energetic Studies on the Interaction of Cationic Surfactants and Cellulose Nanocrystals. *Langmuir* **2016**, *32* (3), 689–698.

(97) Salajkova, M.; Berglund, L. A.; Zhou, Q. Hydrophobic Cellulose Nanocrystals Modified with Quaternary Ammonium Salts. *J. Mater. Chem.* **2012**, *22* (37), 19798.

(98) Abitbol, T.; Marway, H.; Cranston, E. D. Surface Modification of Cellulose Nanocrystals with Cetyltrimethylammonium Bromide. *Nord. Pulp Pap. Res. J.* **2014**, *29* (1), 46–57.

(99) Kaboorani, A.; Riedl, B. Surface Modification of Cellulose Nanocrystals (CNC) by a Cationic Surfactant. *Ind. Crops Prod.* **2015**, *65*, 45–55.

(100) Padalkar, S.; Capadona, J. R.; Rowan, S. J.; Weder, C.; Moon, R. J.; Stanciu, L. A. Self-Assembly and Alignment of Semiconductor Nanoparticles on Cellulose Nanocrystals. *J. Mater. Sci.* **2011**, *46* (17), 5672–5679.

(101) Fortunati, E.; Armentano, I.; Zhou, Q.; Puglia, D.; Terenzi, A.; Berglund, L. A.; Kenny, J. M. Microstructure and Nonisothermal Cold Crystallization of PLA Composites Based on Silver Nanoparticles and Nanocrystalline Cellulose. *Polym. Degrad. Stab.* **2012**, *97* (10), 2027–2036.

(102) Fortunati, E.; Luzi, F.; Puglia, D.; Petrucci, R.; Kenny, J. M.; Torre, L. Processing of PLA Nanocomposites with Cellulose Nanocrystals Extracted from Posidonia Oceanica Waste: Innovative Reuse of Coastal Plant. *Ind. Crops Prod.* **2015**, *67*, 439–447.

(103) Arrieta, M. P.; Fortunati, E.; Dominici, F.; Rayón, E.; López, J.; Kenny, J. M. Multifunctional PLA-PHB/Cellulose Nanocrystal Films: Processing, Structural and Thermal Properties. *Carbohydr. Polym.* **2014**, *107* (1), 16–24.

(104) Arrieta, M. P.; Fortunati, E.; Dominici, F.; Rayón, E.; López, J.; Kenny, J. M. PLA-PHB/Cellulose Based Films: Mechanical, Barrier and Disintegration Properties. *Polym. Degrad. Stab.* **2014**, *107*, 139–149.

(105) Padalkar, S.; Capadona, J. R.; Rowan, S. J.; Weder, C.; Won, Y. H.; Stanciu, L. A.; Moon, R. J. Natural Biopolymers: Novel Templates for the Synthesis of Nanostructures. *Langmuir* **2010**, *26* (11), 8497–8502.

(106) Teipel, B. R.; Grunlan, J. Synergy in Epoxy Nanocomposites with Cellulose Nanocrystals and Boehmite. *Green Mater.* **2014**, *2* (4), 222–231.

(107) Jackson, J. K.; Letchford, K.; Wasserman, B. Z.; Ye, L.; Hamad, W. Y.; Burt, H. M. The Use of Nanocrystalline Cellulose for the Binding and Controlled Release of Drugs. *Int. J. Nanomedicine* **2011**, *6*, 321–330.

(108) Kaboorani, A.; Auclair, N.; Riedl, B.; Landry, V. Physical and Morphological Properties of UV-Cured Cellulose Nanocrystal (CNC) Based Nanocomposite Coatings for Wood Furniture. *Prog. Org. Coatings* **2016**, *93*, 17–22.

(109) Fortunati, E.; Mattioli, S.; Armentano, I.; Kenny, J. M. Spin Coated Cellulose Nanocrystal/Silver Nanoparticle Films. *Carbohydr. Polym.* **2014**, *113*, 394–402.

(110) Hu, Z.; Ballinger, S.; Pelton, R.; Cranston, E. D. Surfactant-Enhanced Cellulose Nanocrystal Pickering Emulsions. *J. Colloid Interface Sci.* **2015**, *439*, 139–148.

(111) Cranston, E. D.; Gray, D. G. Morphological and Optical Characterization of Polyelectrolyte Multilayers Incorporating Nanocrystalline Cellulose. *Biomacromolecules* **2006**, *7* (9), 2522–2530.

(112) Cranston, E. D.; Gray, D. G. Formation of cellulose-based electrostatic layer-by-layer films in a magnetic field. *Sci. Technol. Adv. Mater.* **2006**, *7* (4), 319–321.

(113) Cranston, E. D.; Gray, D. G. Birefringence in spin-coated films containing cellulose nanocrystals. *Colloids Surfaces A Physicochem. Eng. Asp.* **2008**, *325* (1–2), 44–51.

(114) Cranston, E. D.; Gray, D. G.; Rutland, M. W. Direct Surface Force Measurements of Polyelectrolyte Multilayer Films Containing Nanocrystalline Cellulose. *Langmuir* **2010**, *26* (22), 17190–17197.

(115) Gill, U.; Sutherland, T.; Himbert, S.; Zhu, Y.; Rheinstädter, M. C.; Cranston, E. D.; Moran-Mirabal, J. M. Beyond buckling: humidity-independent measurement of the mechanical properties of green nanobiocomposite films. *Nanoscale* **2017**, *9* (23), 7781–7790.

(116) Zhou, Q.; Brumer, H.; Teeri, T. T. Self-Organization of Cellulose Nanocrystals Adsorbed with Xyloglucan Oligosaccharide-Poly(ethylene glycol)-Polystyrene Triblock Copolymer. *Macromolecules* **2009**, *42* (15), 5430–5432.

(117) Lee, K. Y.; Tang, M.; Williams, C. K.; Bismarck, A. Carbohydrate derived copoly(lactide) as the compatibilizer for bacterial cellulose reinforced polylactide nanocomposites. *Compos. Sci. Technol.* **2012**, *72* (14), 1646–1650.

(118) Zhou, Q.; Malm, E.; Nilsson, H.; Larsson, P. T.; Iversen, T.; Berglund, L. a.; Bulone, V. Nanostructured biocomposites based on bacterial cellulosic nanofibers compartmentalized by a soft hydroxyethylcellulose matrix coating. *Soft Matter* **2009**, *5* (21), 4124.

(119) Hu, Z.; Cranston, E. D.; Ng, R.; Pelton, R. Tuning Cellulose Nanocrystal Gelation with Polysaccharides and Surfactants. *Langmuir* **2014**, *30* (10), 2684–2692.

(120) Nagalakshmaiah, M.; Pignon, F.; El Kissi, N.; Dufresne, A. Surface adsorption of triblock copolymer (PEO–PPO–PEO) on cellulose nanocrystals and their melt extrusion with polyethylene. *RSC Adv.* **2016**, *6* (70), 66224–66232.

(121) Hu, Z.; Patten, T.; Pelton, R.; Cranston, E. D. Synergistic Stabilization of Emulsions and Emulsion Gels with Water-Soluble Polymers and Cellulose Nanocrystals. *ACS Sustain. Chem. Eng.* **2015**, *3* (5), 1023–1031.

(122) Hu, Z.; Marway, H. S.; Kasem, H.; Pelton, R.; Cranston, E. D. Dried and Redispersible Cellulose Nanocrystal Pickering Emulsions. *ACS Macro Lett.* **2016**, *5* (2), 185–189.

(123) Kedzior, S. A.; Dubé, M. A.; Cranston, E. D. Cellulose Nanocrystals and Methyl Cellulose as Co-stabilizers for Nanocomposite Latexes with Double Morphology. *Submitt. to ACS Sustain. Chem. Eng.* **2017**.

(124) Araki, J.; Wada, M.; Kuga, S. Steric Stabilization of a Cellulose Microcrystal Suspension by Poly(ethylene glycol) Grafting Steric Stabilization of a Cellulose Microcrystal Suspension by Poly (ethylene glycol) Grafting. *Cellulose* **2001**, No. 17, 21–27.

(125) Okita, Y.; Fujisawa, S.; Saito, T.; Isogai, A. TEMPO-oxidized cellulose nanofibrils dispersed in organic solvents. *Biomacromolecules* **2011**, *12* (2), 518–522.

(126) Abitbol, T.; Marway, H. S.; Kedzior, S. A.; Yang, X.; Franey, A.; Gray, D. G.; Cranston, E. D. Hybrid fluorescent nanoparticles from quantum dots coupled to cellulose nanocrystals. *Cellulose* **2017**, *24* (3), 1287–1293.

(127) Morandi, G.; Thielemans, W. Synthesis of Cellulose Nanocrystals Bearing Photocleavable Grafts by ATRP. *Polym. Chem.* **2012**, *3* (6), 1402–1407.

(128) Ljungberg, N.; Bonini, C.; Bortolussi, F.; Boisson, C.; Heux, L.; Cavaillé, J. Y. New nanocomposite materials reinforced with cellulose whiskers in atactic polypropylene: Effect of surface and dispersion characteristics. *Biomacromolecules* **2005**, *6* (5), 2732–2739.

(129) Kloser, E.; Gray, D. G. Surface grafting of cellulose nanocrystals with poly(ethylene oxide) in aqueous media. *Langmuir* **2010**, *26* (16), 13450–13456.

(130) Li, Z. Q.; Zhou, X. D.; Pei, C. H. Synthesis of PLA-co-PGMA Copolymer and its Application in the Surface Modification of Bacterial Cellulose. *Int. J. Polym. Mater.* **2010**, *59* (9), 725–737.

(131) Habibi, Y.; Dufresne, A. Highly filled bionanocomposites from functionalized polysaccharide nanocrystals. *Biomacromolecules* **2008**, *9* (7), 1974–1980.

(132) Rosilo, H.; Kontturi, E.; Seitsonen, J.; Kolehmainen, E.; Ikkala, O. Transition to Reinforced State by Percolating Domains of Intercalated Brush-Modified Cellulose Nanocrystals and Poly(butadiene) in Cross-Linked Composites Based on Thiol–ene Click Chemistry. *Biomacromolecules* **2013**, *14* (5), 1547–1554.

(133) Morandi, G.; Heath, L.; Thielemans, W. Cellulose Nanocrystals Grafted with Polystyrene Chains Through Surface-Initiated Atom Transfer Radical Polymerization (SI-ATRP). *Langmuir* **2009**, *25* (14), 8280–8286.

(134) Zoppe, J. O.; Habibi, Y.; Rojas, O. J.; Venditti, R. A.; Johansson, L. S.; Efimenko, K.; Österberg, M.; Laine, J. Poly(N-isopropylacrylamide) Brushes Grafted from Cellulose Nanocrystals via Surface-Initiated Single-Electron Transfer Living

Radical Polymerization. *Biomacromolecules* **2010**, *11* (10), 2683–2691.
(135) Misra, B. N.; Chandel, P. S. Grafting onto wool. I. Ceric ion-initiated grafting of poly(methyl acrylate) onto wool. *J. Polym. Sci. Polym. Chem. Ed.* **1977**, *15* (7), 1545–1548.
(136) Schwab, E.; Stannett, V.; Rakowitz, D.; Magrane, J. Paper grafted with vinyl monomers using the ceric ion method. *TAPPI J.* **1962**, No. 45, 390–400.
(137) McDowall, D. J.; Gupta, B. S.; Stannett, V. T. Grafting of vinyl monomers to cellulose by ceric ion initiation. *Prog. Polym. Sci.* **1984**, *10* (1), 1–50.
(138) Arthur, J. C.; Baugh, P. J.; Hinojosa, O. ESR study of reactions of cellulose initiated by the ceric ion method. *J. Appl. Polym. Sci.* **1966**, *10* (10), 1591–1606.
(139) Gupta, K. C.; Sahoo, S. Graft copolymerization of acrylonitrile and ethyl methacrylate comonomers on cellulose using ceric ions. *Biomacromolecules* **2001**, *2* (1), 239–247.
(140) Gupta, K. C.; Khandekar, K. Graft copolymerization of acrylamide-methylacrylate comonomers onto cellulose using ceric ammonium nitrate. *J. Appl. Polym. Sci.* **2002**, *86* (10), 2631–2642.
(141) Gupta, K. C.; Sahoo, S.; Khandekar, K. Graft Copolymerization of Ethyl Acrylate onto Cellulose Using Ceric Ammonium Nitrate as Initiator in Aqueous Medium. *Biomacromolecules* **2002**, *3* (5), 1087–1094.
(142) Gupta, K. C.; Khandekar, K. Temperature-responsive cellulose by ceric(IV) ion-initiated graft copolymerization of N-isopropylacrylamide. *Biomacromolecules* **2003**, *4* (3), 758–765.
(143) Littunen, K.; Hippi, U.; Saarinen, T.; Seppälä, J. Network formation of nanofibrillated cellulose in solution blended poly(methyl methacrylate) composites. *Carbohydr. Polym.* **2013**, *91* (1), 183–190.
(144) Hamad, W.; Su, S. Thermoplastic nanocomposite material based on nanocrystalline cellulose (NCC). 110201755, 2013.
(145) Kan, K. H. M.; Li, J.; Wijesekera, K.; Cranston, E. D. Polymer-Grafted Cellulose Nanocrystals as pH-Responsive Reversible Flocculants. *Biomacromolecules* **2013**, *14* (9), 3130–3139.
(146) Kedzior, S. A.; Graham, L.; Moorlag, C.; Dooley, B. M.; Cranston, E. D. Poly(methyl methacrylate)-Grafted Cellulose Nanocrystals: One-step Synthesis, Nanocomposite Preparation, and Characterization. *Can. J. Chem. Eng.* **2016**, *94* (5), 811–822.
(147) Zhou, C.; Wu, Q.; Yue, Y.; Zhang, Q. Application of Rod-Shaped Cellulose Nanocrystals in Polyacrylamide Hydrogels. *J. Colloid Interface Sci.* **2011**, *353* (1), 116–123.
(148) Zhou, C.; Wu, Q.; Zhang, Q. Dynamic Rheology Studies of in situ Polymerization Process of Polyacrylamide-Cellulose Nanocrystal Composite Hydrogels. *Colloid Polym. Sci.* **2011**, *289* (3), 247–255.
(149) Yang, J.; Han, C.-R.; Duan, J.-F.; Ma, M.-G.; Zhang, X.-M.; Xu, F.; Sun, R.-C.; Xie, X.-M. Studies on the Properties and Formation Mechanism of Flexible Nanocomposite Hydrogels from Cellulose Nanocrystals and Poly(acrylic acid). *J. Mater. Chem.* **2012**, *22* (42), 22467–22480.
(150) Habibi, Y.; Goffin, A.-L.; Schiltz, N.; Duquesne, E.; Dubois, P.; Dufresne, A. Bionanocomposites Based on Poly(ε-caprolactone)-Grafted Cellulose Nanocrystals

by Ring-Opening Polymerization. *J. Mater. Chem.* **2008**, *18* (41), 5002.

(151) Goffin, A.-L.; Raquez, J.-M.; Duquesne, E.; Siqueira, G.; Habibi, Y.; Dufresne, A.; Dubois, P. Poly(ε-caprolactone) Based Nanocomposites Reinforced by Surface-Grafted Cellulose Nanowhiskers via Extrusion Processing: Morphology, Rheology, and Thermo-Mechanical Properties. *Polymer (Guildf).* **2011**, *52* (7), 1532–1538.

(152) Chen, G.; Dufresne, A.; Huang, J.; Chang, P. R. A Novel Thermoformable Bionanocomposite Based on Cellulose Nanocrystal-graft-Poly(ε -caprolactone). *Macromol. Mater. Eng.* **2009**, *294* (1), 59–67.

(153) Lin, N.; Chen, G.; Huang, J.; Dufresne, A.; Chang, P. R. Effects of Polymer-Grafted Natural Nanocrystals on the Structure and Mechanical Properties of Poly(lactic acid): A Case of Cellulose Whisker-Graft-Polycaprolactone. *J. Appl. Polym. Sci.* **2009**, *113* (5), 3417–3425.

(154) Labet, M.; Thielemans, W. Citric Acid as a Benign Alternative to Metal Catalysts for the Production of Cellulose-Grafted-Polycaprolactone Copolymers. *Polym. Chem.* **2012**, *3* (3), 679.

(155) Goffin, A.-L.; Raquez, J.-M.; Duquesne, E.; Siqueira, G.; Habibi, Y.; Dufresne, A.; Dubois, P. From Interfacial Ring-Opening Polymerization to Melt Processing of Cellulose Nanowhisker-Filled Polylactide-Based Nanocomposites. *Biomacromolecules* **2011**, *12* (7), 2456–2465.

(156) Braun, B.; Dorgan, J. R.; Hollingsworth, L. O. Supra-Molecular EcoBioNanocomposites Based on Polylactide and Cellulosic Nanowhiskers: Synthesis and Properties. *Biomacromolecules* **2012**, *13* (7), 2013–2019.

(157) Braunecker, W. A.; Matyjaszewski, K. Controlled/living radical polymerization: Features, developments, and perspectives. *Prog. Polym. Sci.* **2007**, *32* (1), 93–146.

(158) Barbey, R.; Lavanant, L.; Paripovic, D.; Schüwer, N.; Sugnaux, C.; Tugulu, S.; Klok, H. Polymer Brushes via Surface-Initiated Controlled Radical Polymerization: Synthesis, Characterization, Properties, and Applications. *Chem. Rev.* **2009**, *109* (11), 5437–5527.

(159) Roeder, R. D.; Garcia-Valdez, O.; Whitney, R. A.; Champagne, P.; Cunningham, M. F. Graft Modification of Cellulose Nanocrystals via Nitroxide-Mediated Polymerisation. *Polym. Chem.* **2016**, *7* (41), 6383–6390.

(160) Wang, J.-S.; Matyjaszewski, K. Controlled/"living" radical polymerization. atom transfer radical polymerization in the presence of transition-metal complexes. *J. Am. Chem. Soc.* **1995**, *117* (20), 5614–5615.

(161) Patten, T. E.; Matyjaszewski, K. Atom Transfer Radical Polymerization and the Synthesis of Polymeric Materials. *Adv. Mater.* **1998**, *10* (12), 901–915.

(162) Matyjaszewski, K. Transition Metal Catalysis in Controlled Radical Polymerization : Atom Transfer Radical Polymerization. *Chem. Eur. J.* **1999**, *5* (11), 3095–3102.

(163) Matyjaszewski, K.; Xia, J. Atom Transfer Radical Polymerization. *Chem. Rev.* **2001**, *101* (9), 2921–2990.

(164) Rosen, B. M.; Percec, V. Single-electron transfer and single-electron transfer degenerative chain transfer living radical polymerization. *Chem. Rev.* **2009**, *109* (11), 5069–5119.

(165) Tasdelen, M. A.; Uygun, M.; Yagci, Y. Photoinduced controlled radical

polymerization. *Macromol. Rapid Commun.* **2011**, *32* (1), 58–62.

(166) Anastasaki, A.; Nikolaou, V.; Zhang, Q.; Burns, J.; Samanta, S. R.; Waldron, C.; Haddleton, A. J.; McHale, R.; Fox, D.; Percec, V.; et al. Copper(II)/Tertiary Amine Synergy in Photoinduced Living Radical Polymerization: Accelerated Synthesis of ω-Functional and α,ω-Heterofunctional Poly(acrylates). *J. Am. Chem. Soc.* **2014**, *136* (3), 1141–1149.

(167) Anastasaki, A.; Nikolaou, V.; Simula, A.; Godfrey, J.; Li, M.; Nurumbetov, G.; Wilson, P.; Haddleton, D. M. Expanding the Scope of the Photoinduced Living Radical Polymerization of Acrylates in the Presence of CuBr2 and Me6-Tren. *Macromolecules* **2014**, *47* (12), 3852–3859.

(168) Anastasaki, A.; Nikolaou, V.; Pappas, G. S.; Zhang, Q.; Wan, C.; Wilson, P.; Davis, T. P.; Whittaker, M. R.; Haddleton, D. M. Photoinduced sequence-control via one pot living radical polymerization of acrylates. *Chem. Sci.* **2014**, *5* (9), 3536.

(169) Anastasaki, A.; Nikolaou, V.; McCaul, N. W.; Simula, A.; Godfrey, J.; Waldron, C.; Wilson, P.; Kempe, K.; Haddleton, D. M. Photoinduced synthesis of α,ω-telechelic sequence-controlled multiblock copolymers. *Macromolecules* **2015**, *48* (5), 1404–1411.

(170) Anastasaki, A.; Nikolaou, V.; Nurumbetov, G.; Truong, N. P.; Pappas, G. S.; Engelis, N. G.; Quinn, J. F.; Whittaker, M. R.; Davis, T. P.; Haddleton, D. M. Synthesis of Well-Defined Poly(acrylates) in Ionic Liquids via Copper(II)-Mediated Photoinduced Living Radical Polymerization. *Macromolecules* **2015**, *48* (15), 5140–5147.

(171) Hatton, F. L.; Kedzior, S. A.; Cranston, E. D.; Carlmark, A. Grafting-from Cellulose Nanocrystals via Photoinduced Cu-mediated Reversible-deactivation Radical Polymerization. *Carbohydr. Polym.* **2017**, *157*, 1033–1040.

(172) Carlmark, A.; Malmström, E. Atom Transfer Radical Polymerization from Cellulose Fibers at Ambient Temperature. *J. Am. Chem. Soc.* **2002**, *124* (6), 900–901.

(173) Yi, J.; Xu, Q.; Zhang, X.; Zhang, H. Chiral-Nematic Self-Ordering of Rodlike Cellulose Nanocrystals Grafted with Poly(styrene) in Both Thermotropic and Lyotropic States. *Polymer (Guildf).* **2008**, *49* (20), 4406–4412.

(174) Yin, Y.; Tian, X.; Jiang, X.; Wang, H.; Gao, W. Modification of Cellulose Nanocrystal via SI-ATRP of Styrene and the Mechanism of its Reinforcement of Polymethylmethacrylate. *Carbohydr. Polym.* **2016**, *142*, 206–212.

(175) Wang, H.-D.; Roeder, R. D.; Whitney, R. A.; Champagne, P.; Cunningham, M. F. Graft Modification of Crystalline Nanocellulose by Cu(0)-mediated SET Living Radical Polymerization. *J. Polym. Sci. Part A Polym. Chem.* **2015**, *53* (24), 2800–2808.

(176) Boujemaoui, A.; Mongkhontreerat, S.; Malmström, E.; Carlmark, A. Preparation and Characterization of Functionalized Cellulose Nanocrystals. *Carbohydr. Polym.* **2015**, *115*, 457–464.

(177) Rosilo, H.; McKee, J. R.; Kontturi, E.; Koho, T.; Hytönen, V. P.; Ikkala, O.; Kostiainen, M. A. Cationic Polymer Brush-Modified Cellulose Nanocrystals for High-Affinity Virus Binding. *Nanoscale* **2014**, *6* (20), 11871–11881.

(178) Yi, J.; Xu, Q.; Zhang, X.; Zhang, H. Temperature-Induced Chiral Nematic Phase Changes of Suspensions of Poly(N,N-dimethylaminoethyl methacrylate)-Grafted

Cellulose Nanocrystals. *Cellulose* **2009**, *16* (6), 989–997.

(179) Arredondo, J.; Jessop, P. G.; Champagne, P.; Bouchard, J.; Cunningham, M. F. Synthesis of Carbon Dioxide Responsive Cellulose Nanocrystals by Surface-Initiated Cu(0)-Mediated Polymerisation. *Green Chem.* **2017**.

(180) Hemraz, U. D.; Lu, A.; Sunasee, R.; Boluk, Y. Structure of Poly(N-isopropylacrylamide) Brushes and Steric Stability of Their Grafted Cellulose Nanocrystal Dispersions. *J. Colloid Interface Sci.* **2014**, *430*, 157–165.

(181) Zoppe, J. O.; Dupire, A. V. M.; Lachat, T. G. G.; Lemal, P.; Rodriguez-Lorenzo, L.; Petri-Fink, A.; Weder, C.; Klok, H. Cellulose Nanocrystals with Tethered Polymer Chains: Chemically Patchy versus Uniform Decoration. *ACS Macro Lett.* **2017**, 892–897.

(182) Wu, W.; Huang, F.; Pan, S.; Mu, W.; Meng, X.; Yang, H.; Xu, Z.; Ragauskas, A. J.; Deng, Y. Thermo-Responsive and Fluorescent Cellulose Nanocrystals Grafted with Polymer Brushes. *J. Mater. Chem. A* **2015**, *3* (5), 1995–2005.

(183) Zoppe, J. O.; Xu, X.; Känel, C.; Orsolini, P.; Siqueira, G.; Tingaut, P.; Zimmermann, T.; Klok, H.-A. Effect of Surface Charge on Surface-Initiated Atom Transfer Radical Polymerization from Cellulose Nanocrystals in Aqueous Media. *Biomacromolecules* **2016**, *17*, 1404–1413.

(184) Hemraz, U. D.; Campbell, K. A.; Burdick, J. S.; Ckless, K.; Boluk, Y.; Sunasee, R. Cationic Poly(2-aminoethylmethacrylate) and Poly(N-(2-aminoethylmethacrylamide) Modified Cellulose Nanocrystals: Synthesis, Characterization, and Cytotoxicity. *Biomacromolecules* **2015**, *16*, 319–325.

(185) Majoinen, J.; Walther, A.; McKee, J. R.; Kontturi, E.; Aseyev, V.; Malho, J. M.; Ruokolainen, J.; Ikkala, O. Polyelectrolyte Brushes Grafted from Cellulose Nanocrystals using Cu-mediated Surface-Initiated Controlled Radical Polymerization. *Biomacromolecules* **2011**, *12* (8), 2997–3006.

(186) Xu, Q.; Yi, J.; Zhang, X.; Zhang, H. A Novel Amphotropic Polymer Based on Cellulose Nanocrystals Grafted with Azo Polymers. *Eur. Polym. J.* **2008**, *44* (9), 2830–2837.

(187) Yu, J.; Wang, C.; Wang, J.; Chu, F. In Situ Development of Self-reinforced Cellulose Nanocrystals Based Thermoplastic Elastomers by Atom Transfer Radical Polymerization. *Carbohydr. Polym.* **2016**, *141*, 143–150.

(188) Zhang, X.; Zhang, J.; Dong, L.; Ren, S.; Wu, Q.; Lei, T. Thermoresponsive poly(poly(ethylene glycol) methylacrylate)s grafted cellulose nanocrystals through SI-ATRP polymerization. *Cellulose* **2017**.

(189) Eyley, S.; Thielemans, W. Surface Modification of Cellulose Nanocrystals. *Nanoscale* **2014**, *6*, 7764–7779.

(190) Dorris, G. M.; Gray, D. G. The surface analysis of paper and wood fibers by ESCA - electron spectroscopy for chemical analysis I. Applications to cellulose and lignin. *Cellul. Chem. Technol.* **1978**, *12*, 9–23.

(191) Johansson, L. S.; Campbell, J. M. Reproducible XPS on biopolymers: Cellulose studies. *Surf. Interface Anal.* **2004**, *36* (8), 1018–1022.

(192) Roman, M.; Winter, W. T. Effect of sulfate groups from sulfuric acid hydrolysis on the thermal degradation behavior of bacterial cellulose. *Biomacromolecules* **2004**, *5* (5), 1671–1677.

(193) Angell, C. A.; Ngai, K. L.; McKenna, G. B.; McMillan, P. F.; Martin, S. W.

Relaxation in glassforming liquids and amorphous solids. *J. Appl. Phys.* **2000**, *88* (6), 3113–3157.

(194) Wang, J.; Siqueira, G.; Müller, G.; Rentsch, D.; Huch, A.; Tingaut, P.; Levalois-Grützmacher, J.; Grützmacher, H. Synthesis of new bis(acyl)phosphane oxide photoinitiators for the surface functionalization of cellulose nanocrystals. *Chem. Commun.* **2016**, *52* (13), 2823–2826.

(195) VanderHart, D. L.; Atalla, R. H. Studies of microstructure in native celluloses using solid-state carbon-13 NMR. *Macromolecules* **1984**, *17* (8), 1465–1472.

(196) Earl, W. L.; VanderHart, D. L. High Resolution, Magic Angle Sample Spinning 13C NMR of Solid Cellulose I. *J. Am. Chem. Soc.* **1980**, *102* (9), 3251–3252.

(197) Heux, L.; Dinand, E.; Vignon, M. R. Structural aspects in ultrathin cellulose microfibrils followed by 13C CP-MAS NMR. *Carbohydr. Polym.* **1999**, *40* (2), 115–124.

(198) Newman, R. H. Estimation of the lateral dimensions of cellulose crystallites using 13C NMR signal strengths. *Solid State Nucl. Magn. Reson.* **1999**, *15* (1), 21–29.

(199) Montanari, S.; Roumani, M.; Heux, L.; Vignon, M. R. Topochemistry of carboxylated cellulose nanocrystals resulting from TEMPO-mediated oxidation. *Macromolecules* **2005**, *38* (5), 1665–1671.

(200) Peng, S. X.; Chang, H.; Kumar, S.; Moon, R. J.; Youngblood, J. P. A comparative guide to controlled hydrophobization of cellulose nanocrystals via surface esterification. *Cellulose* **2016**, *23* (3), 1–22.

(201) Azzam, F.; Heux, L.; Putaux, J.-L.; Jean, B. Preparation By Grafting Onto, Characterization, and Properties of Thermally Responsive Polymer-Decorated Cellulose Nanocrystals. *Biomacromolecules* **2010**, *11* (12), 3652–3659.

(202) Gårdebjer, S.; Bergstrand, A.; Idström, A.; Börstell, C.; Naana, S.; Nordstierna, L.; Larsson, A. Solid-state NMR to quantify surface coverage and chain length of lactic acid modified cellulose nanocrystals, used as fillers in biodegradable composites. *Compos. Sci. Technol.* **2015**, *107*, 1–9.

(203) Bibette, J.; Leal-Calderon, F. Surfactant-stabilized emulsions. *Curr. Opin. Colloid Interface Sci.* **1996**, *1* (6), 746–751.

(204) Ramsden, W. Separation of Solids in the Surface-Layers of Solutions and Suspensions. *Proc. R. Soc. London* **1903**, *72*, 156–164.

(205) Pickering, S. U. The chemistry of bordeaux mixture. *J. Chem. Soc. Trans.* **1907**, *91*, 1988.

(206) Binks, B. P. Particles as surfactants - similarities and differences. *Curr. Opin. Colloid Interface Sci.* **2002**, *7*, 21–41.

(207) Binks, B. P.; Horozov, T. S. Aqueous Foams Stabilized Solely by Silica Nanoparticles. *Angew. Chemie* **2005**, *117*, 3788–3791.

(208) Aveyard, R.; Binks, B. P.; Clint, J. H. Emulsions stabilised solely by colloidal particles. *Adv. Colloid Interface Sci.* **2003**, *100–102*, 503–546.

(209) Wang, W.; Zhou, Z.; Nandakumar, K.; Xu, Z.; Masliyah, J. H. Effect of charged colloidal particles on adsorption of surfactants at oil-water interface. *J. Colloid Interface Sci.* **2004**, *274* (2), 625–630.

(210) Saleh, N.; Sarbu, T.; Sirk, K.; Lowry, Gregory, V.; Matyjaszewski, K.; Tilton, R. D. Oil-in-water Emulsions Stabilized by Highly Charged Polyelectrolyte-Grafted Silica Nanoparticles. *Langmuir* **2005**, *21* (22), 9873–9878.

(211) Vignati, E.; Piazza, R.; Lockhart, T. P. Pickering emulsions: Interfacial tension, colloidal layer morphology, and trapped-particle motion. *Langmuir* **2003**, *19* (17), 6650–6656.
(212) Binks, B. P.; Whitby, C. P. Nanoparticle silica-stabilised oil-in-water emulsions: Improving emulsion stability. *Colloids Surfaces A Physicochem. Eng. Asp.* **2005**, *253* (1–3), 105–115.
(213) Vignati, E.; Piazza, R.; Lockhart, T. P. Pickering Emulsions: Interfacial Tension, Colloidal Layer Morphology, and Trapped-Particle Motion. *Langmuir* **2003**, *19* (17), 6650–6656.
(214) Binks, B. P.; Lumsdon, S. O. Pickering emulsions stabilized by monodisperse latex particles: effects of particle size. *Langmuir* **2001**, *17* (7), 4540–4547.
(215) Melle, S.; Lask, M.; Fuller, G. G. Pickering Emulsions with Controllable Stability. *Langmuir* **2005**, *21* (6), 2158–2162.
(216) Suzuki, D.; Tsuji, S.; Kawaguchi, H. Janus Microgels Prepared by Surfactant-Free Pickering Emulsion-Based Modification and Their Self-Assembly. *J. Am. Chem. Soc.* **2007**, *129* (26), 8088–8089.
(217) Ashby, N. P.; Binks, B. P. Pickering emulsions stabilised by Laponite clay particles. *Phys. Chem. Chem. Phys.* **2000**, *2* (24), 5640–5646.
(218) Kim, J.; Cote, L. J.; Kim, F.; Yuan, W.; Shull, K. .; J. Huang, J. Graphene Oxide Sheets at Interfaces. *J. Am. Chem. Soc.* **2010**, *132* (14), 8180–8186.
(219) Tzoumaki, M. V.; Moschakis, T.; Kiosseoglou, V.; Biliaderis, C. G. Oil-in-water emulsions stabilized by chitin nanocrystal particles. *Food Hydrocoll.* **2011**, *25* (6), 1521–1529.
(220) Kalashnikova, I.; Bizot, H.; Cathala, B.; Capron, I. New Pickering Emulsions Stabilized by Bacterial Cellulose Nanocrystals. *Langmuir* **2011**, *27* (12), 7471–7479.
(221) De Folter, J. W. J.; Hutter, E. M.; Castillo, S. I. R.; Klop, K. E.; Philipse, A. P.; Kegel, W. K. Particle shape anisotropy in pickering emulsions: Cubes and peanuts. *Langmuir* **2014**, *30* (4), 955–964.
(222) Zhang, J.; Pelton, R. Poly(N-isopropylacrylamide) Microgels at the Air−Water Interface. *Langmuir* **1999**, *15* (23), 8032–8036.
(223) Cathala, B.; Capron, I.; Bizot, H.; Buleon, A.; Kalashnikova, I. Composition in the form of an emulsion, comprising a hydrophobic phase dispersed in an aqueous phase, 2013.
(224) Capron, I.; Cathala, B. Surfactant-Free High Internal Phase Emulsions Stabilized by Cellulose Nanocrystals. *Biomacromolecules* **2013**, *14* (2), 291–296.
(225) Peddireddy, K. R.; Nicolai, T.; Benyahia, L.; Capron, I. Stabilization of Water-in-Water Emulsions by Nanorods. *ACS Macro Lett.* **2016**, *5* (3), 283–286.
(226) Cherhal, F.; Cousin, F.; Capron, I. Structural Description of the Interface of Pickering Emulsions Stabilized by Cellulose Nanocrystals. *Biomacromolecules* **2016**, *17* (2), 496–502.
(227) Zoppe, J. O.; Venditti, R. A.; Rojas, O. J. Pickering Emulsions Stabilized by Cellulose Nanocrystals Grafted with Thermo-Responsive Polymer Brushes. *J. Colloid Interface Sci.* **2012**, *369* (1), 202–209.
(228) Tang, J.; Lee, M. F. X.; Zhang, W.; Zhao, B.; Berry, R. M.; Tam, K. C. Dual Responsive Pickering Emulsion Stabilized by Poly[2-(dimethylamino) ethyl

methacrylate] Grafted Cellulose Nanocrystals. *Biomacromolecules* **2014**, *15* (8), 3052–3060.

(229) Tang, J.; Berry, R. M.; Tam, K. C. Stimuli-Responsive Cellulose Nanocrystals for Surfactant-Free Oil Harvesting. *Biomacromolecules* **2016**, *17* (5), 1748–1756.

(230) Nypelö, T.; Rodriguez-Abreu, C.; Kolen'ko, Y. V.; Rivas, J.; Rojas, O. J. Microbeads and Hollow Microcapsules Obtained by Self-Assembly of Pickering Magneto-Responsive Cellulose Nanocrystals. *ACS Appl. Mater. Interfaces* **2014**, *6* (19), 16851–16858.

(231) Low, L. E.; Tey, B. T.; Ong, B. H.; Chan, E. S.; Tang, S. Y. Palm Olein-in-Water Pickering Emulsion Stabilized by Fe3O4-Cellulose Nanocrystal Nanocomposites and Their Responses to pH. *Carbohydr. Polym.* **2017**, *155*, 391–399.

(232) Visanko, M.; Liimatainen, H.; Sirviö, J. A.; Heiskanen, J. P.; Niinimäki, J.; Hormi, O. Amphiphilic Cellulose Nanocrystals from Acid-Free Oxidative Treatment: Physicochemical Characteristics and Use as an Oil-Water Stabilizer. *Biomacromolecules* **2014**, *15* (7), 2769–2775.

(233) Cunha, A. G.; Mougel, J.-B.; Cathala, B.; Berglund, L. A.; Capron, I. Preparation of Double Pickering Emulsions Stabilized by Chemically Tailored Nanocelluloses. *Langmuir* **2014**, *30* (31), 9327–9335.

(234) Svagan, A. J.; Musyanovych, A.; Kappl, M.; Bernhardt, M.; Glasser, G.; Wohnhaas, C.; Berglund, L. A.; Risbo, J.; Landfester, K. Cellulose Nanofiber/Nanocrystal Reinforced Capsules: A Fast and Facile Approach Toward Assembly of Liquid-Core Capsules with High Mechanical Stability. *Biomacromolecules* **2014**, *15* (5), 1852–1859.

(235) Saidane, D.; Perrin, E.; Cherhal, F.; Guellec, F.; Capron, I. Some Modification of Cellulose Nanocrystals for Functional Pickering Emulsions. *Philos. Trans. R. Soc. A Math. Phys. Eng. Sci.* **2016**, *374* (2072), 1–11.

(236) Ojala, J.; Sirviö, J. A.; Liimatainen, H. Nanoparticle Emulsifiers Based on Bifunctionalized Cellulose Nanocrystals as Marine Diesel Oil-Water Emulsion Stabilizers. *Chem. Eng. J.* **2016**, *288*, 312–320.

(237) Sundberg, D. C.; Durant, Y. G. Latex Particle Morphology, Fundamental Aspects: A Review. *Polym. React. Eng.* **2003**, *11* (3), 379–432.

(238) Steward, P. A.; Hearn, J.; Wilkinson, M. C. An overview of polymer latex film formation and properties. *Adv. Colloid Interface Sci.* **2000**, *86* (3), 195–267.

(239) Chern, C. S. Emulsion polymerization mechanisms and kinetics. *Prog. Polym. Sci.* **2006**, *31* (5), 443–486.

(240) Verwey, E. J. W.; Overbeek, J. G. *Theory of the stability of lyophobic colloids*; Elsevier: New York, 1943.

(241) Asua, J. M. Miniemulsion Polymerization. *Prog. Polym. Sci.* **2002**, *27* (7), 1283–1346.

(242) Cunningham, M. F. Microsuspension Polymerization of Methyl Methacrylate. *Polym. React. Eng.* **1999**, *7* (2), 231–257.

(243) Yuan, H. G.; Kalfas, G.; Ray, W. H. Suspension Polymerization. *J. Macromol. Sci. Part C Polym. Rev.* **1991**, *31* (2–3), 215–299.

(244) Jovanović, R.; Ouzineb, K.; McKenna, T. F.; Dubé, M. A. Butyl acrylate/methyl methacrylate latexes: adhesive properties. *Macromol. Symp.* **2004**, *206* (1), 43–56.

(245) Jovanović, R.; Dubé, M. A. Emulsion-Based Pressure-Sensitive Adhesives: A

Review. *J. Macromol. Sci. Part C Polym. Rev.* **2004**, *44* (1), 1–51.

(246) Czech, Z.; MacIejewski, Z.; Kondratowicz-Maciejewska, K. Water-borne pressure-sensitive adhesives acrylics modified using amorphous silica nanoparticles. *Polish J. Chem. Technol.* **2016**, *18* (4), 124–128.

(247) Sardeh Moghadam, R.; Moghbeli, M. R. Effect of organoclay and chain-transfer agent on molecular parameters and adhesion performance of emulsion pressure-sensitive adhesives. *J. Adhes. Sci. Technol.* **2016**, *30* (3), 284–299.

(248) Li, H.; Yang, Y.; Yu, Y. Acrylic emulsion pressure-sensitive adhesives (PSAS). *J. Adhes. Sci. Technol.* **2004**, *18* (15), 1759–1770.

(249) Favier, V.; Canova, G. R.; Cavaillé, J. Y.; Chanzy, H.; Dufresne, A.; Gauthier, C. Nanocomposite materials from latex and cellulose whiskers. *Polym. Adv. Technol.* **1995**, *6* (5), 351–355.

(250) Elmabrouk, A. Ben; Thielemans, W.; Dufresne, A.; Boufi, S. Preparation of Poly(styrene-co-hexylacrylate)/Cellulose Whiskers Nanocomposites via Miniemulsion Polymerization. *J. Appl. Polym. Sci.* **2009**, *114* (5), 2946–2955.

(251) Mabrouk, A. Ben; Vilar, M. R.; Magnin, A.; Belgacem, M. N.; Boufi, S. Synthesis and Characterization of Cellulose Whiskers/Polymer Nanocomposite Dispersion by Mini-Emulsion Polymerization. *J. Colloid Interface Sci.* **2011**, *363* (1), 129–136.

(252) Geng, S.; Haque, M. M. U.; Oksman, K. Crosslinked Poly(vinyl acetate) (PVAc) Reinforced with Cellulose Nanocrystals (CNC): Structure and Mechanical Properties. *Compos. Sci. Technol.* **2016**, *126*, 35–42.

(253) Pracella, M.; Haque, M. M. U.; Puglia, D. Morphology and Properties Tuning of PLA/Cellulose Nanocrystals Bio-Nanocomposites by Means of Reactive Functionalization and Blending with PVAc. *Polymer (Guildf).* **2014**, *55* (16), 3720–3728.

(254) Dastjerdi, Z.; Cranston, E. D.; Dubé, M. A. Synthesis of Poly(n-butyl acrylate/methyl methacrylate)/CNC Latex Nanocomposites via In Situ Emulsion Polymerization. *Macromol. React. Eng.* **2017**, *201700013*, 1700013.

(255) Dastjerdi, Z.; Cranston, E. D.; Dubé, M. A. Adhesive Property Modification using Cellulose Nanocrystals. *Int. J. Adhes. Adhes.* **2017**, submitted.

Chapter 3

Poly(methyl methacrylate)-Grafted Cellulose Nanocrystals: One-step Synthesis, Nanocomposite Preparation, and Characterization.

The modification of cellulose nanocrystals with hydrophobic polymers is required for a number of applications but the modification methods available pose many challenges. CNCs have minimal colloidal stability in organic solvents, and therefore water-based modification routes are ideal. In this work, we have functionalized CNCs with PMMA in a one step, one pot, water-based free radical polymerization initiated using ceric ammonium nitrate. The PMMA-grafted CNCs were extensively characterized in order to determine the ratio of polymer to cellulose. PMMA nanocomposites were prepared via wet ball milling and melt mixing with unmodified and polymer-grafted CNCs. This work was one of the first comprehensive reports to include polymer grafting, characterization, and nanocomposite preparation and testing.

In this work, I prepared and characterized the PMMA-grafted CNCs and wrote the majority of the manuscript with editorial assistance from my supervisor, Dr. Emily Cranston. Lexa Graham (MASc student) carried out the nanocomposite preparation and testing with guidance from Dr. Carolyn Moorlag and Dr. Brynn Dooley at Xerox Research Centre of Canada. Dr. Tiffany Abitbol performed the AFM and technicians carried out the XPS, TGA, XRD, and solid state NMR as described in the acknowledgements. This chapter is reprinted as it appears in *The Canadian Journal of Chemical Engineering*, with permission from Wiley © 2016.

Poly(methyl methacrylate)-Grafted Cellulose Nanocrystals: One-step Synthesis, Nanocomposite Preparation, and Characterization
Stephanie A. Kedzior, Lexa Graham, Carolyn Moorlag, Brynn M. Dooley, and Emily D. Cranston
The Canadian Journal of Chemical Engineering, **2016**, *94* (5), pp 811-822
DOI: 10.1002/cjce.22456

POLY(METHYL METHACRYLATE)-GRAFTED CELLULOSE NANOCRYSTALS: ONE-STEP SYNTHESIS, NANOCOMPOSITE PREPARATION, AND CHARACTERIZATION

Stephanie A. Kedzior,[1] Lexa Graham,[1] Carolyn Moorlag,[2] Brynn M. Dooley[2] and Emily D. Cranston[1]*

1. Department of Chemical Engineering, McMaster University, 1280 Main St. West, Hamilton, ON, L8S 4L7, Canada

2. Xerox Research Centre of Canada, 2660 Speakman Drive, Mississauga, ON, L5K 2L1, Canada

Cellulose nanocrystals (CNCs) are ideal reinforcing agents for polymer nanocomposites because they are lightweight and nano-sized with a large aspect ratio and high elastic modulus. To overcome the poor compatibility of hydrophilic CNCs in non-polar composite matrices, we grafted poly(methyl methacrylate) (PMMA) from the surface of CNCs using an aqueous, one-pot, free radical polymerization method with ceric ammonium nitrate as the initiator. The hybrid nanoparticles were characterized by CP/MAS NMR, X-ray photoelectron spectroscopy, infrared spectroscopy, contact angle, thermogravimetric analysis, X-ray diffraction, and atomic force microscopy. Spectroscopy demonstrates that 0.11 g/g (11 wt %) PMMA is grafted from the CNC surface, giving PMMA-*g*-CNCs, which are similar in size and crystallinity to unmodified CNCs but have an onset of thermal degradation 45 °C lower. Nanocomposites were prepared by compounding unmodified CNCs and PMMA-*g*-CNCs (0.0025–0.02 g/g (0.25–2 wt %) loading) with PMMA using melt mixing and wet ball milling. CNCs improved the performance of melt-mixed nanocomposites at 0.02 g/g (2 wt %) loading compared to the PMMA control, while lower loadings of CNCs and all loadings of PMMA-*g*-CNCs did not. The difference in Young's modulus between unmodified CNC and polymer-grafted CNC composites was generally insignificant. Overall, ball-milled composites had inferior mechanical and rheological properties compared to melt-mixed composites. Scanning electron microscopy showed aggregation in the samples with CNCs, but more pronounced aggregation with PMMA-*g*-CNCs. Despite improving interfacial compatibility between the nanoparticles and the matrix, the effect of PMMA-*g*-CNC aggregation and decreased thermal stability dominated the composite performance.

Keywords: cellulose nanocrystals, ceric-initiated polymer grafting, poly(methyl methacrylate), melt compounding, ball milling

INTRODUCTION

Cellulose nanocrystals (CNCs) are nanoparticles derived from cellulose, the most abundant natural polymer in the world. CNCs have favourable material properties, including a specific Young's modulus comparable to Kevlar and steel, a high aspect ratio, a high crystallinity, and general biocompatibility.[1,2] As such, CNCs have great potential to replace inorganic or petrochemical-based nanoparticles as the load-bearing component in composites, both for traditional plastic composite applications and in specialty composites like gels, foams, coatings, and scaffolds.

The commercialization of CNCs has accelerated over the past five years and major programs for developing CNC products have begun in Canada, the United States, and Europe.[3] Aside from CNCs, other types of cellulosic nanomaterials also exist. Recent efforts to standardize terminology and test methods for cellulosic nanomaterials have been undertaken by the Canadian Standards Association, TAPPI, and the International Standards Organization. For further information, the reader is directed to a number of excellent reviews on CNCs[1,4] and cellulosic nanomaterials in general.[5–7]

CNCs are rigid, rod-like particles with widths of 5–10 nm and lengths from 50 nm to several micrometers, depending on the cellulose source.[5] They are typically extracted from plant, animal, or bacterial cellulose via controlled acid hydrolysis with sulphuric acid[1] which preferentially breaks down the more accessible disordered regions of the fibres into small polysaccharides and sugars. The remaining crystalline (or paracrystalline) portions of the cellulose can then be isolated by centrifugation and dialysis. Hydrolysis using sulphuric acid leaves anionic sulphate half-ester groups (i.e. sulphate groups connected to cellulose through one of their oxygens) on the surface of the CNCs, which provides colloidal stability in water.[8] While the CNCs used in this work were produced "in-house" from cotton, they are generally indistinguishable from those industrially produced by sulphuric acid hydrolysis of wood pulp, based on standard characterization of commercially-sourced CNCs undertaken in our lab (to be published in an upcoming "benchmarking" study).

Unfortunately, the high hydrophilicity and low thermal stability of CNCs can be problematic for preparing nanocomposites via high-temperature processing with hydrophobic polymers, such as by melt mixing. CNC hydrophilicity is attributed to the three hydroxyl groups on each glucose unit (and intermittent surface sulphate half-esters) which lead to reported water contact angles of 13–25°.[9] The onset of thermal degradation for CNCs is between 200–300 °C, depending on the heating rate and surface modification, and has been observed to decrease with increasing surface sulphation.[10] Impurities and small polysaccharides adsorbed to CNCs[11] may also reduce thermal stability and cause discolouration when subjected to heat. Both the hydrophilicity and thermal stability of nanocelluloses can be tuned through chemical or physical modification using small molecules, polymers, or surfactants.[13,14]

---

* *Author to whom correspondence may be addressed.*
E-mail address: ecranst@mcmaster.ca

Can. J. Chem. Eng. 94:811–822, 2016

DOI 10.1002/cjce.22456

Grafting polymers onto the surface of CNCs is a promising method to improve compatibility between CNCs and polymer matrices. This is possible with two strategies, namely "grafting to" with pre-synthesized polymers or "grafting from," as shown here. Habibi et al. were the first to report "grafting from" CNCs using caprolactone and a ring-opening polymerization technique.[14] Since then, controlled polymerization methods such as atom transfer radical polymerization (ATRP) have been extended from working with cellulose filter paper[14–16] to CNCs.[17–19] ATRP from the surface of filter paper,[14–16] wood,[20] or pulp fibres[21] is relatively straightforward, since the pre-polymerization step to attach the initiator can easily be done (and purified) in various solvents. However, when modifying CNCs with ATRP, initiator attachment involves lengthy solvent exchange steps and destabilization of CNC dispersions.[17–19] While ATRP allows for good control over grafting density and chain length, it is both costly and time-ineffective.

To overcome some of the setbacks of ATRP with CNCs, Boujemaoui et al. recently prepared initiator-functionalized CNCs in a single step by combining acid hydrolysis with Fischer esterification, which allows for CNCs with surface-bound initiators to be made during nanoparticle production.[22] They went on to graft poly(methyl methacrylate) (PMMA) from initiator-functionalized CNCs using ATRP in anisole.[22] When ATRP is used to graft from the CNCs, the length can be controlled by varying the reaction time or by using a sacrificial initiator to grow homopolymer alongside the polymer-grafted CNCs where the graft length is controlled by the ratio of the sacrificial initiator to the CNC surface hydroxyl groups. The latter approach allows for easy quantification, assuming the same kinetics of the free-forming polymer as the graft polymer, and in the former case, the grafts need to be cleaved off the surface in order to determine the graft length.[18] However, when grafting takes place directly from an activated carbon atom on the CNC surface, as shown here, there is no facile method to cleave polymer grafts or fully control the number of activated grafting sites.

In this work, we use ceric ammonium nitrate (CAN) to initiate radical polymerization directly from the cellulose backbone. CAN is a useful redox initiator for CNCs specifically because it is effective in water where CNCs are colloidally stable. CAN has been used to graft vinyl monomers from cellulose, starch, and poly(vinyl alcohol).[23–31] CAN was expected to work only in amorphous cellulose regions, implying that CNCs may be too crystalline for grafting to proceed. To the contrary, a recent patent presents the results of grafting MMA and vinyl acetate from CNCs using CAN.[31] Here, we also use MMA and CAN to modify CNCs, and our research group has reported using CAN to graft water-soluble poly(4-vinyl pyridine) and poly(N-isopropylacrylamide) from the surface of CNCs as well.[32,33] To the best of our knowledge, this is the first peer-reviewed description in the academic literature of this grafting method including the full experimental protocol and characterization of purified products. However, the disadvantage of this polymerization technique is the formation of homopolymer alongside grafted CNCs, whereas ATRP is restricted to graft polymerization only and does not require removing homopolymer after the reaction. Despite this setback, this reaction can be considered more economically and industrially feasible than ATRP since it is a one-step, water-based reaction that does not require tedious steps to modify CNCs with initiators or linkers.

To date, CNCs have been successfully used as reinforcing agents in some hydrosoluble polymer matrices,[34–36] and a few hydrophobic polymers. However, using CNCs in commodity polymers such as polyethylene[36] and PMMA[37–41] has been more challenging. PMMA is a relatively common thermoplastic used as a glass substitute due to its optical transparency, thermal stability, low density, and high impact strength.[42,43] Furthermore, PMMA is easily melt-processed and is relatively low cost, leading to a number of nanocomposite examples with clays,[42,43] carbon nanotubes (CNT),[44–47] and inorganic crystals.[46] In 2010, Liu et al.[40] were the first to report PMMA/CNC composites by sonicating up to 0.1 g/g (10 wt %) CNCs and PMMA in DMF and preparing films by solvent casting. Since then, Sain and colleagues[37,48–52] prepared similar nanocomposites using in situ suspension polymerization of PMMA in the presence of CNCs and ex situ dispersion techniques, followed by solvent casting (from chloroform). Generally, they report a weak interface between CNCs and PMMA but a small increase in T_g of the composites and improved mechanical properties at high temperatures, similar to Kiziltas et al. whose solvent cast composites from acetone.[51] When CNCs were grafted with maleic anhydride to improve interfacial compatibility,[52,54] or MMA was pre-mixed with CNCs and heated,[37] no significant improvement in composite properties was observed. More recently, electrospun fibre composites of PMMA and CNCs in DMF have been prepared with up to 0.4 g/g (40 wt %) CNCs, showing improved mechanical properties only above a 0.17 g/g (17 wt %) loading.[38] As such, most prior work uses simple mixing or sonication to combine CNCs and PMMA in organic solvents, which implies some CNC aggregation and unstable mixtures, and focuses on solvent casting as a fabrication technique.

Herein we compare CNCs and PMMA-grafted CNCs (PMMA-*g*-CNCs) in PMMA nanocomposites prepared through melt mixing and wet ball milling. The work spans all stages of preparing nanocomposites from CNC production, surface modification, and characterization, through nanocomposite compounding, sample fabrication, and final composite testing. Characterization includes spectroscopy, microscopy, thermal analysis, crystallinity, contact angle, rheology, and mechanical testing of starting materials and composites. No previous report of wet ball milling CNC composites has been presented as this method is generally reserved for ceramic composites, pharmaceutical solids, metallurgy, and cement.[52–55] However, it has advantages for CNCs because it can be done at ambient temperatures using a range of liquids.[56]

EXPERIMENTAL

Materials

Ceric ammonium nitrate (CAN; also called diammonium cerium-(IV) nitrate), sodium chloride, inhibitor removers, poly(methyl methacrylate) (PMMA, $M_w = 120\,000$ g/mol), and methyl methacrylate (MMA) were purchased from Sigma-Aldrich. Nitric acid (0.7 g/g (70 wt %)) was obtained from EMD Chemicals, polyallylamine hydrochloride (PAH, $M_w = 120\,000–200\,000$ g/mol) was purchased from Polysciences Inc., sulphuric acid (0.96 ± 0.0015 g/g (96 ± 0.15 wt %)) was purchased from Fischer Scientific, and sodium hydroxide (0.1 mol/L) and hydrochloric acid (0.1 mol/L) were purchased from LabChem Inc.

Error Calculations

Unless otherwise stated, error bars are confidence intervals calculated from the standard deviation (S_x) of repeated measurements (N) i.e. $\Delta x = S_x \times t\text{-value}/(N)^{1/2}$, where the *t*-value is the Student's *t*-distribution at a confidence level of 95 % for *N*–1 degrees of freedom.

Preparation of Cellulose Nanocrystals

Suspensions of CNCs were prepared by sulphuric acid hydrolysis as described previously.[57] Forty grams of cotton filter aid (Whatman ashless filter aid, GE Healthcare, Canada) were treated with sulphuric acid (700 mL, 0.64 g/g (64 wt %)) at 45 °C for 45 min with mechanical stirring. Following hydrolysis, the suspension was diluted 10-fold with cold purified water (resistivity of 18.2 MΩ cm, Barnstead NANOpure Diamond system, Thermo Scientific) to quench the reaction. The resulting suspension was centrifuged repeatedly to concentrate the cellulose and remove excess acid and water. The suspension was then dialyzed against purified water until a constant neutral pH was achieved. The suspension was sonicated in an ice bath for 45 min (Sonifier 450, Branson Ultrasonics, Danbury, CT) at 60 % output. The final suspension was ~0.01 g/g (1 wt %) cellulose with a sulphur content of 0.55–0.71 % (depending on the batch), determined by conductometric titration with NaOH.[58]

Preparation of PMMA-*g*-CNCs

PMMA-*g*-CNCs were prepared in a similar way as described in the recent patent[31] using the following method: 40 mL of a 0.01 g/g (1 wt %) CNC suspension in water was added to a 50 mL three-neck round-bottom flask. MMA monomer was purified by passing it through an inhibitor column, and 1.17 mL purified MMA was added to the round-bottom flask along with 0.75 mL of 0.7 g/g (70 wt %) nitric acid. Constant N_2 gas flow facilitated de-oxygenation and maintained an inert N_2 blanket over the reaction, and the mixture was probe-sonicated at 60 % output in an ice bath. After 45 min of de-oxygenating, 143 mg CAN was dissolved in 1 mL of purified (but not de-oxygenated) water and added to the round-bottom flask. The resulting mixture was sonicated continuously for 2 h in an ice bath, then left stirring overnight at ambient temperature under N_2 atmosphere. Excess acid and PMMA homopolymer were removed by ultracentrifugation at 50 000 rpm twice. The supernatant was removed and the pellet was redistributed using sonication and filtered through a glass microfibre filter (Whatman Grade GF/B, VWR, USA) to remove any metal particles released from the sonicator probe. The product was then dialyzed against purified water. Additional cleaning involved filtering with an ultrafiltration stirred cell (Millipore solvent-resistant stirred cell with 76 mm ultrafiltration discs, EMD Millipore) first with water, then with acetone in order to remove the homopolymer. After 5 rinses with acetone, the suspension was removed from the stirred cell and solvent exchanged back to water to yield a 0.005 g/g (0.5 wt %) PMMA-*g*-CNC suspension, which was then stored in the refrigerator. Samples destined for ball milling were cleaned by ultrafiltration with methyl ethyl ketone (MEK) and stored in MEK for compounding, while PMMA-*g*-CNCs for melt mixing were freeze-dried from water at neutral pH.

Preparation of CAN-Oxidized CNCs

As a control, CNCs were oxidized with CAN using the same reaction profile as above, but without an MMA monomer. Oxidized CNCs were extensively purified by dialysis and ultrafiltration to remove residual CAN and any degraded polysaccharides.

Preparation of CNC/PMMA Nanocomposites

A series of composites with 0.0025, 0.005, 0.01, and 0.02 g/g (0.25, 0.5, 1, and 2 wt %) CNC loadings with respect to PMMA for ball-milled and melt-mixed PMMA-*g*-CNC/PMMA and CNC/PMMA nanocomposites were prepared, for a total of 16 samples. As a control, pure PMMA without nanocrystals was also melt-mixed and ball-milled under the same conditions.

Nanocomposites by wet ball milling

Freeze-dried CNCs were sonicated into MEK for 10 min, while PMMA-*g*-CNCs were never freeze-dried and were already present in MEK. The ball milling preparation method is the same for each set of samples: 0.01 g/g (1 wt %) solutions of CNCs and PMMA-*g*-CNCs in MEK were added to plastic Nalgene bottles with approximately 50 g PMMA and 250 mL MEK. Stainless steel milling media (0.8 mm diameter beads) were added to each container at approximately half the liquid volume. The mixture was processed by roll milling (175 rpm) for 24 h. The mixture was then filtered to remove milling media and poured into a large container to facilitate MEK evaporation inside the fume hood. Once evaporated, the solid composite was mechanically broken up using a household blender (BL10450HB, Black and Decker, USA), transferred into an open container, and put in a vacuum oven at 60 °C for one week to remove remaining MEK. Following this, the composite was melt-pressed at 160 °C, 3175.147 kg (Carver Benchtop Standard Auto Series, Carver Inc., USA) to remove any MEK and to obtain uniform films.

Nanocomposites by melt mixing

Freeze-dried CNCs and PMMA-*g*-CNCs were compounded with 50 g of PMMA. Samples were slowly added to a Haake melt mixer (Haake Rheomix, Thermo Scientific, USA) at 160 °C and allowed to mix for 10 min at 60 rpm. Following this, the composite was melt-pressed at 160 °C, 3175.147 kg (Carver Press) to obtain uniform films.

Characterization of Cellulose Nanocrystals and PMMA-*g*-CNCs

Fourier transform infrared spectroscopy (FTIR)

Freeze-dried CNCs and PMMA-*g*-CNCs were incorporated into KBr pellets at approximately 0.01 g/g (1 wt %), as was done for a neat PMMA sample. FTIR spectra were recorded in transmission mode on a Nicolet 6700 FT-IR spectrometer (Thermo Scientific) running a background of 32 scans and 64 sample scans with a resolution of 4 cm^{-1}.

Solid-state nuclear magnetic resonance spectroscopy (NMR)

Solid-state NMR spectra for freeze-dried CNCs and PMMA-*g*-CNCs were obtained using a Bruker AVANCE3-850HD NMR spectrometer operating at 20.0 T (214 MHz for carbon-13) and equipped with a 3.2 mm H/C-Si/N E-free CP/MAS probe. Spectra were recorded at a magic angle spinning speed of 15 kHz. The CP/MAS spectra were acquired using a 1 ms contact pulse, a 3.1 μs ^{1}H 90-degree pulse, a 15 ms acquisition time, and a 5 s recycle delay. Bloch decay spectra were recorded using a 3.39 μs ^{13}C 90-degree pulse and a recycle delay of 120 s. High-power proton decoupling was carried out using a SPINAL64 sequence on all spectra.

Water contact angle

Contact angle measurements were obtained for films on Piranha-cleaned Si wafers for CNC, CAN-oxidized CNC, and PMMA-*g*-CNC films using the sessile drop method on a Future Digital Scientific OCA 20 High Speed Contact Angle Measurer (USA). Films of CNCs and CAN-oxidized CNCs were spin-coated 3 times from 0.03 g/g (3 wt %) aqueous suspensions (4000 rpm for 30 s, Chemat Technology KW-4A, USA) giving films ~100 nm thick. PMMA-*g*-CNC films were solvent cast of Si wafers from 0.001 g/g (0.1 wt %) acetone suspension, giving films ~500 nm thick.

X-ray photoelectron spectroscopy (XPS)

XPS samples consisted of unmodified CNCs, CAN-oxidized CNCs, and PMMA-*g*-CNCs spin-coated (4000 rpm, 30 s) on Piranha-cleaned Si wafers. Spectra were recorded using a Physical Electronics (PHI) Quantera II spectrometer equipped with an Al anode source for X-ray generation and a quartz crystal monochromator for focusing the generated X-rays. A monochromatic Al K-α X-ray (1486.7 eV) source was operated at 50 W and 15 kV. The system base pressure was no higher than 0.1333 μPa (1.0×10^{-9} torr), with an operating pressure that did not exceed 2.666 μPa (2.0×10^{-8} torr). A pass energy of 280 eV obtained survey spectra and 26 eV for high-resolution C1s. All spectra were obtained at 45° takeoff angles, and a dual beam charge compensation system for neutralization of all samples. The instrument was calibrated using a sputter-cleaned piece of Ag, where the Ag $3d_{5/2}$ peak had a binding energy of 368.3 ± 0.1 eV, and full width at half maximum for the Ag $3d_{5/2}$ peak was at least 0.52 eV. Data manipulation was performed using PHI MultiPak Version 9.4.0.7 software.

Thermogravimetric analysis (TGA)

Thermogravimetric analysis measurements were performed using a thermoanalyzer (STA-409 Luxx, Netzsch Instruments, USA). 20–25 mg of freeze-dried CNCs, CAN-oxidized CNCs, and PMMA-*g*-CNCs were heated to 900 °C with a heating rate of 10 °C/min under a dry air atmosphere.

Atomic force microscopy (AFM)

Polished silicon wafers (Grinm Semiconductor Materials Co. Ltd., China) were cut into 1 cm × 1 cm squares and dipped into a 1 mg/g (0.1 wt %) PAH solution for 1 h and rinsed in purified water to adsorb a cationic precursor layer on the substrate. The silicon wafers were then dropped with either 0.01 mg/g (0.001 wt %) CNC or PMMA-*g*-CNC suspensions and spun at 4000 rpm on a spin coater. The CNC-coated silicon wafers were imaged by AFM using a Nanoscope IIIa Multimode Scanning Probe Microscope with an E scanner (Bruker AXS, Santa Barbara, USA). The tapping mode images were collected in air with silicon cantilevers (AC 160TS, Olympus Canada Inc., Canada).

NanoSight nanoparticle tracking analysis (NTA)

Suspensions of 0.001 mg/g (0.0001 wt %) CNCs, CAN-oxidized CNCs, or PMMA-*g*-CNCs in purified water were prepared and analyzed using a NanoSight LM10 single nanoparticle tracking instrument (Malvern Instruments Ltd., UK).

Electrophoretic mobility

The electrophoretic mobility was measured using a Zeta Potential ZetaPlus Analyzer (Brookhaven, USA). All samples were measured at 0.001 g/g (0.1 wt %) CNC concentrations, with 10 mmol/L NaCl at 25 °C.

X-ray diffraction (XRD)

X-ray diffraction was performed on freeze-dried CNCs, CAN-oxidized CNCs, and PMMA-*g*-CNCs on Piranha-cleaned Si wafers using a Bruker D8 DAVINCI diffractometer (Bruker, USA) with a cobalt sealed tube ($\lambda_{avg} = 0.179\ 026$ nm), 35 kV, 45 mA, and 0.5 mm micro-slit. Two frames were collected to obtain a 2θ range of 8–44°. Frames were also obtained for a blank Si wafer, which were subtracted from the sample frames. To determine the degree of crystallinity, the background corrected intensity versus the 2θ plots were fitted to five symmetric Lorentzian peaks, four peaks corresponding to the (100), (010), (002), and (040) crystalline planes,[59] and one broad amorphous peak fixed at 24.1°. The degree of crystallinity was calculated by the peak deconvolution method as the ratio of the area for the crystalline peaks over the total area for the diffraction plots using a manual peak insertion method (not the Rietveld method). There are a number of accepted XRD fitting methods (height, deconvolution, subtraction)[60,61] to determine the degree of crystallinity for CNCs. All methods have limitations, and as such, we have used the peak deconvolution method, making the values presented here internally consistent. However, the values should not be taken as absolute crystallinity nor compared with reports that fit XRD data using a different method. The error in this measurement and fitting procedure is taken to be 1–2 %.

Characterization of Composites

Tensile testing

Nanocomposite samples were melt-cast into dogbone shapes consistent with ASTM D638 (gauge length 31.8 mm, width 4.4–4.6 mm, thickness 2–3 mm) for tensile testing using a 5 kN load cell at 1 mm/min cross speed. These measurements were taken using a table-mounted Instron Universal tensile tester Model 3366 (Instron Corp., USA). The datasets for each pair of complementary samples were statistically analyzed using a *t*-test assuming unequal variance with $p < 0.05$. The significance levels at which the populations were from different groups are reported with statistical standards for p values.

Rheology

Shear viscosity measurements of CNC/PMMA and PMMA-*g*-CNC/PMMA composites were carried out on an ARES Rheometer at 200 °C on disks that were 7 mm in diameter and 2 mm thick. The individual strain rate for each sample was found by performing a strain sweep test. Strain rates near the centre of the linear region were taken as the strain rate for each sample. Frequency sweep tests were performed for each sample's strain rate. All data reported are an average of three test samples.

Scanning electron microscopy (SEM)

A Hitachi SU8000 STEM (Hitachi, Japan) was used to image nanocomposite samples. Melt-mixed samples of broken dogbone shapes used for tensile measurements were imaged at the break point. Top-view samples were cut using a Leica Ultra Cut-E Microtome fitted with a diamond knife, and all samples were coated with 6 nm of Pt/Pd using a Cressington HR208 high-resolution sputter coater before imaging.

RESULTS AND DISCUSSION

Characterization of Poly(methyl methacrylate)-Grafted-CNCs

PMMA-*g*-CNCs were prepared using CAN-initiated "grafting from" radical polymerization. The aqueous, one-pot synthesis is shown schematically in Figure 1a. We find that probe sonication during polymerization is crucial to avoid the aggregation of CNCs. The initiation mechanism of CAN with cellulose is still debated, but it is thought that oxidative cleavage of the cellulose backbone at the vicinal diol position allows the creation of reactive aldehydes (Figure 1b).[24,61] The ceric ion likely forms a chelated complex with the cellulose backbone and electrons are transferred from cellulose to Ce(IV), leading to Ce(III) and a radical site on the cellulose backbone from which polymerization propagates.[62,63]

The PMMA-*g*-CNCs were extensively purified by centrifugation, filtration, dialysis, and ultrafiltration using water and acetone to

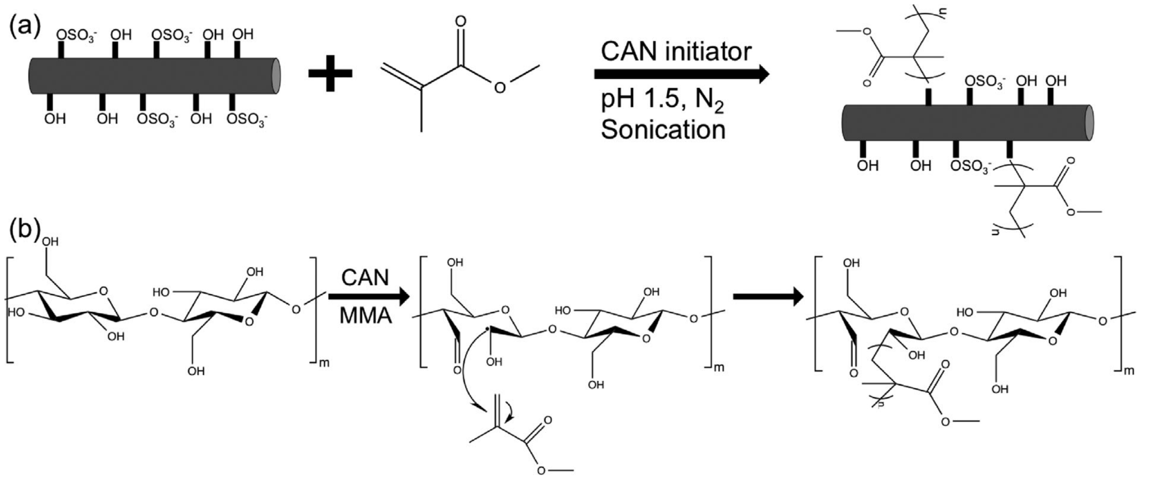

Figure 1. Schematic representation of: (a) the "grafting from" polymerization of PMMA from sulphated cellulose nanocrystals with CAN redox initiator under probe sonication, and (b) a simplified view of the reaction mechanism for cellulose with methyl methacrylate and CAN to form PMMA-*g*-CNCs. PMMA homopolymer is also produced during this reaction, which requires an additional washing step to ensure unbound polymer is removed.

remove all excess acid, initiator, and unbound PMMA homopolymer. The worked-up suspensions show limited colloidal stability and slowly sediment in water, ethanol, methyl ethyl ketone, and acetone. As grafted polymer amounts were low in our previous studies with CNCs and CAN,[33,65] we believe the reduction in colloidal stability arises from having attached sufficient PMMA to make CNCs incompatible with water, but too little PMMA to make the hybrid nanoparticles colloidally stable in PMMA-compatible solvents such as MEK and acetone. Under the grafting reaction conditions used we do not expect hydrolytic desulphation of CNCs to occur. This expectation is based on previously reported desulphation requirements[8] and the grafting of other polymers from CNCs using the same protocol.[33]

The presence of PMMA on the surface of the CNCs was confirmed by FTIR (Figure 2) and CP/MAS solid-state NMR spectroscopy (Figure 3). The FTIR transmittance bands at 2990 and 1730 cm^{-1} correspond to characteristic C–H and C=O PMMA stretching modes, respectively. The NMR spectrum of PMMA-*g*-CNCs (Figure 3a) reveals chemical shifts for PMMA at 180, 65, 45, and 20 ppm. These peaks are not present in the unmodified CNC spectrum (Figure 3b). Unfortunately, peak integration and quantification of grafted polymers using NMR Bloch decay methods were not possible due to the low signal-to-noise ratio, even after 3000 scans (data not shown). Water contact angle indicates that the surface modification increases the CNC hydrophobicity; an increase in contact angle of 17° (to 34.5° for a spin-coated PMMA-*g*-CNCs film on Si) was observed after

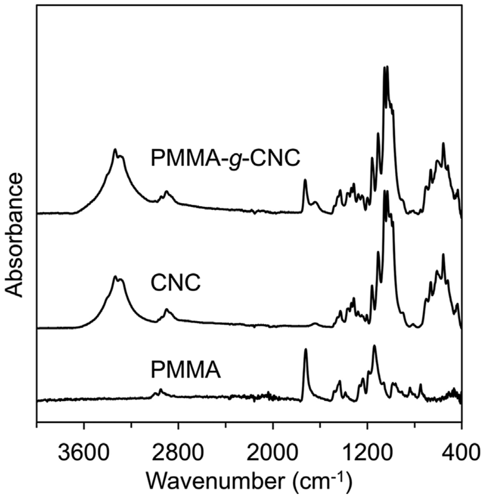

Figure 2. FTIR spectra of PMMA, unmodified CNCs, and PMMA-*g*-CNCs. Peaks at 2990 and 1730 cm^{-1} in the PMMA-*g*-CNC sample confirm the presence of PMMA.

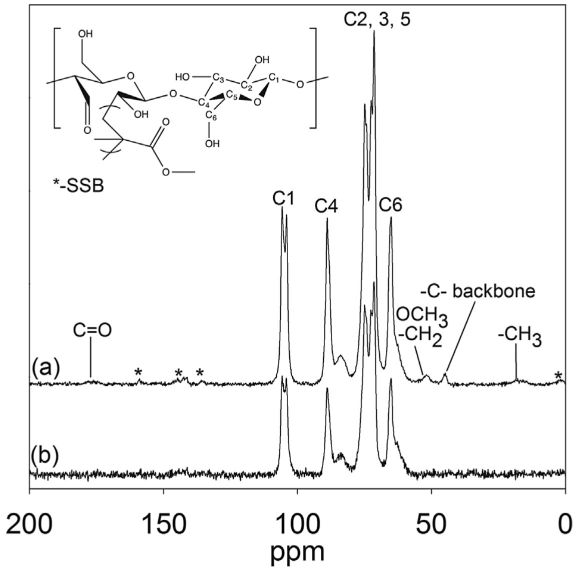

Figure 3. CP/MAS solid state NMR spectra showing: (a) PMMA-*g*-CNCs and (b) unmodified CNCs. PMMA-*g*-CNCs show characteristic peaks at 180, 65, 45, and 20 ppm, corresponding to the PMMA grafted from the CNCs. *-SSB = spinning side bands, and numbered carbon peaks correspond to carbons in the cellulose structure as labelled in the inset.

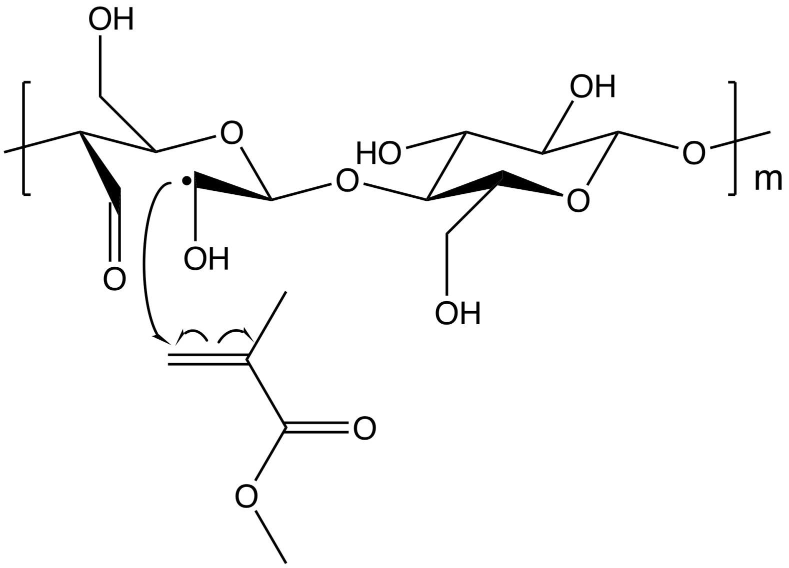

Figure 1S. Schematic of radical addition from the cellulose backbone to an MMA monomer. Corrected from Figure 1(b).

Table 1. Comparison of unmodified CNCs, PMMA-*g*-CNCs, and CAN-oxidized CNCs

	Apparent diameter* (nm)	Electrophoretic mobility (10^{-8} m^2/Vs)	C3/C4 (XPS ratio)	Onset of thermal degradation (°C)	Crystallinity index (%)†	Contact angle (°)
Unmodified CNCs	87 ± 33	-2.7 ± 0.2	–	295	90 %	17.6 ± 0.9
Oxidized CNCs	95 ± 37	-2.0 ± 0.2	–	250	89 %	28.7 ± 1.8
PMMA-*g*-CNCs	105 ± 40	-2.1 ± 0.3	4.3	250	87 %	34.5 ± 0.9

*Measured by NanoSight nanoparticle tracking analysis assuming spherical particles; confidence intervals are one standard deviation
†Crystallinity index determined by the peak deconvolution method with assumed error of 1–2 %

grafting (Table 1). A slight increase in hydrophobicity is also observed for CAN-oxidized CNCs (i.e. CNCs submitted to the same polymerization reaction conditions with CAN but without MMA monomer) because aldehyde groups are less polar than hydroxyl groups. Though these results provide evidence for the presence of PMMA on the surface of CNCs, they cannot distinguish between PMMA that is covalently bound and PMMA that is closely associated with the CNCs. Owing to the previous experience grafting vinyl monomers to CNCs[33] and the exhaustive purification used here to remove homopolymer, we are confident that PMMA is in fact bound to the CNC surface.

XPS high-resolution carbon (C 1s) spectra for PMMA-*g*-CNCs show a C4 peak that is not present in unmodified CNCs (Figure 4). This peak can be attributed to the carbonyl carbon in methyl methacrylate. By taking the ratio of C3/C4 peak areas, where C3 is the C_1 carbon in cellulose (see Figure 3 inset for cellulose structure and carbon labels), we obtain a C3/C4 ratio of 4.3 for PMMA-*g*-CNC samples. This implies that for every 4.3 anhydroglucose units (AGU), there is one MMA monomer which is equivalent to a grafted mass of 0.11 g/g (11 wt %). Assuming that 37 % of AGUs in a nanocrystal are on the surface[33] and grafting can only occur at the surface, we have one MMA monomer for every 1.6 surface AGUs. These numbers indicate that ~95 % of the MMA added to the reaction turned into homopolymer. However, we note that for modifying CNCs with grafted polymers intended for compounding with the same polymer matrix, this low efficiency is less significant and the washing step to remove unbound polymer becomes unnecessary.

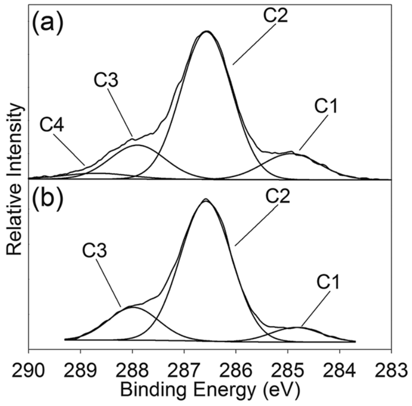

Figure 4. XPS high-resolution C 1s spectra showing: (a) PMMA-*g*-CNCs, and (b) unmodified CNCs. C4 peak is attributed to the carbonyl group on each MMA monomer. Peak fitting was used to extrapolate the mass ratio of PMMA to CNCs.

The previous report of grafting PMMA to CNCs by ATRP found chain lengths of 25–45 kDa (i.e. $25–45 \times 10^3$ g/mol).[22] If our chains were in this size range we would have only one high molecular mass PMMA chain on every third to fifth CNC. However, it is more likely to have a few short grafts per CNC as implied previously by mass spectrometry.[33] Our grafted mass of 0.11 g/g (11 wt %) is low compared to using controlled radical polymerization from CNCs, which typically yields grafted masses ranging from 0.5–0.92 g/g (50–92 wt %).[20,23] It is also slightly lower than the grafting yields reported in the patent disclosing graft-polymerization of PMMA with CAN on CNCs.[31] One possibility is that during the polymerization some MMA monomers are hydrolyzed to methacrylic acid which could reduce the reaction efficiency due to free radical instabilities and chelation of methacrylic acid with ceric ions. However, similar CAN-initiated grafting of PMMA from cellulose nanofibrils, which have significantly more amorphous/accessible cellulose than crystalline CNCs, found a grafted mass of 0.36–0.49 g/g (36–49 wt %) but did not find the presence of methacrylic acid.[30] Varying the ratio of MMA to CNCs during the grafting reaction has also been found to affect the final grafting yield and some mechanistic explanations have been offered.[31] The grafting procedure was not optimized in our work. Although we cannot determine the exact graft density or length, XPS provides insight into the efficiency of the reaction and implies that the overall quantity of PMMA grafted to the CNC surface is low.

To verify that the CNC nanoparticle size, degree of aggregation, morphology, and surface charge were not significantly changed during the polymer grafting reaction, samples were characterized by AFM (Figure 5), light scattering, XRD, and electrophoretic mobility (Table 1). AFM height images show that PMMA-*g*-CNCs are similar in size to unmodified CNCs, but that small polymer particles (bright spots in Figure 5c, which is a sample spin-coated from a more concentrated suspension) are present. AFM also shows that PMMA-*g*-CNCs are slightly more aggregated than unmodified CNCs. This result is unsurprising, given the visible flocculation in the suspension after the reaction and the tendency of CNCs to cluster during the reaction at low pH. Despite the appearance of some aggregates, individualized nanocrystals are also visible.

The apparent mean diameters of unmodified CNCs (87 ± 33 nm), PMMA-*g*-CNCs (105 ± 40 nm), and CAN-oxidized CNCs (95 ± 37 nm) suspended in water were measured using NanoSight nanoparticle tracking analysis. The term *apparent* is used in recognition that this technique calculates particle size assuming a spherical shape, which is not the case for CNCs, which are rod-like particles. The diameters are within similar ranges to each other, and similar to other CNC batches prepared in our lab. CAN-oxidized CNCs are not significantly different in size from the starting CNCs. NanoSight results also imply limited aggregation in the PMMA-*g*-CNC sample in water, yet the particles still sediment

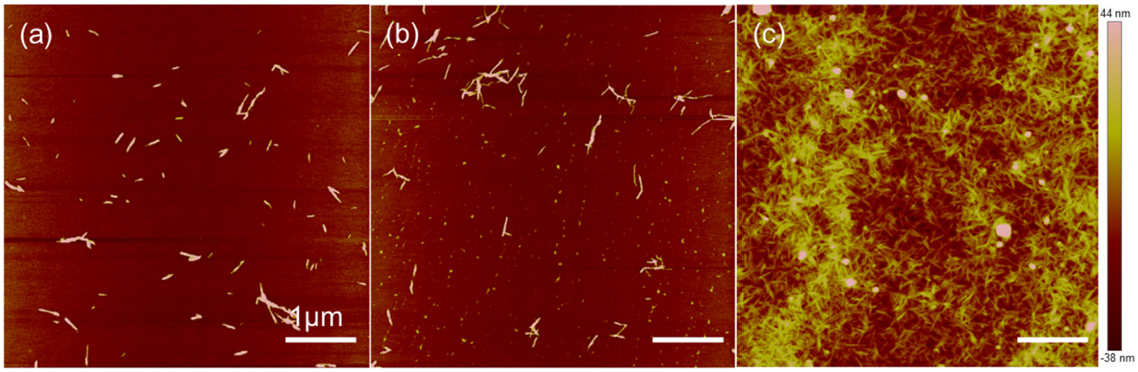

Figure 5. AFM height images of: (a) individual unmodified CNCs, (b) individual PMMA-*g*-CNCs spin-coated from 0.01 mg/g (0.001 wt %) suspensions onto a PAH-coated Si wafer, showing similar nanocrystal size and minor aggregation, and (c) a full surface-coverage film of PMMA-*g*-CNCs. All scale bars are 1 μm.

over time due to their incompatibility with water. The electrophoretic mobility of grafted CNCs and CAN-oxidized CNCs was slightly reduced compared to unmodified CNCs, which may be due to a combination of the oxidation by CAN and/or masking of anionic surface charge by the uncharged grafted polymer chains.

Polymer-grafted CNCs exhibited decreased thermal stability compared to unmodified CNCs (Figure 6). Specifically, the primary onset of thermal degradation shifted from 295 °C for unmodified CNCs to 250 °C for both PMMA-*g*-CNCs and CAN-oxidized CNCs (Table 1). This implies that the opening of the cellulose glucose units at the C_2-C_3 position and creation of aldehyde groups yield a material which undergoes thermal degradation at a lower temperature. PMMA alone degrades at 385 °C and is expected to improve the thermal stability of CNCs through grafting. However, this was not observed here. The two thermal degradation peaks observed for PMMA-*g*-CNCs below 385 °C may be due to non-uniform polymer grafting, or because oxidized glucose rings with grafted polymer on adjacent carbons are more thermally stable than dialdehyde groups. Overall the thermal analysis supports PMMA-*g*-CNCs being new hybrid nanoparticles with altered thermal properties, and that the sample is not a blend of associated CNCs and PMMA.

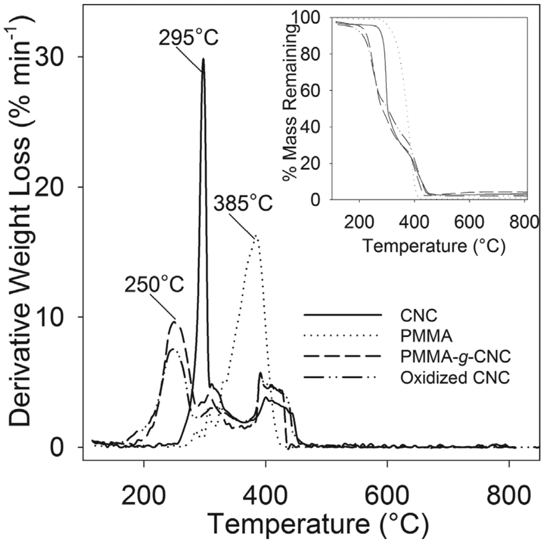

Figure 6. TGA derivative mass loss as a function of temperature (% mass loss in inset) for unmodified CNCs (solid line), PMMA (dotted line), PMMA-*g*-CNCs (dashed line), and CAN-oxidized CNCs (dashed-dotted line) showing that CAN-oxidized CNCs and PMMA-*g*-CNCs have a lower thermal degradation onset temperature (250 °C) than CNCs (295 °C) and PMMA (385 °C).

X-ray diffraction was further performed on unmodified, polymer-grafted, and CAN-oxidized CNCs to determine whether the grafting reaction has an effect on the degree of crystallinity (Table 1). Since the ceric initiator ring opens part of the cellulose backbone and was observed to lower the thermal stability of the CNCs, it was expected that CNCs oxidized in the presence of CAN would have a lower degree of crystallinity. It was previously shown that CNCs oxidized with sodium periodate exhibit reduced crystallinity[66] and polymer grafting from CNCs decreases the overall product degree of crystallinity.[67] As anticipated, unmodified CNCs had the highest degree of crystallinity at 90 %, which is consistent with reported values,[68] CAN-oxidized CNCs are slightly less crystalline at 89 %, and PMMA-*g*-CNCs are 87 % crystalline. These small decreases in crystallinity are within the accepted 1–2 % error interval of the technique and may not be significant despite agreeing with literature trends. While a 3 % decrease in crystallinity from unmodified to PMMA-grafted CNCs is not expected to significantly affect the mechanical properties of CNCs, it does provide some evidence for the effectiveness of the grafting reaction and is consistent with the thermal degradation results.

CNC/PMMA Nanocomposites

CNC/PMMA nanocomposites were compounded by melt mixing with a Haake mixer at 160 °C for 10 min and by wet ball milling in MEK for 24 h. Both unmodified CNCs and PMMA-*g*-CNCs were incorporated into bulk PMMA at loadings of 0.0025, 0.005, 0.01, and 0.02 g/g (0.25, 0.5, 1, and 2 wt %) with respect to PMMA. Ball-milled samples were mixed at ambient temperature. However, in order to prepare samples for mechanical testing, all nanocomposites were hot-pressed at 160 °C.

Although the final hot-pressed samples could be prepared reproducibly and were uniform in appearance, all ball-milled samples initially contained residual MEK, believed to be trapped within the nanocomposite (confirmed by NMR, data not shown). This led to a foam structure forming as the MEK evaporated during hot pressing. Repeated pressing eliminated foaming and after several press cycles, homogeneous and optically clear pellets were

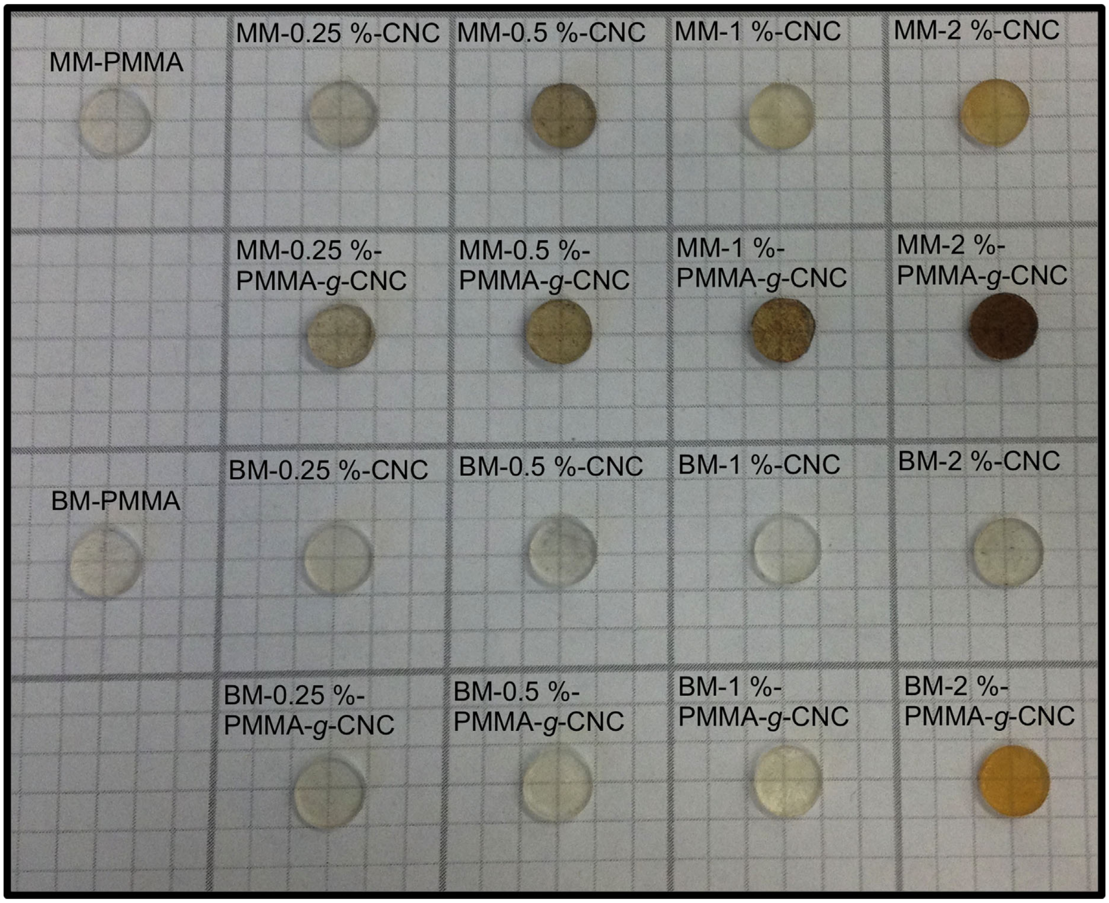

Figure 7. Photographs of CNC/PMMA nanocomposites with various loadings of unmodified cellulose nanocrystals or PMMA-*g*-CNCs, as indicated, showing the optical transparency and different colours obtained from (top two rows) melt-mixed (MM) and (bottom two rows) ball-milled (BM) compounding methods after hot pressing. Background paper has a 0.5 cm grid and disks are ~2 mm thick.

isolated. Melt-mixed samples did not exhibit any foaming. Once the foam structure in ball-milled composites was removed by hot pressing, the overall transparency and colour of ball-milled samples were similar to the PMMA control, whereas the melt-mixed samples exhibited significant discolouration (Figure 7).

Melt-mixed composites showed more variation in colour (darker brown with increasing CNC loading), likely because they experienced longer exposure to a high temperature (10 min), compared to the ball-milled samples which were only heated during pressing ($30\,s^{-2}\cdot min$). In addition, the PMMA-*g*-CNC composites were noticeably darker than the composites containing unmodified CNCs (Figure 6). We also observed that adding wet CNCs, or CNCs from aqueous suspension, led to even more discolouration. We attribute the colour change to a combination of caramelization (browning of surface-adsorbed sugars[11] above 160 °C), a heat-catalyzed desulphation of the CNCs to produce H_2SO_4 which hydrolyzes the cellulose in the presence of trace amounts of water,[12,64] and the non-uniform temperature profile within the Haake mixer which may expose regions of the melted composite to temperatures higher than the setpoint. We do not believe the colour arises from trace CAN, as all initiator was thoroughly removed after polymerization, and wide-spectrum scans by XPS did not show the presence of Ce. The discolouration is non-ideal, as PMMA is often used in optical applications. However, it is possible that the melt processing and degree of PMMA grafting may produce nanocomposites with less discolouration. It is unlikely the discolouration is due to a significant degradation of the CNCs, but this highlights the thermal sensitivity of the material and the importance of temperature control and heating rates. Importantly, the transparency of PMMA was maintained in all ball-milled composites and low CNC loading melt-mixed composites, implying reasonable dispersion of the nanoparticles overall.

Mechanical and Rheological Performance of CNC/PMMA Nanocomposites

Tensile tests were conducted on hot-pressed samples to compare unmodified CNC/PMMA and PMMA-*g*-CNC/PMMA nanocomposites to the PMMA control. Figure 8 presents the measured Young's moduli (E). Based on a *t*-test assuming unequal variance with $p < 0.05$, the majority of values within a given compounding method and between modified versus unmodified CNCs are statistically the same, implying the surface grafting of CNCs with PMMA did not improve the composite performance. Only the composite with the highest nanoparticle loading (0.02 g/g (2 wt %) CNCs) prepared by melt mixing shows a significant increase in modulus compared to the PMMA control ($E = 2.82 \pm 0.04$ versus 2.66 ± 0.03 GPa). In melt-mixed samples with

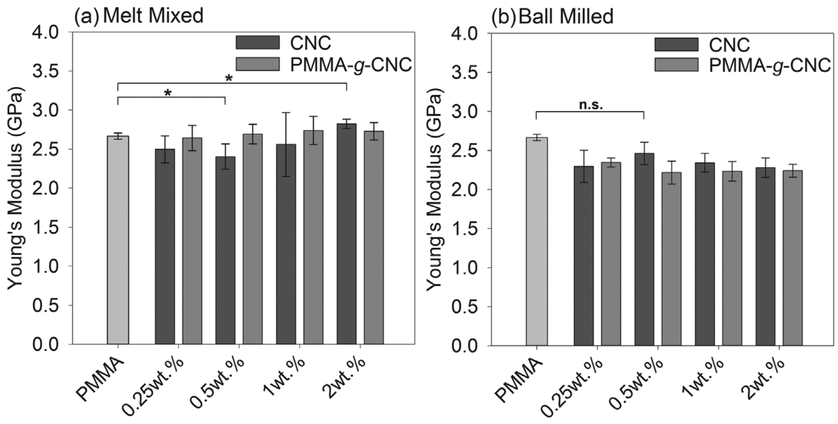

Figure 8. Comparison of Young's modulus for melt-mixed (a) and ball-milled (b) PMMA nanocomposites with unmodified CNCs and PMMA-*g*-CNCs. Loadings are indicated along the x axis in wt % (g/100 g). (Note: * represents statistically significant ($p < 0.05$) compared to the control (processed PMMA without nanocrystals, leftmost bar) and n.s. represents not statistically significant compared to the control. In (b) all loadings except 0.005 g/g (0.5 wt %) are statistically lower than the control. Statistical analysis of unmodified versus polymer-grafted CNC series are not indicated on the plot but were calculated, and only the 0.005 g/g loading for both compounding methods shows a significant difference between unmodified CNCs and PMMA-*g*-CNCs.)

0.005 g/g (0.5 wt %) CNCs, the modulus was lower than the control and for ball-milled samples. In all loadings except 0.005 g/g (0.5 wt %), CNCs were statistically lower than the control. This result is disappointing, considering that a simple law of mixtures[69] predicts a modulus of 4.8 GPa for 0.02 g/g (2.0 wt %) loading, assuming CNCs and PMMA have Young's moduli of 105 and 1.8–3.1 GPa,[70] respectively, and 0.02 g/g (2.0 wt %) CNCs is equivalent to 0.027 L/L (2.7 vol %).[5,68]

Overall, the ball-milled samples had lower moduli than their melt-mixed counterparts, including the control, which may be due to trapped solvent (MEK is a good plasticizer for PMMA) or the effect of vaporizing MEK out of the composites during hot pressing. After processing by ball milling, PMMA polymer globules in dilute solution may not have sufficient time to interact/entangle and crystallization is likely influenced when the wet samples are quickly heated under high pressure.[71,72] It is improbable that we induced PMMA degradation (which occurs above 300 °C) or crosslinking in any of the compounding or pressing steps. Furthermore, no trend in modulus with the degree of discolouration is seen, implying that the colour is not linked to reduced mechanical properties or significant degradation of the composite components.

Based on tensile testing, all samples had the same toughness within error (~0.8 MPa, data not shown), further supporting that the mechanical performance is primarily dictated by the PMMA matrix. The difficulty in determining clear trends from these measurements stems from the large confidence intervals (i.e. error bars shown in Figure 8), however in all cases the reproducibility in tensile testing was higher for unmodified CNC composites compared to PMMA-*g*-CNC composites. Additionally, the melt-mixed composites exhibited a slight increase in stiffness with particle loading, whereas stiffness decreased with increasing particle loading for the ball-milled composites. These results are consistent with previous reports of solvent cast nanocellulose/PMMA composites which show no statistically significant change in stiffness[52,67] or a small increase in stiffness with CNC loading.[49,53] Substantial mechanical improvements were only observed above 0.03 g/g (3 wt %) loading[40] or even 0.17 g/g (17 wt %) loading for electrospun composites, implying that our loadings may be below the onset of significant reinforcement by CNCs.[38] In the majority of studies performend by Sain et al.[37,48–52] 0.1 g/g (10 wt %) CNC loadings were employed, which led to a 14 % increase in modulus but a slight decrease in tensile strength.[47] A recent study comparing nanocelluloses in PMMA composites found slight mechanical improvements above the polymer T_g with 0.005 g/g (0.5 wt %) loadings and showed that higher aspect ratios and high crystallinity contribute to improved composite performance.[51]

Overall the mechanical characterization presented here suggests grafting PMMA from CNCs had a minimal effect on the mechanical properties of this series of nanocomposites. A few possible explanations exist: this may be due to the grafting density/length of PMMA which is unknown; it may be linked to changes in the degree of aggregation of PMMA-*g*-CNCs during compounding; or it may be due to the CNCs' ability to act as a nucleating agent.[73] If unmodified CNCs can act as nucleating agents for polymer matrix crystallization[74] and if polymer grafts on modified CNCs are not of sufficient molecular weight to co-crystallize with the polymer matrix, nucleation cannot take place due to different crystallization rates of grafts versus matrix leading to inferior composites. Ball milling shows promise for use in future compounding applications, as this processing technique does not require the use of high temperatures. Solvents other than MEK that are more easily evaporated and less compatible with the PMMA matrix may give higher modulus composites with less tendency to foam.

With the goal of elucidating the strength of the interactions between CNCs and PMMA, and any mechanical improvement above the T_g/T_m of PMMA, rheology of composites was carried out at 200 °C (Figure 9). Similar to the tensile testing, melt-mixed PMMA had a higher storage modulus than ball-milled PMMA (and the shear viscosity was 44 % higher), suggesting that the processing method changed the way the polymer chains interact with each other. In almost all cases, ball-milled samples mechanically underperform compared to melt-mixed samples.

In the composite melts, a higher viscosity and shear modulus was observed for the unmodified CNCs compared to the polymer-grafted CNCs, which may be attributed to PMMA-*g*-CNC nanoparticle

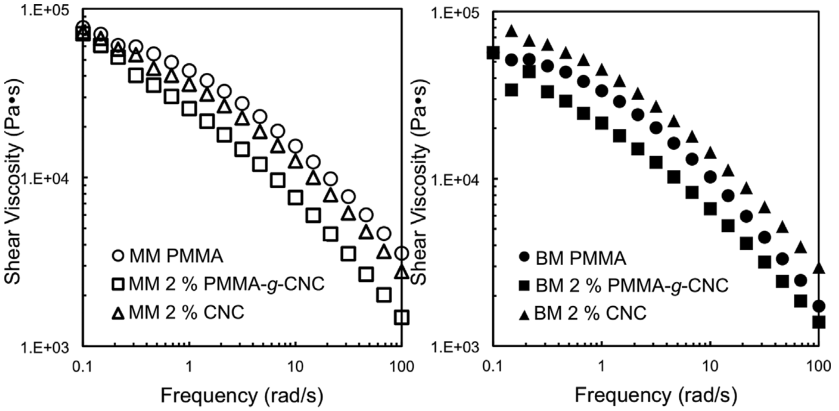

Figure 9. Shear viscosity at 200 °C for: (left) melt-mixed (MM) and (right) ball-milled (BM) composites with 0.02 g/g (2 wt %) loadings of unmodified CNCs (triangles) or PMMA-*g*-CNCs (squares) in a PMMA matrix, and the control PMMA (circles).

aggregation. Different processing conditions resulted in different rheological performance relative to the PMMA control. In the case of the melt-mixed samples, the control had the highest shear viscosity. However, when the ball-milled composites were compared, the PMMA/CNC composite exhibited the highest shear viscosity (Figure 9). The PMMA-*g*-CNC composites had the lowest shear viscosity of the series regardless of processing technique. It appears that while the ball milling process reduced the viscosity of the PMMA matrix (potentially due to trapped MEK), this decrease in mechanical and rheological properties could be compensated for by adding unmodified CNCs. However, PMMA-*g*-CNCs further reduced these properties.

As the CNC loadings in all composites described herein are below the percolation threshold of CNCs (0.025 g/g (~2.5 wt %)[75]) and the concept of percolation has less relevance in the case of surface-modified CNCs, it is thought that the primary reinforcing mechanism in this system is the formation of networks and entanglements between the polymer chains and nanoparticles. The dispersion of CNCs in the PMMA matrix is therefore of utmost importance. In fact, the effect of dispersibility on mechanical performance appears to dominate over interfacial interactions between the nanoparticle and matrix. While PMMA-*g*-CNCs have better interfacial compatibility with PMMA than unmodified CNCs based on contact angle measurements, the degree of functionalization may not be sufficient and reduced dispersibility in both water and MEK gives them a higher tendency to aggregate due to colloidal instability and polymer bridging. Aggregation leads to poor dispersion, less polymer-particle surface area for network formation, and disruption of the polymer-polymer interactions. As such, all composites with PMMA-*g*-CNCs exhibited lower shear viscosity than either the CNC composites or PMMA control, and as mentioned, changes in crystallization kinetics for the PMMA matrix and the nucleating effect of CNCs versus PMMA-*g*-CNCs may also contribute.

Representative scanning electron microscopy images of melt-mixed composites with 0.02 g/g (2 wt %) CNCs or PMMA-*g*-CNCs are shown in Figure 10 and support the suggestion that reduced mechanical properties are a result of nanoparticle aggregation. While the exact identification of components by SEM is

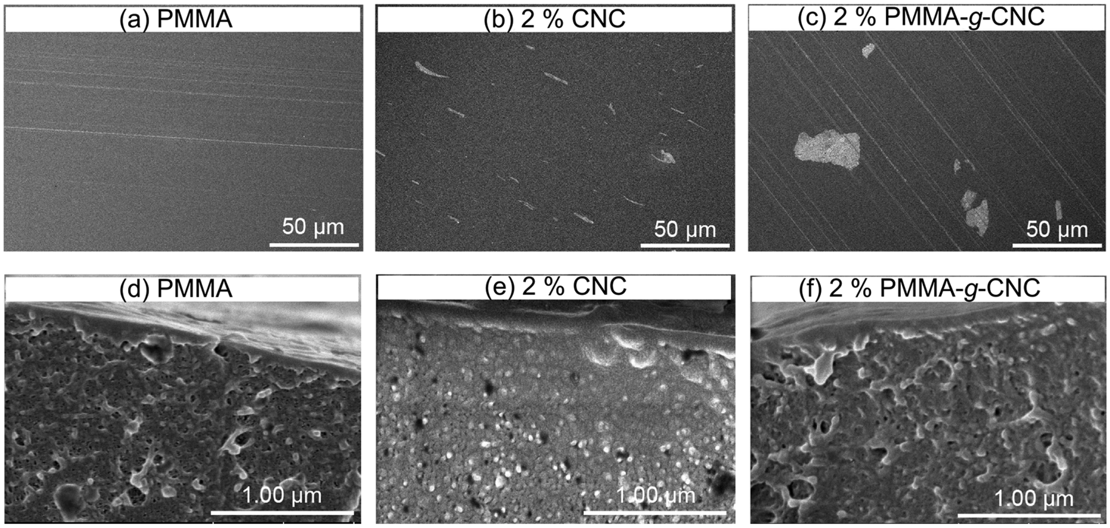

Figure 10. SEM images of melt-mixed PMMA composites (dogbone samples prepared for tensile testing). Top row = microtomed section top-view with scale bar 50 μm; bottom row = freeze-fractured edges with scale bar 1 μm. (a, d) PMMA control; (b, e) 0.02 g/g (2 wt %) loading of unmodified CNCs; (c, f) 0.02 g/g (2 wt %) loading of PMMA-*g*-CNCs.

challenging, the white particulates are likely CNCs while the darker regions are attributed to the PMMA matrix. Figure 10 shows that the microtomed sections are smooth and relatively featureless for pure PMMA, while CNC-rich areas are observed at a 0.02 g/g (2 wt %) CNC loading (Figures 10b–c). The CNC agglomerates are larger in the PMMA-*g*-CNC samples compared to unmodified CNC samples. The higher resolution edge view shows a dense network of PMMA while CNC is visible as bright white spots. The edge view suggests improved dispersion of the unmodified CNCs relative to the PMMA-*g*-CNCs as individual CNC particles are less easily observed in the PMMA-*g*-CNC composite when viewed at high resolution on the fractured edge.

CONCLUSIONS

This work thoroughly investigates all stages of preparing CNC-reinforced nanocomposites starting with CNC production, polymer grafting, compounding, sample fabrication, and final composite testing. We focus specifically on grafting polymers from CNCs using a CAN-initiated radical polymerization because it is a quick, aqueous-based reaction and can be scaled up industrially.[31] Although the total mass of grafted polymer is reasonable, more methods to quantify graft length and graft density are still required. Overall, PMMA-*g*-CNCs had similar size, morphology, and crystallinity to unmodified CNCs after excess homopolymer was removed using ultrafiltration. Evidence that PMMA was successfully bound to CNCs was provided by various spectroscopies, contact angle, and thermal analysis. Importantly, XPS enabled quantification of the total mass of grafted polymer.

This is the first report of cellulose nanocrystal/PMMA composites where compounding is performed by melt mixing and ball milling. Only sonication and simple mixing of components in solvents or in situ polymerization have been demonstrated previously. We believe our methods are scalable and the insight gained here will bring CNC composites closer to commercial realization. This is also the first time PMMA-*g*-CNCs have been compounded with high molecular weight bulk PMMA and its properties tested. While an enhancement of mechanical performance was not observed, we believe that this is due to heightened particle aggregation after grafting and the low nanoparticle loadings used overall (and potential changes in matrix crystallization kinetics). In the case of ball milling, the interaction of PMMA with MEK and heat decreased polymer-polymer entanglement led to reduced stiffness and shear viscosity for all nanocomposites and the control. Increased nanoparticle loadings and improved melt compounding conditions, such as compounding below the T_g of PMMA to increase shear and improve dispersion quality, may yield materials with improved mechanical properties and reduced discolouration.

This study recognizes that modifying CNC surface chemistry is not sufficient to predict its ability to reinforce polymers. In this case, polymer graft density and length would need to be tailored further. Improving interfacial compatibility and particle-polymer interactions may not lead to stronger composites if particle-particle aggregation/bridging cannot be overcome. We urge more researchers to tackle this issue and share testing of compounding methods and composite mechanical properties in series with CNC surface modification, rather than keeping chemical synthesis and materials science and engineering separate. Certainly, there are many challenges in tuning CNCs for optimal polymer matrix compatibility; this work is one step towards tailored nanomaterials that take advantage of CNC strength and dimensions to enhance the properties of polymer products.

ACKNOWLEDGMENTS

The authors thank D. Covelli at the McMaster BioInterfaces Institute for XPS analysis, Professors B. Berno and G. Goward at the McMaster NMR Facility, the Canadian Center for Electron Microscopy, and F. Gibbs and V. Jarvis at the Brockhouse Institute for Materials Research. S. Gardner at the Xerox Research Centre of Canada is gratefully acknowledged for SEM analysis. We also thank Dr. T. Abitbol, Professor T. Hoare, Professor J. Moran-Mirabal, and Professor R. Pelton for equipment and expertise. This work was supported in part by the Natural Sciences and Engineering Research Council of Canada (Discovery and Industrial Postgraduate Scholarship programs), the Xerox Research Centre of Canada, and the Faculty of Engineering at McMaster University.

REFERENCES

[1] Y. Habibi, L. A. Lucia, O. J. Rojas, *Chem. Rev.* **2010**, *110*, 3479.

[2] M. Roman, *Ind. Biotechnol.* **2015**, *11*, 25.

[3] Future Markets Inc., *The Global Market for Nanocellulose to 2020*, 2nd edition, Future Markets **2013**.

[4] B. L. Peng, N. Dhar, H. L. Liu, K. C. Tam, *Can. J. Chem. Eng.* **2011**, *89*, 1191.

[5] R. J. Moon, A. Martini, J. Nairn, J. Simonsen, J. Youngblood, *Chem. Soc. Rev.* **2011**, *40*, 3941.

[6] D. Klemm, F. Kramer, S. Moritz, T. Lindström, M. Ankerfors, D. Gray, A. Dorris, *Angew. Chemie* **2011**, *50*, 5438.

[7] S. J. Eichhorn, A. Dufresne, M. Aranguren, N. E. Marcovich, J. R. Capadona, S. J. Rowan, C. Weder, W. Thielemans, M. Roman, S. Renneckar, W. Gindl, S. Veigel, J. Keckes, H. Yano, K. Abe, M. Nogi, A. N. Nakagaito, A. Mangalam, J. Simonsen, A. S. Benight, A. Bismarck, L. A. Berglund, T. Peijs, *J. Mater. Sci.* **2010**, *45*, 1.

[8] S. Beck, J. Bouchard, *Nord. Pulp Pap. Res. J.* **2014**, *29*, 6.

[9] T. A. Dankovich, D. Gray, *J. Adhes. Sci. Technol.* **2011**, *25*, 699.

[10] M. Roman, W. T. Winter, *Biomacromolecules* **2004**, *5*, 1671.

[11] M. Labet, W. Thielemans, *Cellulose* **2011**, *18*, 607.

[12] D. Roy, M. Semsarilar, J. T. Guthrie, S. Perrier, *Chem. Soc. Rev.* **2009**, *38*, 2046.

[13] Y. Habibi, *Chem. Soc. Rev.* **2014**, *43*, 1519.

[14] Y. Habibi, A.-L. Goffin, N. Schiltz, E. Duquesne, P. Dubois, A. Dufresne, *J. Mater. Chem.* **2008**, *18*, 5002.

[15] S. Hansson, E. Östmark, A. Carlmark, E. Malmström, *ACS Applied Materials & Interfaces* **2009**, *1*, 2651.

[16] S. Hansson, A. Carlmark, E. Malmström, L. Fogelström, *J. Appl. Polym. Sci.* **2015**, *41434*, 1.

[17] J. Yi, Q. Xu, X. Zhang, H. Zhang, *Cellulose* **2009**, *16*, 989.

[18] J. O. Zoppe, Y. Habibi, O. J. Rojas, R. A. Venditti, L. S. Johansson, K. Efimenko, M. Österberg, J. Laine, *Biomacromolecules* **2010**, *11*, 2683.

[19] J. O. Zoppe, R. A. Venditti, O. J. Rojas, *J. Colloid Interf. Sci.* **2012**, *369*, 202.

[20] Y. Fu, G. Li, H. Yu, Y. Liu, *Appl. Surf. Sci.* **2012**, *258*, 2529.

[21] E. Malmström, A. Carlmark, *Polym. Chem.* **2012**, *3*, 1702.

[22] A. Boujemaoui, S. Mongkhontreerat, E. Malmström, A. Carlmark, *Carbohyd. Polym.* **2015**, *115*, 457.

[23] B. N. Misra, P. S. Chandel, *J. Polym. Sci. A* **1977**, *15*, 1545.

[24] E. Schwab, V. Stannett, D. Rakowitz, J. Magrane, *TAPPI* **1962**, 390.

[25] D. J. McDowall, B. S. Gupta, V. T. Stannett, *Prog. Polym. Sci.* **1984**, *10*, 1.

[26] J. C. Arthur, P. J. Baugh, O. Hinojosa, *J. Appl. Polym. Sci.* **1966**, *10*, 1591.

[27] K. C. Gupta, K. Khandekar, *Biomacromolecules* **2003**, *4*, 758.

[28] K. C. Gupta, S. Sahoo, *Biomacromolecules* **2001**, *2*, 239.

[29] K. C. Gupta, S. Sahoo, K. Khandekar, *J. Macromol. Sci. A* **2007**, *44*, 707.

[30] K. Littunen U. Hippi, L. S. Johansson, M. Österberg, T. Tammelin, J. Laine, J. Seppälä, *Carbohydr. Polym.* **2011**, *84*, 1039.

[31] US 8,349,948 (**2013**), PFInnovations, invs.: W. Hamad, S. Su.

[32] H. M. Kan, *Responsive Polymer-Grafted Cellulose Nanocrystals from Ceric (IV) Ion-Initiated Polymerization*, MASc thesis, McMaster University, Hamilton, ON **2013**.

[33] K. H. M. Kan, J. Li, K. Wijesekera, E. D. Cranston, *Biomacromolecules* **2013**, *14*, 3130.

[34] X. Cao, Y. Habibi, L. Lucia, *J. Mater. Chem.* **2009**, *19*, 7137.

[35] C. Miao, W. Y. Hamad, *Cellulose* **2013**, *20*, 2221.

[36] A. Dufresne, *Nanocellulose: from Nature to High Performance Tailored Materials*, Walter de Gruyter, Berlin **2012**.

[37] M. Banerjee, S. Sain, A. Mukhopadhyay, S. Sengupta, T. Kar, D. Ray, *J. Appl. Polym. Sci.* **2014**, *131*, 1.

[38] H. Dong, K. E. Strawhecker, J. F. Snyder, J. A. Orlicki, R. S. Reiner, A. W. Rudie, *Carbohyd. Polym.* **2012**, *87*, 2488.

[39] F. Fahma, N. Hori, T. Iwata, A. Takemura, *J. Appl. Polym. Sci.* **2013**, *128*, 1563.

[40] H. Liu, D. Liu, F. Yao, Q. Wu, *Bioresource Technol.* **2010**, *101*, 5685.

[41] S. Maiti, S. Sain, D. Ray, D. Mitra, *Polym. Degrad. Stabil.* **2013**, *98*, 635.

[42] S. Li, M. S. Toprak, Y. S. Jo, J. Dobson, D. K. Kim, M. Muhammed, *Adv. Mater.* **2007**, *19*, 4347.

[43] E. Džunuzović, M. Marinović-Cincović, J. Vuković, K. Jeremić, J. M. Nedeljković, *Polym. Composite.* **2009**, *30*, 737.

[44] R. Haggenmueller, *Chem. Phys. Lett.* **2000**, *330*, 219.

[45] L. Chen, R. Ozisik, L. S. Schadler, *Polymer* **2010**, *51*, 2368.

[46] L. Chen, J. Zhu, Q. Li, S. Chen, Y. Wang, *Eur. Polym. J.* **2007**, *43*, 4593.

[47] S. Sain, M. Bose, D. Ray, A. Mukhopadhyay, S. Sengupta, T. Kar, C. J. Ennis, P. K. S. M. Rahman, M. Misra, *J. Reinf. Plast. Comp.* **2013**, *32*, 147.

[48] S. Sain, D. Ray, A. Mukhopadhyay, *Polym. Composite.* **2014**, *36*, 1748.

[49] S. Sain, D. Ray, A. Mukhopadhyay, S. Sengupta, T. Kar, C. J. Ennis, P. K. S. M. Rahman, *J. Appl. Polym. Sci.* **2012**, *126*, E127.

[50] S. Sain, S. Sengupta, A. Kar, A. Mukhopadhyay, S. Sengupta, T. Kar, D. Ray, *Polym. Degrad. Stabil.* **2014**, *99*, 156.

[51] E. E. Kiziltas, A. Kiziltas, S. C. Bollin, D. J. Gardner, *Carbohyd. Polym.* **2015**, *127*, 381.

[52] H. J. Fecht, E. Hellstern, Z. Fu, W. L. Johnson, *Metall. Trans. A* **1990**, *21*, 2333.

[53] A. W. Weeber, H. Bakker, *Physica B* **1988**, *153*, 93.

[54] A. Jankovic, W. Valery, E. Davis, *Miner. Eng.* **2004**, *17*, 1075.

[55] E. L. Parrott, *J. Pharm. Sci.* **1974**, *63*, 813.

[56] M. Hussain, *Mater. Lett.* **1996**, *26*, 177.

[57] J.-F. F. J. Revol, H. Bradford, J. Giasson, R. H. Marchessault, D. G. Gray, *Int. J. Biol. Macromol.* **1992**, *14*, 170.

[58] T. Abitbol, E. Kloser, D. G. Gray, *Cellulose* **2013**, *20*, 785.

[59] B. Briois, T. Saito, C. Pétrier, J. L. Putaux, Y. Nishiyama, L. Heux, S. Molina-Boisseau, *Cellulose* **2013**, *20*, 597.

[60] Canadian Standards Association, *Cellulosic nanomaterials — Test methods for characterization (CSA Z5100-14)* **2014**, URL: http://shop.csa.ca/en/canada/sustainable-forest-management/z5100-14/invt/27036672014.

[61] S. Park, J. O. Baker, M. E. Himmel, P. A. Parilla, D. K. Johnson, *Biotechnology for Biofuels* **2010**, *3*, 10.

[62] K. C. Gupta, S. Sahoo, K. Khandekar, *Biomacromolecules* **2002**, *3*, 1087.

[63] D. J. McDowall, B. S. Gupta, V. T. Stannett, *Prog. Polym. Sci.* **1984**, *10*, 1.

[64] O. Y. Mansour, A. Nagaty, *Prog. Polym. Sci.* **1985**, *11*, 91.

[65] K. H. M. Kan, *Responsive Polymer-Grafted Cellulose Nanocrystals*, MASc thesis, McMaster University, Hamilton, ON **2013**.

[66] B. Sun, Q. Hou, Z. Liu, Y. Ni, *Cellulose* **2015**.

[67] S. Eyley, W. Thielemans, *Nanoscale* **2014**, *6*, 7764.

[68] R. J. Moon, A. Martini, J. Nairn, J. Simonsen, J. Youngblood, *Chem. Soc. Rev.* **2011**, *40*, 3941.

[69] S. N. Bhattacharya, *Polymeric Nanocomposites: Theory and Practice*, 1st edition, Hanser Gardner, Munich **2008**.

[70] C. Livermore, J. Voldman, "MIT Material Property Database," *MIT* **2015**, accessed on 2014 September 10, http://web.mit.edu/6.777/www/matprops/matprops.htm.

[71] L. H. Sperling, *Introduction to Physical Polymer Science*, 4th edition, John Wiley & Sons, New York **2006**.

[72] K. Littunen, U. Hippi, T. Saarinen, J. Seppälä, *Carbohyd. Polym.* **2013**, *91*, 183.

[73] D. G. Gray, *Cellulose* **2007**, *15*, 297.

[74] Y. Habibi, A.-L. Goffin, N. Schiltz, E. Duquesne, P. Dubois, A. Dufresne, *J. Mater. Chem.* **2008**, *18*, 5002.

[75] T. Abitbol, B. G. Prevo, C. Galli, S. Choudhary, J. Corwin, F. Villalpando-Paez, L. Nguyen, A. Komarov, M. Villalobos, S. C. Veldhuis, E. D. Cranston, *Green Mater.* **2014**, *2*, 206.

Manuscript received May 11, 2015; revised manuscript received October 21, 2015; accepted for publication October 21, 2015.

Chapter 4

Grafting-from Cellulose Nanocrystals via Photoinduced Cu-mediated Reversible-deactivation Radical Polymerization.

In the previous chapter, CNCs were modified with an uncontrolled polymer grafting approach based on free radical polymerization. In this chapter, a novel controlled photoinduced Cu-mediated reversible-deactivation radical polymerization method was applied to CNCs for the first time. This polymer grafting technique proved highly versatile for the modification of CNCs with hydrophobic poly(methyl acrylate) (PMA), where considerably high amounts of polymer grafting was achieved in short reaction times with simple purification. This work led to modified CNCs with controlled polymer graft lengths and graft densities. While hydrophobic CNCs are needed for various applications, a similar method to that described here is used in Chapter 8 to compatibilize CNCs to allow for their incorporation into polymer latex particles.

In this work, I produced the unmodified CNCs, initiator-modified CNCs, and the initial UV RDRP from CNCs, and prepared samples for XRD and XPS while on exchange at KTH Royal Institute of Technology in Sweden. Dr. Fiona Hatton (KTH Royal Institute of Technology) performed the subsequent series of UV RDRP experiments and carried out the NMR, SEC, FTIR, TGA, DSC, and contact angle characterization. XPS and XRD were performed at McMaster by technicians as described in the acknowledgements and I interpreted the results. The manuscript was drafted by myself and Dr. Fiona Hatton and edited by our academic advisors, Dr. Emily Cranston and Dr. Anna Carlmark (KTH Royal Institute of Technology). This chapter and Supporting Information (Appendix 1) are reprinted as they appear in *Carbohydrate Polymers*, with permission from Elsevier © 2017.

Grafting-from Cellulose Nanocrystals via Photoinduced Cu-mediated Reversible-deactivation Radical Polymerization
Fiona L. Hatton, Stephanie A. Kedzior, Emily D. Cranston, and Anna Carlmark
Carbohydrate Polymers, **2017**, *157*, pp 1033-1040
DOI: 10.1016/j.carbpol.2016.10.064

Carbohydrate Polymers 157 (2017) 1033–1040

Contents lists available at ScienceDirect

Carbohydrate Polymers

journal homepage: www.elsevier.com/locate/carbpol

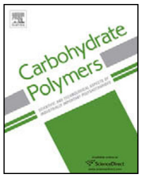

Grafting-from cellulose nanocrystals via photoinduced Cu-mediated reversible-deactivation radical polymerization

Fiona L. Hatton[a,*,1], Stephanie A. Kedzior[b], Emily D. Cranston[b], Anna Carlmark[a,*]

[a] KTH Royal Institute of Technology, School of Chemical Science and Engineering, Department of Fibre and Polymer Technology, Teknikringen 56, SE-100 44 Stockholm, Sweden
[b] McMaster University, Department of Chemical Engineering, 1280 Main Street West, Hamilton, Ontario L8S 4L7, Canada

ARTICLE INFO

Article history:
Received 26 August 2016
Received in revised form 10 October 2016
Accepted 21 October 2016
Available online 21 October 2016

Keywords:
Cellulose nanocrystals
Photoinduced polymerization
RDRP
Polymer-grafted CNC
Characterization
Nanoparticle compatibilization

ABSTRACT

In this work we describe the grafting of cellulose nanocrystals (CNCs) by surface-initiated photoinduced Cu-mediated reversible-deactivation radical polymerization (RDRP). Initially, CNCs obtained through sulfuric acid hydrolysis were functionalized with a tertiary bromo-ester moiety as an initiating group for the subsequent RDRP of methyl acrylate, targeting three different degrees of polymerization for the polymer grafts: 50, 300 and 600. The polymerizations proceeded in DMSO in the presence of $CuBr_2$ and Me_6TREN as the catalytic system utilizing a UV source ($\lambda_{max} \approx 360$ nm). The technique proved highly versatile for the modification of CNCs with poly(methyl acrylate), where considerably high grafting was achieved in short reaction times (90 min), with simple purification steps. CNC morphology was maintained and polymer grafts were evident through FT-IR spectroscopy, thermal analysis, contact angle measurements, X-ray photoelectron microscopy and x-ray diffraction.

1. Introduction

The increasing interest in utilizing renewable, sustainable materials has sparked a large field of research into the use of nanocellulose in advanced materials such as composites, cosmetics, food and biomedical applications (Habibi 2014; Klemm et al., 2011). Cellulose nanocrystals (CNCs) are extracted from cellulose fibers by the preferential acid hydrolysis of amorphous cellulose resulting in highly crystalline, needle-shaped particles which exhibit several interesting properties including excellent mechanical strength, high aspect ratio, low density and liquid crystalline behavior (Habibi, Lucia, & Rojas, 2010; Moon, Martini, Nairn, Simonsen, & Youngblood, 2011). For the utilization of CNCs in many applications, modification is necessary to improve compatibility between the cellulose surface and the surrounding polymer matrix or non-polar liquids (Eichhorn 2011). Modifications are often achieved through chemical functionalization of the CNC surface with small molecules or polymer chains (Eyley & Thielemans, 2014; Habibi 2014). This modification usually occurs after the production of the CNCs; however, a few publications report the chemical modification during the hydrolysis step (Boujemaoui, Mongkhontreerat, Malmström, & Carlmark, 2015; Braun & Dorgan, 2009; Espino-Pérez, Domenek, Belgacem, Sillard, & Bras, 2014). Modification of CNCs, or any cellulose substrate, with polymers relies upon covalent grafting (Malmström & Carlmark, 2012; Roy, Semsarilar, Guthrie, & Perrier, 2009), or physical adsorption (Hatton, Malmström, & Carlmark, 2015). Covalent grafting can be achieved via either grafting pre-formed polymer chains to the CNC surface, grafting-to, or by polymerization of monomer(s) from the CNC surface, grafting-from.

Polymer grafting-from CNCs has been reported utilizing techniques such as free radical polymerization (FRP), ring opening polymerization (ROP) and Cu-mediated reversible-deactivation radical polymerization (RDRP) (Kang, Liu, & Huang, 2015). Whilst free radical grafting-from CNCs is a straight-forward and convenient approach, it is not possible to control or predict the grafting densities, grafted chain lengths or specific polymer architectures (i.e. block copolymer structures) (Kan, Li, Wijesekera, & Cranston, 2013; Kedzior, Graham, Moorlag, Dooley, & Cranston, 2016). Furthermore, the formation of free, unbound homopolymer is unavoidable (Kedzior et al., 2016). ROP grafting-from allows more control over the chain lengths and polymer architectures; however, the grafting density cannot be controlled as the initiating sites for the polymerization are the abundant native hydroxyl groups at

---

* Corresponding authors.
E-mail addresses: f.l.hatton@sheffield.ac (F.L. Hatton), kedziosa@mcmaster.ca (S.A. Kedzior), ecranst@mcmaster.ca (E.D. Cranston), annac@kth.se (A. Carlmark).

[1] Present address: University of Sheffield, Department of Chemistry, Dainton Building, Brook Hill, Sheffield S3 7HF, UK.

http://dx.doi.org/10.1016/j.carbpol.2016.10.064
0144-8617/© 2016 Elsevier Ltd. All rights reserved.

the CNC surface. Therefore, several groups have reported the use of Cu-mediated RDRP techniques to graft-from CNCs (Kang et al., 2015).

RDRP was first used in conjunction with cellulose in 2002 (Carlmark & Malmström, 2002; Carlmark & Malmström, 2003) and has since proved a versatile technique for the grafting-from modification of numerous cellulose substrates (Hansson, Carlmark, Malmström, & Fogelström, 2015; Hansson, Ostmark, Carlmark, & Malmström, 2009). The surface-initiated (SI) RDRP of polystyrene (PS) from CNC was initially reported in 2008, using atom-transfer radical-polymerization (ATRP) (Yi, Xu, Zhang, & Zhang, 2008). Subsequent investigations into the SI-ATRP of PS from CNCs were conducted by Thielemans and coworkers (Morandi, Heath, & Thielemans, 2009). They found that the grafting density could be tuned by varying the amount of reagents used in the initiator immobilization step. Furthermore, the grafted polymer was cleaved from the surface, proving that a good-control of the SI-ATRP was achieved (Morandi & Thielemans, 2012). Since these developments, various functional polymers have been grafted-from CNCs via Cu-mediated RDRP, including: PS (Morandi et al., 2009; Yi et al., 2008; Yin, Tian, Jiang, Wang, & Gao, 2016), poly(methyl acrylate) (PMA) (Wang, Roeder, Whitney, Champagne, & Cunningham, 2015), poly(methyl methacrylate) (PMMA) (Boujemaoui et al., 2015), poly(dimethylaminoethyl methacrylate) (Rosilo et al., 2014; Yi, Xu, Zhang, & Zhang, 2009), poly(*N*-isopropylacrylamide) (PNIPAm) (Hemraz, Lu, Sunasee, & Boluk, 2014; Zoppe, Habibi, & Rojas, 2010), PNIPAm fluorescent copolymers (Wu, Huang, & Pan, 2015), poly(*N*,*N*-dimethylacrylamide) (Zoppe, Xu, & Känel, 2016), poly(2-aminoethylmethacrylate) and poly(2-aminoethylmethacrylamide) (Hemraz et al., 2015), poly(acrylic acid) through hydrolysis of poly(*tert*-butyl acrylate) (Majoinen, Walther, & McKee, 2011), poly(6-(4-(4-methoxyphenylazo)phenoxy)hexyl methacrylate) (Xu, Yi, Zhang, & Zhang, 2008) and copolymers of poly(MMA-*co*-butyl acrylate) (Yu, Wang, Wang, & Chu, 2016). As well as stimuli-responsive polymers, the grafting of more hydrophobic polymers with lower T_g values (e.g. PMA) is highly interesting in the application of polymer-grafted CNCs in nanocomposites, emulsions and adhesives, for example, due to the compatibilization these polymers afford between CNCs and hydrophobic liquids, matrices or surfaces.

Previously, Yagci and coworkers reported a temporal photoinduced Cu-mediated RDRP procedure for the polymerization of methyl methacrylate (Tasdelen, Uygun, & Yagci, 2011). Anastasaki, Nikolaou, & Zhang, 2014 utilized this technique for the homopolymerization of acrylates using low amounts of copper catalyst ($CuBr_2$) and ligand (Me_6TREN) in a UV box ($\lambda_{max} \approx 360$ nm) commonly used in nail salons (Anastasaki, Nikolaou, Zhang et al., 2014). Since 2014, this polymerization methodology has been further expanded by Haddleton and coworkers to include various functional monomers (Anastasaki, Nikolaou, & Simula, 2014), sequence control (Anastasaki, Nikolaou, & McCaul, 2015; Anastasaki, Nikolaou, & Pappas, 2014) and has been performed in ionic liquids (Anastasaki, Nikolaou, Nurumbetov, 2015). Due to the short reaction times, mild conditions and small amount of catalyst/ligand required, this UV-initiation presents itself as an ideal methodology for the SI-photoinduced RDRP from CNCs. Indeed, CNCs have recently been grafted with PS, PMMA, poly(2-isopropenyl-2-oxazoline) and poly(*N*-hydroxysuccinimide methacrylate) by photopolymerization (Hou et al., 2016). However, this approach proceeded via FRP and does not facilitate control over the density of initiating sites, polymer chain molecular weights or architectures as with RDRP techniques. The photoinduced Cu-mediated RDRP technique allows for low amounts of catalyst, low temperatures and mild conditions, whilst maintaining control over the polymer molecular weights, where other Cu-mediated RDRP techniques typically require 50-fold more catalyst, or the addition of a reducing agent. Additionally, we recently successfully applied the Cu-mediated photoinduced RDRP of methyl acrylate (MA) and diethylene glycol acrylate (DEGA) to SI grafting from a cellulose surface (filter paper) (Larsson, Pendergraph, Kaldeus, Malmström, & Carlmark, 2015). Successful grafting was evident through FT-IR and SEM characterization and thermoresponsive properties were endowed to the filter paper when PDEGA was present. Photoinduced Cu-mediated RDRP promises a facile, convenient approach to preparing polymer-grafted CNCs with control over the grafted polymer chains, potentially allowing various polymer architectures, compositions and grafting densities, while maintaining a low amount of Cu catalyst which leads to a more simple purification of the final product.

2. Materials and methods

2.1. Materials

α-Bromoisobutyryl bromide (BiB, 98%), ethyl α-bromoisobutyrate (EBiB, 98%), dimethylformamide (DMF, ≥99.9%), 4-(dimethylamino)pyridine (DMAP, 99%) and copper(II) bromide ($Cu(II)Br_2$, 99%) were purchased from Sigma Aldrich. Triethylamine (TEA, 99%) and dimethyl sulfoxide (DMSO, 99.0%) were purchased from Merck. Tris(2-(dimethylamino)ethyl)amine (Me_6TREN), was synthesized as reported elsewhere (Ciampolini & Nardi, 1966). Methyl acrylate (MA, 99%) was purchased from Aldrich and passed through a column of basic aluminium oxide prior to use. All materials were used as received unless stated otherwise.

2.2. Instrumentation

^1H NMR spectra were recorded at room temperature with a Bruker Avance 400 MHz spectrometer, using d_6-DMSO as the deuterated solvent. Tetramethylsilane (TMS) and the solvent residual peak were used as internal standards.

Fourier transform infrared spectroscopy (FT-IR) was performed using a Perkin-Elmer Spectrum 2000 FT-IR equipped with a MKII Golden Gate, single reflection ATR System from Specac Ltd, (London, UK). The ATR-crystal used was a MKII heated Diamond 45° ATR Top Plate. For each spectrum 16 scans were recorded.

Size-exclusion chromatography (SEC) was used to determine average molar masses of PMA (number-average molar mass, M_n, and weight-average molar mass, M_w) and molar-mass dispersity ($Đ_M = M_w/M_n$) using a Malvern Viscotek GPCmax system equipped with a Viscotek VE3580 RI detector, a TGuard column and 2 LT4000L columns with THF as the mobile phase at 35 °C and a flow rate of 1.0 mL min^{-1}. A conventional calibration method was employed using polystyrene standards and *N*,*N*-dimethylacetamide was used as the internal flow marker.

Thermogravimetric analysis (TGA) was performed to characterize thermal degradation profiles for the polymers and polymer-grafted CNCs using a TA Instruments Hi-Res TGA 2950 analyzer, operating under a N_2 flow of 30 mL min^{-1}, a heating rate of 10 °C min^{-1}, heating the samples from 40 to 700 °C.

Differential scanning calorimetry (DSC) measurements were performed with a DSC 1 from Mettler-Toledo. Samples were measured through a cycle of heating-cooling-heating, with a starting temperature of −50 °C, up to 150 °C at a heating/cooling rate of 10 °C min^{-1}, under a N_2 flow of 30 mL min^{-1}. T_g values reported were taken from the second heating step.

Sessile drop water contact angles were measured on films prepared by drop casting each sample from a 1 wt% dispersion in THF onto a glass slide which had previously been cleaned with acetone and ethanol. The measurements were conducted at 50% RH and 23 °C on a KSV instrument CAM 200 equipped with a Basler A602f camera, using 5 μL droplets of MilliQ water. A Young-Laplace fitting model was used to process the images. Contact angle values reported were those observed after 30 s of measurement. Measurements were performed in triplicate.

X-ray diffraction (XRD) samples were prepared by freeze drying unmodified and BiB-CNCs and vacuum drying purified CNC-g-PMA$_{50}$, CNC-g-PMA$_{300}$, and CNC-g-PMA$_{600}$. Measurements were performed using a Bruker D8 DAVINCI diffractometer with a cobalt sealed tube source (λ_{avg} = 1.79026 Å), 35 kV, 45 mA with a parallel focus Goebel Mirror, 0.5 mm micro-slit and 0.5 mm short collimator over a 2θ range of 8–45°. Si wafer blanks were subtracted from all measurements. Percent crystallinity was determined by deconvolution using the cellulose I single crystal information file (CIF) with a linear background and a fixed amorphous peak at 21.4°. A pseudo-voigt function was used to fit peak intensity and peak shape. While XRD fitting methods are highly debated (Ahvenainen, Kontro, & Svedström, 2016; Driemeier 2014; Driemeier & Calligaris, 2011; Oliveira & Driemeier, 2013) we note that fitting is done internally consistent making the comparison between unmodified and polymer-grafted CNCs valid and the error in these measurements is taken to be 1–2%.

X-ray photoelectron spectroscopy (XPS) samples of blank-CNCs and BiB-CNCs were prepared by freeze drying, while samples of CNC-*g*-PMA$_n$ were prepared by vacuum drying after purification. Spectra were recorded using a Physical Electronics (PHI) Quantera II spectrometer equipped with an Al anode source for X-ray generation and a quartz crystal monochromator for focusing the generated X-rays. A monochromatic Al K-α X-ray (1486.7 eV) source was operated at 50W 15 kV. The system base pressure was no higher than 1.0×10^{-9} Torr, with an operating pressure that did not exceed 2.0×10^{-8} Torr. A pass energy of 280 eV was used to obtain survey spectra and 26 eV for high resolution C1s. All spectra were obtained at 45° take off angles, and a dual beam charge compensation system for neutralization of all samples. The instrument was calibrated using a sputter-cleaned piece of Ag, where the Ag $3d_{5/2--}$ peak had a binding energy of 368.3 ± 0.1 eV and full width at half maximum for the Ag 3d--$_{5/2}$ peak was at least 0.52 eV. Data manipulation was performed using PHI MultiPak Version 9.4.0.7 software.

2.3. Methods and procedures

2.3.1. Preparation of CNCs through sulfuric acid hydrolysis

CNCs were prepared by sulfuric acid hydrolysis of cotton ashless filter aid as described previously (Cranston & Gray, 2006). Ground Whatman filter aid (40 g, Whatman ashless filter aid, GE Healthcare) was added to 64 wt.% sulfuric acid (700 mL) under mechanical stirring for 45 min at 45 °C, after which the reaction was quenched with cold purified water (resistivity of 18.2 MΩ cm, Barnstead NANOpure Diamond system, Thermo Scientific). The resulting suspension was then centrifuged at 6000 rpm for 10 min intervals until the excess acid was removed and the suspension no longer formed a pellet. The suspension was then further purified by dialysis against purified water for several days. Finally, the CNC suspension was sonicated using a probe sonicator (Sonifier 450, Branson Ultrasonics) for 45 min in an ice bath and filtered in order to remove metal particles from the probe sonication. The resulting cellulose nanocrystals (CNCs) contained 0.7 wt% sulfur (determined by conductometric titration (Beck, Method, & Bouchard, 2015) and confirmed with elemental analysis) which corresponds to 1.3×10^{20} equivalents of charge per g of cellulose. The CNCs had a zeta potential of −40 mV measured using a Zeta Potential ZetaPlus Analyzer (Brookhaven, USA) at 0.1 wt% with 10 mM added NaCl and average dimensions of approximately 120 nm × 12 nm measured by atomic force microscopy (MF*P*-3D, Asylum Research, Santa Barbara, CA).

2.3.2. Initiator immobilization on CNCs

BiB-CNCs were prepared by redispersing freeze dried blank-CNCs (2 g) in DMF (200 mL, final concentration of 1 wt%). The suspension was sonicated in a sonicator bath (Symphony ultrasonic bath, 35 kHz) for 45 min to ensure good dispersion. Triethylamine (3.34 g, 33 mmol) was added along with a catalytic amount of 4-dimethylaminopyridine and the flask was then sealed and degassed by bubbling argon while stirring for 15 min 2-Bromoisobutyryl bromide (4.60 g, 20 mmol) was then added dropwise and subsequently degassed for 5 min. The reaction was then sealed and placed in an oil bath at 70 °C for 18 h. The resulting product, BiB-CNCs, was purified by centrifugation and washing in ethanol (3×, 14 000 rpm, 10 min, 5 °C) then purified water (2×, 14 000 rpm, 10 min, 5 °C), dialyzed against purified water and freeze dried.

2.3.3. Photoinduced Cu-mediated RDRP of methyl acrylate

In a typical experiment, MA (2.0 mL, 22.1 mmol), EBiB (65 μL, 0.44 mmol), Me$_6$TREN (12.3 mg, 53 μmol), CuBr$_2$ (2.0 mg, 8.8 μmol) and DMSO (2.0 mL) were added to a vial and sealed with a septum. The reaction mixture was degassed with Argon for 15 min, after which it was placed inside the UV nail box to commence the polymerization. The UV nail box was equipped with four 9 W light bulbs, $\lambda_{max} \approx 360$ nm, as previously described by Haddleton and coworkers (Anastasaki, Nikolaou, Zhang et al., 2014). The polymers were obtained after 90 min exposure with an intensity of approximately 40 mW cm^{-2}. Samples were removed periodically and analyzed by ^{1}H NMR and SEC analyses. Following polymerization the reaction mixture was diluted with acetone, passed through a basic alumina column and concentrated *in vacuo*. The polymer was purified by precipitation into cold methanol and dried in a vacuum oven at 50 °C.

2.3.4. Photoinduced grafting-from BiB-CNCs

For the grafting-from CNC experiments the same procedure was followed for the photoinduced Cu-mediated RDRP polymerization of methyl acrylate described above, however, the DMSO used as the solvent was substituted for 1 wt% dispersions of BiB-CNCs in DMSO. In addition to this the polymerizations were scaled-up to ensure a higher mass of grafted CNCs was recovered for the appropriate analyses.

Following polymerization the reaction mixture was diluted with acetone and the free polymer and CNC-*g*-PMA were separated by centrifugation at 15 000 rpm for 20 min at 20 °C. The supernatant was collected and the pellet was redispersed in acetone and centrifuged twice more. The supernatant containing free polymer was purified as described above. The remaining CNC-*g*-PMA pellet was dried in a vacuum oven at 50 °C overnight before further analyses.

2.3.5. Photoinduced Cu-mediated RDRP of MA in the presence of blank-CNCs

The blank-CNCs in the presence of the RDRP of MA proceeded as described for the photoinduced Cu-mediated RDRP polymerization of methyl acrylate described above, however, the DMSO used as the solvent was substituted for 1 wt% dispersions of blank-CNCs in DMSO.

Following polymerization the reaction mixture was diluted with acetone and the free polymer and CNC-*g*-PMA were separated by centrifugation at 10,000 rpm for 20 min at 20 °C. The supernatant was collected and the pellet was redispersed in acetone and centrifuged twice more. The supernatant containing free polymer was purified as described above. The remaining pellet of blank-CNCs was dried in a vacuum oven at 50 °C overnight before further analyses.

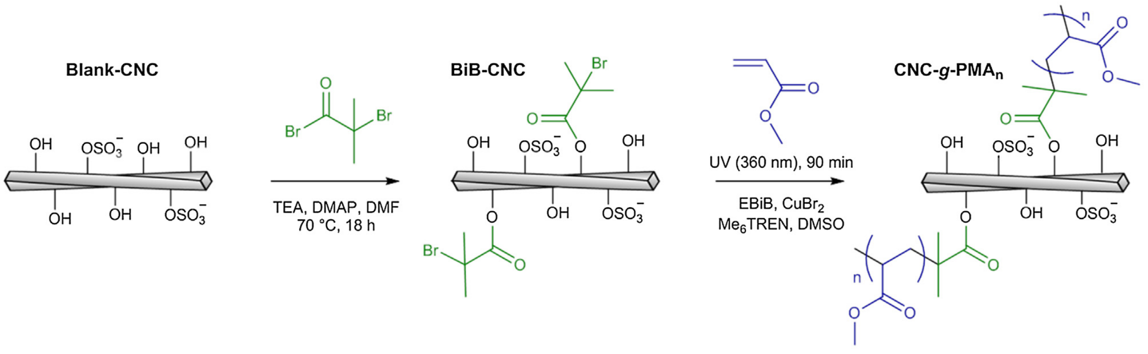

Scheme 1. Schematic representation of the initiator immobilization and the SI-photoinduced RDRP of MA from BiB-CNC.

3. Results and discussion

Expanding on our previous work, herein we describe the SI-photoinduced RDRP of MA from initiator-modified CNCs, as shown in Scheme 1. The aim is to demonstrate the applicability of this UV-induced procedure to nanocellulose as a facile, mild route to polymer grafting from CNCs, with a simple purification.

The CNCs used in this work were produced from the sulfuric acid hydrolysis of cotton and are individual rod-shaped nanoparticles ranging from 100 to 120 nm in length and 10 to 12 nm in cross section as determined by atomic force microscopy (Online Resource Fig. S1). Bromoisobutyryl bromide (BiB) was used in the esterification reaction with the hydroxyl groups on the CNC surface, following a previously described protocol; to yield initiator immobilized BiB-CNCs (Morandi et al., 2009; Zoppe et al., 2010). Characterization of the BiB-CNCs by FT-IR (Fig. 1) showed a small carbonyl peak at 1730 cm^{-1} corresponding to the carbonyl in the ester group in the initiating BiB group. Thermal gravimetric analysis (TGA, Fig. 2) showed a clear difference between the blank-CNCs and BiB-CNCs as the thermal stability was reduced in the BiB-CNCs, also observed by others (Hemraz et al., 2015; Wu et al., 2015). Whilst the sulfate half-ester groups present on the sulfuric acid hydrolyzed blank-CNC can lower the CNC thermal stability (Roman & Winter, 2004), the presence of the BiB group had more of an effect on lowering the thermal stability in this work. This was most likely due to the presence of Br, which upon heating may be cleaved from the CNCs to form HBr, causing accelerated acid degradation of the cellulose (Boujemaoui et al., 2015).

The grafting-from polymerizations were performed in DMSO with 1 wt% BiB-CNCs, maintaining a ratio of monomer:sacrificial initiator:catalyst:ligand ($MA:EBiB:CuBr_2:Me_6TREN$) of n:1:0.02:0.12, where n was 50, 300 or 600, depending on the targeted degree of polymerization (DP_n) of PMA. It is worth noting the low amounts of Cu and ligand needed here, compared to traditional Cu-mediated RDRP techniques. Ethyl α-bromoisobutyrate (EBiB) was added in the reaction medium as a sacrificial initiator which allowed for the targeting of the DP_n and provided unbound (free) polymer for analysis. After 90 min reaction time conversions between 89 and 92% were obtained, see Table 1. The free polymer and CNC-g-PMA were separated by centrifugation, and the CNC-g-PMA were further purified using centrifugation in acetone to remove unreacted monomer, copper, and ligand. This is significantly more straight-forward compared to the purification required after typical SI-ATRP of CNCs where up to 50 times the amount of copper is added, requiring several more centrifugation steps in order to isolate the modified CNCs. The supernatant containing the free polymer was purified and the free polymers were analyzed by size-exclusion chromatography (SEC) showing similar molecular weights and dispersities to the reference polymerizations conducted in the absence of the BiB-CNCs (Table 1). The kinetic evaluation of the free PMA_{300} in the CNC-g-PMA_{300} polymerization (Online Resource Fig. S2) showed that the

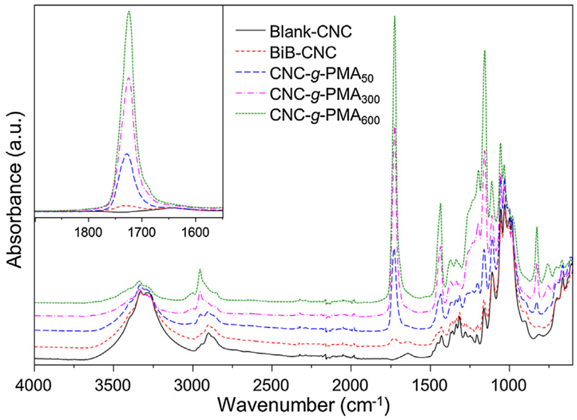

Fig. 1. FT-IR spectra overlaid and offset for blank-CNC, BiB-CNC and CNC-g-PMA_n samples, inset shows the increasing carbonyl peak with PMA graft length, in the region 1900–1650 cm^{-1} (not offset).

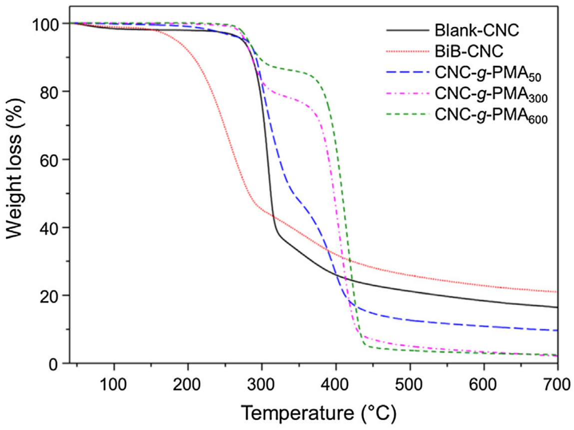

Fig. 2. Thermogravimetric weight loss curves for the blank-CNC, BiB-CNC and CNC-g-PMA_n samples.

Table 1
Conversion, molecular weights and dispersity indices of PMA_n synthesized by UV-photoinduced RDRP.

CNCs present	PMA DP_n	Conv[a] (%)	M_n[b] ($g\,mol^{-1}$)	M_w[b] ($g\,mol^{-1}$)	Đ[b]
–	50	90	5 000	5 300	1.07
	300	93	27 100	28 800	1.06
	600	92	47 700	51 900	1.08
Blank-CNCs	50	93	4 800	5 200	1.09
	300	92	25 600	27 700	1.08
	600	92	44 800	50 400	1.12
BiB-CNCs	50	91	5 300	5 700	1.08
	300	92	27 100	29 100	1.07
	600	89	46 500	51 100	1.10

[a] Calculated by ^1H NMR.
[b] Determined by SEC analysis utilizing tetrahydrofuran (THF) as eluent with conventional calibration using PS standards.

polymerization followed first order kinetics, with a linear increase in molecular weight with increasing conversion, in accordance with reference polymerizations (Online Resource Fig. S3), and as expected for a RDRP polymerization.

The presence of polymer grafts in the CNC-*g*-PMA_n samples was confirmed by FT-IR, TGA, differential scanning calorimetry (DSC), contact angle measurements (CA), x-ray photoelectron spectroscopy (XPS), X-ray diffraction (XRD) and redispersion in various organic solvents. With increasing DP_n of PMA the intensity of the carbonyl peak ($1730\,cm^{-1}$) observed by FT-IR increased drastically (Fig. 1), as did other peaks corresponding to the PMA segment (2950, 1440, 1155, and $825\,cm^{-1}$). The broad peak corresponding to the hydroxyl groups present in the CNC, 3100–3500 cm^{-1}, decreased with increasing PMA content accordingly. In TGA, Fig. 2, the thermal degradation patterns showed a clear difference between each sample and were used to estimate the relative wt% of CNC and PMA in the samples. The first derivatives of the weight loss curves showed two defined peaks corresponding to CNC and polymer content (Online Resource Fig. S4). From the inflection points of the first derivative curves the wt% content of CNC and PMA was estimated showing increased wt% of PMA with increasing target DP_n values (Table 2).

Comparable to previous studies, our blank-CNCs and CNC-*g*-PMA_n have the same onset of thermal degradation as other sulfuric acid-hydrolyzed CNCs at ca. 300 °C (Roman & Winter, 2004) (which is improved compared to the BiB-CNCs). The higher value of residue at the end of the TGA experiment for the BiB-CNC compared with the Blank-CNC can be ascribed to the blocking of primary oxide groups with the bromo ester which could possibly prevent the depolymerization of cellulose by acting as a flame retardant (Kandola, Horrocks, Price, & Coleman, 1996). This is in accordance to previous work performed in our group in which BiB-CNC was synthesized and analyzed by TGA (Boujemaoui, Mazieres, Malmström, Destarac, & Carlmark, 2016).

CNC-*g*-PMA_n samples also exhibited a secondary degradation curve which is shifted towards the onset of thermal degradation temperature of pure PMA, implying that our final modified CNCs possess degradation properties of both CNCs and PMA, which is in line with other reports of polymer-grafted CNCs prepared by ATRP (Majoinen et al., 2011; Zoppe et al., 2010).

DSC analysis was performed on the PMA homopolymers and the CNC-*g*-PMA_n samples (Online Resource Fig. S5, Table S1). The T_g values for samples PMA_{50}, PMA_{300} and PMA_{600}, were 5.3, 10.9, and 16.5 °C respectively, showing an increase in T_g with increasing polymer molecular weight. Analysis of the CNC-*g*-PMA_n samples showed that the T_g of the polymer in the grafted samples was 16.3, 19.8 and 21.3 °C for CNC-*g*-PMA_{50}, CNC-*g*-PMA_{300} and CNC-*g*-PMA_{600} respectively. This corresponds to an increase of 11, 8.9 and 4.8 °C of the T_g of the grafted PMA_n compared to the corresponding free polymer. This has also been observed in other polymer-grafted CNCs and is due to the reduced mobility of the grafted (i.e. tethered) polymer chains (Wang, Siqueira, & Muller, 2016; Zoppe et al., 2010). These results confirm that the polymers chains in the CNC-*g*-PMA_n samples were covalently bound to the CNC surface and were not simply free polymer *blended* with CNCs.

Water CA measurements of films prepared from the CNC samples on glass slides showed that the BiB-CNCs were more hydrophobic than the blank-CNCs as the contact angle increased from 11 to 36° (Table 2). The CNC-*g*-PMA_{50} sample showed a contact angle of 90° and the CNC-*g*-PMA_{300} and CNC-*g*-PMA_{600} samples showed very similar contact angles of 125 and 126°. This indicates that with increasing PMA content the contact angle increases, until the sample is almost entirely constituted of PMA.

High resolution carbon XPS spectra were obtained in order to deconvolute the C1 s peak; the C1 carbon (carbon bonded to no oxygen) was of primary interest. Theoretically, unmodified CNCs only contain C2 and C3 carbon peaks which correspond to carbon bonded to one and two oxygens, respectively. In our case, the control (blank-CNCs), had a small C1 peak (7.2%, Table 2), attributed to minor hydrocarbon-containing contaminants (Dorris & Gray, 1978a; Dorris & Gray, 1978b). BiB-CNCs showed an increase in C1 carbon due to the isopropyl group in the bromo-ester moiety. For the CNC-*g*-PMA_n samples, a distinct increase in C1 content due to the hydrocarbon polymer backbone was observed (46.1% for CNC-*g*-PMA_{50}, 52.9% for CNC-*g*-PMA_{300}, and 81.6% for CNC-*g*-PMA_{600}) corresponding to an increase in grafted polymer molecular weight with target DP_n.

The CNC crystalline morphology is maintained after grafting as evidenced by characteristic cellulose I peaks visible in the X-ray diffraction data (Table 2). See Online Resource Fig. S6 for the X-ray diffractograms. Upon modification with the BiB initiating group, BiB-CNCs had a lower degree of crystallinity compared to blank-CNCs (86.4% and 95.6%, respectively). This is due to the disruption of the crystalline structure at the surface of CNCs where initiator groups are attached. CNC-g-PMA_n with increasing DP similarly

Table 2
Weight% of CNCs and PMA in the samples determined by TGA, water CA of solvent cast films, and high resolution C1 peak from XPS of blank-CNC, BiB-CNC and CNC-g-PMA_n samples.

Sample	Wt% CNC[a]	Wt% PMA[a]	CA (°)[b]	C1%[c]	Degree of Crystallinity (%)[d]
Blank-CNCs	–	–	11 ± 2	7.2	96
BiB-CNCs	–	–	36 ± 1	14.4	87
CNC-g-PMA_{50}	61	39	90 ± 3	46.1	73
CNC-g-PMA_{300}	24	76	125 ± 1	52.9	46
CNC-g-PMA_{600}	15	85	126 ± 3	81.6	48

[a] Estimated from TGA analysis, average of duplicate samples.
[b] Standard deviation calculated over 3 measurements.
[c] Fitted from XPS high resolution carbon spectra.
[d] Determined using XRD.

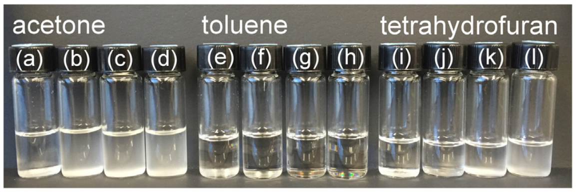

Fig. 3. (a) Photographs of blank-CNC and CNC-*g*-PMA$_n$ dispersed in various organic solvents; (a) blank-CNCs, (b) CNC-*g*-PMA$_{50}$, (c) CNC-*g*-PMA$_{300}$ and (d) CNC-*g*-PMA$_{600}$ in acetone; (e) blank-CNCs, (f) CNC-*g*-PMA$_{50}$, (g) CNC-*g*-PMA$_{300}$ and (h) CNC-*g*-PMA$_{600}$ in toluene; (i) blank-CNCs, (j) CNC-*g*-PMA$_{50}$, (k) CNC-*g*-PMA$_{300}$ and (l) CNC-*g*-PMA$_{600}$ in tetrahydrofuran. All blank-CNCs and CNC-*g*-PMA$_n$ suspensions were prepared at 0.1 wt% in the appropriate solvent.

resulted in a lower degree of crystallinity, as the degree of crystallinity was 72.5% for CNC-g-PMA$_{50}$, 45.9% for CNC-g-PMA$_{300}$ and 48.1% for CNC-g-PMA$_{600}$. The small increase from CNC-g-PMA$_{300}$ to CNC-g-PMA$_{600}$ is attributed to measurement error and is not statistically significant. The decrease in degree of crystallinity with increase in polymer grafting was expected and has been reported (Vandamme, Eyley, Van den Mooter, Muylaert, & Thielemans, 2015) and related the change in crystallinity to the amount of modification (i.e. grafted polymer increases the amorphous XRD peak). Using the assumption presented in their work, the percent polymer in the CNC-g-PMA$_{50}$ sample is calculated to be 23%, compared to 50% for CNC-g-PMA$_{300}$ and CNC-g-PMA$_{600}$. These values are comparable but lower than those determined by TGA.

These data support the composition of the CNC-g-PMA$_n$ samples, however, one further method which could be utilized would involve cleaving the polymer chains from the CNC surface for subsequent analysis. In several cases using a cleavable initiator has proven incredibly useful for this purpose (Hansson et al., 2013; Larsson et al., 2015; Morandi & Thielemans, 2012). However, it assumes that the reactivity of the initiating moiety in the cleavable initiator is the same as the non-cleavable initiator. In the case of hydrolysis of the sample (Wang et al., 2015), this also hydrolyses the ester bonds along the polymer chain resulting in poly(acids) which are typically troublesome to analyze by SEC, or require methylation for analysis. For this work we found that the amounts of PMA grafted from the CNCs increased as expected, with the relative increase in DP between samples, therefore we deemed it unnecessary to explore cleaving the polymer chains from the CNCs further.

Blank-CNCs, CNC-g-PMA$_{50}$, CNC-g-PMA$_{300}$, and CNC-g-PMA$_{600}$ samples were dispersed in acetone, toluene and THF as shown in Fig. 3. Unmodified CNCs settled to the bottom of the vials in all solvents, whereas the grafted CNCs dispersed to varying degrees, where increasing cloudiness indicates larger agglomerates of nanoparticles. The high transparency in toluene is due to refractive index matching of cellulose and toluene. Overall, compared to blank-CNCs, CNCs with all three PMA DPs show good dispersion in the organic solvents, implying that the grafted polymer allows for better compatibility between the CNC surface and the solvents tested.

It is well-known that UV irradiation of cellulose causes the formation of free radical species (Phillips, Hinojosa, Arthur, & Mares, 1966), however, in cases where UV light was used to initiate free radical grafting-from CNCs (Biyani, Jorfi, Weder, & Foster, 2014; Wang et al., 2016), and also light-induced cellulose cross-linking (Hufendiek, Carlmark, Meier, & Barner-Kowollik, 2016), no degradation of the CNCs has been reported. Therefore, to investigate the effects, if any, the UV irradiation had on the CNCs, and to show that UV-initiated free radical polymerization was not playing a significant role in the grafting reactions, blank-CNCs were introduced to the polymerizations. Dispersions of 1 wt% blank-CNCs in DMSO were prepared and subjected to identical conditions to the polymerizations described above. The conversions, molecular weights and dispersities of the free polymers were in accordance with those found for the PMA$_n$ synthesized in the presence of BiB-CNCs and the absence of any CNCs (Table 1). Kinetic evaluation of the PMA$_{300}$ free polymer in the presence of blank-CNCs was very similar to the corresponding polymerization with BiB-CNCs, see Online Resource Fig. S2, and also the reference polymerization in the absence of CNCs (Online Resource Fig. S3). The kinetic results and the agreement in molecular weights and dispersities between the PMA$_n$ free polymers and reference PMA$_n$ samples indicated that the presence of CNC in the polymerization mixtures did not adversely affect the polymerization mechanism. ^{1}H NMR and FT-IR analyses confirmed the PMA structure, see Online Resource Fig. S7 and S8 for typical spectra.

The characterization of each blank-CNC sample by FT-IR showed a small peak at 1730 cm^{-1} (Online Resource Fig. S9) corresponding to a carbonyl stretch, which could be attributed to small numbers of monomer units which are covalently bound to the CNC, or free polymer which had not been removed fully during the centrifugation purification step. TGA analyses of the blank-CNC-PMA$_n$ samples show very similar degradation patterns to the blank-CNCs (Online Resource Fig. S10), and very different degradation patterns from the homopolymers (Online Resource Fig. S11), indicating that little to no polymer grafting had occurred.

4. Conclusions

To conclude, we have prepared CNC-*g*-PMA$_n$ through a mild and facile surface-initiated *photoinduced* Cu-mediated reversible-deactivation radical polymerization technique. The inclusion of CNCs in the polymerization reaction appeared to have no effect on the polymerization of the free polymer, established using sacrificial initiator. It was also shown that the BiB immobilization on the CNC surface was necessary to achieve large amounts of grafted PMA chains from the CNC surface, which were clearly observable by FT-IR, TGA, XPS and XRD analyses. DSC analysis of the PMA$_n$ and CNC-*g*-PMA$_n$ provided evidence that the polymer grafts were indeed tethered to the CNC surface, due to an increase in the T_g compared with the free polymer. Redispersion of the modified CNCs in organic solvents showed that the CNC morphology was maintained while allowing for improved compatibility in acetone, toluene and THF compared to unmodified CNCs which are not colloidally stable in these solvents. The described technique provides an excellent route for the grafting of CNC owing to high levels of grafting in short reaction times with a facile purification. This stems from the fact that utilizing a UV source allows for the reduction in Cu concentrations by 50-fold. This enables the further application of this photoinduced Cu-mediated RDRP to achieve various compositions and architectures of polymer-grafted CNCs. These polymer-grafted CNCs may have use in emulsion stabilizing and composite applications, where the hydrophobic polymer allows for compatibilization between the CNCs and surrounding hydrophobic liquid or polymer matrix, and further investigations are being conducted.

Acknowledgements

We gratefully acknowledge Dr. Jamie Godfrey (KTH Royal Institute of Technology) for synthesizing Me$_6$TREN. Additional thanks to Dr. Danielle Covelli at the Biointerfaces Institute (McMaster University) for performing the XPS measurements and Victoria Jarvis at the MAX Diffraction Facility (McMaster University) for performing the XRD measurements. FH would like to thank the Tunholmen foundation for financial support. EC and SK are grateful to the Faculty of Engineering and VP International Affairs Office at McMaster University for financial support for SK to travel to

Sweden for this collaboration. Funding Sources: Tunholmen Foundation (FH), and Natural Sciences and Engineering Research Council of Canada (Discovery Grants RGPIN 402329) and Faculty of Engineering, McMaster University (SK, EC).

References

Ahvenainen, P., Kontro, I., & Svedström, K. (2016). Comparison of sample crystallinity determination methods by X-ray diffraction for challenging cellulose I materials. *Cellulose*, *23*, 1073–1086.

Anastasaki, A., Nikolaou, V., McCaul, N. W., et al. (2015). Photoinduced synthesis of α,ω-telechelic sequence-controlled multiblock copolymers. *Macromolecules*, *48*, 1404–1411.

Anastasaki, A., Nikolaou, V., Nurumbetov, G., et al. (2015). Synthesis of well-Defined poly(acrylates) in ionic liquids via copper(II)-mediated photoinduced living radical polymerization. *Macromolecules*, *48*, 5140–5147.

Anastasaki, A., Nikolaou, V., Pappas, G. S., et al. (2014). Photoinduced sequence-control via one pot living radical polymerization of acrylates. *Chemical Science*, *5*, 3536–3542.

Anastasaki, A., Nikolaou, V., Simula, A., et al. (2014). Expanding the scope of the photoinduced living radical polymerization of acrylates in the presence of CuBr2 and Me6-Tren. *Macromolecules*, *47*, 3852–3859.

Anastasaki, A., Nikolaou, V., Zhang, Q., et al. (2014). Copper(II)/tertiary amine synergy in photoinduced living radical polymerization: Accelerated synthesis of ω-Functional and α,ω-heterofunctional poly(acrylates). *Journal of the American Chemical Society*, *136*, 1141–1149.

Beck, S., Method, M., & Bouchard, J. (2015). General procedure for determining cellulose nanocrystal sulfate half-ester content by conductometric titration. *Cellulose*, *1*, 101–116.

Biyani, M. V., Jorfi, M., Weder, C., & Foster, E. J. (2014). Light-stimulated mechanically switchable: Photopatternable cellulose nanocomposites. *Polymer Chemistry*, *5*, 5716–5724.

Boujemaoui, A., Mongkhontreerat, S., Malmström, E., & Carlmark, A. (2015). Preparation and characterization of functionalized cellulose nanocrystals. *Carbohydrate Polymers*, *115*, 457–464.

Boujemaoui, A., Mazieres, S., Malmström, E., Destarac, M., & Carlmark, A. (2016). SI- RAFT /MADIX polymerization of vinyl acetate on cellulose nanocrystals for nanocomposite applications. *Polymer*, *99*, 240–249.

Braun, B., & Dorgan, J. R. (2009). Single-Step method for the isolation and surface functionalization of cellulosic nanowhiskers. *Biomacromolecules*, *10*, 334–341.

Carlmark, A., & Malmström, E. (2002). Atom transfer radical polymerization from cellulose fibers at ambient temperature. *Journal of the American Chemical Society*, *124*, 900–901.

Carlmark, A., & Malmström, E. E. (2003). ATRP grafting from cellulose fibers to create block-copolymer grafts. *Biomacromolecules*, *4*, 1740–1745.

Ciampolini, M., & Nardi, N. (1966). Five-coordinated high-spin complexes of bivalent cobalt, nickel, and copper with tris(2-dimethylaminoethyl)amine. *Inorganic Chemistry*, *5*, 41–44.

Cranston, E. D., & Gray, D. G. (2006). Morphological and optical characterization of polyelectrolyte multilayers incorporating nanocrystalline cellulose. *Biomacromolecules*, *7*, 2522–2530.

Dorris, G. M., & Gray, D. G. (1978a). The surface analysis of paper and wood fibers by ESCA (Electron spectroscopy for chemical analysis). I. application to cellulose and lignin. *Cellulose Chemistry and Technology*, *12*, 9–23.

Dorris, G. M., & Gray, D. G. (1978b). The surface analysis of paper and wood fibers by ESCA (Electron spectroscopy for chemical analysis). II. surface composition of mechanical pulps. *Cellulose Chemistry and Technology*, *12*, 721–734.

Driemeier, C., & Calligaris, G. A. (2011). Theoretical and experimental developments for accurate determination of crystallinity of cellulose I materials. *Journal of Applied Crystallography*, *44*, 184–192.

Driemeier, C. (2014). Two-dimensional Rietveld analysis of celluloses from higher plants. *Cellulose*, *21*, 1065–1073.

Eichhorn, S. J. (2011). Cellulose nanowhiskers: Promising materials for advanced applications. *Soft Matter*, *7*, 303–315.

Espino-Pérez, E., Domenek, S., Belgacem, N., Sillard, C., & Bras, J. (2014). Green process for chemical functionalization of nanocellulose with carboxylic acids. *Biomacromolecules*, *15*, 4551–4560.

Eyley, S., & Thielemans, W. (2014). Surface modification of cellulose nanocrystals. *Nanoscale*, *6*, 7764–7779.

Habibi, Y., Lucia, L. A., & Rojas, O. J. (2010). Cellulose nanocrystals: Chemistry, self-Assembly and applications. *Chemical Reviews*, *110*, 3479–3500.

Habibi, Y. (2014). Key advances in the chemical modification of nanocelluloses. *Chemical Society Reviews*, *43*, 1519–1542.

Hansson, S., Ostmark, E., Carlmark, A., & Malmström, E. (2009). ARGET ATRP for versatile grafting of cellulose using various monomers. *ACS Applied Materials & Interfaces*, *1*, 2651–2659.

Hansson, S., Trouillet, V., Tischer, T., Goldmann, A. S., Carlmark, A., Barner-Kowollik, C., et al. (2013). Grafting efficiency of synthetic polymers onto biomaterials: A comparative study of grafting-from versus grafting-to. *Biomacromolecules*, *14*, 64–74.

Hansson, S., Carlmark, A., Malmström, E., & Fogelström, L. (2015). Toward industrial grafting of cellulosic substrates via ARGET ATRP. *Journal of Applied Polymer Science*, *132*, 10.

Hatton, F. L., Malmström, E., & Carlmark, A. (2015). Tailor-made copolymers for the adsorption to cellulosic surfaces. *European Polymer Journal*, *65*, 325–339.

Hemraz, U. D., Lu, A., Sunasee, R., & Boluk, Y. (2014). Structure of poly(*N*-isopropylacrylamide) brushes and steric stability of their grafted cellulose nanocrystal dispersions. *Journal of Colloid and Interface Science*, *430*, 157–165.

Hemraz, U. D., Campbell, K. A., Burdick, J. S., Ckless, K., Boluk, Y., & Sunasee, R. (2015). Cationic poly(2-aminoethylmethacrylate) and poly(*N*-(2-aminoethylmethacrylamide) modified cellulose nanocrystals: Synthesis, characterization, and cytotoxicity. *Biomacromolecules*, *16*, 319–325.

Hou, L., Bian, H., Wang, Q., Zhang, N., Liang, Y., & Dong, D. (2016). Direct functionalization of cellulose nanocrystals with polymer brushes via UV-induced polymerization: Access to novel heterogeneous visible-light photocatalysts. *RSC Advances*, *6*, 53062–53068.

Hufendiek, A., Carlmark, A., Meier, M. A. R., & Barner-Kowollik, C. (2016). Fluorescent covalently cross-linked cellulose networks via light-induced ligation. *ACS Macro Letters*, *5*, 139–143.

Kan, K. H. M., Li, J., Wijesekera, K., & Cranston, E. D. (2013). Polymer-grafted cellulose nanocrystals as pH responsive reversible flocculant. *Biomacromolecules*, *14*, 3130–3139.

Kandola, B. K., Horrocks, A. R., Price, D., & Coleman, G. V. (1996). Flame-Retardant treatments of cellulose and their influence on the mechanism of cellulose pyrolysis. *Journal of Macromolecular Science, Reviews in Macromolecular Chemistry and Physics, C*, *36*, 721–794.

Kang, H., Liu, R., & Huang, Y. (2015). Graft modification of cellulose: Methods, properties and applications. *Polymer*, *70*, A1–A16.

Kedzior, S. A., Graham, L., Moorlag, C., Dooley, B. M., & Cranston, E. D. (2016). Poly(methyl methacrylate)-grafted cellulose nanocrystals: One-step synthesis, nanocomposite preparation, and characterization. *The Canadian Journal of Chemical Engineering* [n/a-n/a].

Klemm, D., Kramer, F., Moritz, S., Lindström, T., Ankerfors, M., Gray, D., et al. (2011). Nanocelluloses: A new family of nature-based materials. *Angewandte Chemie International Edition*, *50*(543), 8–5466.

Larsson, E., Pendergraph, S. A., Kaldeus, T., Malmström, E., & Carlmark, A. (2015). Cellulose grafting by photoinduced controlled radical polymerisation. *Polymer Chemistry*, *6*, 1865–1874.

Majoinen, J., Walther, A., McKee, J. R., et al. (2011). Polyelectrolyte brushes grafted from cellulose nanocrystals using Cu-mediated surface-initiated controlled radical polymerization. *Biomacromolecules*, *12*, 2997–3006.

Malmström, E., & Carlmark, A. (2012). Controlled grafting of cellulose fibres – an outlook beyond paper and cardboard. *Polymer Chemistry*, *3*, 1702–1713.

Moon, R. J., Martini, A., Nairn, J., Simonsen, J., & Youngblood, J. (2011). Cellulose nanomaterials review: Structure: properties and nanocomposites. *Chemical Society Reviews*, *40*, 3941–3994.

Morandi, G., & Thielemans, W. (2012). Synthesis of cellulose nanocrystals bearing photocleavable grafts by ATRP. *Polymer Chemistry*, *3*, 1402–1407.

Morandi, G., Heath, L., & Thielemans, W. (2009). Cellulose nanocrystals grafted with polystyrene chains through surface-Initiated atom transfer radical polymerization (SI-ATRP). *Langmuir*, *25*, 8280–8286.

Oliveira, R. P., & Driemeier, C. (2013). CRAFS: A model to analyze two-dimensional X-ray diffraction patterns of plant cellulose. *Journal of Applied Crystallography*, *46*, 1196–1210.

Phillips, G. O., Hinojosa, O., Arthur, J. C., & Mares, T. (1966). Photochemical initiation of free radicals in cotton cellulose. *Textile Research Journal*, *36*, 822–827.

Roman, M., & Winter, W. T. (2004). Effect of sulfate groups from sulfuric acid hydrolysis on the thermal degradation behavior of bacterial cellulose. *Biomacromolecules*, *5*, 1671–1677.

Rosilo, H., McKee, J. R., Kontturi, E., Koho, T., Hytonen, V. P., Ikkala, O., et al. (2014). Cationic polymer brush-modified cellulose nanocrystals for high-affinity virus binding. *Nanoscale*, *6*, 11871–11881.

Roy, D., Semsarilar, M., Guthrie, J. T., & Perrier, S. (2009). Cellulose modification by polymer grafting: A review. *Chemical Society Reviews*, *38*, 2046–2064.

Tasdelen, M. A., Uygun, M., & Yagci, Y. (2011). Photoinduced controlled radical polymerization. *Macromolecular Rapid Communications*, *32*, 58–62.

Vandamme, D., Eyley, S., Van den Mooter, G., Muylaert, K., & Thielemans, W. (2015). Highly charged cellulose-based nanocrystals as flocculants for harvesting Chlorella vulgaris. *Bioresource Technology*, *194*, 270–275.

Wang, H.-D., Roeder, R. D., Whitney, R. A., Champagne, P., & Cunningham, M. F. (2015). Graft modification of crystalline nanocellulose by Cu(0)-mediated SET living radical polymerization. *Journal of Polymer Science Part A: Polymer Chemistry*, *53*, 2800–2808.

Wang, J., Siqueira, G., Muller, G., et al. (2016). Synthesis of new bis(acyl)phosphane oxide photoinitiators for the surface functionalization of cellulose nanocrystals. *Chemical Communications*, *52*, 2823–2826.

Wu, W., Huang, F., Pan, S., et al. (2015). Thermo-responsive and fluorescent cellulose nanocrystals grafted with polymer brushes. *Journal of Materials Chemistry A*, *3*, 1995–2005.

Xu, Q., Yi, J., Zhang, X., & Zhang, H. (2008). A novel amphotropic polymer based on cellulose nanocrystals grafted with azo polymers. *European Polymer Journal*, *44*, 2830–2837.

Yi, J., Xu, Q., Zhang, X., & Zhang, H. (2008). Chiral-nematic self-ordering of rodlike cellulose nanocrystals grafted with poly(styrene) in both thermotropic and lyotropic states. *Polymer*, *49*, 4406–4412.

Yi, J., Xu, Q., Zhang, X., & Zhang, H. (2009). Temperature-induced chiral nematic phase changes of suspensions of poly(*N*,*N*-dimethylaminoethyl methacrylate)-grafted cellulose nanocrystals. *Cellulose*, *16*, 989–997.

Yin, Y., Tian, X., Jiang, X., Wang, H., & Gao, W. (2016). Modification of cellulose nanocrystal via SI-ATRP of styrene and the mechanism of its reinforcement of polymethylmethacrylate. *Carbohydrate Polymers*, *142*, 206–212.

Yu, J., Wang, C., Wang, J., & Chu, F. (2016). In situ development of self-reinforced cellulose nanocrystals based thermoplastic elastomers by atom transfer radical polymerization. *Carbohydrate Polymers*, *141*, 143–150.

Zoppe, J. O., Habibi, Y., Rojas, O. J., et al. (2010). Poly(*N*-isopropylacrylamide) brushes grafted from cellulose nanocrystals via surface-initiated single-electron transfer living radical polymerization. *Biomacromolecules*, *11*, 2683–2691.

Zoppe, J. O., Xu, X., Känel, C., et al. (2016). Effect of surface charge on surface-initiated atom transfer radical polymerization from cellulose nanocrystals in aqueous media. *Biomacromolecules*, *17*, 1404–1413.

Appendix 1: Chapter 4 Supporting Information

Electronic Supplementary Material

Grafting-from Cellulose Nanocrystals via Photoinduced Cu-mediated Reversible-Deactivation Radical Polymerization

Fiona L. Hatton,[a†] Stephanie A. Kedzior,[b] Emily D. Cranston[b] and Anna Carlmark[a,*]

[a]*KTH Royal Institute of Technology, School of Chemical Science and Engineering, Department of Fibre and Polymer Technology, Teknikringen 56, SE-100 44 Stockholm, Sweden*

f.l.hatton@sheffield.ac.uk, annac@kth.se

[†]*Present address: University of Sheffield, Department of Chemistry, Dainton Building, Brook Hill, Sheffield, S3 7HF, UK*

[b]*McMaster University, Department of Chemical Engineering, 1280 Main Street West, Hamilton, Ontario, L8S 4L7, Canada*

kedziosa@mcmaster.ca, ecranst@mcmaster.ca

*Email: annac@kth.se, Tel: +46(0)87908027

Electronic Supplementary Material

1. Experimental Section

1.1 Atomic Force Microscopy (AFM) samples were prepared by spin coating a 0.1 wt.% poly(allylamine hydrochloride) (PAH) layer (4000 rpm, 30 s, Chemat Technology KW-4A, USA) onto a Piranha-cleaned Si wafer. A 0.01 wt.% suspension of unmodified CNCs was then spin coated onto the PAH layer using the same procedure. The films were then dried at 80 °C overnight. Images were obtained using a MFP-3D atomic force microscope (Asylum Research an Oxford Instrument Company, Santa Barbara, CA) in tapping mode using a FMR Si probe from Nanoworld with a force constant of 2.8 N/m and a fundamental frequency of 75 kHz. The scan size was 5.0 µm × 5.0 µm and the image was obtained using a scan rate of 0.5 Hz and 512 dots per line.

2. Results

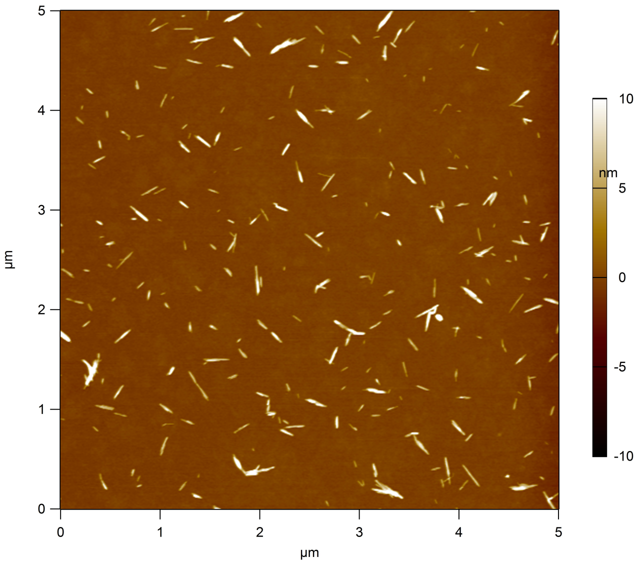

Fig S1. Atomic force microscopy height image (5 µm × 5 µm) of unmodified CNCs spin coated onto a Si wafer coated with a cationic poly(allylamine hydrochloride) precursor layer.

Electronic Supplementary Material

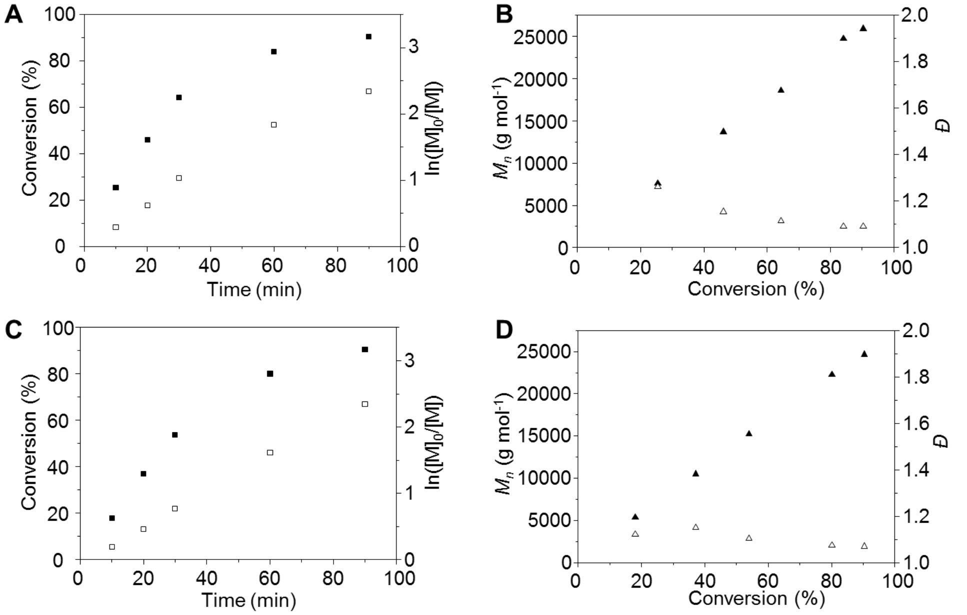

Fig. S2 Kinetic evaluation of free polymer PMA_{300} with blank and BiB-CNCs present; (A and B) blank-CNC-PMA_{300}, (C and D) CNC-*g*-PMA_{300}. Conversion (filled squares) and ln($[M]_0$/[M]) (open squares) *vs.* time (A, C), and M_n (filled triangles) and Đ (open triangles) *vs.* conversion (B, D).

Electronic Supplementary Material

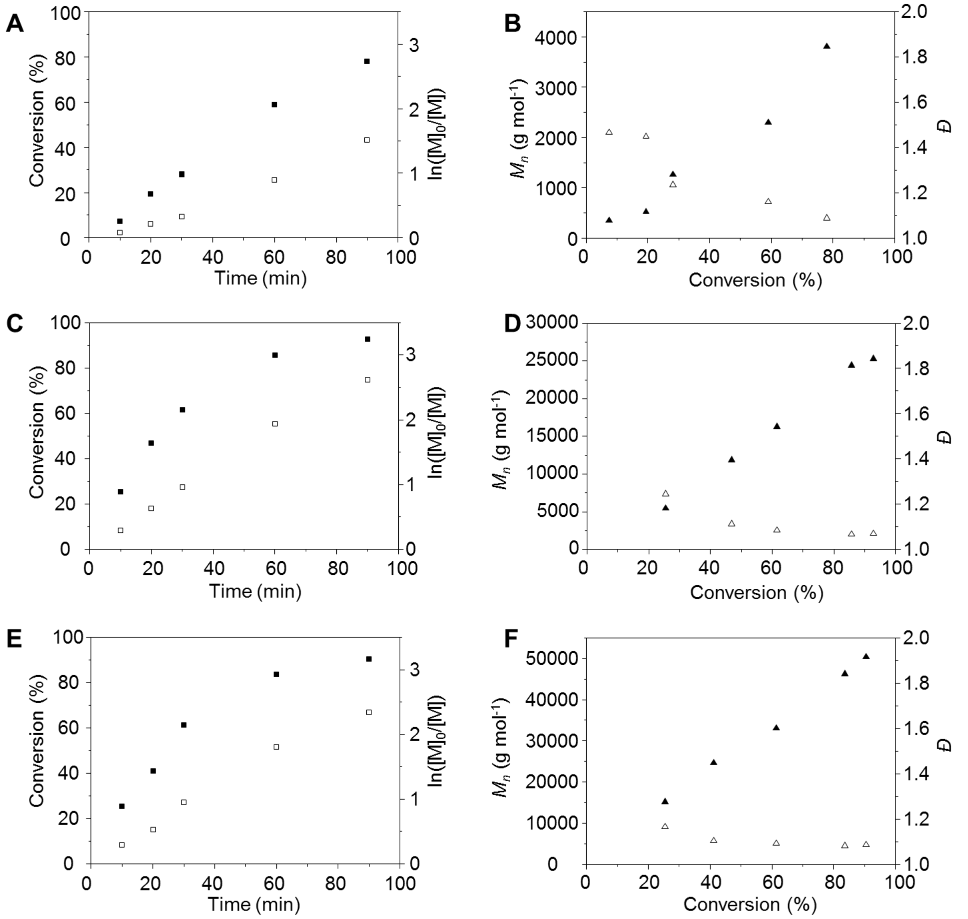

Fig. S3 Kinetic evaluation of polymerizations without CNCs; (A and B) PMA$_{50}$, (C and D) PMA$_{300}$ and (E and F) PMA$_{600}$. Conversion (filled squares) and ln([M]$_0$/[M]) (open squares) *vs.* time (A, C, E), and M_n (filled triangles) and Đ (open triangles) *vs.* conversion (B, D, F).

Electronic Supplementary Material

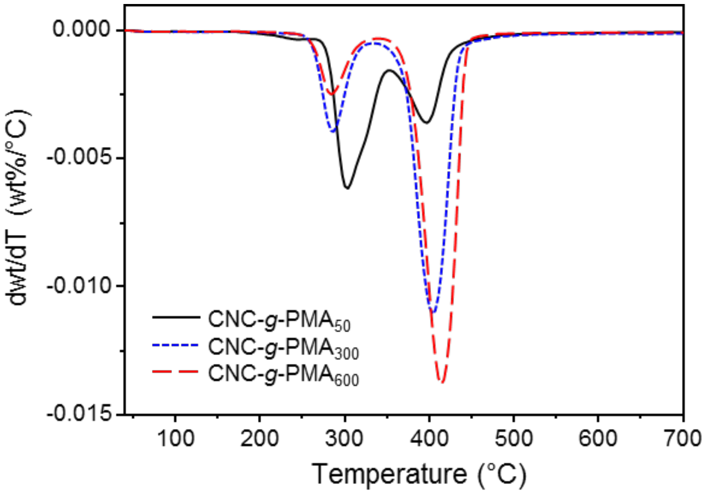

Fig. S4 Thermogravimetric derivative curves of the CNC-*g*-PMA$_n$ samples.

Table S1 Glass transition temperatures (T_g) for the PMA$_n$ homopolymers and CNC-*g*-PMA$_n$ graft copolymers.

Sample	T_g (°C)^a
PMA$_{50}$	5.3
PMA$_{300}$	13.9
PMA$_{600}$	16.9
CNC-*g*-PMA$_{50}$	16.3
CNC-*g*-PMA$_{300}$	20.4
CNC-*g*-PMA$_{600}$	20.7

^{a}Calculated from the 2nd heating curve, average of two runs

Electronic Supplementary Material

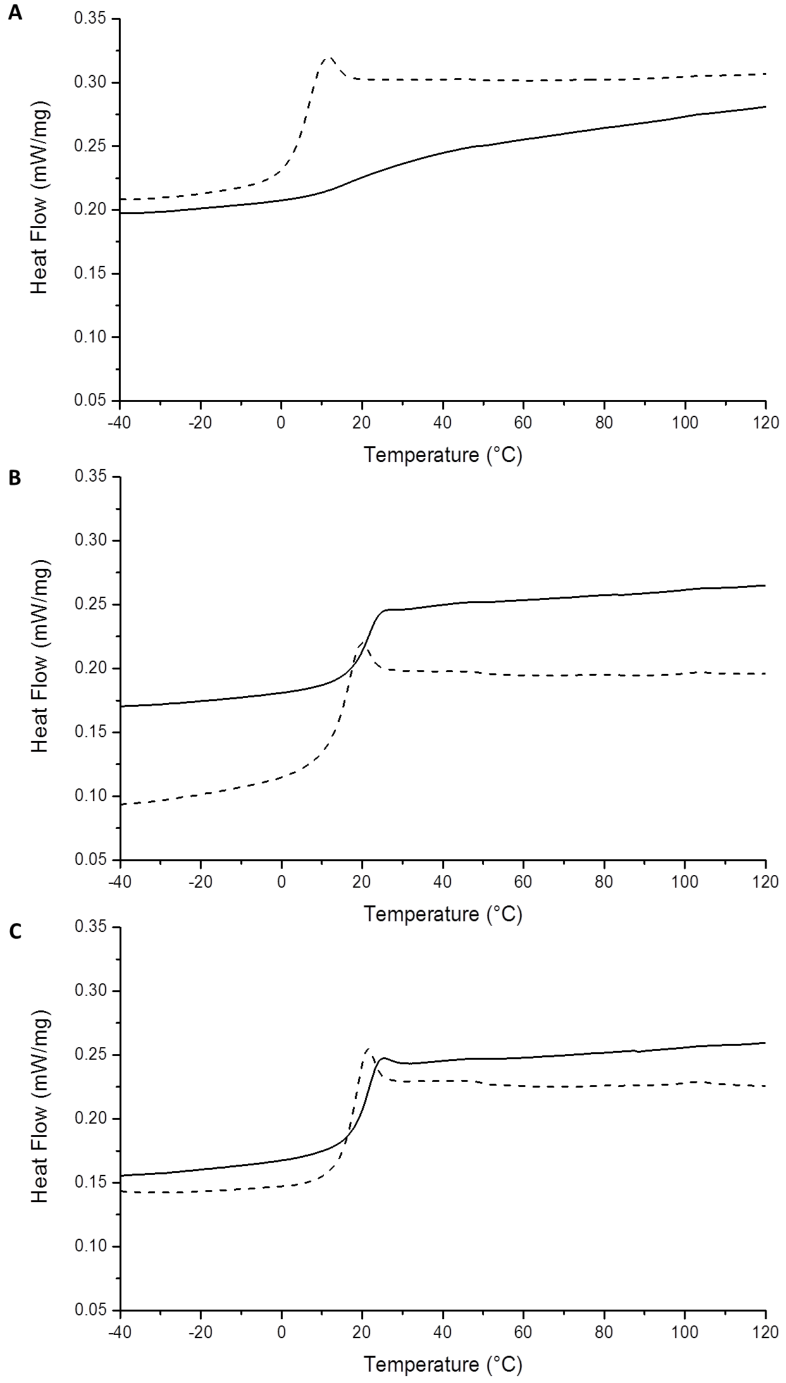

Fig. S5 DSC curve overlays from the 2nd heating cycle of PMA$_n$ homopolymers (dotted lines) and CNC-g-PMA$_n$ grafted samples (solid lines) for (A) n = 50, (B) n = 300 and (C) n = 600.

Electronic Supplementary Material

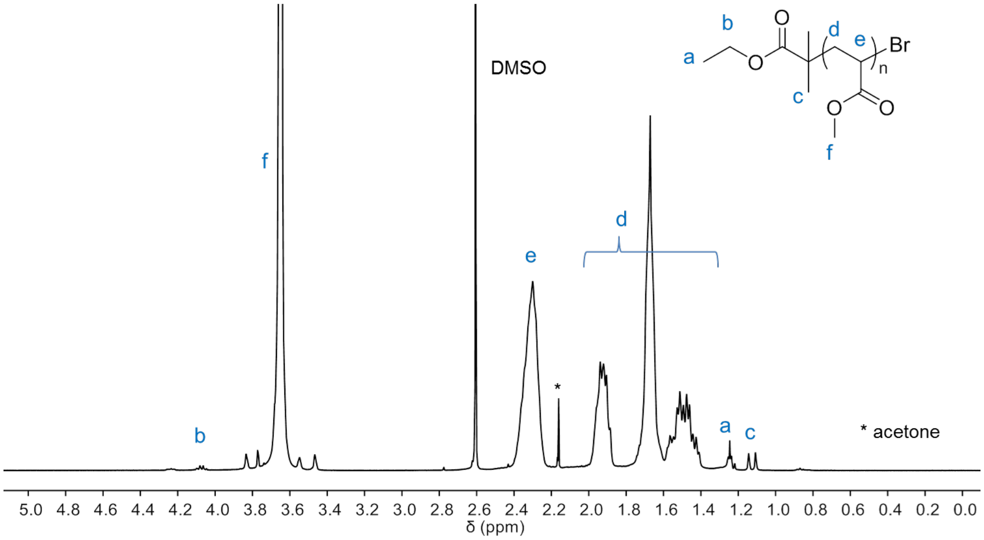

Fig. S6 ^{1}H NMR ($CDCl_3$, 300 MHz) spectrum of the PMA_{300} final polymer obtained from the polymerization conducted without CNCs present.

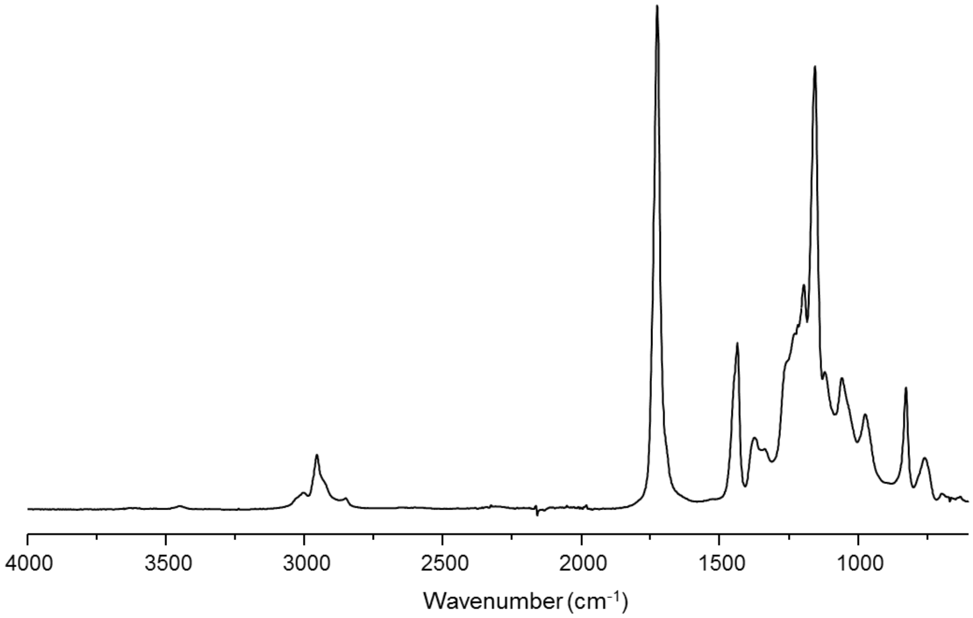

Fig. S7 FT-IR spectrum of the PMA_{300} final polymer obtained from the polymerization conducted without CNCs present.

Electronic Supplementary Material

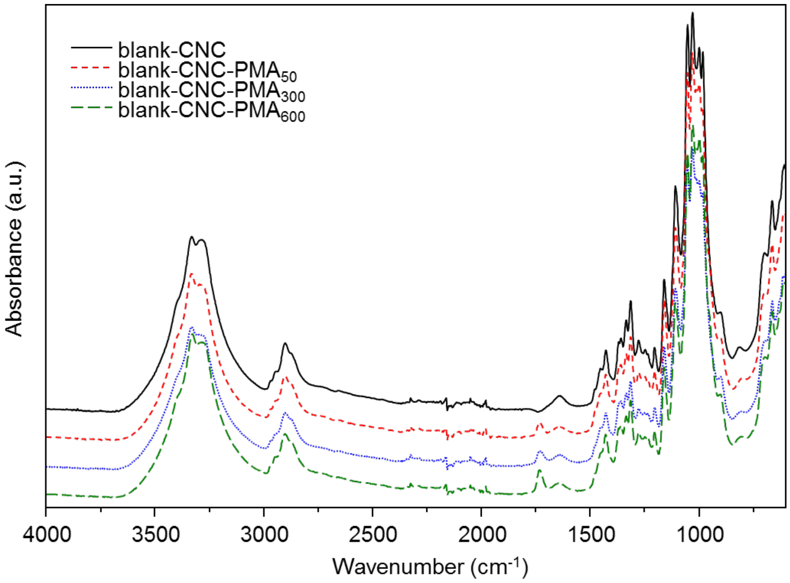

Fig. S8 Offset FT-IR spectra overlays of blank-CNC and the blank-CNC-PMA$_n$ samples.

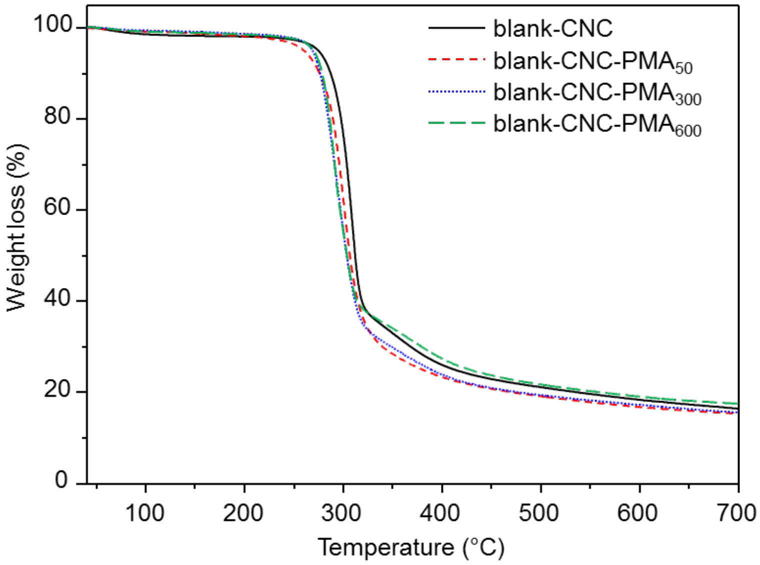

Fig. S9 Thermogravimetric weight loss curves of blank-CNC and the blank-CNC-PMA$_n$ samples.

Chapter 5

Liquids NMR Toolbox for the Analysis of Chemically Modified Nanocellulose.

In Chapter 3, a free radical polymer grafting technique was used to modify CNCs with PMMA. This modification resulted in CNCs with uncontrolled polymer graft lengths and graft densities and a large range of characterization techniques were used to infer the amount of grafted polymer. This chapter provides a novel NMR-based method to characterize polymer-grafted CNCs. PMMA-grafted CNCs were dissolved in ionic liquid and the grafted polymer was isolated by methanolysis. Solution state NMR was used to quantify the total polymer amount and degree of polymerization. A similar controlled polymer grafting method to that demonstrated in Chapter 4 (i.e. surface initiated atom transfer radical polymerization, SI-ATRP) was also used in this work to produce PMMA-grafted cellulose filter paper (in the presence of sacrificial initiator) which was used to confirm the new NMR method. This is the first report of using solution state NMR to quantify polymer-grafted CNCs when the polymer chains cannot be easily cleaved from the nanocrystals. This NMR method can be extended to other types of nanocellulose and other CNC surface modifications.

In this work, I prepared and characterized the PMMA-grafted CNCs via ceric-initiated free radical grafting. I also prepared the control samples of PMMA-grafted filter paper and determined the free polymer molecular weight by GPC. Dr. Alistair King (principle investigator at the University of Helsinki) carried out some of the NMR sample preparation, measurements and analyzed the data. Drs. Tiina Laaksonen (Analyst – Neste Oil), Ashley Holding (Consultant – Worn Again), Sami Heikkinen (University of Helsinki), and Valtteri Mäkelä (Professor – University of Helsinki) as well as Jussi Helminen (PhD Candidate – University of Helsinki) also contributed to optimizing the cellulose dissolution process, polymer cleavage and running of NMR experiments. The manuscript was drafted by myself and Dr. Alistair King and edited by my supervisor, Dr. Emily Cranston as well as Dr. Ilkka Kilpeläinen. This chapter will be submitted to the *Journal of the American Chemical Society* for publication.

Liquids NMR Toolbox for the Analysis of Chemically Modified Nanocelluloses
Alistair W. T. King, Stephanie A. Kedzior, Tiina Laaksonen, Ashley J. Holding, Jussi K. J. Helminen, Sami Heikkinen,Valtteri Mäkelä, Emily D. Cranston, and Ilkka Kilpeläinen
Journal of the Americal Chemical Society, to be submitted.

Liquids NMR toolbox for the analysis of chemically modified nanocelluloses.

Alistair W. T. King,*† Stephanie A. Kedzior,§ Tiina Laaksonen,† Ashley J. Holding,† Jussi K. J. Helminen,† Sami Heikkinen,† Valtteri Mäkelä,† Emily D. Cranston,§ Ilkka Kilpeläinen.*†

† Materials Chemistry Division, Chemistry Department, University of Helsinki, AI Virtasen Aukio 1, Helsinki, Finland, email: alistair.king@helsinki.fi, ilkka.kilpelainen@helsinki.fi

§ Department of Chemical Engineering, McMaster University, 1280 Main Street West, Hamilton, ON, L8S 4L7, Canada

KEYWORDS. *DOSY, HSQC, nanocellulose, polymer grafting, ionic liquid.*

ABSTRACT: Recent developments in ionic liquid electrolytes for cellulose or biomass dissolution has allowed for high-resolution ^{1}H and ^{13}C NMR on very high molecular weight cellulose. This allows for the development of advanced liquid-state quantitative NMR methods for characterisation of nano-structured celluloses, before and after chemical modification. As such, we present the use of tetrabutylphosphonium acetate ([P_{4444}][OAc]) in the 1 and 2D NMR characterization of cellulose nanocrystals (CNCs) and poly(methylmethacrylate) (PMMA)-grafted CNCs, as a difficult model to study. Diffusion filtered HSQC was shown to be effective in the discrimination between polymer grafts and low molecular weight peaks, arising from the solvent system. Bulk ratio of MMA to AGU was determined using a combination of HSQC and quantitative ^{13}C NMR. After recovery of the PMMA grafts through methanolysis, DOSY NMR was used to determine the average self-diffusion coefficient and hence molecular weight of the grafts, compared against self-diffusion coefficients for PMMA GPC standards, which finally lead to a rough calculation of both graft length and graft density.

INTRODUCTION

Nanocellulose (i.e. cellulose nanocrystals (CNCs) and cellulose nanofibrils (CNFs)) are currently being intensively researched for their applications, mainly in material science.[1–3] Many niche applications are under development, but for high volume applications the bulk areas of interest are in the formation of regenerated nanocelluloses and their composites (e.g. films[4,5] and staple fibres or yarn[6–9]), as surfactants or emulsion stabilizers,[10–13] as foam stabilizers,[14] or as rheology modifiers[15–17] and in packaging.[18–20] Many of these applications require topochemical modification at the nanocellulose surface to tune dispersion in particular media.[21] Typical examples of chemical modification to enhance the dispersion of nanocelluloses in aqueous media are surface 2,2,6,6-tetramethyl-1-piperidinyloxy (TEMPO) oxidation,[22–26] sulphate formation during hydrolysis[27] and carboxymethylation[28] which are used to increase electrostatic charge on the surface. Many of these techniques are applied during the initial isolation stages for preparation of nanocelluloses. Further chemical modifications can then be applied commonly to residual hydroxyl or carboxylate functionalities, to further tune dispersability or introduce additional functionality. Specific modifications of interest for bulk application include grafting polymers onto the surface of nanocelluloses in order to better compatibilize the particles within a hydrophobic polymer matrix, or to better disperse in a polar or non-polar solvent. These can be through typical ionic reaction mechanisms such as etherification or esterification reactions.[29] The degree of polymerization (i.e. chain length) and grafting density can be highly tuned, as is in the case of atom transfer radical polymerisation (ATRP),[30–34] although this is typically expensive and reserved for model studies or high-value applications. Alternatively, a potentially cheaper industrial method can be through radical grafting.[35–37] However, with this technique the introduction of radicals and grafting of monomers does not have very specific chemoselectivity and regioselectivity. As such, mechanistic understanding is difficult to come by when dealing with heterogeneous systems.

Methods for following the degree of reaction and selectivity of chemically modified nanocelluloses but of polymer-grafted-cellulose nanocrystals in particular, are mostly based on solid-state analyses. These are at best semi-quantitative and include X-ray photoelectron spectroscopy (XPS), ^{13}C-cross polarisation magic angle spinning (CP-MAS) nuclear magnetic resonance (NMR), ^{1}H-high resolution magic angle spinning (HR-MAS) NMR, attenuated total reflection (ATR)-IR spectroscopy and elemental analysis. Solution-phase analysis after hydrolysis is also problematic as the cellulose nanocrystals are often highly unreactive in < 65 % sulphuric acid, due to their highly crystalline state. Avoiding degradation under these conditions is very difficult. However, there is demonstrated potential for liquid-state quantitative analyses after dissolution into direct-dissolution solvents, such as ionic liquids.

Recently we demonstrated the dissolution and NMR analysis of different technical cellulose samples in the ionic liquid electrolyte methyltrioctylphosphonium acetate ([P_{8881}][OAc]):DMSO-d_6.[38] Using this system, it was possible to even run ^{1}H-^{13}C heteronuclear single quantum correlation (HSQC) NMR on high molecular weight samples, such as bacterial cellulose, due to the excellent solvating power and relatively low viscosity of the electrolyte at the concentrations prepared. Therefore, we would like to present our results concerning the use of a novel ionic liquid electrolyte and methods for analysis of a difficult to analyse model modified nanocellulose. This is poly(methyl methylacrylate)-grafted cellulose nanocrystals (PMMA-*g*-CNCs), prepared by Kedzior et al., through ceric ammonium nitrate initiated grafting of methylmethacrylate (MMA).[37] The PMMA-*g*-CNCs were determined to be nanocrystalline with similar dimensions and crystallinity (Cellulose I) to the starting CNCs. Grafting was confirmed using ^{13}C-CP-MAS, contact angle (increased hydrophobicity), thermogravimetric analysis (TGA) and XPS. However, the degree of incorporation of MMA vs cellulose, the number of surface attachment points and hence the graft length, were not accurately determined. Atomic force microscopy (AFM) results also suggested that chain-chain termination was not occurring to any significant degree as the PMMA-*g*-CNCs were easily redispersed in the bulk phase. As such, in the present publication we aimed to determine the polymer graft length and the grafting density of the samples using quantitative ^{1}H & ^{13}C, diffusion-ordered spectroscopy (DOSY) and several HSQC variants to investigate the possibility of decreasing or removing our ionic liquid signals and potentially increasing resolution.

EXPERIMENTAL

Preparation of the PMMA-*g*-CNCs (Model Nanocellulose)

PMMA-*g*-CNCs were prepared using the procedure by Kedzior et al.[37] following the scheme in Figure 1. In short, sulphuric acid hydrolysed CNCs dispersed in water were added to methylmethacrylate (MMA) monomer in nitric acid under a nitrogen blanket. After dispersion by sonication, the reaction was initiated by addition of ceric ammonium nitrate (CAN) in an ice bath under constant probe sonication. The PMMA-*g*-CNCs were then purified by centrifugation, dialysis, and stirred cell ultrafiltration in acetone. They were then solvent exchanged back to water and freeze dried for further analysis.

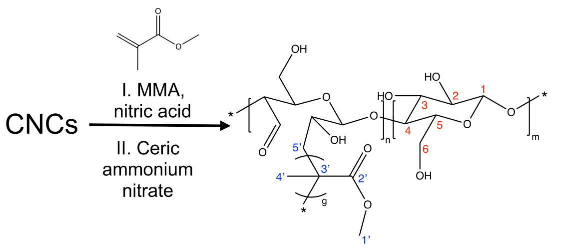

Figure 1. Preparation of PMMA-*g*-CNCs and numbering scheme used throughout the manuscript.[37]

Preparation of [P_{4444}][OAc]:DMSO-d_6 (NMR Solvent)

Tetrabutylphosphonium acetate ([P_{4444}][OAc]) was prepared according to a previous publication (Figure 2);[39] Tetrabutylphosphonium chloride ([P_{4444}]Cl, CYPHOS 443W, 80 wt% in water) was dried by rotary evaporation and the chloride anion was exchanged by addition of silver acetate in isopropyl alcohol (IPA). After settling and filtration through celite to remove excess salts, the IPA was evaporated away, fresh methanol was then added and evaporated to help remove traces of IPA and finally the product was dried under high vacuum to yield a crystalline material (mp 46 °C). To prepare the stock NMR electrolyte solution, [P_{4444}][OAc] was added to DMSO-d_6 in the w/w ratio of 1:4. This was found to be sufficient for dissolution of microcrystalline cellulose up to about 8 wt% before increasing viscosity prohibited transfer of the solution to the 5 mm NMR tube.

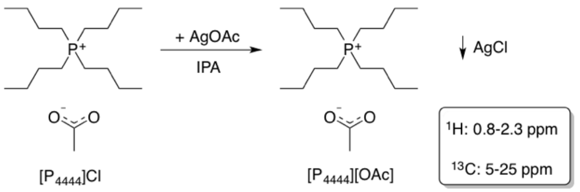

Figure 2. Preparation of [P_{4444}][OAc] and the spectral regions where the alkyl signals occupy.

Preparation of the CNC Solutions for NMR Analysis

CNC samples (40 mg of freeze-dried CNCs and PMMA-*g*-CNCs) were added to the stock solution of [P_{4444}][OAc]:DMSO-d_6 (1:4 w/w, 600 μL) and heated at 65 °C under argon for 1 hr. The samples were initially dispersed with a fine needle to avoid formation of gelled cellulose, which would dissolve over a longer period. Once the solutions were clear, the samples were then transferred into a 5 mm NMR tube for analysis.

Graft Cleavage Procedure

PMMA-*g*-CNCs were treated with a mixture of 1.27 M acetyl chloride in methanol (to generate 1.27 M hydrochloric acid in methanol) at 80 °C for 18 hr. After the treatment, the system was rotary evaporated to dryness and extracted into $CDCl_3$. DOSY NMR, utilising the bipolar pulse pair stimulated echo (BPPSTE)[40,41] pulse sequence was performed directly on this sample to determine the graft number-average molecular weight (DP_n), against DOSY-analysed PMMA gel-permeation chromatography (GPC) standards.

NMR Experiments

Standard ^{1}H and ^{13}C experiments were recorded for both CNC samples. Quantitative ^{13}C (inverse gated decoupling), HSQC[42-45], Carr-Purcell-Meiboom-Gill (CPMG[46,47])-filtered HSQC[48], diffusion-filtered HSQC and 1D diffusion-filtered HSQC experiments were collected for the PMMA-*g*-CNC sample. The diffusion-edited HSQC was achieved by applying the diffusion-editing at the start of the HSQCs first INEPT step. A

DOSY (BPPSTE) experiment was set up for analysis of the cleaved PMMA grafts and PMMA GPC standards (5 mg in 1 ml $CDCl_3$).

All spectra were processed using MestReNova 10.0,[49] (www.mestrelab.com) except the DOSY spectra which were processed using 'DOSY Toolbox' by Nilsson et al.[50] Self-diffusion coefficient (D_i, m^2/s) for the PMMA methyl ester (D_{Polm}) and residual $CHCl_3$ (D_{Solv}) were determined using the DOSY module in 'DOSY Toolbox' as follows: A 20 Hz Gaussian line broadening was applied and each increment was phased individually. Only the methyl ester and residual $CHCl_3$ regions were selected. A threshold was also applied to limit additional peaks on the baseline. Monoexponential fitting was then performed which yielded the average self-diffusion coefficients for the two resonances.

Calculation of Graft Ratio, Length and Density

The relative self-diffusion coefficients (D_{REL}) were obtained according to equation 1, where D_{Polym} and D_{Solv} are the self-diffusion coefficients for the graft and $CHCl_3$, respectively. These were then plotted against the number-average degree of polymerisation (DP_n) for the PMMA standards. This yielded a master curve for determination of graft lengths, which could be fitted with a power law relationship (R^2=0.99), shown in equation 2. This method of determination of polymer molecular mass is based on an article by Crutchfield et al.[52]

$$D_{REL} = \frac{D_{Polym}}{D_{Solv}} \qquad \text{(equation 1)}$$

$$DP_n = \frac{1.0849}{D_{REL}^{\;0.61}} \qquad \text{(equation 2)}$$

The PMMA graft to cellulose anhydroglucose unit (AGU) ratio ($R_{G/AGU}$) was determined from quantitative ^{13}C NMR by essentially integrating the cellulose resonances against the PMMA resonances, that were not overlapping with $[P_{4444}][OAc]$ or each other. The values were averaged for those peaks, or clusters of peaks, that could be cleanly integrated for each polymer, as follows: the average molar integral value for each polymer (EQ_S) was determined by initial summation of the integral values (I_x) divided by the number of carbons contributing to those resonances (N_C), for integrals χ in set S; where, for cellulose, S is C1 region (N_C=1), C2-5 region (N_C=4) and C6 region (N_C=1); where, for PMMA, S is C2′ (N_C=1) C1′& C5′ region (N_C=2) and C3′region (N_C=1). The summations were then divided by the number of separate resonances in each set that were integrated (C_S), to finally give EQ_S (equation 3). $R_{G/AGU}$ was then determined according to equation 4. The graft density (σ_G) was then determined according to equation 5.

$$EQ_S = \frac{1}{C_S} \times \sum_{x \in S} \frac{I_x}{N_C} \qquad \text{(equation 3)}$$

$$R_{G/AGU} = \frac{EQ_G}{EQ_{AGU}} \qquad \text{(equation 4)}$$

$$\sigma_G = \frac{R_{G/AGU}}{DP_n} \qquad \text{(equation 5)}$$

RESULTS AND DISCUSSION

Ionic Liquid Choice

While we have published the use of $[P_{8881}][OAc]$ for NMR analysis of cellulose,[38] $[P_{4444}][OAc]$ dissolves cellulose sufficiently for NMR analysis, even at a dilution of 80 wt% DMSO-d_6. At this concentration, it was possible to dissolve up to 10 wt% MCC but practically about 6-8 wt % is the maximum concentration that can be transferred into a 5 mm NMR tube, due to high viscosity and depending on the molecular weight of the analyte. $[P_{4444}][OAc]$ also contains a more symmetric cation and has less atoms than $[P_{8881}][OAc]$, which significantly reduces the potential for overlap of resonances in the saturated alkyl ppm range. Previously we have also demonstrated the utility of this electrolyte in analysing pretreated wood samples.[52] When dissolving cellulose, the use of a saturated tetraalkylphosphonium cation-containing electrolyte salts allows for no overlap of solvent peaks with the cellulose backbone signals in the ^1H and ^{13}C spectra (Figure 3). By comparison, dialkylimidazolium-based ionic liquids, e.g. 1-ethyl-3-methylimidazolium acetate ([emim][OAc]), have 2 α-alkyl signals at ~ 4 ppm; one for the 1 position and one for the

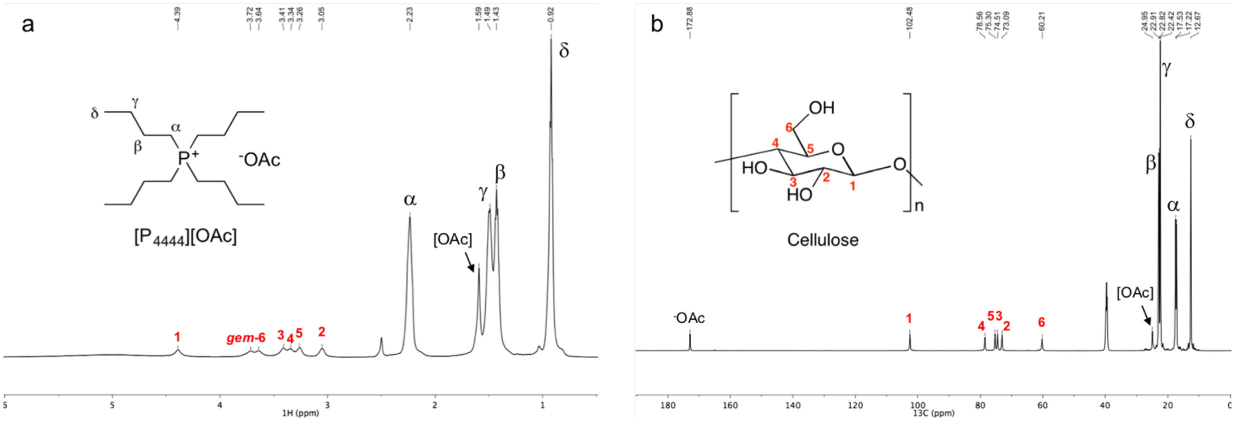

Figure 3. ^1H and ^{13}C spectra for the unmodified CNCs dissolved in $[P_{4444}][OAc]$:DMSO-d_6 (1:4 w/w).

3 position on the imidazolium ring. In the ^{13}C dimension, there is no overlap between the ionic liquid resonances and cellulose backbone. However, the more critical issue for developing an NMR solvent for this purpose is to avoid reaction between the solvent and the solute. In the case of cellulose, it is well known that [emim][OAc] will react with cellulose,[53-55] due to a combination of anion basicity and acidity of the imidazolium ring (carbene formation).[56] Fortunately, tetraalkylphosphoniums, with saturated alkyl chains, are much more thermally and chemically stable. They are also very effective at dissolving cellulose, but only as the electrolyte solutions with dipolar aprotic solvents, e.g. DMSO.[39] This does not matter as we require a locking solvent (DMSO-d_6). In addition, the more molecular co-solvent there is the lower the viscosity and therefore the higher the resolution.

Initial 2D Resonance Assignments and Resolution

A multiplicity-edited HSQC was performed on the sample dissolved in $[P_{4444}][OAc]$:DMSO-d_6 (Figure 4). 65 °C was found to be the most suitable temperature to maximise resolution and signal to noise. It was thought that higher temperatures might start to significantly degrade the cellulosic components. From Figure 4 it is obvious that we can clearly resolve the cellulose backbone peaks (Figure 4, in red) from the grafted PMMA chains (Figure 4, blue). It is also visible at this stage that the meso-racemo tetrads for 5′-CH_2s in the PMMA chains are somewhat separable. However, due to the high abundance of the ionic liquid peaks somewhat limiting dynamic range, overlapping with the PMMA 4′-Me triads and generally causing phasing problems (particularly with the multiplicity-edited spectra), full resolution and signal to noise are not adequate. Thus, we sought to improve either signal-to-noise and resolution, somehow.

Diffusion-Editing for Additional Resolution

To achieve this, we investigated the application of DOSY for separation of the high and low molecular weight components. This can be implemented as a ^1H 1D experiment or incorporated as single diffusion delay time diffusion-filtering into the HSQC pulse sequence (Figure 5).

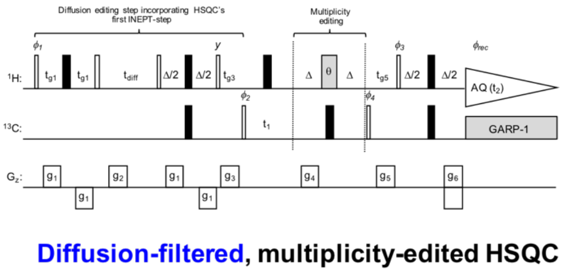

Figure 5. Implementation of pulsed-field gradients into the HSQC sequence.

Using this sequence, we found it possible to optimise the conditions for removal of the $[P_{4444}][OAc]$ signals from the 1D diffusion-edited HSQC, by initial optimisation of the diffusion gradient and then the post-diffusion gradient delay time (ms). An array of delay values showed the gradual disappearance of the $[P_{4444}][OAc]$ signals and evolution of both the cellulose backbone and PMMA-graft signals (Figure 6a). Similarly, optimisation of the DOSY (BPPSTE) experiment yielded a gradient array, stacked and normalised to the largest peak, which demonstrated the same thing, expectedly with much better signal-to-noise. Even from the ^1H DOSY we can see clear emergence of the PMMA-graft resonances, which greatly aids in identifying the polymeric material (Figure 6b).

After these promising results we analysed the PMMA-*g*-CNC sample, yielded a spectrum where we could significantly diminish the $[P_{4444}][OAc]$ signals from the spectrum, maximising the gain and thus dynamic range (Figure 7a). Naturally, however, incorporating the diffusion delay into the existing long HSQC pulse sequence is expected reduce signal to noise due to the short T_2 values typically demonstrated for the rigid

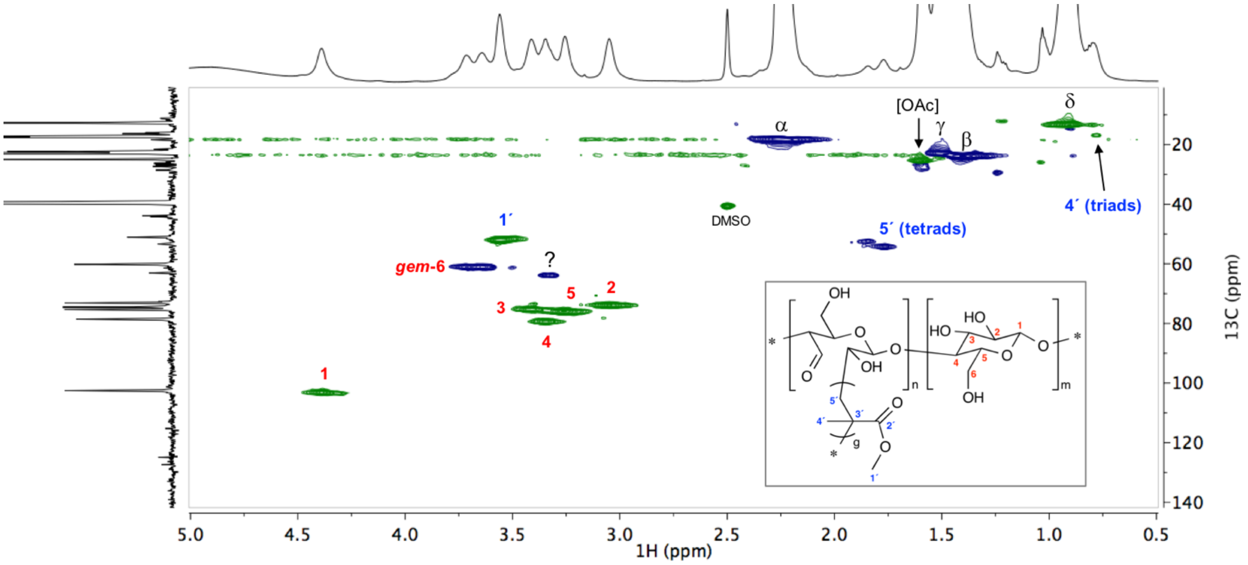

Figure 4. Multiplicity-edited HSQC spectrum for PMMA-*g*-CNCs dissolved in $[P_{4444}][OAc]$:DMSO-d_6 (1:4 w/w); The cellulose backbone resonances are numbered in red and the PMMA-graft resonances are numbered in blue.

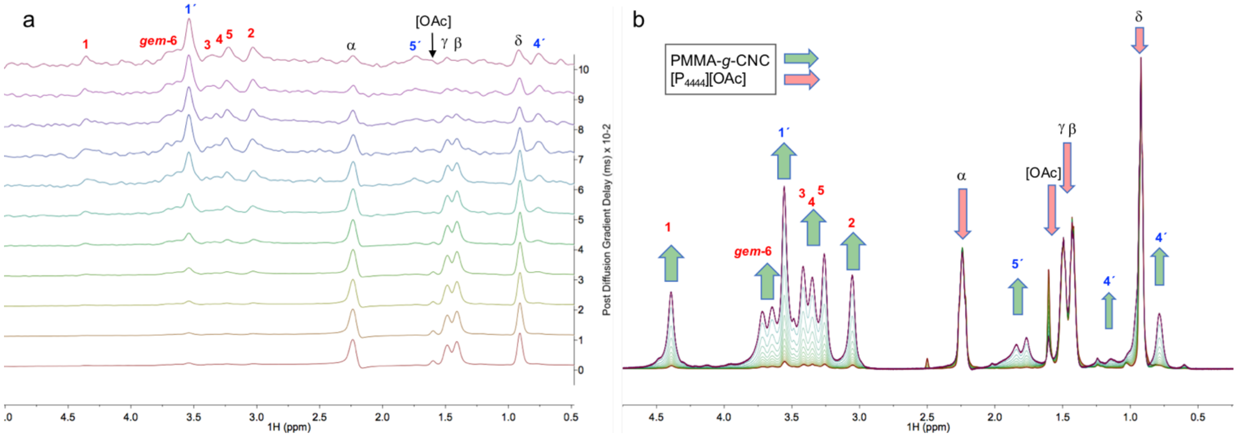

Figure 6. Arrayed spectra for: a) 1D HSQC with increasing post-gradient diffusion delay, b) DOSY with increasing gradient strength.

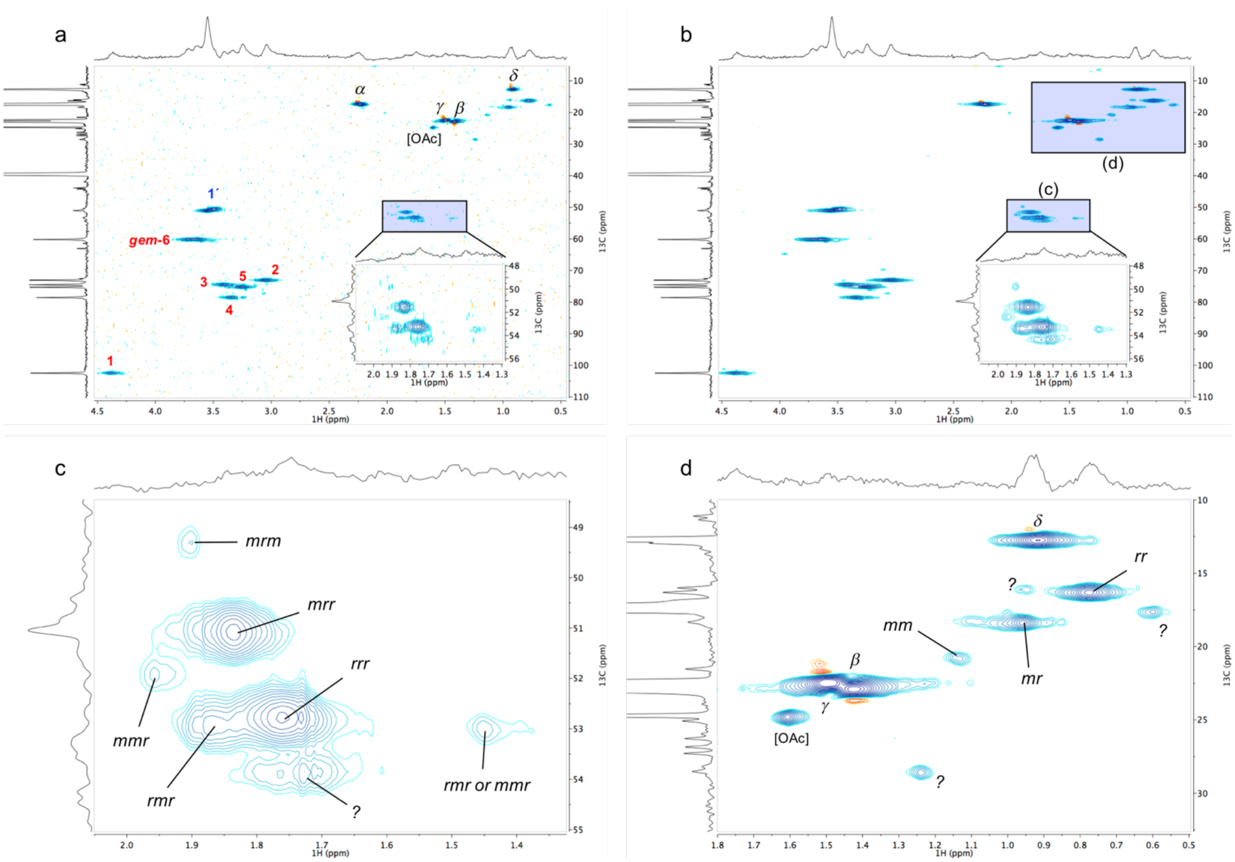

Figure 7. Diffusion-filtered HSQC spectra for PMMA-*g*-CNC in [P_{4444}][OAc]:DMSO-d_6: a) Initial post-processed spectrum, b) spectrum where the end of the FID was attenuated by 17 %, c) PMMA-graft CH_2 tetrad region, d) PMMA-graft Me triad region.

cellulose and PMMA polymers.

In these cases, with longer sequences, the acquisition phase does not begin until after the signal has started to decay so there is a compromise between how long the diffusion delay can be, before signal-to-noise is eroded. From Figure 7a we can see much better resolution for the PMMA-graft Me (triad) and PMMA-graft CH_2 (tetrad) regions. However, in this spectrum, the baseline noise is visible. Thus, we attenuated the fid (removal of 17 % from the end of the fid) in a bid to increase signal-to-noise, at the expense of resolution (Figure 7b). This allowed for a modest improvement in signal-to-noise of the PMMA-graft CH_2 region and further reduction in [P_{4444}][OAc] signals (long T_2). Resolution was still sufficient to assign and integrate the different tetrad peaks (Figure 7c). Assignments are based on previous assignments by Brar et al.[57] but new peaks are also apparent which do not have previous assignment in the literature. Similarly, the PMMA-graft Me region (Figure 7d) yielded 3 peaks which agreed with literature assignments by Goñi et al.[58] However, new polymeric peaks also appeared, which do not have literature assignments. At this point, further studies were not made to assign these peaks as our preliminary goal was to assess these electrolyte solutions for general resonance identification and quantitation, through the combination of accessible NMR techniques.

Quantification –Graft Ratio

Now that it is possible to assign the expected resonances in the PMMA-*g*-CNC sample, the real value of this procedure will be in the quantification of the grafting, for further process development. As mentioned previously, long pulse sequences, such as HSQC, with rigid polymeric materials suffer from attenuation of resonances with short T_2 values. This very much limits the potential for quantitative 2D analyses, unless the species for quantification are very similar. This might allow for determination of relative quantities of the species, *e.g.* for PMMA-graft CH_2s. Fortunately, we still have excellent resolution in the ^{13}C spectrum. A quantitative ^{13}C experiment was performed to determine the ratio of the graft ratio ($R_{G/AGU}$), *i.e.* molar ratio of methylmethacrylate (MMA) monomer to the bulk AGU. To minimise error, this was achieved by integrating the separable cellulose peak regions against the separable PMMA peak regions and averaging the values. A graft ratio ($R_{G/AGU}$) for MMA to AGU of 0.46 was determined, with a standard deviation of 0.058 between the different integral regions. The value determined through XPS by Kedzior et al.,[37] was 0.23; by determining the ratio of the peak areas for the PMMA carbonyl (C2´) and C1 in cellulose. While XPS is a quantitative technique to determine elemental composition, it very much depends on surface penetration depth on the nm scale, thus, surface layers give different values to bulk sample. In addition, while signal-to-noise is reasonably good,[37] resolution of the different carbons is poor, requiring deconvolution to determine the area compositions. While there are these sources of error to contend with, a rough estimate for $R_{G/AGU}$ can be given. By contrast, how to perform quantitative liquid 1D NMR is very well understood. Resolution of peaks is very good but the main limitation is signal-to-noise. In the NMR case a worthy standard deviation of 12.6 % is given from integration of the different peak regions.

Quantification – Graft Length and Density

These quantitative ^{13}C results, however, do not tell us anything about the graft length (DP_n, number average molecular weight for each graft) or graft density (σ_G, number of graft points per bulk AGU). To determine this, we must remove the grafts from the surface of the CNCs for molecular weight determination. This was achieved by treatment of the PMMA-*g*-CNCs with a methanolic HCl solution. A methanolic solution was chosen to avoid hydrolysis of the PMMA chains. This yielded a $CDCl_3$ soluble PMMA sample. DP_n for these grafts were determined by measuring and determining the relative (to $CHCl_3$) self-diffusion coefficients (D_{REL}) in $CDCl_3$. D_{REL} was calculated for the PMMA methyl ester peak. Monoexponential fitting was used to give a single value. DP_n was then calculated from the numerical relationship determined after measuring D_{REL} for PMMA gel-permeation chromatography (GPC) standards, of known DP_n values (Figure 8 and equation 2).

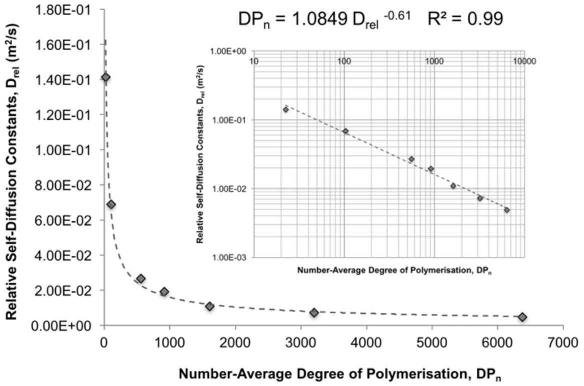

Figure 8. Master curves and equation for conversion of PMMA graft relative self-diffusion coefficient (D_{rel}), determined by DOSY, into the number-average degree of polymerization (DP_n).

The DP_n value was determined to be 168 through the DOSY method. For comparison, GPC (THF eluent) was also used for comparison and DP_n was determined to be 184, rather close to the NMR determination. A DP_n of 168 allowed for graft density (σ_G) determination of 0.0027 graft points per AGU. Or, $1/\sigma_G$ as 365 AGUs per PMMA graft. Or put more clearly, for a hypothetical cotton nanocrystal (cellulose source for the PMMA-*g*-CNCs) of 13 × 13 × 231 AGUs[59] (39039 AGUs), there are only 107 linkages per CNC. This is really a rather surprising result, as a higher value was expected. It should be noted that there is of course a small error with the quantitative ^{13}C but it is not significant enough to radically alter the graft density values. The graft cleavage procedure is also unoptimised. However, if degradation of the PMMA chains was occurring this would actually yield a lower graft density (grafts per CNC).

Future Developments and Best Practice

This work was designed to demonstrate the potential for liquids NMR on modified nanocelluloses and celluloses in general. So far, liquid-state analyses have been lacking due to the insolubility and general recalcitrance of nanocelluloses towards mild acid. The use of tetraalkylphosphonium acetate ionic liquids are key to the success of this due to their high chemical stability and cellulose-dissolving capability as the DMSO-d_6 electrolyte solutions. This technique should open the door to much more thorough characterisation of chemically modified nanocelluloses but can essentially be applied to all kinds of cellulose. From the analyses described herein, the main sources of error are in the initial quantification by ^{13}C NMR. To absolutely guarantee true quantitivity, T_1 values for ^{13}C should be determined but in reality, this takes too much spectrometer time due to the already poor signal-to-noise. In practise, a modest pre-relaxation delay time of 20 s was applied. A potentially larger source of error is the poor signal-to-noise afforded by quantitative ^{13}C, due to a combination of poor sensitivity towards ^{13}C and strictly applied delay times.

To achieve suitable signal-to-noise, many days collection times should be used on a probe sensitive for ^{13}C. If possible, averaging of integrals for different resonances should be applied to minimise errors due to incomplete relaxation. Thus, a compromise in sources of errors can be applied to minimise collection time and maximise sample throughput. Unfortunately, in NMR, signal-to-noise is proportional to the square root of the collection time. Therefore, maximising concentration, without compromising on resolution, is also necessary.

The method presented herein, for cleavage of grafts is also unoptimised. However, clearly it works in principal but should be validated in the future, using different well characterised samples. Within this method, hydrolysis or decarboxylation of PMMA may yield a polymer which has a different hydrodynamic radius in solution, which introduces error to the molecular weight determination. There is also potential for depolymerisation but significant depolymerisation is not apparent after this procedure and HSQC NMR analysis of the recovered grafts does not show significant degradation. In any case, different methods must be sought for different grafted polymers. Radical-initiated polymer grafting is also an extreme case as generation of radicals is often non-specific. Carbon-carbon bonds are also typically formed, which are difficult to break, requiring hydrolysis of the attached sugar. Functionality that can be introduced or cleaved through two electron transfer processes, e.g. esterifications, etherifications, should be easier to analyse, potentially allowing for assignment and integration of the attachment points or the functionality itself. Thus, in this case we have the drawback that we have not been able to identify these. The structure proposed in Figure 1 is also likely inaccurate, based on the many articles on CAN-initiated grafting onto cellulose. More than likely, the graft points are not specific to C2 or C3, aldehydes formed will be in the form of acetals and oxidation may preferentially occur at C6 or even the reducing end. This requires further detailed work with carefully prepared models to elucidate the mechanisms.

An additional feature of this method that would have been useful was if it would be possible to quantify surface sulphate groups, arising from sulphuric acid digestion of the cotton substrate. However, sulphate esters are known to be labile and are likely cleaved off by trace water in the samples. In the future, it may be possible to use a scavenger to bind and quantify sulphate esters. Storage of the NMR stock solution over molecular sieves would also be good practise.

CONCLUSIONS

It has been demonstrated that it is possible to determine graft ratio, length and density through liquids NMR analysis of PMMA-*g*-CNCs, derived from ceric ammonium nitrate initiated monomer grafting. This is a very difficult model to analyse as the attachment points are likely non-selective and have not been well defined in the literature for cellulose, compared to, *e.g.*, ATRP polymerisation where a reactive C2,3 or 6 ester forms the initiation point. In fact, prior to now there has been no high resolution methods to do this type of non-destructive quantitative analyses. While the ratio of MMA monomer to AGU was possible to determine using quantitative ^{13}C NMR, cleavage of the grafts by methanolysis and DOSY NMR analysis, against PMMA GPC standards allowed for an integrated method of determining also the graft length and density. It was found that for this specific PMMA-*g*-CNC sample, the grafting density (PMMA grafts per AGU or crystallite) was surprisingly low. Furthermore, diffusion-edited HSQC allowed for rough relative quantification of the tacticity of the PMMA grafts on the CNC backbone, after dissolution.

The media used for the dissolution is a highly chemically stable ionic liquid, $[P_{4444}][OAc]$, in DMSO-d_6. This of course not only dissolves nanocelluloses but can be applied to technical celluloses and many forms of chemically modified celluloses. Thus, the PMMA-*g*-CNCs served as a good model to demonstrate the potential of this method for process optimisation where the modified cellulose samples are not soluble in molecular solvents. This is particularly relevant for heterogeneous cellulose chemistry or reactions where very low DS products are formed.

AUTHOR INFORMATION

Corresponding Author

* alistair.king@helsinki.fi.

ACKNOWLEDGMENTS

The authors wish to acknowledge CLIC Innovation Oy for support under the Future Biorefinery (FuBio) and Advanced Cellulose to Novel Products (ACel) programs.

REFERENCES

(1) Kalia, S.; Dufresne, A.; Cherian, B. M.; Kaith, B. S.; Avérous, L.; Njuguna, J.; Nassiopoulos, E. Cellulose-based bio- and nanocomposites: A review. *Int. J. Polym. Sci.* **2011**, *2011*, 1–35 DOI: 10.1155/2011/837875.

(2) Klemm, D.; Kramer, F.; Moritz, S.; Lindström, T.; Ankerfors, M.; Gray, D.; Dorris, A. Nanocelluloses: a new family of nature-based materials. *Angew. Chemie* **2011**, *50* (24), 5438–5466 DOI: 10.1002/anie.201001273.

(3) Salas, C.; Nypelö, T.; Rodriguez-Abreu, C.; Carrillo, C.; Rojas, O. J. Nanocellulose properties and applications in colloids and interfaces. *Curr. Opin. Colloid Interface Sci.* **2014**, *19* (5), 383–396 DOI: 10.1016/j.cocis.2014.10.003.

(4) Lagerwall, J. P. F.; Schütz, C.; Salajkova, M.; Noh, J.; Hyun Park, J.; Scalia, G.; Bergström, L. Cellulose nanocrystal-based materials: from liquid crystal self-assembly and glass formation to multifunctional thin films. *NPG Asia Mater.* **2014**, *6* (1), 1–12 DOI: 10.1038/am.2013.69.

(5) Martin, C.; Jean, B. Nanocellulose / polymer multilayered thin films : tunable architectures towards tailored physical properties. *Nord. Pulp Pap. Res. J.* **2014**, *29* (1), 19–30.

(6) John, M. J.; Anandjiwala, R.; Oksman, K.; Mathew, A. P. Melt-spun polylactic acid fibers: Effect of cellulose nanowhiskers on processing and properties. *J. Appl. Polym. Sci.* **2013**, *127* (1), 274–281 DOI: 10.1002/app.37884.

(7) Hooshmand, S.; Aitom??ki, Y.; Skrifvars, M.; Mathew, A. P.; Oksman, K. All-cellulose nanocomposite fibers produced by melt spinning cellulose acetate butyrate and cellulose nanocrystals. *Cellulose* **2014**, *21* (4), 2665–2678 DOI: 10.1007/s10570-014-0269-4.

(8) Blaker, J. J.; Lee, K. Y.; Walters, M.; Drouet, M.; Bismarck, A. Aligned unidirectional PLA/bacterial cellulose nanocomposite fibre reinforced PDLLA composites. *React. Funct. Polym.* **2014**, *85*, 185–192 DOI: 10.1016/j.reactfunctpolym.2014.09.006.

(9) Hooshmand, S.; Cho, S.-W.; Skrifvars, M.; Mathew, A.; Oksman, K. Melt spun cellulose nanocomposite fibres: comparison of two dispersion techniques. *Plast. Rubber Compos.* **2014**, *43* (1), 15–24 DOI: 10.1179/1743289813Y.0000000066.

(10) Abitbol, T.; Marway, H.; Cranston, E. D. Surface modification of cellulose nanocrystals with cetyltrimethylammonium bromide. *Nord. Pulp Pap. Res. J.* **2014**, *29* (1), 46–57.

(11) Hu, Z.; Ballinger, S.; Pelton, R.; Cranston, E. D. Surfactant-enhanced cellulose nanocrystal Pickering emulsions. *J. Colloid Interface Sci.* **2015**, *439*, 139–148 DOI: 10.1016/j.jcis.2014.10.034.

(12) Capron, I.; Cathala, B. Surfactant-free high internal phase emulsions stabilized by cellulose nanocrystals. *Biomacromolecules* **2013**, *14* (2), 291–296 DOI: 10.1021/bm301871k.

(13) Kalashnikova, I.; Bizot, H.; Bertoncini, P.; Cathala, B.; Capron, I. Cellulosic nanorods of various aspect ratios for oil in water Pickering emulsions. *Soft Matter* **2013**, *9* (3), 952 DOI: 10.1039/c2sm26472b.

(14) Wege, H. A.; Kim, S.; Paunov, V. N.; Zhong, Q.; Velev, O. D. Long-term stabilization of foams and emulsions with in-situ formed microparticles from hydrophobic cellulose. *Langmuir* **2008**, *24* (17), 9245–9253 DOI: 10.1021/la801634j.

(15) Li, M. C.; Wu, Q.; Song, K.; Qing, Y.; Wu, Y. Cellulose nanoparticles as modifiers for rheology and fluid loss in bentonite water-based fluids. *ACS Appl. Mater. Interfaces* **2015**, *7* (8), 5009–5016 DOI: 10.1021/acsami.5b00498.

(16) Ureña-Benavides, E. E.; Ao, G.; Davis, V. A.; Kitchens, C. L. Rheology and Phase Behavior of Lyotropic Cellulose Nanocrystal Suspensions. *Macromolecules* **2011**, *44* (22), 8990–8998 DOI: 10.1021/ma201649f.

(17) Wu, Q.; Meng, Y.; Wang, S.; Li, Y.; Fu, S.; Ma, L.; Harper, D. Rheological behavior of cellulose nanocrystal suspension: Influence of concentration and aspect ratio. *J. Appl. Polym. Sci.* **2014**, *131* (15), 1–8 DOI: 10.1002/app.40525.

(18) Paunonen, S. Strength and Barrier Enhancements of Cellophane and Cellulose Derivative Films: A Review. *BioResources* **2013**, *8* (2), 3098–3121.

(19) Khan, A.; Huq, T.; Khan, R. a.; Riedl, B.; Lacroix, M. Nanocellulose-Based Composites and Bioactive Agents for Food Packaging. *Crit. Rev. Food Sci. Nutr.* **2014**, *54*, 163–174 DOI: 10.1080/10408398.2011.578765.

(20) Li, F.; Mascheroni, E.; Piergiovanni, L. The Potential of NanoCellulose in the Packaging Field: A Review. *Packag. Technol. Sci.* **2015**, *28*, 475–508 DOI: 10.1002/pts.

(21) Eichhorn, S. J. Cellulose nanowhiskers: promising materials for advanced applications. *Soft Matter* **2011**, *7* (2), 303 DOI: 10.1039/c0sm00142b.

(22) Habibi, Y.; Lucia, L. A.; Rojas, O. J. Cellulose Nanocrystals: Chemistry, Self-Assembly and Applications. *Chem. Rev.* **2010**, *110*, 3479–3500.

(23) Siró, I.; Plackett, D. Microfibrillated cellulose and new nanocomposite materials: a review. *Cellulose* **2010**, *17* (3), 459–494 DOI: 10.1007/s10570-010-9405-y.

(24) Moon, R. J.; Martini, A.; Nairn, J.; Simonsen, J.; Youngblood, J. *Cellulose nanomaterials review: structure, properties and nanocomposites*; 2011; Vol. 40.

(25) Saito, T.; Nishiyama, Y.; Putaux, J. L.; Vignon, M.; Isogai, A. Homogeneous suspensions of individualized microfibrils from TEMPO-catalyzed oxidation of native cellulose. *Biomacromolecules* **2006**, *7* (6), 1687–1691 DOI: 10.1021/bm060154s.

(26) Isogai, A.; Kato, Y. Preparation of polyuronic acid from cellulose by TEMPO-mediated oxidation. *Cellulose* **1998**, *5* (3), 153–164 DOI: 10.1007/s10570-008-9245-1.

(27) Beck-Candanedo, S.; Roman, M.; Gray, D. Effect of conditions on the properties behavior of wood cellulose nanocrystals suspensions. *Biomacromolecules* **2005**, *6*, 1048–1054.

(28) Wågberg, L. Decher, G.; Norgren, M.; Lindström, T.; Axnäs, K. The Build-Up of Polyelectrolyte Multilayers of Microfibrillated Cellulose and Cationic Polyelectrolytes. *Langmuir*, **2008**, *24 (3)*, 784-795.

(29) Habibi, Y. Key advances in the chemical modification of nanocelluloses. *Chem. Soc. Rev.* **2014**, *43* (5), 1519–1542 DOI: 10.1039/c3cs60204d.

(30) Carlmark, A.; Malmström, E. Atom Transfer Radical Polymerization from Cellulose Fibers at Ambient Temperature. *J. Am. Chem. Soc.* **2002**, *124* (6), 900–901 DOI: 10.1021/ja016582h.

(31) Carlmark, A.; Malmström, E. E. ATRP grafting from cellulose fibers to create block-copolymer grafts. *Biomacromolecules* **2003**, *4* (6), 1740–1745 DOI: 10.1021/bm030046v.

(32) Xiao, M.; Li, S.; Chanklin, W.; Zheng, A.; Xiao, H. Surface-initiated atom transfer radical polymerization of butyl acrylate on cellulose microfibrils. *Carbohydr. Polym.* **2011**, *83* (2), 512–519 DOI: 10.1016/j.carbpol.2010.08.011.

(33) Morandi, G.; Heath, L.; Thielemans, W. Cellulose nanocrystals grafted with polystyrene chains through Surface-Initiated Atom Transfer Radical Polymerization (SI-ATRP). *Langmuir* **2009**, *25* (14), 8280–8286 DOI: 10.1021/la900452a.

(34) Zoppe, J. O.; Habibi, Y.; Rojas, O. J.; Venditti, R. A.; Johansson, L. S.; Efimenko, K.; Österberg, M.; Laine, J. Poly(N - isopropylacrylamide) brushes grafted from cellulose nanocrystals via surface-initiated single-electron transfer living radical polymerization. *Biomacromolecules* **2010**, *11* (10), 2683–2691 DOI: 10.1021/bm100719d.

(35) Littunen, K.; Hippi, U.; Johansson, L. S.; Österberg, M.; Tammelin, T.; Laine, J.; Seppälä, J. Free radical graft copolymerization of nanofibrillated cellulose with acrylic monomers. *Carbohydr. Polym.* **2011**, *84* (3), 1039–1047 DOI: 10.1016/j.carbpol.2010.12.064.

(36) Kan, K. H. M.; Li, J.; Wijesekera, K.; Cranston, E. D. Polymer-grafted cellulose nanocrystals as pH-responsive reversible flocculants. *Biomacromolecules* **2013**, *14* (9), 3130–3139 DOI: 10.1021/bm400752k.

(37) Kedzior, S. A.; Graham, L.; Moorlag, C.; Dooley, B. M.; Cranston, E. D. Poly(methyl methacrylate)-grafted cellulose nanocrystals: One-step synthesis, nanocomposite preparation, and characterization. *Can. J. Chem. Eng.* **2016**, *9999*, n/a – n/a DOI: 10.1002/cjce.22456.

(38) Holding, A. J.; Mäkelä, V.; Tolonen, L.; Sixta, H.; Kilpeläinen, H.; King, A. W. T. Solution-State One- and Two-Dimensional NMR Spectroscopy of High-Molecular-Weight Cellulose. *ChemSusChem*, **2016**, *9*, 880-892.

(39) Holding, A. J.; Heikkilä, M.; Kilpeläinen, I., King, A. W. T. Amphiphilic and Phase-Separable Ionic Liquids for Biomass Processing, *ChemSusChem*, **2014**, *7*, 1422-1434.

(40) D. H. Wu, A. D. Chen, C. S. Johnson, *J. Magn. Reson. Ser. A*, **1995**, *115*, 260.

(41) A. Jerschow, N. Muller, *J. Magn. Reson*., **1997**, 125, 372.

(42) L. E. Kay and A. Bax, *J. Magn. Reson*. **1989**, *84*, 598.

(43) D. G. Davis, *J. Magn. Reson*. **1991**, *91*, 665.

(44) P. Schmieder, T. Domke, D. G. Norris, M. Kurz, H. Kessler and D. Leibfritz, *J. Magn. Reson*. **1991**, *93*, 430.

(45) W. Willker, D. Leibfritz, R. Kerssebaum and W. Bermel, *Magn. Reson. Chem.* **1993**, *31*, 287.

(46) H. Y. Carr, E. M. Purcell, Effects of Diffusion on Free Precession in Nuclear Magnetic Resonance Experiments. *Phys. Rev*., **1954**, *94*, 630-638.

(47) S. Meiboom, D. Gill, Modified Spin-Echo Method for Measuring Nuclear Relaxation Times, Rev. Sci. Inst., 1958, 29, 688-691.

(48) F. A. A. Mulder, C. A. E. M. Spronk, M. Slijper, R. Kaptein, R. Boelens, Improved HSQC experiments for the observation of exchange broadened signals. *J. Biomol. NMR*, **1996**, 8, 223-228.

(49) www.mestrelab.com

(50) Nilsson, M. The DOSY Toolbox: A new tool for processing PFG NMR diffusion data, J. Mag., Res., 2009, 200, 296-302.

(51) http://dosytoolbox.chemistry.manchester.ac.uk/dosytoolbox

(52) C. A. Crutchfield, D. J. Harris, Molecular mass estimation by PFG NMR spectroscopy. *J. Mag. Res*., **2007**, *185*, 179-182.

(52) Deb, S.; Labafzadeh, S. R.; Liimatainen, U.; Parviainen, A.; Hauru, L. K. J.; Azhar, S.; Lawoko, M.; Kulomaa, T.; Kakko, T.; Fiskari, J.; Borrega, M.; Sixta, H.; Kilpeläinen, I.; King, A. W. T. Application of mild autohydrolysis to facilitate the dissolution of wood chips in direct-dissolution solvents. *Green Chem*., **2016**, *18*, 3286-3294.

(53) T. Liebert, T. Heinze, *Bioresources*, **2008**, *3*, 576-601.

(54) G. Ebner, S. Schiehser, A. Potthast, T. Rosenau, *Tetrahedron Lett*., **2008**, *49*, 7322-7324.

(55) M. T. Clough, K. Geyer, P. A. Hunt, S. Son, U. Vagt, T. Welton, *Green Chem*., **2015**, *17*, 231-243.

(56) A. W. T. King, A. Parviainen, P. Karhunen, J. Matikainen, L. K. J. Hauru, H. Sixta, I. Kilpeläinen, *RSC Adv*., **2012**, *2*, 8020-8026.

(57) A. S. Brar, A. K. Goyal, S. Hooda, *Pure Appl. Chem*., **2009**, *81*, 389-415.

(58) I. Goñi, M. Gurruchaga, M. Valero, G. M. Guzmán, *Polymer*, **1992**, 33, 3089-3094.

(59) S. Elazzouzi-Hafraoui, Y. Nishiyama, J-L. Putaux, L. Heux, F. Debreuil, C. Rochas, *Biomacromol*., **2008**, *9*, 57-65.

Chapter 6

Tailoring Cellulose Nanocrystal and Surfactant Behavior in Miniemulsion Polymerization.

While Chapters 3 and 4 discussed covalent surface modification methods to impart new properties to CNCs, this chapter focuses on non-covalent modification via electrostatic interactions. This chapter aims to better understand the interactions between CNCs and the surfactants commonly used in latex synthesis. Anionic and cationic CNCs were combined with anionic and cationic surfactants and their binding was studied in suspension and using model CNC films. The surfactant-CNC combinations were used to stabilize the miniemulsion polymerization of methyl methacrylate; whether electrostatic interactions led to surfactant-modified CNCs or non-interacting surfactant-CNC pairs controlled the latex particle size and polymer molecular weight. This work aims to extend the use of CNCs in latex systems where surfactants are present and provides a method of incorporating CNCs into existing formulations to produce adhesives, paints and coatings.

In this work, I designed and performed all syntheses and characterization experiments except the colloid probe AFM measurements, carried out by Heera Marway (MASc student). I analyzed and interpreted all data and wrote the manuscript. The manuscript was edited by Heera Marway and my supervisor, Dr. Emily Cranston. This chapter and the Supporting Information (Appendix 2) are reprinted as they appear in *Macromolecules*, with permission from the American Chemical Society © 2017.

Tailoring Cellulose Nanocrystal and Surfactant Behavior in Miniemulsion Polymerization
Stephanie A. Kedzior, Heera S. Marway, and Emily D. Cranston
Macromolecules, **2017**, *50* (7), pp 2645-2655
DOI: 10.1021/acs.macromol.7b00516

Macromolecules
Article
pubs.acs.org/Macromolecules

Tailoring Cellulose Nanocrystal and Surfactant Behavior in Miniemulsion Polymerization

Stephanie A. Kedzior, Heera S. Marway, and Emily D. Cranston*

Department of Chemical Engineering, McMaster University, 1280 Main Street West, Hamilton, ON, Canada L8S 4L8

Supporting Information

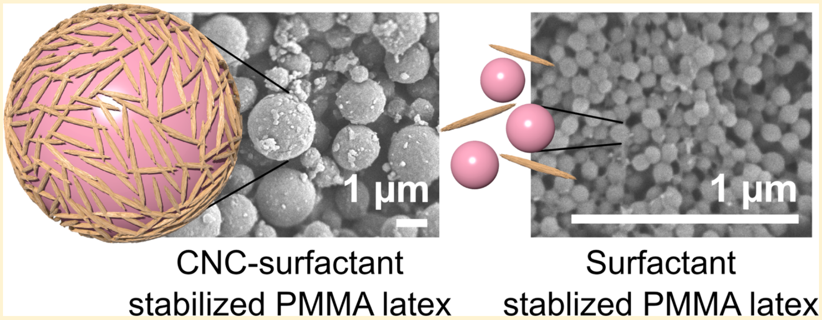

ABSTRACT: Cellulose nanocrystals (CNCs) combined with surfactants were used to stabilize miniemulsion polymerization reactions. Anionic CNCs with H^+ and Na^+ counterions and cationic-modified CNCs were investigated with anionic and cationic surfactants. When oppositely charged CNCs and surfactants were mixed, CNC size increased and absolute zeta-potential decreased, indicating surfactant adsorption and the ability to costabilize the monomer/water interface. Colloid-probe atomic force microscopy showed that surfactant adsorption to CNCs is strongly dependent on the CNC surface charge and counterion. Miniemulsion polymerization of poly(methyl methacrylate) (PMMA) was performed in the presence of CNC−surfactant mixtures; latexes were produced giving PMMA *nano*particles when there was no interaction between CNCs and surfactant and PMMA *micro*particles when CNCs and surfactant acted as costabilizers. This shows that CNCs can be used with surfactants to stabilize miniemulsion polymerization, reducing the need for a hydrophobe and leading to latexes with tunable properties (size, size distribution, surface charge, and polymer molecular weight) for coatings, adhesives, and household/personal care products.

INTRODUCTION

Cellulose nanocrystals (CNCs) are rigid, rod-shaped nanoparticles derived from renewable resources such as wood pulp and cotton.[1,2] Typically, a sulfuric acid hydrolysis is used to isolate the ordered (crystalline) nanoparticles from the disordered (amorphous) regions of the starting cellulosic material, resulting in stable colloidal suspensions. Hydrolysis with sulfuric acid grafts anionic sulfate half ester groups (OSO_3^-) on the CNC surface, which in the "acid form" possess an H^+ counterion. Acid-form CNCs may be neutralized using sodium hydroxide, effectively exchanging the counterion to sodium, a step necessary if the CNCs are to be dried and redispersed at a later time.[3] CNCs can also be rendered cationic by grafting trimethylammonium moieties to the surface using water-based epoxide chemistry.[4] This cationization requires a partial desulfation of CNCs prior to the grafting of cationic groups. Although the resulting CNCs have a net positive surface charge, both anionic and cationic surface groups are present. Controlling the type of counterion associated with CNCs as well as the overall surface charge density will play an important role in expanding the use of CNCs in formulated liquid products such as a variety of traditionally surfactant-based systems.

There has been a growing interest in using CNCs and surfactants together. Habibi et al. were the first to exploit electrostatic attraction between anionic CNCs and a cationic surfactant to prepare Langmuir−Schaefer model films.[5] Following that work, reports of modifying CNCs by adsorbing cationic surfactants and studying the governing parameters for adsorption have emerged. Dhar et al.[6] investigated the adsorption of cationic tetradecyltrimethylammonium bromide (TTAB) with anionic CNCs by isothermal titration calorimetry and showed that the formation of CNC−TTAB complexes are electrostatically driven, followed by hydrophobically driven micellization of TTAB on the CNC surface. This work was expanded upon by Brinatti et al.,[7] who studied the interactions between C_nTAB ($n = 12$, 14, and 16) and anionic CNCs. They identified the same driving forces for surfactant adsorption and micellization as Dhar et al. and furthermore showed that when the surfactant concentration was increased, charge neutraliza-

Received: March 9, 2017
Published: March 20, 2017

ACS Publications

DOI: 10.1021/acs.macromol.7b00516
Macromolecules 2017, 50, 2645−2655

tion and association of the surfactant-coated CNCs led to flocculation.[7] This indicates the delicate balance of surfactant adsorption and CNC colloidal stability which must be optimized if CNCs and surfactants are to be used in combination.

In other CNC and surfactant work, Salajková et al.[8] used quaternary ammonium surfactants to hydrophobically modify carboxylated CNCs. This study was intended as a facile surface modification route for CNCs and was similarly demonstrated using the more common sulfated CNCs with CTAB.[9,10] This modification is essentially an ion exchange reaction where the CNC counterion is exchanged for a bulky amphiphilic salt. Since these pioneering studies, cationic surfactant-modified CNCs have been used in the preparation of a range of materials including semiconducting nanoparticles,[11] poly(lactic acid) composites,[12,13] poly(lactic acid)−poly(hydroxybutyrate) blends,[14,15] metal nanoparticles,[16] nanoclay/epoxy composites,[17] drug delivery vehicles,[18] coatings,[19] and films.[20] However, to the best of our knowledge, no prior work has systematically studied the use of CNCs and surfactants as stabilizers for miniemulsion polymerization.

It was Capron and co-workers who recently discovered that CNCs can effectively stabilize oil−water interfaces and produce robust oil-in-water emulsions.[21−24] CNCs with higher aspect ratios and/or lower surface charge densities were found to be the best emulsion stabilizers.[22] To screen the surface charge on sulfated CNCs (with ca. 0.5 charges/nm^2), they demonstrated that salt can be added which allows CNCs to pack close enough to provide adequate oil droplet coverage,[22] in either a monolayer or a multilayer at the interface, depending on the surface charge.[25] To improve the inherent stabilizing properties of CNCs, their surface activity can be enhanced by covalently grafting polymer brushes,[26−28] small molecules,[29−33] and functional nanoparticles[34,35] or through adsorption of surface active polymers[36,37] and surfactants.[38] These surface modifications generally provide emulsions which are more stable to coalescence and eliminate the need to remove or screen CNC surface charge. This newly recognized amphiphilicity of CNCs, and ways to augment it, can also be taken advantage of to stabilize emulsion gels,[24] double emulsions,[30] water-in-water emulsions,[39] and dried oil powders,[38] which demonstrates the versatility of CNCs as Pickering stabilizers.

Despite the existing work on CNCs in emulsions, little work has examined emulsion or suspension polymerization with CNCs. In the few cases that have been reported, CNCs did not play a role in the monomer droplet or latex particle stabilization due to the choice of components.[40−43] For example, CNCs were shown to act as a nanofiller in the final composite when styrene and hexyl acrylate were copolymerized via miniemulsion polymerization using an anionic surfactant.[40,41] There was no driving force for the CNCs and surfactant to act as costabilizers due to their similar charge, and the TEM images indicated that the CNCs and latex particles remained as separate entities in the final dispersion.[40,41] Similarly, CNCs were blended with a poly(butyl acrylate-*co*-methyl methacrylate) latex prepared using an anionic surfactant in a traditional emulsion polymerization and were able to increase the mechanical properties of the resulting latex composite; however, the CNCs were added to the preprepared latex and therefore did not act as stabilizers during the polymerization.[42] Furthermore, Mabrouk et al.[43] prepared poly(butyl methacrylate) particles via miniemulsion polymerization with a cationic surfactant and anionic CNCs and found that due to electrostatic attraction the CNCs were anchored around the particles. Polymerizing polymers *in situ* with CNCs is one of the many routes that researchers have attempted to produce CNC−polymer composites (to overcome the general challenge of compatibilizing CNCs with hydrophobic polymers). In this work, we have used anionic and cationic surfactants with anionic and cationic CNCs to directly probe the difference between interacting costabilizers and noninteracting stabilizers to elucidate the range of roles that CNCs can play in miniemulsion polymerization specifically.

The interest in miniemulsion polymerization stems from the fact that uniform nanoscale particles of a wide range of polymers can be prepared, often allowing for an increase in solids content which is important for industrial applications of latexes. Miniemulsion polymerization is differentiated from traditional emulsion polymerization by the use of sonication to compartmentalize nanoscale monomer droplets (i.e., “nanoreactors” which have kinetics similar to bulk or solution polymerization) with limited diffusion of monomer during the reaction.[44] The addition of a hydrophobe is typically used to prevent droplet coalescence and monomer diffusion such that the size of the monomer droplets and corresponding polymer particles are the same.[45] Applications of latexes produced by miniemulsion polymerization include adhesives,[46] packaging films,[47] microencapsulation,[34] and drug delivery,[48] among many others.

Herein, we describe the use of anionic acid-form (H-CNCs), anionic sodium-form (Na-CNCs), and cationic cellulose nanocrystals (Cat-CNCs) with anionic and cationic surfactants as miniemulsion polymerization stabilizers. The interactions between surfactants and CNCs in suspension and on model surfaces were used to predict the ability of oppositely charged CNC−surfactant combinations to act as costabilizers during polymerization. This work aims to understand the fundamental interactions between CNCs and surfactants with the goal of expanding their use to emulsion polymerization systems. We believe this is a straightforward way to synthesize hybrid CNC−polymer materials which may find application in paints, coatings, and household and personal care products and whereby CNCs may enhance the mechanical, adhesive, rheological, shelf life, and structural properties of latex products.

■ EXPERIMENTAL SECTION

Materials. 2,3-Epoxypropyltrimethylammonium chloride (EPTMAC), cetyltrimethylammonium bromide (CTAB) with a critical micelle concentration (CMC) of 1 mM,[49] sodium dodecyl sulfonate (SDS) with a CMC of 8.2 mM,[50] aluminum oxide (activated, basic), benzoyl peroxide (Luperox A98), methyl methacrylate (MMA), Dowex Marathon hydrogen form ion-exchange resin, and cellulose dialysis tubing (14 kDa MWCO) were purchased from Sigma-Aldrich. MMA was purified to remove inhibitor by passing it through an aluminum oxide column before use. Dowex Marathon hydrogen form ion-exchange resin was rinsed with purified water before use. Whatman ashless filter aid was purchased from GE Healthcare Canada. Sodium hydroxide (NaOH) pellets, sulfuric acid, and sodium chloride (NaCl) were purchased from Caledon Laboratories Ltd.

Preparation of Sodium and Acid Form CNCs. Cellulose nanocrystals used in the miniemulsion polymerization of methyl methacrylate were provided by CelluForce Inc. Acid form CNCs (H-CNCs) were prepared by redispersing dried sodium form CelluForce CNCs (Na-CNCs, or CNCs where the counterion on the sulfate half ester group is a sodium ion, at a pH of 6.4) in purified water (2 wt %) and passing the suspension through an ion-exchange resin column (Dowex Marathon hydrogen form). The resulting H-CNCs (where the counterion is a proton) were then collected, diluted to 1.5 wt %, and characterized.

CNCs used in the zeta-potential, NanoSight particle size analysis, and colloid-probe atomic force microscopy study were prepared according to previous literature[51] and are considered to be comparable to CelluForce CNCs.[52] Briefly, 40 g of Whatman ashless filter aid was ground and added to a 45 °C water bath. 64 wt % sulfuric acid was added, and the hydrolysis was allowed to proceed for 45 min under mechanical agitation. The resulting suspension was then quenched with cold purified water (10× dilution) and centrifuged at 6000 rpm in 10 min increments until a pellet was no longer formed. Residual acid was then removed from the suspension by dialysis against purified water for several water changes. Finally, the resulting CNCs were sonicated with a probe sonicator (Sonifier 450, Branson Ultrasonics, Danbury, CT) for 45 min in an ice bath and filtered to remove excess metal from the probe. The resulting H-CNCs were used as is and as Na-CNCs after being neutralized with sodium hydroxide to replace all proton counterions with sodium ions.

Preparation of Cationic CNCs. In order to prepare cationic CNCs (Cat-CNCs), dried Na-CNCs were redispersed in purified water and concentrated to 10 wt %. The 10 wt % suspension was then desulfated by the addition of an equal volume of 3 M NaOH for 5 h at 65 °C. The resulting CNCs (DS-CNCs) had approximately two-thirds of the sulfur content as the starting CNCs and were dialyzed against purified water until a neutral pH was obtained. Cat-CNCs were prepared by bringing DS-CNCs to a pH of 13.2 and adding EPTMAC dropwise at a 1:16 CNC:EPTMAC weight ratio under constant stirring and at 65 °C. The suspension turned light yellow and was allowed to react for 5 h. Upon completion of the reaction, the product was dialyzed against purified water and diluted to 1.5 wt %, and a neutral pH of 8.4 was measured.

Miniemulsion Polymerization. The miniemulsion water phase was prepared by dissolving surfactant at 2 times the CMC for the given surfactant (CTAB or SDS) in a 1.5 wt % CNC suspension. The oil phase was prepared by dissolving benzoyl peroxide (BPO) in purified methyl methacrylate. In a typical reaction with CTAB and Na-CNCs, 5.1 mg of CTAB was dissolved in 7 mL of 1.5 wt % Na-CNCs through continuous magnetic stirring. Meanwhile, 2.82 g of purified MMA was weighed into a separate vial, and 0.141 g of BPO was added and dissolved by gentle agitation. The water and oil phase were then mixed and sonicated using a sonicator probe for 30−60 s in an ice bath. The resulting emulsion was 0.3:0.7 oil:water by volume. The emulsion was then added to a round-bottom flask with a magnetic stir bar, sealed, and degassed by bubbling Ar under continuous stirring in an ice bath for 15 min. The emulsion was then added to an oil bath at 60 °C, and the reaction was allowed to proceed for 6 h, after which the reaction was terminated by exposing the resulting latex to air. The PMMA particles were collected for further characterization.

Characterization of CNCs and Surfactant in Suspension. *Zeta-Potential.* Zeta-potential samples of CNC−surfactant suspensions were prepared by diluting a bulk sample of CNCs with the given surfactant concentration (0.2, 0.5, 1, 2, 5, and 10 times the CMC of the surfactant) to 0.1 wt % and adjusting the salt concentration to 10 mM NaCl. Zeta-potential of the resulting suspension was measured using a zeta-potential ZetaPlus analyzer (Brookhaven, USA). Electrophoretic mobility and zeta-potential were both recorded, and it is noted that electrophoretic mobility is directly proportional to the particle surface charge without assumptions of particle shape/size/charge density; however, zeta-potential is more commonly reported in the literature. As such, the Smoluchowski equation was used to covert electrophoretic mobility to zeta-potential.

NanoSight. NanoSight samples were prepared by diluting zeta-potential samples to 0.0001 wt %. The apparent diameter was measured using a NanoSight LM10 single nanoparticle tracking instrument (Malvern Instruments Ltd., UK). The term "apparent diameter" is used in recognition of the fact that NanoSight models spherical particles, as opposed to rod-shaped particles as in the case of CNCs. We take the "apparent diameter" as an approximate size measurements suitable for internal comparison of samples.

Characterization of Surfactant Interactions with CNC Films. *Colloid-Probe Atomic Force Microscopy.* Colloid-probe atomic force microscopy (AFM) was performed on spin-coated films of Na-CNCs, H-CNCs, and Cat-CNCs using a MFP-3D AFM (Asylum Research an Oxford Instrument Company, Santa Barbara, CA). Films were spin-coated onto Si wafers cleaned with piranha solution from a 1 wt % CNC suspension at 4000 rpm for 30 s (G3P Spin-coat, Specialty Coating Systems Inc., Indianapolis, IN). Colloid-probe AFM was used to measure normal forces between CNC films and a 2.5 μm Si colloid glued to an AFM cantilever with a nominal spring constant of 0.09 N/m (Novascan Technologies Inc., Ames, IA) in aqueous surfactant environments. An "open fluid cell" made by adding the surfactant solution dropwise to the sample surface until a drop was formed was used to perform these experiments. The Si probe was calibrated using the Sader method.[53] For normal force measurements, the probe was withdrawn from the surface, and "force pulls" were collected by ramping the probe perpendicular to the substrate at a scan rate of 0.5 Hz (500 nm/s), using a trigger point of 0.8 V and an approach (pull) distance of 500 nm. The Derjaguin approximation for a sphere of a known radius, R, and a flat plane (eq 1) was used to normalize the force data.[54]

$$F = 2\pi RW \tag{1}$$

where W, expressed as force/$2\pi R$, is the interaction energy per unit area between two flat surfaces. All colloid-probe AFM force data were processed using Igor Pro version 6.3 (Wavemetrics, Portland, OR). Force measurements were performed over 150 measurements, and data presented show one representative curve from each data set.

Characterization of Miniemulsion Polymerization. *Surface Coverage Calculation.* Surface coverage calculations were carried out following previous reports.[23,25,55] The surface coverage C is given by the ratio of the theoretical maximum surface susceptible to be covered by the particles and the total surface displayed by the oil droplet. Assuming that all the particles are adsorbed at the interface, the total coverage (the percentage of droplet surface area covered by CNCs) can be expressed according to eq 2.

$$C = \frac{mD}{6h\rho V_{\mathrm{oil}}} \tag{2}$$

where m is the mass of the CNCs used in the emulsion, D is the diameter of the particle (taken from SEM or measured by Mastersizer as $D_{4/3}$), h is the thickness of the CNCs as determined by AFM,[52] ρ is the density of CNCs (1.5 g/mL),[56,57] and V_{oil} is the volume of the oil phase.

Conversion. Conversion of all miniemulsion polymerization reactions was carried out through gravimetric analysis and calculated via eq 3 using the final wt % of the actual latex (wt $\%_{\mathrm{actual}}$) and the wt % of the latex had all of the monomer reacted (wt $\%_{\mathrm{theoretical}}$).

$$\text{conversion} = \frac{\text{wt }\%_{\mathrm{actual}}}{\text{wt }\%_{\mathrm{theoretical}}} \tag{3}$$

Conversions of less than 100% were achieved in most cases, likely due to the controlled reaction time and long half-life for BPO. Conversion was not optimized in this study.

Zeta-Potential. Zeta-potential samples were prepared by diluting the PMMA particles to 0.1 wt % and adding 10 mM NaCl. Electrophoretic mobility and zeta-potential were measured using a zeta-potential ZetaPlus analyzer (Brookhaven, USA).

Dynamic Light Scattering. Dynamic light scattering (DLS) samples were prepared in order to measure the diameter of the nanoscale monomer droplets (D_{d}) as well as the nanoscale PMMA particles (D_{p}) using a Malvern Zetasizer Nano particle analyzer at 20 °C. Samples were prepared by diluting zeta-potential samples to a concentration of 0.025 wt % and measured by DLS assuming the refractive index (RI) of MMA (1.41)[58] in the case of D_{d} and of PMMA (1.49)[59] in the case of D_{p}.

Mastersizer. Mastersizer was used to measure the diameter of the microscale monomer droplets (D_{d}) and of the microscale PMMA particles (D_{p}) using a Malvern Mastersizer 2000G (Malvern

DOI: 10.1021/acs.macromol.7b00516
Macromolecules 2017, 50, 2645−2655

Instruments, UK) equipped with a HeNe laser operating at 633 nm. The RI of MMA was used in the case of D_d, and the RI of PMMA was used in the case of D_p. The mean droplet diameter was taken to be the volume mean diameter ($D_{4/3}$) from three replicate measurements, which is mathematically expressed as shown in eq 4.

$$D_{4/3} = \frac{\sum D_i^{\,4} N_i}{\sum D_i^{\,3} N_i} \tag{4}$$

Particle size *span* was calculated using $D(0.9)$ which represents the diameter greater than 90% of measured particles, $D(0.1)$ which represents the diameter greater than 10% of measured particles, and $D(0.5)$ which represents the median diameter and is calculated using eq 5.

$$\text{span} = \frac{[D(0.9) - D(0.1)]}{D(0.5)} \tag{5}$$

Differential Scanning Calorimetry. Differential scanning calorimetry (DSC) samples were prepared by drying the latex samples at 80 °C. Samples of 5 mg were sealed in aluminum hemetic pans. DSC curves were collected under Ar using a heat/cool/heat cycle at with a heating rate of 10 °C/min, cooling rate of 5 °C/min, upper temperature of 250 °C, and lower temperature of −20 °C using a Q20 DSC (TA Instruments, New Castle, DE). Glass transition temperature (T_g) was determined using the second heating cycle.

Gel Permeation Chromotography. Gel permeation chromatography (GPC) samples were prepared by drying the latex particles at 80 °C overnight. The dried samples were redispersed in THF in order to solubilize the PMMA polymer. The insoluble CNCs were removed by centrifugation at 11 000 rpm for 10 min. The supernatant was collected, dried, and redispersed in THF to be centrifuged again in order to remove any remaining CNCs. Molecular weight and polydispersity indices (PDI) were analyzed via GPC using a Waters 2695 separations module, equipped with a Waters 2414 refractive index detector, and a Jordi Fluorinated DVB mixed-bed column. Polystyrene standards were used for calibration, with THF as the eluent at a flow rate of 3.0 mL/min.

Scanning Electron Microscopy. Scanning electron microscopy (SEM) samples were prepared by drying the latex at 80 °C. The samples were ground and dispersed on carbon tape on a SEM stub and subsequently coated with 6 nm platinum. Images were obtained using JEOL JSM-7000F SEM with a 3 kV acceleration voltage.

■ RESULTS AND DISCUSSION

Characterization of CNC Starting Materials. Na-CNCs, H-CNCs, and Cat-CNCs were characterized to measure the apparent diameter, zeta-potential, and pH of the starting materials (Table 1). The apparent diameter of Na-CNCs, H-CNCs, and Cat-CNCs were statistically indistinguishable; however, we believe that aggregation is more likely in the Cat-CNC system. This is possible because of the potential for Cat-CNCs to undergo ionic bridging (if they are forced close enough) since they contain both negative and positive surface charge groups. Na-CNCs and H-CNCs showed negative zeta-potential and good colloidal stability in water, while the Cat-CNCs showed a positive zeta-potential. Finally, the pH of all CNCs at 1.5 wt % was measured and showed Na-CNCs and Cat-CNCs were close to neutral pH while the H-CNCs were acidic. While this indicates neutral or acidic reaction conditions during miniemulsion polymerization, the monomer and initiator are not pH sensitive and as such we do not expect pH to play a significant role.

Table 1. Characterization of CNC Starting Materials

	apparent diameter (nm)[a]	zeta-potential (mV)	pH
Na-CNC	100 ± 40	−27 ± 4	6.4
H-CNC	100 ± 40	−29 ± 2	2.7
Cat-CNC	120 ± 40	+30 ± 2	8.4

[a] Measured using NanoSight single nanoparticle tracking analysis and considered "apparent diameter" since spherical particles are assumed and CNCs are rod-shaped.

CNC−Surfactant Interactions in Suspension. In order to elucidate the interactions between the anionic and cationic CNCs and surfactants used in this work, zeta-potential and apparent diameter of Na-CNCs, H-CNCs, and Cat-CNCs with increasing concentration of surfactant were measured. Zeta-potential measurements are plotted against increasing CNC concentration in order to display the trends in surface charge with increasing amounts of surfactant added to a CNC suspension (Figure 1). As the concentration of CTAB in suspension increases with Na-CNCs, the zeta-potential increases sharply, passing through neutral as the cationic surfactant heads neutralize the anionic CNC surface charges, and ultimately reaching a positive zeta-potential due to surfactant aggregates forming on the Na-CNCs (Figure 1a, black circles). This trend is expected and has been shown previously in the literature.[6−10] However, for H-CNCs the increase in zeta-potential with increasing CTAB concentration is more gradual and does not reach as high a positive value as the Na-CNCs (Figure 1a, gray circles), suggesting that H-CNCs do not accommodate the same electrostatic binding of CTAB. Additionally, for Cat-CNCs with increasing CTAB no statistically significant change in zeta-potential is observed (Figure 1a, white circles), indicating little electrostatic attraction. In contrast, anionic SDS with Cat-CNCs shows a sharp decrease in zeta-potential with added surfactant (Figure 1b, white circles). For SDS with Na-CNCs and H-CNCs, no apparent change in zeta-potential is observed (Figure 1b, black and gray circles, respectively).

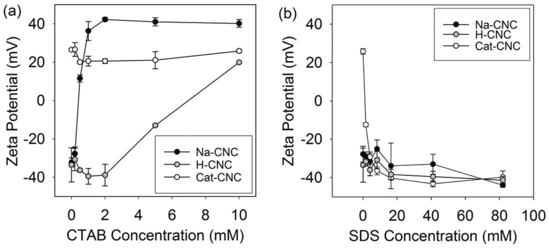

Figure 1. Zeta-potential of CNCs in suspension with increasing concentrations of (a) CTAB and (b) SDS. Surfactant concentrations (x-axis) run from 0 to 10 times the CMC. Each point is an average of three measurements, and error bars represent the standard deviation. Lines drawn between points are provided to guide the eye.

Complementary to the shift in zeta-potential, the apparent diameter of oppositely charged CNCs is expected to increase due to surfactant binding (Figure 2). In the case of CTAB with Na-CNCs, an increase in apparent diameter occurs at the same concentration (1 mM) of CTAB as the sharp increase in zeta-potential (Figure 2a, black circles). In contrast, the apparent diameter of H-CNCs is relatively unchanged (Figure 2a, gray circles), which is the same as Cat-CNCs with CTAB (Figure 2a, white circles).

The difference in CTAB adsorption to Na-CNCs and H-CNCs is attributed to different adsorption mechanisms and bound surfactant morphologies, which stem from the ability of

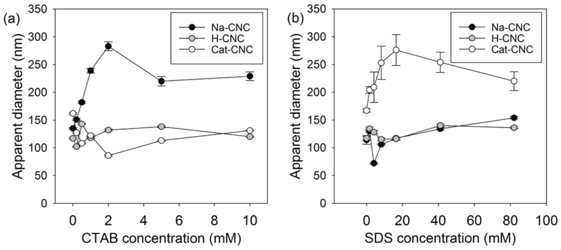

Figure 2. "Apparent diameter" of CNCs in suspension measured by NanoSight, with increasing amounts of (a) CTAB and (b) SDS. Each point represents the mean diameter measured for all particles tracked ($N > 1000$), and error bars are calculated as 95% confidence intervals. Lines drawn between points are provided to guide the eye.

CTAB (or more precisely, CTA$^+$) to displace H$^+$ or Na$^+$ (i.e., reactivity series), or due to the electrostatic/hydrophobic drive in solution for surfactants to adsorb vs aggregate. According to the Hofmeister series, Na$^+$ promotes hydrophobic interactions more than H$^+$.[60] We therefore propose two possibilities: (1) Individual CTAB molecules adsorb onto CNCs and then hydrophobic "tail" interactions lead to more surfactant binding with the cationic surfactant "heads" pointed outward. This would imply significant adsorption at low surfactant concentrations and more uniform surface coverage, which might be more detectable as a particle size increase by NanoSight. The second option (2) is that cationic surfactant aggregates (micelles, hemimicelles, etc.) adsorb to anionic CNCs directly leading to charge overcompensation. This mechanism would only occur above surfactant aggregation concentrations and could imply less uniform surface coverage which might not be detectable by NanoSight.

Na-CNCs appear to follow (1) closer and H-CNCs appear to follow (2). The apparent diameter of Cat-CNCs also shows an increasing trend upon the addition of oppositely charged SDS (Figure 2b, white circles), and the size of Na-CNCs and H-CNCs remains relatively unchanged because of the lack of electrostatic attraction (Figure 2b, black and gray circles, respectively). Overall, NanoSight results agree well with the zeta-potential, as well as trends seen in previous works (which only look at Na-CNCs), and highlight that there are significant differences in interactions and physical properties depending on the CNC surface charge and counterion.[6,7]

Surfactant Interactions with CNC Films. The interactions between CNCs and surfactants can be further elucidated through colloid-probe AFM. Spin-coated CNC films were covered by a CTAB solution at 0.5 times the CMC (though we anticipate a higher local concentration of CTAB at the surface of the film), and precontact interactions were assessed from the AFM force curves on approach. While the force increases monotonically as the probe approaches the surface in all cases (Figure 3), the profiles are not all typical of purely electrostatic interactions. In the case of Na-CNCs (Figure 3a) and H-CNCs (Figure 3b), there are additional features which imply soft surface contact of the probe with structures (i.e., surfactant aggregates) leading to steric forces apparent near the surface. These "soft surface features" are shown in the force curves as an initial limit to the decreasing separation (a bump in the curve), but upon the application of additional force, a "jump" to contact with the hard CNC surface is observed.

The jump-in distance varies indicating that the features have different sizes on Na-CNC vs H-CNC films. For Na-CNCs, the bump in the force curve is at approximately 10 nm, which corresponds to 3 times the length of a fully extended CTAB molecule.[61] Considering that there is also surfactant adsorbed on the anionic silica probe, the feature in the force curve may be due to a bilayer of surfactant adsorbed on each surface (where the tails interpenetrate and thus a bilayer is less than 2 times the surfactant molecule size). This feature is easy to push through, requiring only 0.2 mN/m of force. For H-CNCs, the bump in the force curve is at approximately 6 nm, which corresponds to the size of a CTAB micelle.[62] This highly ordered surfactant aggregate required a significantly larger force (3.3 mN/m) to push through compared to the soft features observed on the Na-CNC film. The inferred CTAB aggregate structures on Na-CNC and H-CNC films are shown in the inset of Figures 3a and 3b, respectively. (Although representative curves are provided in Figure 3, these features are highly reproducible as shown by the overlapping of force curves in Supporting Information Figure S1.) Colloid-probe AFM provides further indication that Na-CNCs and H-CNCs bind CTAB differently, as evidenced by both the size of the features and the forces required to push through the structured surfactant layers.

The lack of bumps in the force curves for CTAB with Cat-CNCs (Figure 3c) implies that there is insignificant adsorption of CTAB to Cat-CNC films but that a cationic layer of CTAB is adsorbed on the silica probe leading to a cationic probe—cationic film interaction. The approach curves for Na-CNCs, H-CNCs, and Cat-CNCs with SDS are nearly identical to Figure 3c (data not shown), suggesting that there is no significant binding of SDS below its CMC to any of the CNC

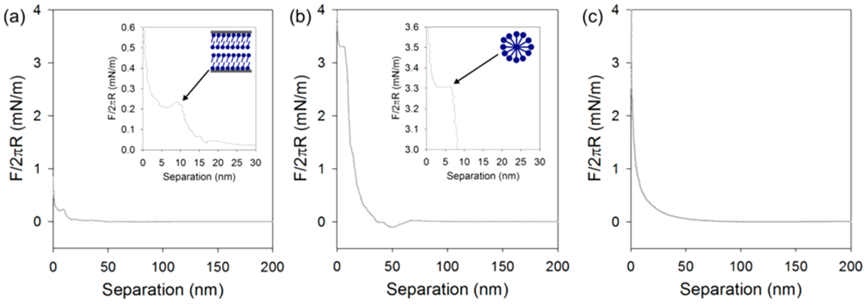

Figure 3. Representative colloid-probe AFM force curves (on approach) in a CTAB solution using a silica probe for a (a) Na-CNC film, (b) H-CNC film, and (c) Cat-CNC film. Insets in (a) and (b) show a zoomed-in curve and suggested surfactant structuring.

surfaces—this was also predicted from the zeta-potential and NanoSight measurements.

The work of adhesion between the probe and the CNC films in the presence of surfactant can provide insight into how strongly CNCs coated with surfactant can adhere at interfaces or to other polymers or particles in composite materials. Adhesion is calculated from the integrated area between the colloid-probe AFM approach and retraction curves (representative curves shown in Supporting Information Figure S2) and averaged over 150 measurements. In cases where surfactant structuring is seen on the CNC surface, such as for H-CNCs with CTAB, a higher adhesion was measured (Table 2). Less adhesion was observed for Na-CNCs with CTAB, likely due to the less ordered bilayer surfactant morphology on the surface. Cat-CNC films in SDS showed some adhesion, which is in line with the interactions measured in solution by zeta-potential and NanoSight. This is consistent with previous AFM studies of surfactants which highlight the difference between ordered and disordered surfactant structures at the surface; generally, there is higher adhesion with more surfactant and more micelles, as the micelle structure is more complete/ordered, and micelles require a higher force for the probe to push through.[63,64] All colloid-probe AFM data on CNC films agree well with the trends seen in suspension, highlighting the potential to elucidate surfactant−CNC interactions (and furthermore, bound surfactant morphologies) for the purpose of predicting particle properties in various systems such as miniemulsion polymerization.

Table 2. Force of Adhesion Measured by Colloid-Probe AFM and Calculated from the Area between the Attraction and Retraction Curves for Solutions of CTAB and SDS at 0.5 × CMC on a Na-CNC, H-CNC, and Cat-CNC Film[a]

	adhesion in CTAB (pJ/m)	adhesion in SDS (pJ/m)
Na-CNCs	47 ± 9	0[b]
H-CNCs	110 ± 10	0[b]
Cat-CNCs	0[b]	19 ± 3

[a] Each value represents an average of 150 measurements, and confidence intervals are the standard deviation. [b] Zero indicates no adhesion measured with a standard deviation of ±15 pJ/m.

Miniemulsion Polymerization. Here we used a combination of cellulose nanocrystals and surfactants to control the monomer droplet size (and corresponding polymer particle size) as well as the latex surface charge in the miniemulsion polymerization of methyl methacrylate. We also compared the resulting polymer particle properties of those made with and without hydrophobe. A schematic of the miniemulsion polymerization is shown in Figure 4.

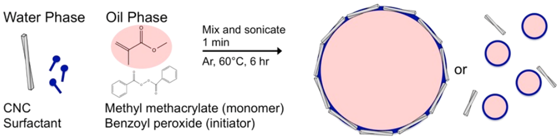

Figure 4. Schematic of miniemulsion polymerization stabilized by CNCs and/or surfactants, where oppositely charged CNCs and surfactants result in PMMA microparticles, and like charged CNCs and surfactants result in PMMA nanoparticles (not drawn to scale).

The stability of the miniemulsions before polymerization was studied in order to assess the resistance to coalescence of the monomer droplets. In the case where CNCs and surfactants costabilize the monomer/water interface (Na-CNCs + CTAB, H-CNCs + CTAB, Cat-CNCs + SDS), the emulsions show improved stability 1 h after emulsification (Figure 5a,b,f) compared to cases where CNCs and surfactants have no affinity for each other (Cat-CNCs + CTAB, Figure 5c; Na-CNCs + SDS, Figure 5d; and H-CNCs + SDS, Figure 5e). Costabilized systems also show improved stability over CTAB alone (Figure 5g) and SDS alone (Figure 5h). Neither Na-CNCs, H-CNCs, nor Cat-CNCs with 50 mmol NaCl were able to effectively stabilize an emulsion of MMA monomer in water on their own (Figure 5i, j, and k, respectively). The emulsion droplet sizes and how they correspond to polymer particle size after polymerization is discussed later.

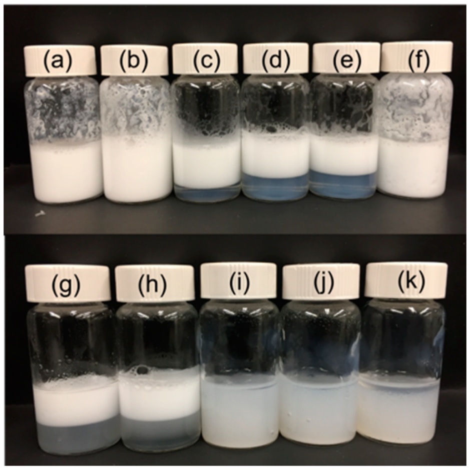

Figure 5. Emulsions of 0.3:0.7 MMA:water by volume stabilized by (a) Na-CNCs + CTAB, (b) H-CNCs + CTAB, (c) Cat-CNCs + CTAB, (d) Na-CNCs + SDS, (e) H-CNCs + SDS, (f) Cat-CNCs + SDS, (g) CTAB only, (h) SDS only, (i) Na-CNCs only, (j) H-CNCs only, and (k) Cat-CNCs only. Emulsions remained at room temperature for 1 h after sonication before the photograph was taken.

Miniemulsion polymerization reactions were carried out with the three types of CNCs combined with either cationic CTAB or anionic SDS at 2 times the CMC. The surfactant concentration is based on our previous work with CTAB which indicates that CNCs are sufficiently coated in surfactant at these concentrations in order to be surface active.[9,38] The reactions with oppositely charged CNCs and surfactants (Na-CNC + CTAB, H-CNC + CTAB, and Cat-CNC + SDS) showed particle sizes in the micrometer range and non-interacting CNC−surfactant systems (Na-CNC + SDS, H-CNC + SDS, and Cat-CNC + CTAB) gave particles in the nanometer range (Table 3). Na-CNCs with CTAB produced PMMA particles that were 9.3 μm, while H-CNCs with CTAB resulted in 4.5 μm PMMA particles (Table 3). We have shown above (Figure 2) that at twice the surfactant CMC CTAB binds more to Na-CNCs than H-CNCs, leading to a larger apparent diameter, which appears to correlate to larger PMMA particles. We note that the droplet size in our particle-stabilized emulsions has a lower limit due to the stabilizing particle size and geometry, and since CNCs are rigid and 100−200 nm in

Table 3. Miniemulsion Polymerization Conditions and Resulting Conversion, Particle Size, Weight Fraction of Micro- and Nanoparticles, Zeta-Potential, and Glass Transition Temperature (T_g)

CNCs present	surfactant	conv[a] (%)	size[b] (nm)	size[c] (μm)	wt fraction nano[d]	wt fraction micro[d]	zeta-potential (mV)	T_g (°C)[e]
Na-CNC	CTAB	64		9 ± 10	0.02	0.98	−31 ± 4	123
H-CNC	CTAB	51		5 ± 3	0.004	0.99	−11 ± 3	122
Cat-CNC	CTAB	46	206 ± 40		0.33	0.67	+11 ± 1	125
	CTAB	59	144 ± 1		1	0	+8 ± 2	122
Na-CNC	SDS	98	133 ± 1		1	0	−43 ± 1	118
H-CNC	SDS	99	124 ± 1		1	0	−38 ± 5	118
Cat-CNC	SDS	21	185 ± 10	18 ± 3	0.73	0.27	−51 ± 6	125
	SDS	85	138 ± 10		1	0	−61 ± 10	118

[a] Determined gravimetrically. [b] Measured by dynamic light scattering; error is the standard deviation from three measurements. [c] Measured by Mastersizer, error is calculated as span, shown in eq 5. [d] Determined gravimetrically by filtering with a 1 μm filter. [e] Measured by DSC.

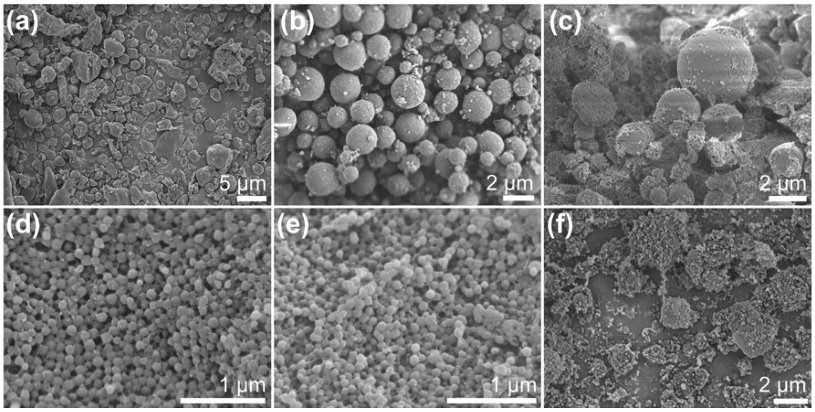

Figure 6. Scanning electron micrographs of PMMA particles stabilized using (a) Na-CNCs + CTAB, (b) H-CNCs + CTAB, (c) Cat-CNCs + CTAB, (d) Na-CNCs + SDS, (e) H-CNCs + SDS, and (f) Cat-CNCs + SDS.

length, nanometer-sized droplets stabilized by CNCs are unfeasible.

The emulsion stability results (Figure 5) and the size of the PMMA particles produced with oppositely charged CNCs and surfactants imply that surfactant-modified CNCs act as stabilizers at the monomer—water interface and remain there during the polymerization. Micrometer-sized particles with CNCs at the interface have also been demonstrated previously in an emulsion polymerization reaction of polystyrene with CNCs (without surfactant).[22,23,36] The presence of CNCs on the surface of the microparticles in costabilized systems is further supported by the fact that the PMMA particles synthesized in the presence of anionic CNCs have negative zeta-potentials, and with cationic CNCs the PMMA particles have positive zeta-potentials (Table 3). This is not the case for Cat-CNCs with SDS where the majority of the polymer particles are nanosized and anionic, likely due to their stabilization by SDS alone.

The particle size distribution was roughly estimated by separating the nano and micro fractions of the PMMA latex. For Na-CNCs and H-CNCs with CTAB, 99% of the particles produced were above 1 μm (by weight, as measured by the percent mass of particles passing through a 1 μm filter, Table 3). However, when Cat-CNCs were combined with CTAB, two-thirds of the particles were microparticles. We attribute this to the fact that Cat-CNCs contain both negative and positive surface charge groups, allowing for the interaction of the anionic surface groups with cationic CTAB to produce some micrometer-sized particles. The opposite was observed for Cat-CNCs with SDS where two-thirds of the particles produced were nanoparticles. In surfactant-only, or noninteracting CNC—surfactant systems, 100% of the particles produced were in the nanometer range, and we infer that they were stabilized by surfactant alone.

In miniemulsion polymerization, the monomer droplet diameter and the resulting polymer particle diameter should be nearly identical.[44] In this study, for the systems where CNCs and surfactants are used as costabilizers, the droplet size was on the same order of magnitude as the polymer particle size (Supporting Information Table S1), though this may not meet the specific criteria for a traditional miniemulsion polymerization. For example, the Na-CNCs + CTAB stabilized monomer droplet diameter increased from 2.3 μm to a particle diameter of 9.2 μm. Similarly, H-CNCs + CTAB stabilized monomer droplets have a diameter of 1.4 μm, while the resulting PMMA particles have a diameter of 4.5 μm. This implies that CNCs have the capacity to prevent droplet coalescence and, furthermore, to reduce monomer diffusion which is generally the role of the hydrophobe. As a direct comparison, we repeated all polymerization reactions reported in Table 3 with the addition of octadecyl acrylate (ODA) as the hydrophobe (the full characterization is shown in Supporting Information Table S2); the same trends were observed but the particles sizes were slightly smaller in the presence of the hydrophobe.

DOI: 10.1021/acs.macromol.7b00516
Macromolecules 2017, 50, 2645−2655

For the three polymerizations with noninteracting CNCs and surfactants (Cat-CNCs + CTAB, Na-CNCs + SDS, and H-CNCs + SDS), we predict that the polymerization proceeds more closely to a traditional emulsion polymerization, whereby the monomer droplets are stabilized by surfactant alone, with the CNCs dispersed in the aqueous phase. In this case, we expect the monomer to be contained in large monomer droplets and the remaining surfactant to form surfactant micelles after the emulsification step.[65] In these three cases, when the droplet size is measured by DLS, a peak is observed between 80 and 150 nm (Supporting Information Table S1 and Figure S3). Because the surfactant micelles are <5 nm,[49,50] and the monomer droplet is larger than what is measurable by DLS, this peak is attributed to the free CNCs in suspension. This is supported by the fact that when CNCs are measured by DLS in a surfactant solution at 2 × CMC, only one predominantly monomodal peak is seen centered around 100 nm (Supporting Information Figure S4). Furthermore, the presence of large monomer droplets in noninteracting CNC−surfactant systems was confirmed via optical microscopy (Supporting Information Figure S5). The PMMA particles produced from these noninteracting systems were 124−206 nm (Table 3).

The polymer particle size and morphology were also investigated by SEM (Figure 6) and agree with the trends shown in Table 3 regarding the fraction of nano- and microparticles. When CNCs and oppositely charged surfactants were used, microparticles were observed. Interestingly, when Na-CNCs were used with CTAB, the particles have a rough, nonspherical morphology. When H-CNCs were used with CTAB, the resulting PMMA microparticles are smoother and spherical. Since H-CNCs with CTAB led to the highest adhesion systems (Table 2), this may suggest that the H-CNCs are more strongly attached to the particle surface, resulting in more spherical particles. Cat-CNCs and CTAB produced some large microparticles which are attributed to the remaining anionic surface groups on Cat-CNCs interacting with CTAB, as discussed above. Particles stabilized with Na-CNCs or H-CNCs with SDS were all nanometers in size, and upon closer investigation, some rodlike nanoparticles can be seen in between the latex particles (Supporting Information Figure S6). Additionally, particles stabilized with CTAB and SDS without CNCs both result in PMMA nanoparticles, as seen in Supporting Information Figure S7. The PMMA particle sizes measured by SEM correlate well with both Mastersizer and DLS which supports that minimal artifacts occurred during SEM sample preparation.

For cases where Na-CNCs or H-CNCs were used as costabilizers with CTAB, no free CNCs could be detected upon separation of the latex particles from the reaction media. As such, we assume that all of the CNCs added to the reaction were used to stabilize monomer droplets and become incorporated on the surface of the latex particles. With this assumption, the surface coverage, C, of the PMMA particles with CNCs can be calculated using eq 2. The surface coverage of the particles may be plotted against the particle diameter (Supporting Information Figure S8). Correlating this plot with the particle size measured by SEM of 2.5 μm, we can conclude that the surface coverage of the particles is 97%. This correlates well with Capron and co-workers, who showed that a surface coverage of 84% is required in order to stabilize polystyrene droplets with CNCs.[23] Therefore, the remaining surface area of the particle is either uncovered or stabilized by surfactant.

Thermal properties of the PMMA particles were investigated by DSC. For the reactions run with either CTAB or SDS and CNCs, the resulting micro- or nanoparticles of PMMA showed similar glass transition temperatures (Table 3) in agreement with literature values for PMMA.[66,67] This suggests that the polymer mobility is unchanged and that the polymers are not tethered to the CNCs themselves.[68] The only significant increase (+7 °C) in T_g was observed for the PMMA particles prepared using Cat-CNCs and SDS (which we assume provide costabilization of the interface) which implies that CNCs are more closely associated, or incorporated into, the latex particles. We also observed that the polymer T_g was increased in all reactions where ODA was used, since ODA is also a hydrophobic monomer that gets incorporated into the PMMA polymer chains and is known to act as a plasticizer (Supporting Information Table S3).[69]

In order to elucidate the kinetic effect of CNCs on miniemulsion polymerization, monomer conversion (Table 3) and polymer molecular weight (MW, Table 4) were measured; however, we emphasize that neither parameter was intended to be optimized in this study. Since the reaction proceeds at 60 °C for 6 h, and the half-life of benzoyl peroxide is 25 h at 60 °C (using styrene monomer as a solvent, comparable to MMA used in this work),[70] the molecular weight values were expected to be very large. Monomer conversion shows that most CTAB reactions do not proceed to complete conversion, while SDS reactions reach 100% conversion more easily. Indeed GPC results, shown in Table 4, confirm that for all cases with SDS (alone and with CNCs) the MW is too large to be measured with the standard calibration curve and is therefore larger than 3000 kDa. In this case, a broad distribution is measured and thus polydispersity cannot be accurately quantified.

Table 4. Molecular Weight Distribution of PMMA Latexes

CNCs present	surfactant	M_n (kDa)	M_w (kDa)	PDI
Na-CNC	CTAB	75	207	2.74
H-CNC	CTAB	207	770	3.72
Cat-CNC	CTAB	118	575	3.23
	CTAB	181	923	5.09
Na-CNC	SDS	>1000[a]	>1000[a]	[b]
H-CNC	SDS	>1000[a]	>1000[a]	[b]
Cat-CNC	SDS	>1000[a]	>1000[a]	[b]
	SDS	>1000[a]	>1000[a]	[b]

[a]Not accurately measurable due to high MW. [b]Not calculated due to inaccuracy in estimated M_n and M_w.

For all CTAB-stabilized polymers, a polydisperse MW was measured; however, the PDI was lower when CNCs were present (Table 4). This suggests again that CNCs provided a barrier for monomer and/or initiator diffusion between particles. Indeed, the lowest PDI measured was for particles stabilized by Na-CNCs and CTAB which have the strongest interaction and most adsorbed surfactant on the CNC surfaces (Figures 1 and 2). Therefore, we propose that the adsorption of surfactants to CNCs, and their ability to costabilize the monomer droplets/polymer particles, hinders monomer diffusion and droplet coalescence, leading to polymers with lower PDI and MW. Similarly, CTAB had some affinity for H-CNCs and Cat-CNCs which produced microparticles with CNCs at the interface, thus leading to relatively good resistance to monomer diffusion and measurable MWs. In comparison, SDS did not show significant adsorption to any type of CNC, thus leading to monomer diffusion and very large MWs. The higher MW produced with SDS compared with CTAB (especially in surfactant-only systems) is primarily due to the concentrations of surfactant used: since the CMCs are different and we were working at 2 × CMC, we used 2 mM CTAB but 16.4 mM SDS; therefore, there are many more SDS micelles[71] and fewer initiator molecules per micelle, which should lead to higher MW.[72] The MW for miniemulsions performed with and without the ODA hydrophobe are comparable (Supporting Information Table S4).

■ CONCLUSIONS

Poly(methyl methacrylate) particles were synthesized by miniemulsion polymerization in the presence of CNCs and surfactants. CNC−surfactant interactions were governed by the CNC counterion, surface charge, and hydrophobic interactions. The choice of CNC and surfactant type could be used to tailor PMMA particle size, particle size distribution, particle roughness, particle zeta-potential, polymer molecular weight, and PDI without affecting the thermal properties or latex stability. Overall, when oppositely charged CNCs and surfactants were used in miniemulsion polymerization, they acted as costabilizers and prevented monomer diffusion between droplets, and the resulting PMMA particles were on the order of micrometers. For noninteracting CNC and surfactant combinations, nanoscale PMMA particles stabilized by surfactant were produced. This work provides design rules for the use of CNCs in surfactant-based systems such as emulsion polymerization and may lead to the use of CNCs in applications including composites, adhesives, cosmetics, and coatings.

■ ASSOCIATED CONTENT

Ⓢ Supporting Information

The Supporting Information is available free of charge on the ACS Publications website at DOI: 10.1021/acs.macromol.7b00516.

> AFM force curves showing the reproducibility of the measurement, colloid-probe AFM retraction curves, droplet diameters of MMA monomer droplets stabilized by CNCs and surfactants (including raw data), DLS measurements for CNCs in noninteracting surfactant solution, synthesis and characterization of PMMA particles prepared with ODA hydrophobe, and SEM images of PMMA particles stabilized by Na-CNCs + SDS, H-CNCs + SDS, and surfactant-only systems (PDF)

■ AUTHOR INFORMATION

Corresponding Author

*(E.D.C.) E-mail: ecranst@mcmaster.ca.

ORCID

Emily D. Cranston: 0000-0003-4210-9787

Funding

Funding for this work was provided by the Natural Sciences and Engineering Research Council of Canada (NSERC) as well as the Biointerfaces Collaborative Research and Training Experience Program (CREATE).

Notes

The authors declare no competing financial interest.

■ ACKNOWLEDGMENTS

The authors are grateful to CelluForce Inc. for providing CNC starting material. Special thanks to Daniel Osorio for obtaining SEM images at the Canadian Center for Electron Microscopy, Marta Kocun for the AFM support, and Michael Reid for assistance in obtaining the optical micrographs. Additional thanks to Drs. Pelton, Hoare, Guarne, and Adronov and the McMaster Biointerfaces Institute for equipment use.

■ REFERENCES

(1) Habibi, Y.; Lucia, L. A.; Rojas, O. J. Cellulose Nanocrystals: Chemistry, Self-Assembly, and Applications. *Chem. Rev.* **2010**, *110* (6), 3479−3500.

(2) Moon, R. J.; Martini, A.; Nairn, J.; Simonsen, J.; Youngblood, J. Cellulose Nanomaterials Review: Structure, Properties and Nanocomposites. *Chem. Soc. Rev.* **2011**, *40* (7), 3941.

(3) Beck, S.; Bouchard, J.; Berry, R. Dispersibility in Water of Dried Nanocrystalline Cellulose. *Biomacromolecules* **2012**, *13* (5), 1486−1494.

(4) Hasani, M.; Cranston, E. D.; Westman, G.; Gray, D. G. Cationic Surface Functionalization of Cellulose Nanocrystals. *Soft Matter* **2008**, *4* (11), 2238.

(5) Habibi, Y.; Hoeger, I.; Kelley, S. S.; Rojas, O. J. Development of Langmuir-Schaeffer Cellulose Nanocrystal Monolayers and Their Interfacial Behaviors. *Langmuir* **2010**, *26* (2), 990−1001.

(6) Dhar, N.; Au, D.; Berry, R. C.; Tam, K. C. Interactions of Nanocrystalline Cellulose with an Oppositely Charged Surfactant in Aqueous Medium. *Colloids Surf., A* **2012**, *415*, 310−319.

(7) Brinatti, C.; Huang, J.; Berry, R. M.; Tam, K. C.; Loh, W. Structural and Energetic Studies on the Interaction of Cationic Surfactants and Cellulose Nanocrystals. *Langmuir* **2016**, *32* (3), 689−698.

(8) Salajkova, M.; Berglund, L. A.; Zhou, Q. Hydrophobic Cellulose Nanocrystals Modified with Quaternary Ammonium Salts. *J. Mater. Chem.* **2012**, *22* (37), 19798.

(9) Abitbol, T.; Marway, H.; Cranston, E. D. Surface Modification of Cellulose Nanocrystals with Cetyltrimethylammonium Bromide. *Nord. Pulp Pap. Res. J.* **2014**, *29* (1), 46−57.

(10) Kaboorani, A.; Riedl, B. Surface Modification of Cellulose Nanocrystals (CNC) by a Cationic Surfactant. *Ind. Crops Prod.* **2015**, *65*, 45−55.

(11) Padalkar, S.; Capadona, J. R.; Rowan, S. J.; Weder, C.; Moon, R. J.; Stanciu, L. A. Self-Assembly and Alignment of Semiconductor Nanoparticles on Cellulose Nanocrystals. *J. Mater. Sci.* **2011**, *46* (17), 5672−5679.

(12) Fortunati, E.; Armentano, I.; Zhou, Q.; Puglia, D.; Terenzi, A.; Berglund, L. A.; Kenny, J. M. Microstructure and Nonisothermal Cold Crystallization of PLA Composites Based on Silver Nanoparticles and Nanocrystalline Cellulose. *Polym. Degrad. Stab.* **2012**, *97* (10), 2027−2036.

(13) Fortunati, E.; Luzi, F.; Puglia, D.; Petrucci, R.; Kenny, J. M.; Torre, L. Processing of PLA Nanocomposites with Cellulose Nanocrystals Extracted from Posidonia Oceanica Waste: Innovative Reuse of Coastal Plant. *Ind. Crops Prod.* **2015**, *67*, 439−447.

(14) Arrieta, M. P.; Fortunati, E.; Dominici, F.; Rayón, E.; López, J.; Kenny, J. M. Multifunctional PLA-PHB/Cellulose Nanocrystal Films: Processing, Structural and Thermal Properties. *Carbohydr. Polym.* **2014**, *107* (1), 16−24.

(15) Arrieta, M. P.; Fortunati, E.; Dominici, F.; Rayón, E.; López, J.; Kenny, J. M. PLA-PHB/Cellulose Based Films: Mechanical, Barrier and Disintegration Properties. *Polym. Degrad. Stab.* **2014**, *107*, 139−149.

(16) Padalkar, S.; Capadona, J. R.; Rowan, S. J.; Weder, C.; Won, Y. H.; Stanciu, L. A.; Moon, R. J. Natural Biopolymers: Novel Templates for the Synthesis of Nanostructures. *Langmuir* **2010**, *26* (11), 8497−8502.

(17) Teipel, B. R.; Grunlan, J. Synergy in Epoxy Nanocomposites with Cellulose Nanocrystals and Boehmite. *Green Mater.* **2014**, *2* (4), 222−231.

(18) Jackson, J. K.; Letchford, K.; Wasserman, B. Z.; Ye, L.; Hamad, W. Y.; Burt, H. M. The Use of Nanocrystalline Cellulose for the Binding and Controlled Release of Drugs. *Int. J. Nanomed.* **2011**, *6*, 321−330.

(19) Kaboorani, A.; Auclair, N.; Riedl, B.; Landry, V. Physical and Morphological Properties of UV-Cured Cellulose Nanocrystal (CNC) Based Nanocomposite Coatings for Wood Furniture. *Prog. Org. Coat.* **2016**, *93*, 17−22.

(20) Fortunati, E.; Mattioli, S.; Armentano, I.; Kenny, J. M. Spin Coated Cellulose Nanocrystal/Silver Nanoparticle Films. *Carbohydr. Polym.* **2014**, *113*, 394−402.

(21) Kalashnikova, I.; Bizot, H.; Cathala, B.; Capron, I. New Pickering Emulsions Stabilized by Bacterial Cellulose Nanocrystals. *Langmuir* **2011**, *27* (12), 7471−7479.

(22) Kalashnikova, I.; Bizot, H.; Cathala, B.; Capron, I. Modulation of Cellulose Nanocrystals Amphiphilic Properties to Stabilize Oil/Water Interface. *Biomacromolecules* **2012**, *13* (1), 267−275.

(23) Kalashnikova, I.; Bizot, H.; Bertoncini, P.; Cathala, B.; Capron, I. Cellulosic Nanorods of Various Aspect Ratios for Oil in Water Pickering Emulsions. *Soft Matter* **2013**, *9* (3), 952−959.

(24) Capron, I.; Cathala, B. Surfactant-Free High Internal Phase Emulsions Stabilized by Cellulose Nanocrystals. *Biomacromolecules* **2013**, *14* (2), 291−296.

(25) Cherhal, F.; Cousin, F.; Capron, I. Structural Description of the Interface of Pickering Emulsions Stabilized by Cellulose Nanocrystals. *Biomacromolecules* **2016**, *17* (2), 496−502.

(26) Zoppe, J. O.; Venditti, R. A.; Rojas, O. J. Pickering Emulsions Stabilized by Cellulose Nanocrystals Grafted with Thermo-Responsive Polymer Brushes. *J. Colloid Interface Sci.* **2012**, *369* (1), 202−209.

(27) Tang, J.; Lee, M. F. X.; Zhang, W.; Zhao, B.; Berry, R. M.; Tam, K. C. Dual Responsive Pickering Emulsion Stabilized by Poly[2-(dimethylamino) ethyl methacrylate] Grafted Cellulose Nanocrystals. *Biomacromolecules* **2014**, *15* (8), 3052−3060.

(28) Tang, J.; Berry, R. M.; Tam, K. C. Stimuli-Responsive Cellulose Nanocrystals for Surfactant-Free Oil Harvesting. *Biomacromolecules* **2016**, *17* (5), 1748−1756.

(29) Visanko, M.; Liimatainen, H.; Sirviö, J. A.; Heiskanen, J. P.; Niinimäki, J.; Hormi, O. Amphiphilic Cellulose Nanocrystals from Acid-Free Oxidative Treatment: Physicochemical Characteristics and Use as an Oil-Water Stabilizer. *Biomacromolecules* **2014**, *15* (7), 2769−2775.

(30) Cunha, A. G.; Mougel, J.-B.; Cathala, B.; Berglund, L. A.; Capron, I. Preparation of Double Pickering Emulsions Stabilized by Chemically Tailored Nanocelluloses. *Langmuir* **2014**, *30* (31), 9327−9335.

(31) Svagan, A. J.; Musyanovych, A.; Kappl, M.; Bernhardt, M.; Glasser, G.; Wohnhaas, C.; Berglund, L. A.; Risbo, J.; Landfester, K. Cellulose Nanofiber/Nanocrystal Reinforced Capsules: A Fast and Facile Approach Toward Assembly of Liquid-Core Capsules with High Mechanical Stability. *Biomacromolecules* **2014**, *15* (5), 1852−1859.

(32) Saidane, D.; Perrin, E.; Cherhal, F.; Guellec, F.; Capron, I. Some Modification of Cellulose Nanocrystals for Functional Pickering Emulsions. *Philos. Trans. R. Soc., A* **2016**, *374* (2072), 20150139.

(33) Ojala, J.; Sirviö, J. A.; Liimatainen, H. Nanoparticle Emulsifiers Based on Bifunctionalized Cellulose Nanocrystals as Marine Diesel Oil-Water Emulsion Stabilizers. *Chem. Eng. J.* **2016**, *288*, 312−320.

(34) Nypelö, T.; Rodriguez-Abreu, C.; Kolen'ko, Y. V.; Rivas, J.; Rojas, O. J. Microbeads and Hollow Microcapsules Obtained by Self-Assembly of Pickering Magneto-Responsive Cellulose Nanocrystals. *ACS Appl. Mater. Interfaces* **2014**, *6* (19), 16851−16858.

(35) Low, L. E.; Tey, B. T.; Ong, B. H.; Chan, E. S.; Tang, S. Y. Palm Olein-in-Water Pickering Emulsion Stabilized by Fe3O4-Cellulose Nanocrystal Nanocomposites and Their Responses to pH. *Carbohydr. Polym.* **2017**, *155*, 391−399.

(36) Hu, Z.; Patten, T.; Pelton, R.; Cranston, E. D. Synergistic Stabilization of Emulsions and Emulsion Gels with Water-Soluble Polymers and Cellulose Nanocrystals. *ACS Sustainable Chem. Eng.* **2015**, *3* (5), 1023−1031.

(37) Hu, Z.; Marway, H. S.; Kasem, H.; Pelton, R.; Cranston, E. D. Dried and Redispersible Cellulose Nanocrystal Pickering Emulsions. *ACS Macro Lett.* **2016**, *5* (2), 185−189.

(38) Hu, Z.; Ballinger, S.; Pelton, R.; Cranston, E. D. Surfactant-Enhanced Cellulose Nanocrystal Pickering Emulsions. *J. Colloid Interface Sci.* **2015**, *439*, 139−148.

(39) Peddireddy, K. R.; Nicolai, T.; Benyahia, L.; Capron, I. Stabilization of Water-in-Water Emulsions by Nanorods. *ACS Macro Lett.* **2016**, *5* (3), 283−286.

(40) Elmabrouk, A. B.; Wim, T.; Dufresne, A.; Boufi, S. Preparation of Poly(styrene-co-hexylacrylate)/Cellulose Whiskers Nanocomposites via Miniemulsion Polymerization. *J. Appl. Polym. Sci.* **2009**, *114* (5), 2946−2955.

(41) Ben Mabrouk, A.; Kaddami, H.; Magnin, A.; Belgacem, M. N.; Dufresne, A.; Boufi, S. Preparation of Nanocomposite Dispersions Based on Cellulose Whiskers and Acrylic Copolymer by Miniemulsion Polymerization: Effect of the Silane Content. *Polym. Eng. Sci.* **2011**, *51* (1), 62−70.

(42) Vatansever, A.; Dogan, H.; Inan, T.; Sezer, S.; Sirkecioglu, A. Properties of Na-Montmorillonite and Cellulose Nanocrystal Reinforced Poly(butyl acrylate-co-methyl methacrylate) Nanocomposites. *Polym. Eng. Sci.* **2015**, *55* (12), 2922−2928.

(43) Ben Mabrouk, A.; Rei Vilar, M.; Magnin, A.; Belgacem, M. N.; Boufi, S. Synthesis and Characterization of Cellulose Whiskers/Polymer Nanocomposite Dispersion by Mini-Emulsion Polymerization. *J. Colloid Interface Sci.* **2011**, *363* (1), 129−136.

(44) Asua, J. M. Miniemulsion Polymerization. *Prog. Polym. Sci.* **2002**, *27* (7), 1283−1346.

(45) Arshady, R. Suspension, Emulsion, and Dispersion Polymerization: A Methodological Survey. *Colloid Polym. Sci.* **1992**, *270* (8), 717−732.

(46) Fonseca, G. E.; McKenna, T. F.; Dubé, M. A. Miniemulsion vs. Conventional Emulsion Polymerization for Pressure-Sensitive Adhesives Production. *Chem. Eng. Sci.* **2010**, *65* (9), 2797−2810.

(47) Zengeni, E.; Hartmann, P. C.; Pasch, H. Encapsulation of Clay by Ad-Miniemulsion Polymerization: The Influence of Clay Size and Modifier Reactivity on Latex Morphology and Physical Properties. *ACS Appl. Mater. Interfaces* **2012**, *4* (12), 6957−6968.

(48) Kumar, P.; Behl, G.; Sikka, M.; Chhikara, A.; Chopra, M. Poly(ethylene glycol)-co-Methacrylamide-co-Acrylic Acid Based Nanogels for Delivery of Doxorubicin. *J. Biomater. Sci., Polym. Ed.* **2016**, *27* (14), 1413−1433.

(49) Patel, V.; Dharaiya, N.; Ray, D.; Aswal, V. K.; Bahadur, P. pH Controlled Size/Shape in CTAB Micelles with Solubilized Polar Additives: A Viscometry, Scattering and Spectral Evaluation. *Colloids Surf., A* **2014**, *455* (1), 67−75.

(50) Yoshii, N.; Okazaki, S. A molecular dynamics study of structural stability of spherical SDS micelle as a function of its size. *Chem. Phys. Lett.* **2006**, *425* (1−3), 58−61.

(51) Cranston, E. D.; Gray, D. G. Morphological and Optical Characterization of Polyelectrolyte Multilayers Incorporating Nanocrystalline Cellulose. *Biomacromolecules* **2006**, *7* (9), 2522−2530.

(52) Reid, M. S.; Villalobos, M.; Cranston, E. D. Benchmarking Cellulose Nanocrystals: From the Laboratory to Industrial Production. *Langmuir* **2017**, *33*, 1583.

(53) Sader, J. E.; Chon, J. W. M.; Mulvaney, P. Calibration of Rectangular Atomic Force Microscope Cantilevers. *Rev. Sci. Instrum.* **1999**, *70* (10), 3967−3969.

(54) Israelachvili, J. *Intermolecular and Surface Forces*, 3rd ed.; Academic Press Inc.: London, 1985.

(55) Gautier, F.; Destribats, M.; Perrier-Cornet, R.; Dechézelles, J.-F.; Giermanska, J.; Héroguez, V.; Ravaine, S.; Leal-Calderon, F.; Schmitt, V. Pickering Emulsions With Stimulable Particles: From Highly- to Weakly-Covered Interfaces. *Phys. Chem. Chem. Phys.* **2007**, *9* (48), 6455−6462.

(56) Mariano, M.; El Kissi, N.; Dufresne, A. Cellulose Nanocrystals and Related Nanocomposites: Review of Some Properties and Challenges. *J. Polym. Sci., Part B: Polym. Phys.* **2014**, *52* (12), 791−806.

(57) Reid, M. S.; Villalobos, M.; Cranston, E. D. Cellulose Nanocrystal Interactions Probed by Thin Film Swelling to Predict Dispersibility. *Nanoscale* **2016**, *8* (24), 12247−12257.

(58) Peng, G. D.; Chu, P. L.; Xiong, Z.; Whitbread, T. W.; Chaplin, R. P. Dye-doped step-index polymer optical fiber for broadband optical amplification. *J. Lightwave Technol.* **1996**, *14* (10), 2215−2223.

(59) Ohtsuka, Y. Light-Focusing Plastic Rod Prepared from diallyl isophthalate-methyl methacrylate Copolymerization. *Appl. Phys. Lett.* **1973**, *23* (5), 247−248.

(60) Vlachy, N.; Jagoda-Cwiklik, B.; Vácha, R.; Touraud, D.; Jungwirth, P.; Kunz, W. Hofmeister Series and Specific Interactions of Charged Headgroups with Aqueous ions. *Adv. Colloid Interface Sci.* **2009**, *146* (1−2), 42−47.

(61) Jha, A. K.; Lee, J.; Tripathi, A.; Bose, A. Three-Dimensional Confinement-Related Size Changes to Mixed-Surfactant Vesicles. *Langmuir* **2008**, *24* (12), 6013−6017.

(62) Tan, G.; Ford, C.; John, V. T.; He, J.; McPherson, G. L.; Bose, A. Surfactant Solubilization and the Direct Encapsulation of Interfacially Active Phenols in Mesoporous Silicas. *Langmuir* **2008**, *24* (3), 1031−1036.

(63) Bremmell, K. E.; Jameson, G. J.; Biggs, S. Forces between surfaces in the presence of a cationic polyelectrolyte and an anionic surfactant. *Colloids Surf., A* **1999**, *155* (1), 1−10.

(64) Vakarelski, I. U.; Brown, S. C.; Rabinovich, Y. I.; Moudgil, B. M. Lateral Force Microscopy Investigation of Surfactant-Mediated Lubrication from Aqueous Solution. *Langmuir* **2004**, *20* (13), 1724−1731.

(65) Ugelstad, J.; El-Aasser, M. S.; Vanderhoff, J. W. Emulsion Polymerization: Initiation of Polymerization in Monomer Droplets. *J. Polym. Sci., Polym. Lett. Ed.* **1973**, *11*, 503−513.

(66) Yeom, E.; Kim, W.; Kim, J.; Lee, S.; Park, M. Synthesis and Characterization of Poly (Methyl Methacrylate)/Montmorillonite Nanocomposites by Emulsifier-Free Emulsion Polymerization. *Mol. Cryst. Liq. Cryst.* **2004**, *425* (1), 85−91.

(67) Huang, X.; Brittain, W. J. Synthesis and Characterization of PMMA Nanocomposites by Suspension and Emulsion Polymerization. *Macromolecules* **2001**, *34* (10), 3255−3260.

(68) Hatton, F. L.; Kedzior, S. A.; Cranston, E. D.; Carlmark, A. Grafting-from Cellulose Nanocrystals via Photoinduced Cu-mediated Reversible-deactivation Radical Polymerization. *Carbohydr. Polym.* **2017**, *157*, 1033−1040.

(69) Jordan, E. F.; Riser, G. R.; Salber, C.; Wrigley, A. N.; Terpolymers, I. The Mechanical Properties and Transition Temperatures of Terpolymers of n-Octadecyl acrylate, Ethyl Acrylate, and Acrylonitrile. *J. Appl. Polym. Sci.* **1972**, *16* (11), 3017−3034.

(70) Brandup, J.; Immergut, E. H.; Grulke, E. A. *Polymer Handbook*, 4th ed.; Wiley: New York, 1999.

(71) Hecht, L. L.; Schoth, A.; Muñoz-Espí, R.; Javadi, A.; Köhler, K.; Miller, R.; Landfester, K.; Schuchmann, H. P. Determination of the Ideal Surfactant Concentration in Miniemulsion Polymerization. *Macromol. Chem. Phys.* **2013**, *214* (7), 812−823.

(72) Kumbhare, M. B. *Effect of Initiator-Monomer Ratio in Polymerization of Vinyl Acetate* **2014**, *5* (2), 80−83.

DOI: 10.1021/acs.macromol.7b00516
Macromolecules 2017, 50, 2645−2655

Appendix 2: Chapter 6 Supporting Information

Supporting Information

Supporting Information

Tailoring Cellulose Nanocrystal and Surfactant Behavior in Miniemulsion Polymerization

Stephanie A. Kedzior[a], Heera S. Marway[a], and Emily D. Cranston[a]*

[a]Department of Chemical Engineering, McMaster University, 1280 Main Street West, Hamilton, ON, Canada, L8S 4L8

*To whom correspondence should be address, email: ecranst@mcmaster.ca

Supporting Information

Methods

Miniemulsion Polymerization with ODA Hydrophobe

The miniemulsion water phase was prepared by dissolving surfactant at 2 times the critical micelle concentration (CMC) for the given surfactant in a 1.5 wt.% CNC suspension. The oil phase was prepared by dissolving benzoyl peroxide (BPO) and octadecyl acrylate (ODA) in purified methyl methacrylate. In a typical reaction with CTAB and Na-CNCs, 5.1 mg CTAB was dissolved in 7 mL 1.5 wt.% Na-CNCs with continuous stirring. Meanwhile, 2.82 g of purified MMA was weighed into a separate vial and 0.141 g ODA and 0.141 g BPO were added and dissolved by gentle agitation. The water and oil phase were then mixed and sonicated using a sonicator probe for 30-60 s in an ice bath. The resulting emulsion was 0.3:0.7 oil:water by volume. The emulsion was then added to a round bottom flask with a magnetic stir bar, sealed, and degassed by bubbling Ar under continuous stirring in an ice bath for 15 min. The emulsion was then added to an oil bath at 60°C and the reaction was allowed to proceed for 6 h, after which the reaction was terminated by exposing the latex to air. The resulting PMMA particles were collected for further characterization.

Dynamic Light Scattering

Dynamic light scattering (DLS) samples were prepared by diluting either the monomer droplets or a 1.5 wt.% suspension of CNCs using a surfactant solution at 2× the critical micelle concentration of the given surfactant. Apparent diameter was measured using a Malvern Zetasizer Nano Particle Analyzer at 20°C.

Optical Microscopy

Optical microscopy samples were prepared by casting a drop of emulsified monomer onto a glass slide and covering the drop with a cover slip. Optical micrographs were obtained at 10 fold magnification using a Nikon Eclipse LV100POL microscope.

Supporting Information

Results

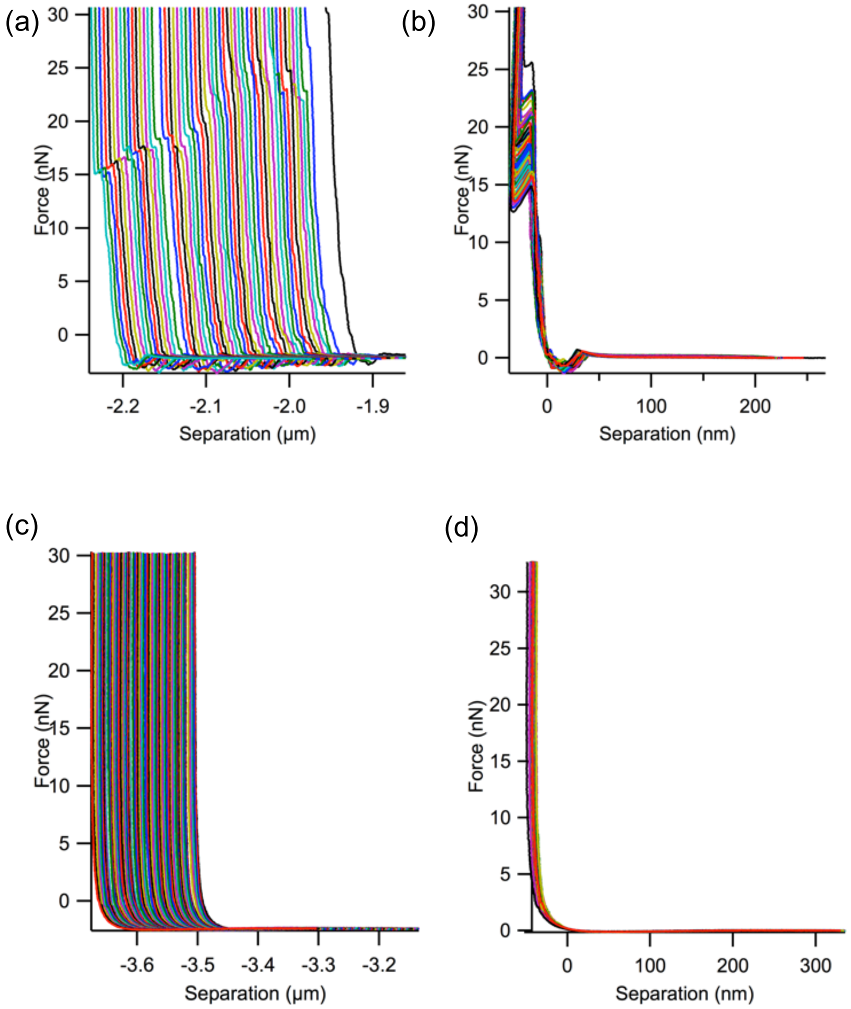

Figure S1. A set of 50 approach force curves between a Si probe and a (a) H-CNC film in a CTAB solution at 0.5× CMC - force curves before shifting to zero separation, (b) the mostly indistinguishable normalized curves in this system. (c) shows 100 approach curves for a Cat-CNC film in a CTAB solution at 0.5× CMC before being normalized and (d) overlapping normalized curves showing the reproducibility in this measurement technique.

Supporting Information

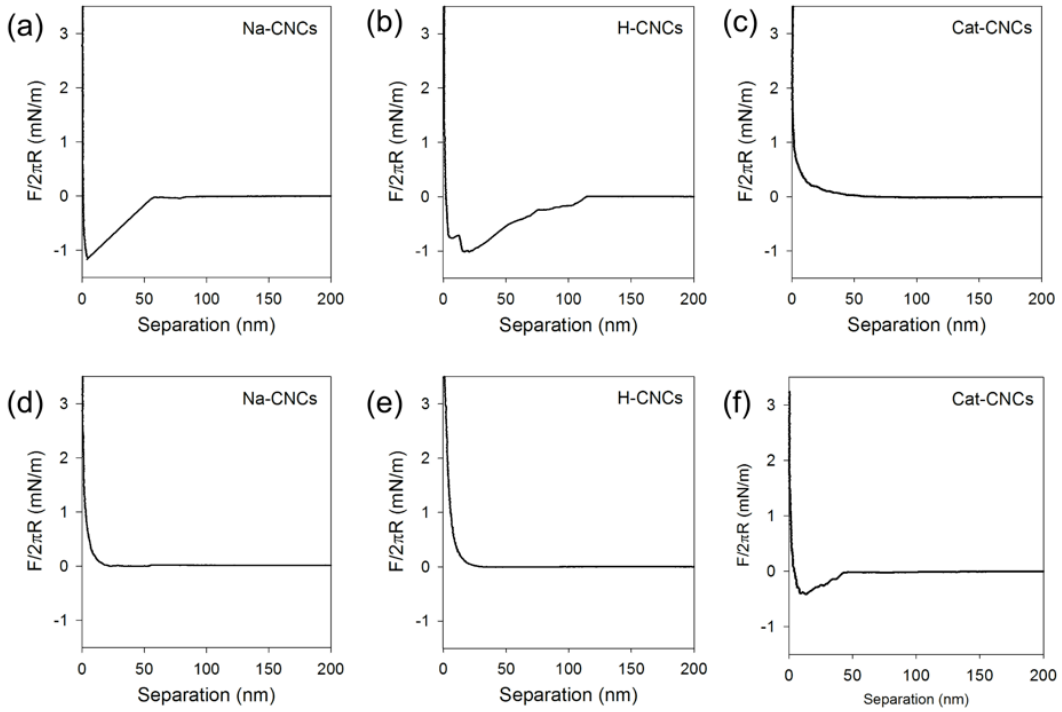

Figure S2. Representative colloid probe AFM retraction curves for films of (a) Na-CNC in a CTAB solution, (b) H-CNC in a CTAB solution, (c) Cat-CNC in a CTAB solution, (d) Na-CNC in a SDS solution, (e) H-CNC in a SDS solution, (f) Cat-CNC in a SDS solution.

Table S1. Droplet diameters for MMA monomer droplets without hydrophobe.

CNCs present	Surfactant	Droplet diameter (nm)$_{b}$	Droplet diameter (μm)^{a}
Na-CNC	CTAB	--	2.3 ± 10
H-CNC	CTAB	--	1.4 ± 5
Cat-CNC	CTAB	150 ± 30	--
--	CTAB	2.3 ± 0.8	--
Na-CNC	SDS	79 ± 2	--
H-CNC	SDS	85 ± 1	--
Cat-CNC	SDS	--	50 ± 2
--	SDS	2.1 ± 0.1	--

[a] Measured with MasterSizer, standard deviation calculated as span, shown in Eq. 1. [b] Measured with dynamic light scattering.

Supporting Information

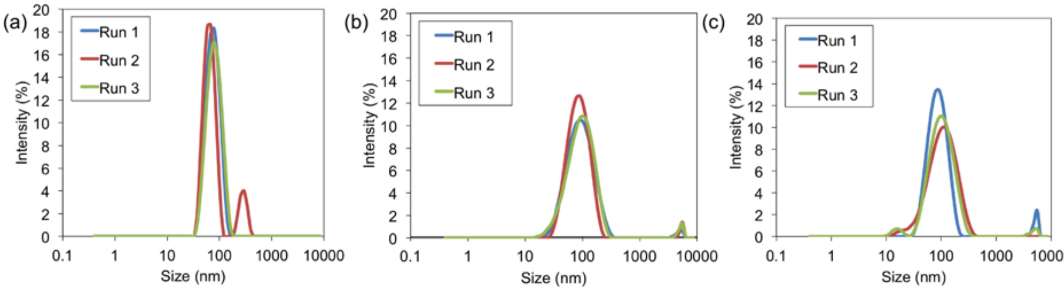

Figure S3. DLS raw data for monomer droplets stabilized by (a) Cat-CNCs+CTAB, (b) Na-CNCs+SDS, and (c) H-CNCs+SDS.

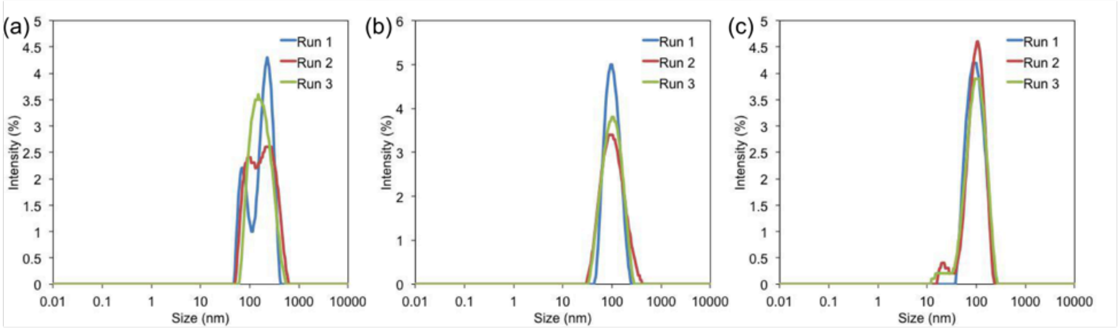

Figure S4. DLS raw data for (a) Cat-CNCs in 2×CMC CTAB, (b) Na-CNCs in 2×CMC SDS, and (c) H-CNCs in 2×CMC SDS.

Supporting Information

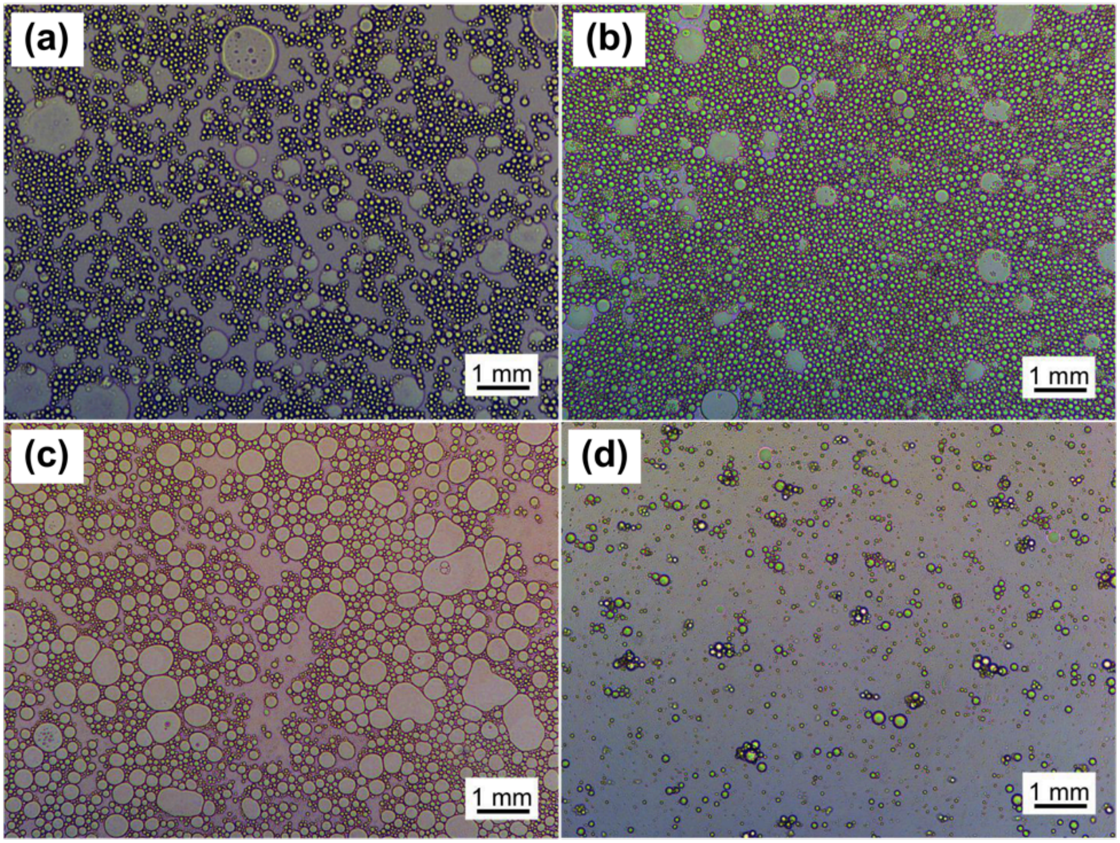

Figure S5. Optical micrographs showing monomer droplet sizes of (a) CTAB+Cat-CNCs, (b) CTAB alone, (c) SDS+Na-CNCs, and (d) SDS alone.

Table S2. Characterization of miniemulsion polymerizations of methyl methacrylate with 5 wt.% ODA.

CNCs present	Surfactant	Monomer	Conv[a] (%)	Size[b] (nm)	Size[c] (μm)	Wt fraction nano[d]	Wt fraction micro[d]	Surface Potential (mV)
Na-CNC	CTAB	MMA, ODA	41	--	2.5 ± 6	0	1	-31 ± 3
H-CNC	CTAB	MMA, ODA	21	--	2.9 ± 10	0	1	-31 ± 2
Cat-CNC	CTAB	MMA, ODA	89	350 ± 40	--	0.91	0.09	52 ± 20
--	CTAB	MMA, ODA	86	330 ± 60	--	1	0	27 ± 5
Na-CNC	SDS	MMA, ODA	91	80 ± 1	--	1	0	-42 ± 7
H-CNC	SDS	MMA, ODA	88	82 ± 1	--	1	0	-46 ± 3
Cat-CNC	SDS	MMA, ODA	31	155 ± 7	--	0.95	0.05	-56 ± 2
--	SDS	MMA, ODA	85	74 ± 1	--	1	0	-42 ± 10

[a] Determined gravimetrically. [b] Measured with dynamic light scattering. [c] Measured with MasterSizer, standard deviation calculated as span, shown in Eq. 1. [d] Determined gravimetrically by filtering with a 1 μm filter.

Supporting Information

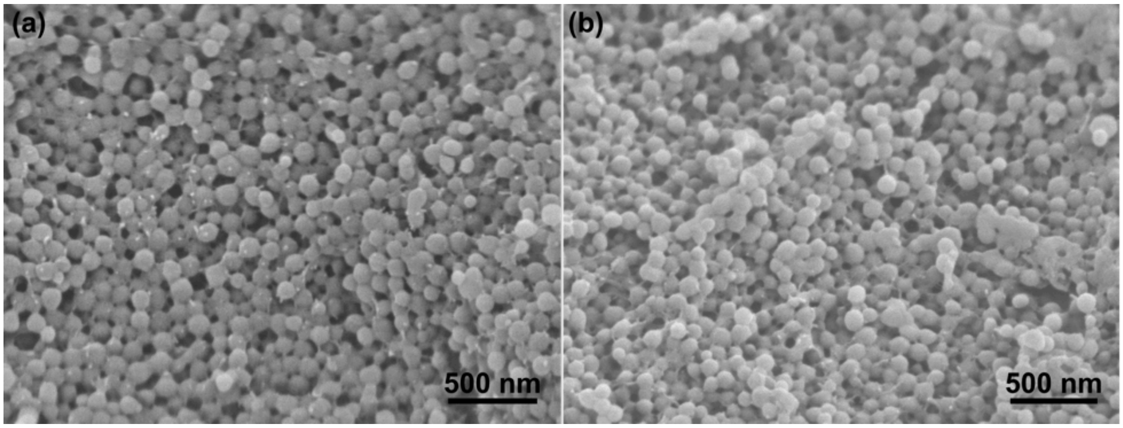

Figure S6. SEM images of PMMA particles stabilized by (a) SDS+Na-CNC and (b) SDS+H-CNC. Images are larger than manuscript figure to show potential CNCs between the polymer particles.

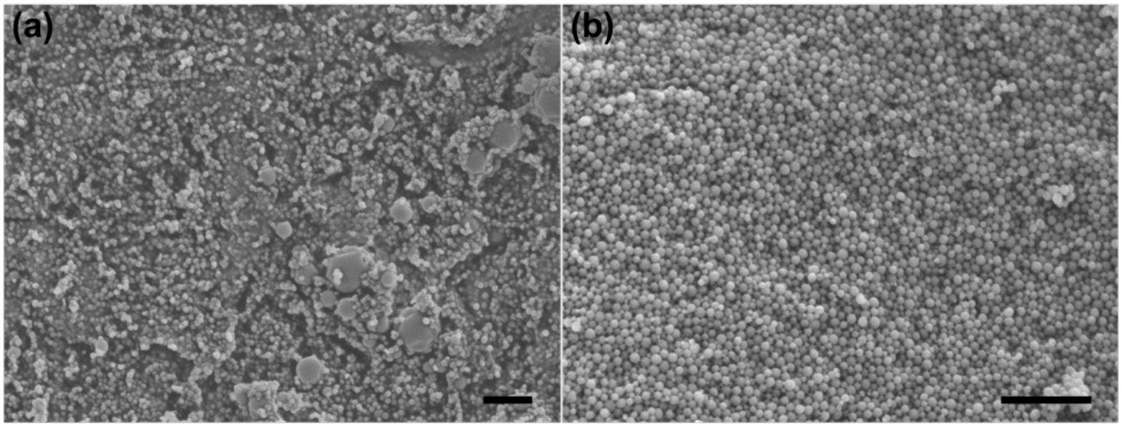

Figure S7. SEM images of PMMA particles stabilized by (a) CTAB only and (b) SDS only. Both scale bars are 1 µm.

Supporting Information

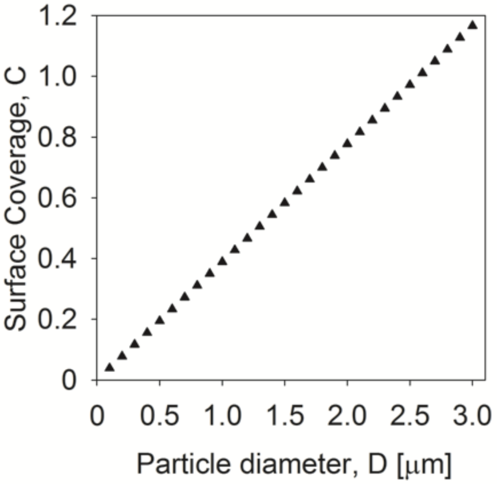

Figure S8. Theoretical droplet surface coverage plotted against particle diameter, as determined by Equation 2.

Table S3. Glass transition temperature of PMMA particles with ODA.

CNCs present	Surfactant	Monomer	T_g (°C)
Na-CNC	CTAB	MMA, ODA	111
H-CNC	CTAB	MMA, ODA	99
Cat-CNC	CTAB	MMA, ODA	107
--	CTAB	MMA, ODA	103
Na-CNC	SDS	MMA, ODA	112
H-CNC	SDS	MMA, ODA	105
Cat-CNC	SDS	MMA, ODA	118
--	SDS	MMA, ODA	111

Table S4. Molecular weight and PDI of PMMA particles prepared with ODA.

CNCs present	Surfactant	M_n (kDa)	M_w (kDa)	PDI
Na-CNC	CTAB	200	878	4.38
H-CNC	CTAB	201	939	4.66
Cat-CNC	CTAB	198	688	3.47
Na-CNC	SDS	>1000*	>1000*	**
H-CNC	SDS	>1000*	>1000*	**
Cat-CNC	SDS	193	331	1.71

* Not accurately measurable due to extremely high MW.
** Not calculated due to inaccuracy in estimated M_n and M_w.

Chapter 7

Cellulose Nanocrystals and Methyl Cellulose as Co-stabilizers for Nanocomposite Latexes with Double Morphology.

In the previous chapter, CNC-surfactant combinations were used to stabilize miniemulsion polymerization. This chapter aims to explore the role CNCs can play as Pickering stabilizers in latex synthesis without using surfactants. CNCs were non-covalently modified with the surface active polymer methyl cellulose (which is known to adsorb to CNCs) in order to stabilize the microsuspension polymerization of methyl methacrylate. PMMA latex particles with hierarchical double morphology were produced and particle size, size distribution and roughness could be tuned based on the ratio of CNC to methyl cellulose used. This work provides a new method for the incorporation of CNCs into surfactant-free polymer latexes.

In this work, I designed and performed all syntheses and characterization experiments and wrote the manuscript. The manuscript was edited by Dr. Marc Dubé (our collaborator and polymer reaction engineering expert from the University of Ottawa) and my supervisor, Dr. Emily Cranston. This chapter has been submitted to *ACS Sustainable Chemistry & Engineering* for publication.

Cellulose Nanocrystals and Methyl Cellulose as Co-stabilizers for Nanocomposite Latexes with Double Morphology.
Stephanie A. Kedzior, Marc A. Dubé, Emily D. Cranston
ACS Sustainable Chemistry & Engineering, submitted (manuscript ID: sc-2017-02510q).

Cellulose Nanocrystals and Methyl Cellulose as Co-stabilizers for Nanocomposite Latexes with Double Morphology

Stephanie A. Kedzior[a], Marc A. Dubé[b], and Emily D. Cranston[a*]

[a]Department of Chemical Engineering, McMaster University, 1280 Main Street West, Hamilton, ON, L8S 4L7, Canada
[b]Department of Chemical and Biological Engineering, Centre for Catalysis Research and Innovation, University of Ottawa, 161 Louis Pasteur Pvt., Ottawa, ON, K1N 6N5, Canada

*To whom correspondence should be addressed
email: ecranst@mcmaster.ca
phone: +1 (905) 525-9140 ex. 24369

Abstract

Cellulose nanocrystals (CNCs) are sustainable rigid rod-shaped nanoparticles that have potential as reinforcing agents in polymer nanocomposites. CNCs can also act as Pickering stabilizers in emulsions and foams due to their amphiphilic nature. In this work, CNCs were rendered surface active through adsorption with the biopolymer methyl cellulose (MC) to produce MC-coated CNCs. MC-coated CNCs were used to stabilize the microsuspension polymerization of methyl methacrylate. Monomer conversion, latex size, and gel content were studied. The microsuspension polymerization resulted in a double morphology where poly(methyl methacrylate) (PMMA) microparticles and nanoparticles were produced simultaneously. The ratio of micro- to nanoparticles could be tuned based on the CNC:MC ratio. Most nanoparticles were attached to the microparticles offering hierarchically structured latexes, although approximately 2 wt.% were free in suspension. Drying conditions could be used to control the surface roughness of the dry latex particles. This work provides a new strategy for the incorporation of CNCs into polymer latexes and the ability to control their morphology. This method could be used to produce CNC-based adhesives, toners, cosmetics, and coatings, providing a greener route compared to solvent-based polymerization while replacing synthetic surfactants with CNCs and MC which are derived from renewable resources.

Keywords
cellulose nanocrystals, methyl cellulose, suspension polymerization, latex, double morphology

Introduction

Cellulose nanocrystals (CNCs) are whisker-like nanoparticles extracted from wood pulp, cotton and other renewable cellulose sources, most commonly via acid hydrolysis.[1] Hydrolysis with sulfuric acid removes the disordered cellulose, leaving ordered, crystalline nanoparticles that possess sulfate half-ester surface groups as well as a hydrophobic plane (void of hydroxyl groups) that provides amphiphilic properties.[2] These amphiphilic, anionic nanoparticles form stable colloidal suspensions in water and are desirable due to their low cost, high strength, and light weight.[3,4] CNCs are finding increasing interest in a broad range of applications due to the shift towards greener chemistry and sustainable practices, and have shown suitable life cycle assessments to be used as a green alternative to synthetic chemicals.[5,6]

In recent years, much work has focused on the incorporation of CNCs into polymer matrices to produce CNC-polymer nanocomposites with improved properties.[7,8] If the polymer matrix is hydrophilic, unmodified CNCs may be easily incorporated, however when hydrophobic polymers are used, the uniform incorporation of unmodified CNCs poses many challenges. Accordingly, surface modification of CNCs to increase their hydrophobicity has been the focus of many recent papers and patents.[9] Various surface modification routes have been applied, mainly polymer grafting,[10–14] polymer adsorption,[15] or small molecule attachment[16–21] in order to provide CNCs with improved compatibility and functionality. These methods typically require organic solvents, hindering colloidal dispersion of CNCs and inducing nanoparticle aggregation, and additionally must be extensively purified in order to remove unreacted species. Because of this, water-based (and green) chemistry approaches have also been developed to functionalize CNCs, with many reports of water-based polymer grafting,[22–26] or non-covalent modification such as polymer adsorption[27–30] and surfactant adsorption.[31,32] Still, these reactions are typically multistep and require purification which is both time and cost inefficient. In this work, we use the biopolymer methyl cellulose which is an uncharged, water-soluble cellulose derivative that binds to CNCs.[29] By mixing CNCs with MC in water, CNCs are surface modified and are rendered surface active through polymer adsorption, and there is no need for further purification. The work presented here shows that MC-coated CNCs are easily incorporated into polymer latexes where they play the role of Pickering stabilizers *in situ* during polymerization.

Pickering emulsions using CNCs were first prepared by Capron and co-workers; they showed that reducing the CNC surface charge density or using salt to screen the anionic surface charge promoted improved CNC packing at the oil-water interface.[2,33] They further demonstrated that changing the aspect ratio of the CNCs had a direct influence on the surface coverage of the oil droplets.[34] Since this pioneering work, Capron's group has also used CNCs to stabilize high internal phase emulsions[35] and water-in-water emulsions;[36] the surface functionality of CNCs has been shown to provide emulsions with tailorable properties.[37] In these studies, the focus was on oil-in-water emulsions but in a few cases, CNC stabilized polystyrene (PS) latexes were prepared to visualize the CNCs at the interface.[2,33,34,37,38] Since this was performed for imaging purposes only there was no optimization of CNC stabilized latex systems. Recent work has shown that heterogeneously modified CNCs can be used to stabilize PS latexes with amino-rich surfaces that can be further treated to produce PS latexes that are crosslinked to one another.[39] Hierarchical structures were formed, however, this morphology was not controlled and required several steps to produce the final crosslinked latex.

Our previous work has used both surface active polymers[29,40,41] and surfactants[28,32] as co-stabilizers with CNCs to produce Pickering emulsions, emulsion gels, oil powders, and aqueous foams. These co-stabilized systems showed better stability to coalescence compared to emulsions stabilized by CNCs alone and due to their enhanced robustness we set out to test and optimize a latex polymerization stabilized by MC-coated CNCs. To the best of our knowledge, this is the first work to use polymer-coated CNCs to produce CNC nanocomposite latexes and furthermore, it is the first to show that a double latex morphology can be readily obtained and tuned using a one pot, water-based microsuspension polymerization route.

Unmodified CNCs have been used previously in nanocomposite latexes where they could be incorporated *in situ* but played a passive role in the polymerization reaction (since a surfactant was used to stabilize the monomer droplets), or the CNCs were blended with the latex post-synthesis. Irrespective of the route of incorporation, CNCs have typically demonstrated the ability to improve latex nanocomposite and coating properties: for example, Elmabrouk et al. used CNCs to reinforce poly(styrene-*co*-hexyl acrylate), poly(styrene-*co*-2-ethyl hexyl acrylate) and poly(butyl methacrylate) latex coatings that were prepared via miniemulsion polymerization with CNCs present in the water phase.[42,43] More recently, Geng et al.[44] and Pracella et al.[45] used CNCs to improve the mechanical properties in a poly(vinyl acetate) latex whereby *in situ* addition of CNCs during polymerization gave better properties than the CNC-latex blend and further mixing of the nanocomposite latex within another bulk polymer also led to improved dispersibility of CNCs. Similarly, CNCs have been added *in situ* during the emulsion polymerization of poly(*n*-butyl acrylate-*co*-methyl methacrylate) by Dastjerdi et al. showing that the gel content, viscosity, elasticity, tack, shear strength and peel strength of the resulting pressure sensitive adhesive films increased with increasing CNC content.[46,47] In these past studies, CNCs were located primarily in the water phase while surfactants were used to stabilize the growing polymer particles, which is in contrast to the work presented here, where the CNCs are necessary in stabilizing the monomer-water interface during the microsuspension polymerization. We also show that the presence of CNCs at the interface influences the resulting latex size, morphology, surface charge and surface roughness.

In contrast to emulsion polymerization and miniemulsion polymerization employed in the work described above, microsuspension polymerization is a type of suspension polymerization used to synthesize particles with sizes above those made by emulsion polymerization (hundreds of nm to 1 μm) yet below those made using conventional suspension polymerization (20-3000 μm).[48] In this polymerization method, a water insoluble monomer with an oil soluble initiator is dispersed in the continuous aqueous phase using a small amount of suspending agent or stabilizer[49] (in our case CNCs), resulting in micron sized monomer droplets that are converted to polymer particles during the polymerization step. The stabilizer hinders the coalescence of the monomer droplets such that each monomer droplet is converted to a polymer particle. Microsuspension polymerization provides many advantages such as low dispersion viscosity, low separation costs, and a final product in particle form.[50] Furthermore, microsuspension polymerization provides a method in which polymer nanocomposites can be prepared by simply adding a reinforcing agent into the continuous phase or by using reinforcing agents as Pickering stabilizers. In this work, MC-coated CNCs are used to stabilize microsuspension polymerization reactions of methyl methacrylate (MMA), providing a facile method for incorporating CNCs into latex polymer particles.

The combination of CNCs and MC as co-stabilizers is shown here to lead to a double morphology in the resultant latex, which is defined as a polymeric system of microparticles decorated with a secondary morphology of nanoparticles (alongside some free nanoparticles in suspension). Other methods to produce polymer particles with hierarchical morphology (e.g., raspberry-like particles) and/or controlled aggregated latex structures include variants on emulsion,[51–53] suspension,[54,55] and dispersion[56] polymerization. Furthermore, a sustainable emulsion polymerization method was recently reported where non-ionic poly(ethylene oxide)-grafted-lignin was used to stabilize PS latexes.[57] The "green" surfactant resulted in a double morphology where both nano and microparticles were prepared, but the morphology was not tuned and was not the focus of the work. Morphological control is generally used to tailor particle interfacial interactions for various applications such as toners.[58] Additionally, a double morphology can increase the total solids content of a latex in a single reaction, as opposed to preparing latexes of two different sizes in two separate reactions and blending. Latexes with multiple sizes or different chemical compositions can be synthesized in various "one pot" reactions, for example, using a multi-step process of seeded conventional emulsion and seeded miniemulsion polymerization.[59,60]

This work aims to provide a facile, water-based approach to prepare CNC nanocomposite latexes with controllable size, surface roughness, and morphology. This is a more sustainable approach to polymerization, polymer morphological control, and compounding compared to traditional solvent-based polymerization and solvent/melt processing of composites, and furthermore only employs bio-based stabilizers and no surfactants. In order to increase the sustainability of the method overall, a more renewable monomer could be chosen, such as alpha-methylene-gamma-valerolactone. However in this work, CNCs and MC were used to stabilize MMA droplets as they were converted to PMMA particles via microsuspension polymerization. PMMA was chosen as a model methacrylate system as its high glass transition temperature allows for facile characterization and imaging. The monomer/polymer properties were tracked over the course of the reaction and the latex properties were shown to be tunable based on the ratio of CNCs to MC in the reaction, as well as the latex drying method.

Experimental Section

Materials

Methyl cellulose (M_n 40 000, D.S. (methoxy) 1.60-1.90), aluminum oxide (activated, basic), benzoyl peroxide (BPO, Luperox A98), methyl methacrylate (MMA), poly(vinylidene fluoride) (PVDF) membrane filters, and cellulose dialysis tubing (14 kDa MWCO) were purchased from Sigma Aldrich. MMA was purified by passing it through an aluminum oxide column to remove inhibitor prior to use. Whatman ashless filter aid was purchased from GE Healthcare Canada. Sodium hydroxide (NaOH) pellets, sulfuric acid, and sodium chloride (NaCl) were purchased from Caledon Laboratories Ltd. All water used had a resistivity of 18.2 MΩ·cm and was purified by a Barnstead GenPure Pro water purification system from Thermo Fisher Scientific (Waltham, USA).

Sulfuric acid hydrolysis of cellulose nanocrystals. Cellulose nanocrystals were prepared according to the literature.[61] Briefly, 40 g of dried Whatman ashless filter aid was ground and placed in a 45 °C water bath. 700 mL of 64 wt.% sulfuric acid was added and the hydrolysis proceeded for 45 minutes, after which the reaction was quenched in 7 L of cold purified water. Residual acid was removed by centrifugation at 6000 rpm for 10 minutes and repeated until a pellet no longer formed, and then by dialysis against purified water until the pH of the CNC suspension in the dialysis tube no longer changed. The resulting suspension was then probe sonicated (Sonifier 450, Branson Ultrasonics, Danbury, CT) for 45 minutes (3 x 15 min intervals) in an ice bath and filtered to remove metal released from the sonicator probe. The CNCs were then neutralized with NaOH and freeze dried. The CNCs had an average length of 130 ± 50 nm and an average cross section of 8 ± 3 nm (determined using AFM), surface charge of 0.4 e/nm^2 (0.7 %S), zeta potential of -30 mV and crystallinity of 93% (determined by X-ray diffraction).[62]

Microsuspension polymerization. The microsuspension polymerization water phase was prepared by mixing 3.5 mL of a 0.6 wt.% CNC aqueous suspension with 3.5 mL of a 0.4 wt.% MC aqueous solution, resulting in a 3:2 CNC:MC ratio and referred to as the "base case". In a separate vial, 0.0564 g BPO (an oil soluble, radical initiator) was added to 2.82 g of purified MMA and dissolved using gentle agitation. It is of note that MMA has a surface tension of 24 mN/m,[63] comparable to that of dodecane (25 mN/m[64]) which we have used in previous work[29] in order to determine the interfacial tension of MC-coated CNCs. The water phase was then added to the oil phase and the mixture was first mixed via vortexing and was then sonicated using a probe sonicator for 60 s. The emulsion was transferred to a round bottom flask with a magnetic stir bar, sealed, and degassed by bubbling Ar under continuous stirring in an ice bath. The emulsion was then added to a 60 °C oil bath and the polymerization proceeded for 6 h until it was removed from the oil bath and exposed to air. Similar reactions were run with varying CNC:MC ratios of 6:2 and 3:4 (by weight) as well as a control with MC only (0.4 wt.% MC).

Dynamic light scattering (DLS). Dynamic light scattering samples were prepared as 0.025 wt.% suspensions. The diameter of the latex particles was measured using a Malvern Zetasizer Nano Particle Analyzer at 20 °C using the refractive index of PMMA (1.49).[65] The apparent size by DLS was also measured for CNC suspensions and MC solutions (also at 0.025 wt.%) and the term "apparent" is used in recognition that the CNCs are rod-shaped and MC is a loose coil therefore neither are hard spheres as assumed by DLS when converting diffusion coefficients to particle diameter.[66] The reported DLS values are an average of three measurements with the error reported as one standard deviation.

Zeta potential. Zeta potential samples were prepared as 0.1 wt.% suspensions in 10 mM NaCl. Zeta potential was measured using a Zeta Potential ZetaPlus Analyzer (Brookhaven, USA) whereby electrophoretic mobility was converted to zeta potential following the Smoluchowski theory.[66] In each measurement, electrophoretic mobility was measured over 10 runs, with the error reported as the standard deviation of the average.

Mastersizer. The PMMA particle diameter was measured using a Malvern Mastersizer 2000 G (Malvern Instruments, UK) equipped with a HeNe laser operating at 633 nm. The refractive index of PMMA (1.49)[65] was used. The mean diameter was taken to be the volume mean diameter ($D_{4/3}$) from 3 replicate measurements which is expressed mathematically in Equation 1.

$$D_{4/3} = \frac{\sum D_i^4 N_i}{\sum D_i^3 N_i} \quad (1)$$

Particle size span (shown as error bars in later figures) was calculated using Equation 2.

$$span = \frac{[D(0.9) - D(0.1)]}{D(0.5)} \quad (2)$$

D(0.9) represents the diameter greater than 90% of measured particles, D(0.1) represents the diameter greater than 10% of measured particles, and D(0.5) represents the median diameter.

Monomer Conversion. Conversion during the microsuspension polymerization was calculated gravimetrically and was based on dried polymer. After each hour, the wt.% of the reaction was calculated and Equation 3 was used to calculate the monomer conversion.

$$monomer\ conversion = \frac{wt.\%_{actual}}{wt.\%_{theoretical}} \times 100\% \quad (3)$$

where wt.%$_{actual}$ is the wt.% measured at the given time point and wt.%$_{theoretical}$ is the wt.% assuming all of the monomer had reacted.

Gel Content. Gel content of the latex was measured in order to provide information about the amount of insoluble high molecular weight (MW) polymer chains within the latex, as the MW of the polymer was too large to be measured by gel permeation chromatography (GPC). Gel content samples were prepared by heat sealing 0.1 g dried nanocomposite latex samples in PVDF membranes that were pre-weighed (membrane weight), and weighed with samples (membrane + sample weight) and submerged in tetrahydrofuran (THF) for 16 hours. After 16 h, the THF was poured off and the membranes were allowed to dry. The dry membranes were then weighed (dry weight). Gel content was calculated according to Equation 4.

$$gel\ content = \frac{(dry\ weight - membrane\ weight)}{(membrane + sample\ weight - membrane\ weight)} \times 100\% \quad (4)$$

Surface Tension. Surface tension of the 3:2 CNC:MC in water and the resulting base case latex was measured by the pendant drop method using a Krüss Drop Shape Analysis System DSA10 instrument. A drop of either 3:2 CNC:MC (total concentration of 0.5 wt.% in water, as used in the microsuspension polymerization), or the resulting latex was formed at the end of a stainless steel needle in air.

Scanning Electron Microscopy (SEM). Scanning electron microscopy samples were prepared by drying the PMMA particle suspension at 60 °C, unless otherwise specified. Dried samples were ground using a mortar and pestle, dispersed on carbon tape on an SEM stub, and coated with a 6 nm gold layer. Images were obtained using a JEOL JSM-7000F SEM with a 3 kV acceleration voltage.

Results and Discussion

Microsuspension Polymerization Kinetics

Microsuspension polymerization was carried out according to the schematic shown in Figure 1. An aqueous suspension of CNCs and a solution of MC were mixed in the water phase prior to adding methyl methacrylate monomer with BPO. The two phases were vortexed and sonicated, which resulted in a stable emulsion with a milky white appearance. While the conversion and polymer molecular weight were not specifically optimized in this study, the particle size, conversion, and gel content of the resulting latex were studied as a function of reaction time. Additionally, the ratio of CNC:MC used as co-stabilizer was varied in order to tune the double morphology of the resulting polymer particles.

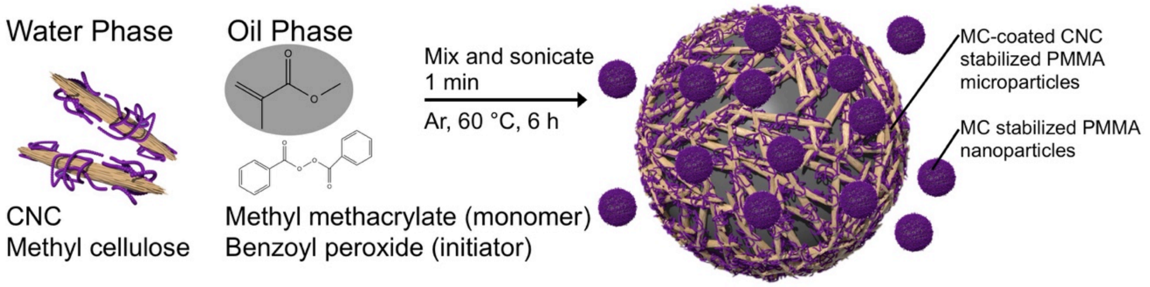

Figure 1. Schematic of the microsuspension polymerization of MMA (grey) stabilized by CNCs (beige) and MC (purple).

Methyl cellulose was used to non-covalently functionalize the CNCs, which on their own are amphiphilic but not sufficiently surface active to stabilize oil-in-water emulsions over long time periods.[29] CNCs also partition slowly to interfaces due to their size, compared with small molecule or polymeric surfactants.[31] Methyl cellulose is surface active and as such, having MC-coated CNCs and some free (or loosely bound) MC helps to lower the energy requirements to quickly form stable monomer-in-water emulsions.

Previous work has studied the adsorption of MC to CNCs and determined that above a ratio of 20:1 CNC:MC, the surface of the CNCs was saturated with MC (corresponding to ca. 0.16 mg of MC per square meter), and the dodecane/water interfacial tension was lowered to the value measured with MC alone.[29] Because of this previous work, and since MMA has similar physical properties to dodecane, comparable behavior was expected. However, at a ratio of 20:1 CNC:MC, the monomer emulsion formed was not stable to coalescence, and could not be uniformly polymerized.[32] Therefore, a base case of 3:2 CNC:MC (by weight) was chosen as it is well above the concentration where the CNC surface is fully covered with MC, and where approximately 90% of the MC is free MC not bound to CNCs. Using this amount of CNCs and MC as co-stabilizers during the microsuspension polymerization resulted in the double morphology of PMMA latex particles depicted in Figure 1.

During the microsuspension polymerization, aliquots were taken after each hour in order to determine the reaction kinetics (Figure 2). Since sonication of the methyl methacrylate in water produced micron-sized droplets and microsuspension polymerization is known to polymerize monomer droplets following bulk polymerization kinetics, the polymer particle size should be maintained throughout the reaction. Figure 2a shows the polymer microparticle size at each time point (t = 1-6 h) for the base case reaction (3:2 CNC:MC). As expected, the diameter of the particles remained fairly constant (8-15 μm) within error as the polymerization proceeded. This size range is of particular interest as it is difficult to achieve with other polymerization methods such as emulsion and suspension polymerization. Notably, the error bars (calculated as the span from Mastersizer measurements) narrowed as the polymerization proceeded, implying that the final latex particle size became less polydisperse with time.

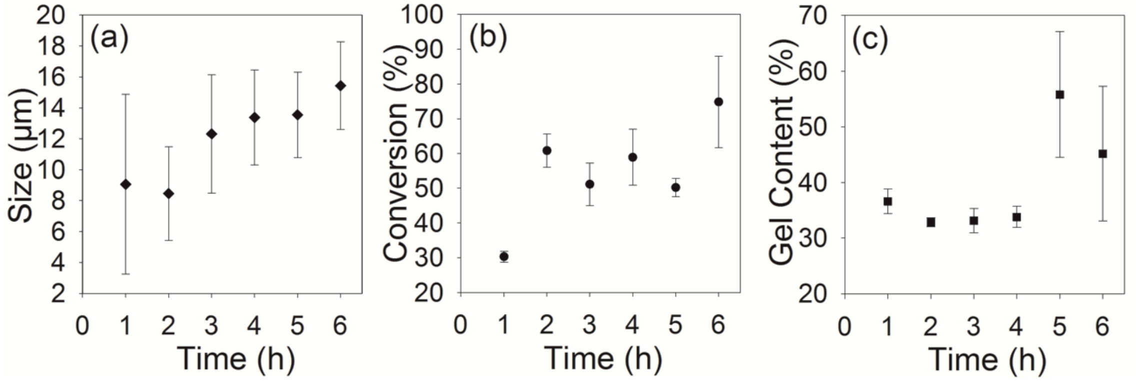

Figure 2. (a) PMMA microparticle size (measured by Mastersizer) over time produced by microsuspension polymerization stabilized by 3:2 CNC:MC, (b) conversion versus time of PMMA produced by microsuspension polymerization stabilized by 3:2 CNC:MC. (each value is the average of three measurements with the error bars representing the standard deviation of the average), and (c) gel content of the PMMA latex produced by microsuspension polymerization stabilized by 3:2 CNC:MC over time.

The monomer conversion in the microsuspension polymerization was also monitored after each hour and is shown in Figure 2b. As expected, the reaction followed kinetics typical of bulk radical polymerization, where the conversion increased relatively quickly in the first few hours and then began to plateau (within error) as the remaining monomer in each droplet was slowly consumed.

In order to indirectly measure the polymer molecular weight as the polymerization proceeded (and since the molecular weight of the polymer chains within the latex particles was too large to determine via GPC), gel content of the latex was studied. Gel content refers to the portion of the latex that consists of crosslinked or essentially insoluble high molecular weight polymer chains that are not able to diffuse from the latex particles through the PVDF membranes. High molecular weight polymer chains are likely a result of limited monomer diffusion between droplets as well as the long half life of BPO,[67] while crosslinking may occur via chain transfer and termination reactions. Gel content measurements assume that all polymer chains that are not entangled in a polymer "gel" (crosslinked or high MW) are soluble in THF. Gel content kinetics (Figure 2c) showed that the gel content remained constant over time at 35% during the first four hours of the polymerization, suggesting that the amount of high MW chains was relatively similar during the same phase as when the conversion began to plateau (Figure 2b). However, after 5 and 6 h respectively, the gel content increased, suggesting that past 4 h of polymerization the molecular weight of the polymer chains increased, and either very high MW polymers or crosslinking (by chain transfer/termination) were formed within the latex particles. This increase in gel content is likely due to the Trommsdorff[68] or gel effect, where high MW polymer limits the diffusion of monomer within individual particles, resulting in "runwaway reactions" and potential crosslinking within individual polymer particles.[69] However, because the high MW polymer chains are contained in the particles, the viscosity of the latex suspension does not increase over time and the latex can be easily processed and handled similar to commercial latex products. Furthermore, this implies that the MC-CNC shell on the droplet/particle may provide an additional barrier that restricts the diffusion of high MW polymers.

In order to determine if any remaining stabilizer such as excess MC or MC-coated CNCs were left after the polymerization, the surface tension of the base case latex was measured. The surface tension of a suspension of 3:2 CNC:MC was measured to be 58 mN/m, while the surface tension of the base case latex was 71.2 mN/m, similar to 72.8 mN/m for water,[70] implying that no excess stabilizer was free in suspension in the final latex.

Latex Particle Morphology

PMMA particle morphology was investigated by SEM and a double morphology was observed, where both PMMA microparticles and PMMA nanoparticles were formed. The double morphology for the 3:2 CNC:MC base case can be seen in Figure 3a, where spherical PMMA microparticles appear to be decorated with spherical nanoparticles. When the amount of CNCs was doubled (6:2 CNC:MC), the microparticles had a smoother surface, and less of the secondary nanoparticle morphology was present (Figure 3b). In contrast, when the amount of MC was doubled (3:4 CNC:MC), the amount of nanoparticles increased and the surface roughness of the microparticles increased as well (Figure 3c). In all cases, the latex microparticles produced were spherical and fairly consistent in size (15 ± 3 μm, measured by Mastersizer) and the nanoparticles produced were spherical and ranged in size from 100 to 200 nm. The microparticle size remained constant for all CNC:MC ratios which is likely a compound effect of the MMA-water interfacial tension and CNC size.

The change in particle morphology and ratio of micro- to nanoparticles was shown to be tunable based on the ratio of CNC:MC stabilizers used. When the polymerization was performed with only MC as the stabilizer, only nanoparticles were observed and tended to be highly aggregated (Figure 3d). This suggests that in the double morphology samples, the microparticles were stabilized by MC-coated CNCs, while the nanoparticles were stabilized by excess MC. Because of the rigid structure of the MC-coated CNCs, the fact that they themselves are 100-200 nm in length, and that previous work demonstrated that CNCs (functionalized or not) can only stabilize micron-sized droplets or polymer particles,[2,29,32,34] the MC-coated CNCs are geometrically unable to stabilize the nanosized fraction of latex particles produced here. Furthermore, having a large excess of MC (~90%) implies the nanoscale morphology to be stabilized by MC alone, hence why adding more MC resulted in more nanoscale particles.

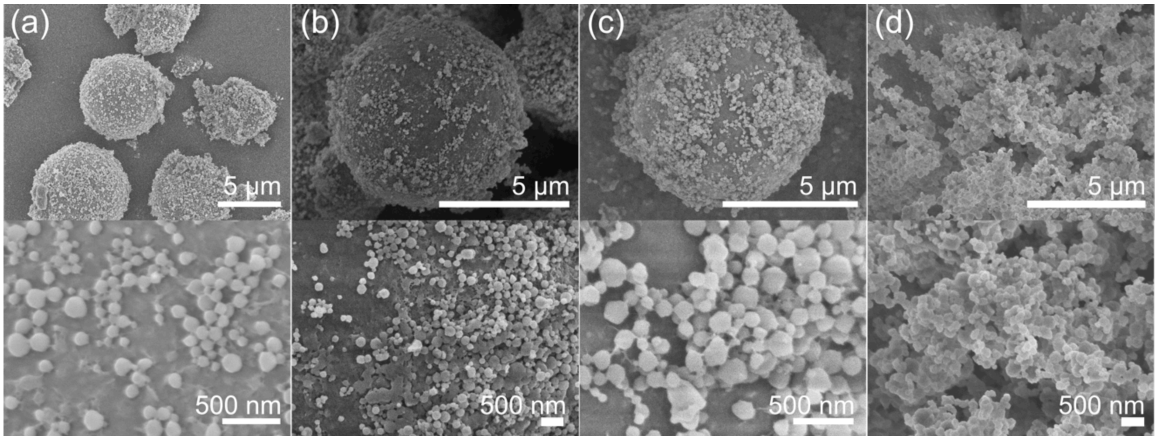

Figure 3. Double morphology of PMMA particles stabilized by (a) 3:2 CNC:MC, (b) 6:2 CNC:MC, (c) 3:4 CNC:MC, (d) MC only. Top row scale bars are 5 μm and bottom row shows a zoomed in version of the top row with scale bars of 500 nm.

In order to further understand the latex double morphology, a suspension of the polymer particles (synthesized using the 3:2 MC:CNC ratio) was diluted, the concentration was measured gravimetrically, and the suspension was then passed through a 1 μm syringe filter. The starting suspension had a total solids content of 1 wt.%. By measuring the concentration of the sample that passed through the filter, it was determined that 2 wt.% of the solids content consisted of free nanoparticles that were able to pass through the filter. The sample was then back-filtered, and the microparticles that did not pass through the filter were imaged by SEM. The microparticles still showed some surface roughness and the presence of the secondary spherical nanoparticle morphology (Figure 4a and b) indicating that most of the nanoparticles were attached to the surface of the microparticles in solution, and the appearance of the nanoparticles on the microparticle surface (such as those shown in Figure 3) was not merely an effect of drying during SEM sample preparation. Additionally, some rod-shaped particles, which we interpret as CNCs, were visible at the surface of the microparticles (Figure 4b). Since a very small amount of stabilizer was used overall (ca. 1.2%), it was difficult to detect the MC/CNC coatings on the latex particles with techniques other than SEM such as spectroscopy and thermal analysis, and DSC measurements showed a glass transition temperature of the base case latex to be the same as pure PMMA. Additionally, SEM images of the microfiltered particles (Figure 4c) revealed a spherical morphology identical to the PMMA latexes that were produced using MC alone (Figure 3d), further indicating that the free nanoscale morphology was PMMA particles stabilized by MC.

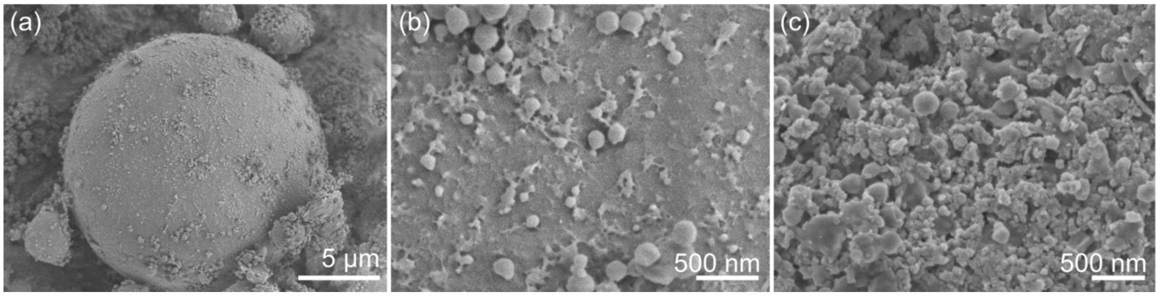

Figure 4. SEM images of (a) back-filtered PMMA latex particle showing the secondary nanoscale morphology attached to the microparticles (stabilized by a 3:2 CNC:MC ratio), (b) surface of a back-filtered microparticle showing the presence of CNCs and (c) filtered PMMA latex showing only the nanoscale morphology.

The size and surface charge of the filtered and back-filtered samples (for the base case of 3:2 CNC:MC) were also measured and the results are shown in Table 1. The initial latex suspension of PMMA particles had a zeta potential of -17 mV, suggesting that the CNCs were at the surface of the PMMA particles as they were the only charged species in the polymerization. When the back-filtered particles (those that did not pass through the 1 μm filter) were collected, they had a zeta potential of -35 mV, comparable to -30 mV for a pure CNC suspension. This further supports that the large particles have CNCs on the surface. Additionally, the filtered nanoparticles had a neutral zeta potential, resulting from an uncharged surface, which is comparable to a solution of MC which is uncharged. Because of this, and since it was confirmed that only nanoparticles were formed when MC was used alone as a stabilizer, it can be concluded that the microparticles of PMMA were stabilized by CNCs coated with MC, and the secondary nanoparticle morphology was stabilized by MC only.

Table 1. Size and zeta potential of particles before and after filtration through a 1μm filter.

	Zeta Potential (mV)	Particle Size
Initial	-17.1 ± 0.5	19 μm[a]
Back-filter	-35 ± 2	43 μm[a]
Filter	-6 ± 3	266 nm[b]
CNC	-30 ± 3	78 nm[c]
MC	-3 ± 2	70 nm [c]

[a]Determined by MasterSizer.
[b]Determined by DLS.
[c]Determined by DLS for a separate CNC suspension and MC solution, unrelated to the filtration/back-filtration investigation of PMMA latexes.

In order to elucidate the effect of drying temperature on the morphology of the PMMA particles, base case 3:2 CNC:MC samples were dried at three different temperatures (Figure 5). Since the glass transition temperature (T_g) of PMMA is around 105 °C,[71] temperatures were chosen above and below the T_g. Importantly, in samples dried at all three temperatures, spherical microparticles with diameters >20 μm were seen, while those <20 μm likely coalesced and were not as apparent in the SEM images. Nonetheless, samples dried below the T_g, at 80 °C (Figure 5a) and 100°C (Figure 5b) showed no difference in surface morphology from those dried at 60 °C (shown in Figure 3); PMMA microparticles decorated with PMMA nanoparticles were observed for both samples. For the sample dried above the T_g at 140 °C (Figure 5c), less of the secondary nanoparticle morphology was observed on the microparticle surface, and at higher magnification the nanoparticles on the surface appear coalesced/sintered, resulting in a smoother surface. This suggests that the PMMA polymer chains inside the nanoparticles were mobile enough above their T_g to coalesce and form a smooth PMMA shell on the surface of the PMMA microparticles. This was also seen when PMMA nanoparticles stabilized by MC alone were dried at 140 °C, they showed a smooth, coalesced morphology where the nanoparticles appeared to be melted into one another (data not shown). Therefore, in the large microparticles produced in the base case latex, no change in the microparticle morphology was observed even at temperatures well above the T_g of the polymer, suggesting that the CNC shell on these particles is able to improve resistance to coalescence at high temperatures and that the microparticle surface morphology may be tuned based on drying conditions.

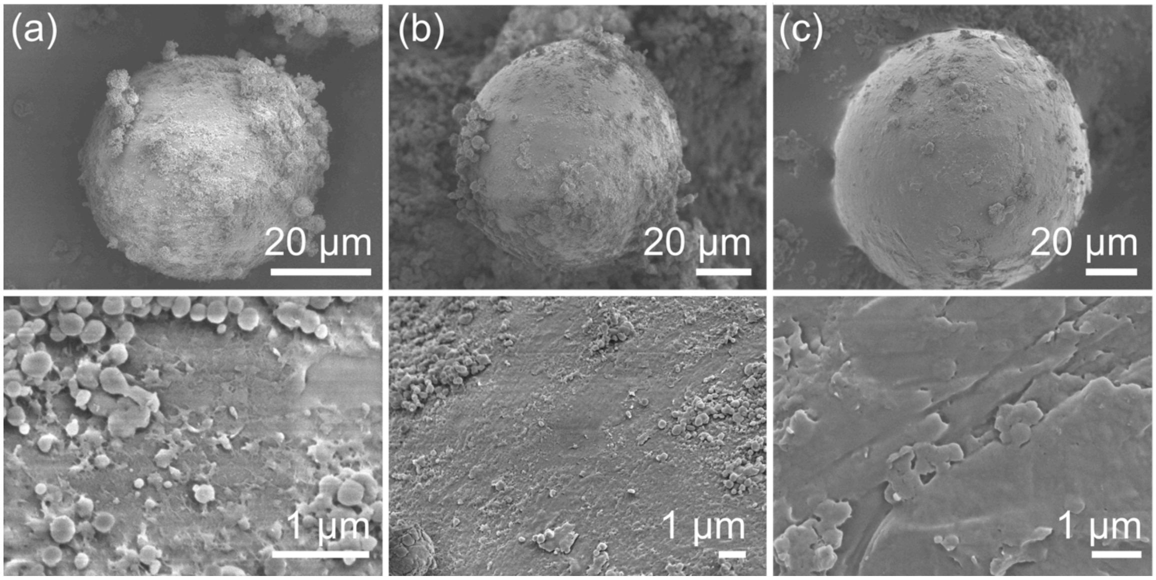

Figure 5. Morphology of PMMA particles stabilized by 3:2 CNC:MC after oven drying for 30 min at (a) 80 °C, (b) 100 °C, (c) 140 °C. Top row shows microparticle morphology (20 µm scale bars) and bottom row shows a zoomed in version of the microparticle surfaces (1 µm scale bars).

This work presents a new "greener" method that uses cellulose nanocrystals and methyl cellulose as co-stabilizers in the microsuspension polymerization of methyl methacrylate to produce PMMA latexes with a double morphology. A higher CNC:MC ratio gave more microparticles stabilized by MC-coated CNCs and a lower CNC:MC ratio gave more nanoparticles stabilized by MC alone. Most of the nanoparticles were attached to the microparticles offering a novel secondary latex structure achievable in only one synthetic step. Overall, the latex morphology, surface charge and roughness were tunable based on the ratio of co-stabilizers and the latex drying protocol, and a facile method to incorporate CNCs into latexes was presented. While PMMA was chosen as a model system, these findings are translatable to other suspension polymer systems and may extend the use of CNCs into products such as adhesives, toners, cosmetics, paints and coatings.

Acknowledgements

The authors thank Xuan Yang and Daniel Osorio for performing the SEM imaging at the Canadian Center for Electron Microscopy at McMaster University. Special thanks to Drs. Pelton, Adronov, and Guarne for equipment use. Additional thanks to Blair Morgan, Erik Joy, Lingli Liu, and Dr. Zhen Hu for useful lab assistance and discussions.

Synopsis

Cellulose nanocrystals and methyl cellulose (both sustainable biopolymers from renewable resources) are used replace toxic and synthetic surfactants to produce polymer latexes with unique morphologies.

References

(1) Habibi, Y.; Lucia, L. A.; Rojas, O. J. Cellulose Nanocrystals: Chemistry, Self-Assembly, and Applications. *Chem. Rev.* **2010**, *110* (6), 3479–3500.
(2) Kalashnikova, I.; Bizot, H.; Cathala, B.; Capron, I. Modulation of Cellulose Nanocrystals Amphiphilic Properties to Stabilize Oil/Water Interface. *Biomacromolecules* **2012**, *13* (1), 267–275.
(3) Salas, C.; Nypelö, T.; Rodriguez-Abreu, C.; Carrillo, C.; Rojas, O. J. Nanocellulose Properties and Applications in Colloids and Interfaces. *Curr. Opin. Colloid Interface Sci.* **2014**, *19* (5), 383–396.
(4) Eichhorn, S. J. Cellulose Nanowhiskers: Promising Materials for Advanced Applications. *Soft Matter* **2011**, *7* (2), 303–315.
(5) Li, Q.; McGinnis, S.; Sydnor, C.; Wong, A.; Renneckar, S. Nanocellulose Life Cycle Assessment. *ACS Sustain. Chem. Eng.* **2013**, *1* (8), 919–928.
(6) de Figueirêdo, M. C. B.; Rosa, M. de F.; Ugaya, C. M. L.; Souza Filho, M. de S. M. de; Silva Braid, A. C. C. da; Melo, L. F. L. de. Life Cycle Assessment of Cellulose Nanowhiskers. *J. Clean. Prod.* **2012**, *35*, 130–139.
(7) Oksman, K.; Aitomäki, Y.; Mathew, A. P.; Siqueira, G.; Zhou, Q.; Butylina, S.; Tanpichai, S.; Zhou, X.; Hooshmand, S. Review of the Recent Developments in Cellulose Nanocomposite Processing. *Compos. Part A Appl. Sci. Manuf.* **2016**, *83*, 2–18.
(8) Dufresne, A. Cellulose Nanomaterial Reinforced Polymer Nanocomposites. *Curr. Opin. Colloid Interface Sci.* **2017**, *29*, 1–8.
(9) Habibi, Y. Key Advances in the Chemical Modification of Nanocelluloses. *Chem. Soc. Rev.* **2014**, *43* (5), 1519–1542.
(10) Morandi, G.; Heath, L.; Thielemans, W. Cellulose Nanocrystals Grafted with Polystyrene Chains Through Surface-Initiated Atom Transfer Radical Polymerization (SI-ATRP). *Langmuir* **2009**, *25* (14), 8280–8286.
(11) Yin, Y.; Tian, X.; Jiang, X.; Wang, H.; Gao, W. Modification of Cellulose Nanocrystal via SI-ATRP of Styrene and the Mechanism of its Reinforcement of Polymethylmethacrylate. *Carbohydr. Polym.* **2016**, *142*, 206–212.
(12) Rosilo, H.; McKee, J. R.; Kontturi, E.; Koho, T.; Hytönen, V. P.; Ikkala, O.;

Kostiainen, M. A. Cationic Polymer Brush-Modified Cellulose Nanocrystals for High-Affinity Virus Binding. *Nanoscale* **2014**, *6* (20), 11871–11881.

(13) Yu, H. Y.; Zhang, D. Z.; Lu, F. F.; Yao, J. New Approach for Single-Step Extraction of Carboxylated Cellulose Nanocrystals for Their Use As Adsorbents and Flocculants. *ACS Sustain. Chem. Eng.* **2016**, *4* (5), 2632–2643.

(14) Mujica-Garcia, A.; Hooshmand, S.; Skrifvars, M.; Kenny, J. M.; Oksman, K.; Peponi, L. Poly(lactic acid) Melt-spun Fibers Reinforced with Functionalized Cellulose Nanocrystals. *RSC Adv.* **2016**, *6* (11), 9221–9231.

(15) Podsiadlo, P.; Choi, S. Y.; Shim, B.; Lee, J.; Cuddihy, M.; Kotov, N. A. Molecularly Engineered Nanocomposites: Layer-by-layer Assembly of Cellulose Nanocrystals. *Biomacromolecules* **2005**, *6* (6), 2914–2918.

(16) Morelli, C. L.; Belgacem, M. N.; Branciforti, M. C.; Bretas, R. E. S.; Crisci, A.; Bras, J. Supramolecular Aromatic Interactions to Enhance Biodegradable Film Properties Through Incorporation of Functionalized Cellulose Nanocrystals. *Compos. Part A Appl. Sci. Manuf.* **2016**, *83*, 80–88.

(17) Morelli, C. L.; Belgacem, N.; Bretas, R. E. S.; Bras, J. Melt Extruded Nanocomposites of Polybutylene adipate-co-terephthalate (PBAT) with Phenylbutyl Isocyanate Modified Cellulose Nanocrystals. *J. Appl. Polym. Sci.* **2016**, *133* (34), 1–9.

(18) Hasani, M.; Cranston, E. D.; Westman, G.; Gray, D. G. Cationic Surface Functionalization of Cellulose Nanocrystals. *Soft Matter* **2008**, *4* (11), 2238–2244.

(19) Goussé, C.; Chanzy, H.; Excoffier, G.; Soubeyrand, L.; Fleury, E. Stable Suspensions of Partially Silylated Cellulose Whiskers Dispersed in Organic Solvents. *Polymer (Guildf).* **2002**, *43* (9), 2645–2651.

(20) Goussé, C.; Chanzy, H.; Cerrada, M. L.; Fleury, E. Surface Silylation of Cellulose Microfibrils: Preparation and Rheological Properties. *Polymer (Guildf).* **2004**, *45* (5), 1569–1575.

(21) Boujemaoui, A.; Mongkhontreerat, S.; Malmström, E.; Carlmark, A. Preparation and Characterization of Functionalized Cellulose Nanocrystals. *Carbohydr. Polym.* **2015**, *115*, 457–464.

(22) Kan, K. H. M.; Li, J.; Wijesekera, K.; Cranston, E. D. Polymer-Grafted Cellulose Nanocrystals as pH-Responsive Reversible Flocculants. *Biomacromolecules* **2013**, *14* (9), 3130–3139.

(23) Kedzior, S. A.; Graham, L.; Moorlag, C.; Dooley, B. M.; Cranston, E. D. Poly(methyl methacrylate)-Grafted Cellulose Nanocrystals: One-step Synthesis, Nanocomposite Preparation, and Characterization. *Can. J. Chem. Eng.* **2016**, *94* (5), 811–822.

(24) Zoppe, J. O.; Habibi, Y.; Rojas, O. J.; Venditti, R. A.; Johansson, L. S.; Efimenko, K.; Österberg, M.; Laine, J. Poly(N-isopropylacrylamide) Brushes Grafted from Cellulose Nanocrystals via Surface-Initiated Single-Electron Transfer Living Radical Polymerization. *Biomacromolecules* **2010**, *11* (10), 2683–2691.

(25) Zoppe, J. O.; Xu, X.; Känel, C.; Orsolini, P.; Siqueira, G.; Tingaut, P.; Zimmermann, T.; Klok, H.-A. Effect of Surface Charge on Surface-Initiated Atom Transfer Radical Polymerization from Cellulose Nanocrystals in Aqueous Media. *Biomacromolecules* **2016**, *17*, 1404–1413.

(26) Haque, M. M.-U.; Puglia, D.; Fortunati, E.; Pracella, M. Effect of Reactive

Functionalization on Properties and Degradability of Poly(lactic acid)/Poly(vinyl acetate) Nanocomposites with Cellulose Nanocrystals. *React. Funct. Polym.* **2017**, *110*, 1–9.

(27) Zhou, Q.; Brumer, H.; Teeri, T. T. Self-Organization of Cellulose Nanocrystals Adsorbed with Xyloglucan Oligosaccharide-Poly(ethylene glycol)-Polystyrene Triblock Copolymer. *Macromolecules* **2009**, *42* (15), 5430–5432.

(28) Hu, Z.; Cranston, E. D.; Ng, R.; Pelton, R. Tuning Cellulose Nanocrystal Gelation with Polysaccharides and Surfactants. *Langmuir* **2014**, *30* (10), 2684–2692.

(29) Hu, Z.; Patten, T.; Pelton, R.; Cranston, E. D. Synergistic Stabilization of Emulsions and Emulsion Gels with Water-Soluble Polymers and Cellulose Nanocrystals. *ACS Sustain. Chem. Eng.* **2015**, *3* (5), 1023–1031.

(30) Hu, Z.; Berry, R. M.; Pelton, R.; Cranston, E. D. One-Pot Water-Based Hydrophobic Surface Modification of Cellulose Nanocrystals Using Plant Polyphenols. *ACS Sustain. Chem. Eng.* **2017**, *5* (6), 5018–5026.

(31) Hu, Z.; Ballinger, S.; Pelton, R.; Cranston, E. D. Surfactant-Enhanced Cellulose Nanocrystal Pickering Emulsions. *J. Colloid Interface Sci.* **2015**, *439*, 139–148.

(32) Kedzior, S. A.; Marway, H. S.; Cranston, E. D. Tailoring Cellulose Nanocrystal and Surfactant Behavior in Miniemulsion Polymerization. *Macromolecules* **2017**, *50* (7), 2645–2655.

(33) Cherhal, F.; Cousin, F.; Capron, I. Structural Description of the Interface of Pickering Emulsions Stabilized by Cellulose Nanocrystals. *Biomacromolecules* **2016**, *17* (2), 496–502.

(34) Kalashnikova, I.; Bizot, H.; Bertoncini, P.; Cathala, B.; Capron, I. Cellulosic Nanorods of Various Aspect Ratios for Oil in Water Pickering Emulsions. *Soft Matter* **2013**, *9* (3), 952–959.

(35) Capron, I.; Cathala, B. Surfactant-Free High Internal Phase Emulsions Stabilized by Cellulose Nanocrystals. *Biomacromolecules* **2013**, *14* (2), 291–296.

(36) Peddireddy, K. R.; Nicolai, T.; Benyahia, L.; Capron, I. Stabilization of Water-in-Water Emulsions by Nanorods. *ACS Macro Lett.* **2016**, *5* (3), 283–286.

(37) Saidane, D.; Perrin, E.; Cherhal, F.; Guellec, F.; Capron, I. Some Modification of Cellulose Nanocrystals for Functional Pickering Emulsions. *Philos. Trans. R. Soc. A Math. Phys. Eng. Sci.* **2016**, *374* (2072), 1–11.

(38) Kalashnikova, I.; Bizot, H.; Cathala, B.; Capron, I. New Pickering Emulsions Stabilized by Bacterial Cellulose Nanocrystals. *Langmuir* **2011**, *27* (12), 7471–7479.

(39) Du, W.; Guo, J.; Li, H.; Gao, Y. Heterogeneously Modified Cellulose Nanocrystals-Stabilized Pickering Emulsion: Preparation and Their Template Application for the Creation of PS Microspheres with Amino-Rich Surfaces. *ACS Sustain. Chem. Eng.* **2017**, acssuschemeng.7b00375.

(40) Hu, Z.; Marway, H. S.; Kasem, H.; Pelton, R.; Cranston, E. D. Dried and Redispersible Cellulose Nanocrystal Pickering Emulsions. *ACS Macro Lett.* **2016**, *5* (2), 185–189.

(41) Hu, Z.; Xu, R.; Cranston, E. D.; Pelton, R. H. Stable Aqueous Foams from Cellulose Nanocrystals and Methyl Cellulose. *Biomacromolecules* **2016**, *17* (12), 4095–4099.

(42) Elmabrouk, A. Ben; Thielemans, W.; Dufresne, A.; Boufi, S. Preparation of

Poly(styrene-co-hexylacrylate)/Cellulose Whiskers Nanocomposites via Miniemulsion Polymerization. *J. Appl. Polym. Sci.* **2009**, *114* (5), 2946–2955.

(43) Mabrouk, A. Ben; Kaddami, H.; Magnin, A.; Belgacem, M. N.; Dufresne, A.; Boufi, S. Preparation of Nanocomposite Dispersions Based on Cellulose Whiskers and Acrylic Copolymer by Miniemulsion Polymerization: Effect of the Silane Content. *Polym. Eng. Sci.* **2011**, *51* (1), 62–70.

(44) Geng, S.; Haque, M. M. U.; Oksman, K. Crosslinked Poly(vinyl acetate) (PVAc) Reinforced with Cellulose Nanocrystals (CNC): Structure and Mechanical Properties. *Compos. Sci. Technol.* **2016**, *126*, 35–42.

(45) Pracella, M.; Haque, M. M. U.; Puglia, D. Morphology and Properties Tuning of PLA/Cellulose Nanocrystals Bio-Nanocomposites by Means of Reactive Functionalization and Blending with PVAc. *Polymer (Guildf).* **2014**, *55* (16), 3720–3728.

(46) Dastjerdi, Z.; Cranston, E. D.; Dubé, M. A. Synthesis of Poly(n-butyl acrylate/methyl methacrylate)/CNC Latex Nanocomposites via In Situ Emulsion Polymerization. *Macromol. React. Eng.* **2017**, *201700013*, 1700013.

(47) Dastjerdi, Z.; Cranston, E. D.; Dubé, M. A. Adhesive Property Modification using Cellulose Nanocrystals. *Int. J. Adhes. Adhes.* **2017**, submitted.

(48) Cunningham, M. F. Microsuspension Polymerization of Methyl Methacrylate. *Polym. React. Eng.* **1999**, *7* (2), 231–257.

(49) Vivaldo-Lima, E.; Wood, P. E.; Hamielec, A. E.; Penlidis, A. An Updated Review on Suspension Polymerization. *Ind. Eng. Chem. Res.* **1997**, *36* (4), 939–965.

(50) Yuan, H. G.; Kalfas, G.; Ray, W. H. Suspension Polymerization. *J. Macromol. Sci. Part C Polym. Rev.* **1991**, *31* (2–3), 215–299.

(51) Perro, A.; Reculusa, S.; Bourgeat-Lami, E.; Duguet, E.; Ravaine, S. Synthesis of Hybrid Colloidal Particles: From Snowman-Like to Raspberry-Like Morphologies. *Colloids Surfaces A Physicochem. Eng. Asp.* **2006**, *284–285*, 78–83.

(52) Tiarks, F.; Landfester, K.; Antonietti, M. Silica Nanoparticles as Surfactants and Fillers for Latexes Made by Miniemulsion Polymerization. *Langmuir* **2001**, *17* (19), 5775–5780.

(53) Cao, Z.; Schrade, A.; Landfester, K.; Ziener, U. Synthesis of Raspberry-Like Organic-Inorganic Hybrid Nanocapsules via Pickering Miniemulsion Polymerization: Colloidal Stability and Morphology. *J. Polym. Sci. Part A Polym. Chem.* **2011**, *49* (11), 2382–2394.

(54) Duan, L.; Chen, M.; Zhou, S.; Wu, L. Synthesis and Characterization of Poly(N-isopropylacrylamide)/Silica Composite Microspheres via Inverse Pickering Suspension Polymerization. *Langmuir* **2009**, *25* (6), 3467–3472.

(55) Omi, S.; Senba, T.; Nagai, M.; Ma, G. Morphology Development of 10-µm Scale Polymer Particles Prepared by SPG Emulsification and Suspension Polymerization. *J. Appl. Polym. Sci.* **2001**, *79*, 2200–2220.

(56) Zhu, H.; Zhang, Q.; Zhu, S. Preparation of Raspberry-Like ZIF-8/PS Composite Spheres via Dispersion Polymerization. *Dalt. Trans.* **2015**, *44* (38), 16752–16757.

(57) Schmidt, B. V. K. J.; Molinari, V.; Esposito, D.; Tauer, K.; Antonietti, M. Lignin-based polymeric surfactants for emulsion polymerization. *Polymer (Guildf).* **2017**, *112*, 418–426.

(58) Tong, X.; Ding, W.; Cetinkaya, C. Effects of Nanoparticle Coating on the

Adhesion of Emulsion Aggregation Toner Particles. *J. Adhes. Sci. Technol.* **2010**, *24* (2), 371–387.

(59) Jovanović, R.; Ouzineb, K.; McKenna, T. F.; Dubé, M. A. Butyl acrylate/methyl methacrylate latexes: adhesive properties. *Macromol. Symp.* **2004**, *206* (1), 43–56.

(60) Ouzineb, K.; Graillat, C.; McKenna, T. F. High-Solid-Content Emulsions. V. Applications of Miniemulsions to High Solids and Viscosity Control. *J. Appl. Polym. Sci.* **2005**, *97* (3), 745–752.

(61) Cranston, E. D.; Gray, D. G. Morphological and Optical Characterization of Polyelectrolyte Multilayers Incorporating Nanocrystalline Cellulose. *Biomacromolecules* **2006**, *7* (9), 2522–2530.

(62) Reid, M. S.; Villalobos, M.; Cranston, E. D. Benchmarking Cellulose Nanocrystals: From the Laboratory to Industrial Production. *Langmuir* **2017**, *33* (7), 1583–1598.

(63) Yaws, C. L. *Thermophysical Properties of Chemicals and Hydrocarbons*; William Andrew: Norwich, NY, 2008.

(64) Schmidt, R. L.; Randall, J. C.; Clever, H. L. The Surface Tension and Density of Binary Hydrocarbon Mixtures: Benzene-n-Hexane and Benzene-n-Dodecane. *J. Phys. Chem.* **1966**, *70* (12), 3912–3916.

(65) Ohtsuka, Y. Light-Focusing Plastic Rod Prepared from diallyl isophthalate-methyl methacrylate Copolymerization. *Appl. Phys. Lett.* **1973**, *23* (5), 247–248.

(66) Bhattacharjee, S. DLS and Zeta Potential - What They Are and What They Are Not? *J. Control. Release* **2016**, *235*, 337–351.

(67) Brandup, J.; Immergut, E. H.; Grulke, E. A. *Polymer Handbook*, Fourth.; Wiley: New York, 1999.

(68) Trommsdorff, V. E.; Köhle, H.; Lagally, P. Zur Polymerisation des Methacrylsäuremethylesters. *Die Makromol. Chemie* **1948**, *1* (3), 169–198.

(69) Tulig, T. J.; Tirrell, M. On the Onset of the Trommsdorff Effect. *Macromolecules* **1982**, *15* (2), 459–463.

(70) Harkins, W. D.; Brown, F. E. The Determination of Surface Tension (Free Surface Energy), and the Weight of Falling Drops: The Surface Tension of Water and Benzene by the Capillary Height Method. *J. Am. Chem. Soc.* **1919**, *41* (4), 499–524.

(71) Huang, X.; Brittain, W. J. Synthesis and Characterization of PMMA Nanocomposites by Suspension and Emulsion Polymerization. *Macromolecules* **2001**, *34* (10), 3255–3260.

Table of Contents Graphic (For table of contents use only)

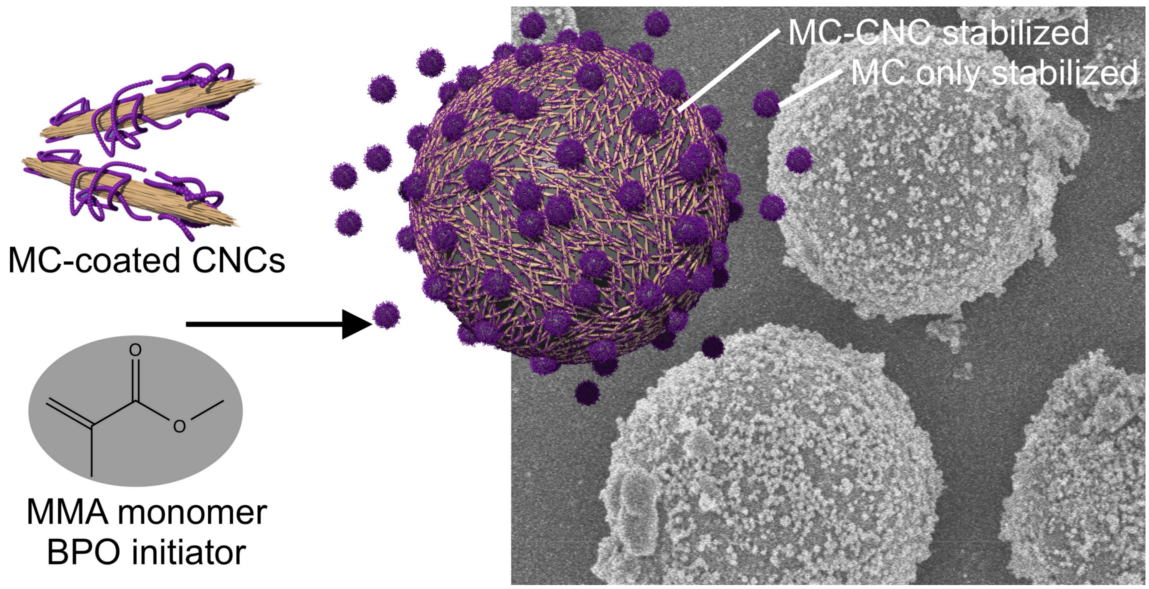

Chapter 8

Polymer-grafted Cellulose Nanocrystals for Incorporation into the Core of Latex Polymer Particles.

This chapter uses controlled polymer grafting techniques similar to those presented in Chapter 4 to graft poly(butyl acrylate) and poly(methyl methacrylate) from CNCs with varying graft lengths. The modified CNCs were added to the hydrophobic monomer phase during the miniemulsion polymerization of MMA to incorporate polymer-grafted CNCs into the core of the polymer latex particles. This is in contrast to Chapter 6 and 7 where CNCs were either passive entities in the water phase during latex synthesis or played the role of Pickering stabilizers (and became incorporated into the polymer at the latex-water interface). This is proof of principle work that demonstrates that CNC surface chemistry can be tailored to control the location of CNCs in latexes where improved mechanical and adhesive properties may be achieved.

In this work, I designed and performed all syntheses and characterization experiments with assistance from Michael Kiriakou (BEng student). Dr. Elina Niinivaara collected the transmission electron microscopy images. I wrote the manuscript with editorial assistance from my supervisor, Dr. Emily Cranston. Prof. Marc Dubé from the University of Ottawa advised on the reaction engineering aspects of the project and guidance was provided by our industrial sponsors, Dr. Carole Fraschini (FPInnovations) and Dr. Richard Berry (CelluForce). This chapter is in the final stages of preparation for submission.

Polymer-grafted Cellulose Nanocrystals for Incorporation into the Core of Latex Polymer Particles

Stephanie A. Kedzior[a], Michael Kiriakou[a], Elina Niinivaara[a], Marc A. Dubé[b], Carole Fraschini[c], Richard Berry[d], Emily D. Cranston[a,*]

[a]Department of Chemical Engineering, McMaster University, 1280 Main Street West, Hamilton, ON, Canada, L8S 4L7

[b]Department of Chemical and Biological Engineering, Centre for Catalyst Research and Innovation, University of Ottawa, 75 Laurier Ave E, Ottawa, ON, Canada, K1N 6N5

[c]FPInnovations, 570 Boulevard St. Jean, Pointe-Claire, QC, Canada, H9R 3J9

[d]CelluForce Inc., 625 Président-Kennedy Avenue, Montreal, QC, Canada, H3A 1K2

*To whom correspondence should be addressed
Dr. Emily D. Cranston, ecranst@mcmaster.ca

ABSTRACT

Cellulose nanocrystals (CNCs) are stiff anisotropic nanoparticles derived from renewable resources such as wood pulp and cotton. CNCs are growing in popularity in academic and industrial research because they have the potential to be used as modifiers and reinforcing agents in nanocomposites. However, challenges due to incompatibility between cellulose and hydrophobic polymers, and processing difficulties such as aggregation and low thermal stability have limited the performance of nanocomposites produced to date. In this work, we have used surface initiated atom transfer radical polymerization to graft hydrophobic poly(butyl acrylate) and poly(methyl methacrylate) (PMMA) from the surface of CNCs to overcome the incompatibility issue. The polymer-grafted CNCs were used in the miniemulsion polymerization of methyl methacrylate whereby the modified CNCs were added to the monomer phase. Polymer-grafted CNCs with short graft lengths (degree of polymerization = 50) were incorporated inside the core of the latex particles, producing a PMMA-CNC nanocomposite latex *in situ*. The effect of grafted polymer type, length and loading on the latex size, surface charge, and morphology was investigated. Transmission electron microscopy indicated that grafted polymer type did not have a significant effect on CNC incorporation and that CNCs with long polymer grafts (degree of polymerization = 200) may be too large/aggregated to be integrated into the latex core. This work provides a novel method for incorporating CNCs into nanocomposite latexes and is anticipated to extend the use of CNCs in applications such as adhesives, coatings, and other synthetic latex-based products.

Introduction

In recent years, cellulose nanocrystals (CNCs) have gained attention in both academic and industrial research due to their unique properties.[1,2] They are strong, rod-shaped, light weight, bio-based nanoparticles that have the potential to be used as reinforcing agents, modifiers, and stabilizers in polymer nanocomposites and hybrid materials.[3] CNCs are most commonly extracted from sources such as wood pulp and cotton through a sulfuric acid hydrolysis which yields anisotropic nanoparticles with anionic sulfate half ester groups on the surface. Both lab-made and industrially produced CNCs are isolated via this process and have near identical properties.[4] Despite having slight amphiphilic properties and a hydrophobic plane void of hydroxyl groups, the majority of the CNC surface has an abundance of hydroxyl groups resulting in a nanoparticle that is overall hydrophilic in the unmodified state. This hydrophilicity leads to compatibility and processing issues when CNCs are combined with hydrophobic polymer matrices.

In order to overcome the hydrophilicity of CNCs, many surface modification methods have been used to prepare hydrophobic CNCs, most of which are summarized in recent reviews.[5,6] In short, ionic interactions between the anionic sulfate half ester groups on the surface of CNCs and quarternary ammonium salts bearing long alkyls tails can be used to prepare hydrophobic CNCs, though ionic bonds may not be robust enough to withstand some processing techniques and solvents.[7–9] Covalent modification with small molecules offers a more robust modification. Methods include esterification,[10,11] modification with urethanes,[12] grafting of castor oil,[13] oxidation,[14] acytelation,[15] the attachment of silane groups,[16] and the use of tannic acid as a primer for decylamine addition.[17] These modification routes provide hydrophobically modified CNCs that retain their morphology, with contact angles typically within 67 to 85°.

CNCs can also be rendered hydrophobic via polymer grafting. Two methods for polymer grafting are typically used: "grafting to" where pre-formed polymers are attached to the surface of CNCs, or "grafting from" where the polymerization is initiated from the CNC surface. Polymer "grafting to" CNCs is typically limited by steric hinderance, and therefore high grafting density is difficult to achieve.[5] Polymer "grafting from" CNCs may occur via free radical polymerization,[18–22] ring opening polymerization,[23–29] nitroxide mediated polymerization,[30] or surface initiated atom transfer radical polymerization (SI-ATRP), which is used in this work.

SI-ATRP from CNCs was first reported by Yi et al.[31] who grafted polystyrene (PS) from CNCs. Morandi et al.[32] also grafted PS from CNCs and presented a series of PS-*g*-CNCs with varying graft densities. In their work, the grafted polymer was cleaved from the surface and characterized to show that good control of the SI-ATRP was achieved.[33] Since these first reports, other polymers have been grafted from CNCs including PS,[31,32,34] poly(methacrylate),[35,36] poly(methyl methacrylate) (PMMA),[37] poly(dimethylaminoethyl methacrylate),[38,39] poly(N-isopropylacrylamide) (PNIPAm),[40–42] PNIPAm fluorescent copolymers,[43] poly(N,N-dimethylacrylamide),[44] poly(2-aminoethylmethacrylate) and poly(2-aminoethylmethacrylamide),[45] poly(acrylic acid) through hydrolysis of poly(tert-butyl acrylate),[46] poly(6-(4-(4-

methoxyphenylazo)phenoxy)hexyl methacrylate),[47] copolymers of poly(MMA-co-butyl acrylate),[48] poly(dimethylaminoethy methacrylate) and poly(diethylaminoethyl methacrylate),[49] poly(ethylene glycol methylacrylate),[50] poly([(2-methacryloyloxy)ethyl]trimethylammonium chloride),[42] and poly(sodium 4-vinylbenzenesulfonate).[42] SI-ATRP provides many benefits over other polymer grafting techniques including the ability to control the polymer graft density (via the ratio of initiating groups to hydroxyl groups on the CNC surface) as well as the polymer graft length (or degree of polymerization, DP). In this work, we have used SI-ATRP to modify CNCs with the hydrophobic polymers poly(butyl acrylate) (PBA) and PMMA, resulting in CNC-*g*-PBA$_n$ or CNC-*g*-PMMA$_n$ (where n is the target DP). PBA was grafted from the CNC surface at two different graft lengths in order to determine the effect of graft length on the incorporation of CNC-*g*-PBA$_n$ into the core of latex polymer particles, with the goal of preparing novel nanocomposite latexes.

Previously, nanocomposite latexes with CNCs have been prepared by blending CNCs with a pre-made latex, or by adding CNCs *in situ* during the (mini)emulsion polymerization. CNC/latex blends were first prepared by Favier and Chanzy.[51,52] In their work, CNCs were blended with low T_g polymer latexes in order to prepare nanocomposite films. Transmission electron microscopy (TEM) showed a good distribution of CNCs within the polymer film, and the nanocomposite film exhibited superior mechanical properties compared to polymer alone. The CNCs were unmodified and remained in the water phase. Similar to this work, Vatansever et al.[53] blended CNCs with a poly(butyl acrylate-co-methyl methacrylate) latex and showed good dispersion of the CNCs within the latex suspension and an increase in mechanical properties. Blending CNCs with latex provides a facile method for the addition of CNCs into latex nanocomposites, however the location of the CNCs is restricted to the water phase. In this work, we aim to incorporate CNCs into the hydrophobic core of the polymer latex particles.

Elmabrouk and coworkers used unmodified CNCs *in situ* in order to improve the properties of a latex-based coating.[54] The CNCs were added to the water phase in the miniemulsion polymerization of poly(styrene-co-hexyl acrylate). Upon imaging the films with TEM, the CNCs were observed between the latex particles, and remained in the water phase during the polymerization. The nanocomposite latex films showed improved properties compared to those without CNCs. Elmabrouk et al. also prepared poly(butyl methacrylate) latexes by miniemulsion polymerization in the presence of CNCs,[55] where unmodified CNCs were added to the water phase with a cationic surfactant as the stabilizer.[55] In this case, the anionic CNCs tended to appear anchored around the cationic latex particles. Furthermore, Elmabrouk et al. studied the preparation of poly(styrene-co-2-ethyl hexylacrylate) latexes using a reactive silane (methacryloxypropyl triethoxysilane) in order to stabilize the dispersion and to promote the anchoring of CNCs on the polymer particles via hydrogen bonding between the silanol groups and the hydroxyl groups on the CNC surface. This provided improved mechanical properties in the resulting films. Most recently, Dastjerdi et al.[56] added unmodified CNCs to the water phase in the preparation of poly(*n*-butyl acrylate/methyl methacrylate)/CNC latex nanocomposites. They showed a significant increase in gel content, latex viscosity, and storage and loss moduli. We have also shown the ability to use CNCs as co-stabilizers in miniemulsion[57] and microsuspension polymerization[58] of PMMA latexes whereby CNCs were combined with either surfactant or polymer in order to enhance their surface activity and their use as Pickering stabilizers. In all of these cases, the CNCs were trapped in between latex particles or incorporated at the latex-water interface, and to the best of our knowledge there are no literature examples of CNCs inside the core of a latex particle.

In the work presented here, we have used SI-ATRP to prepare polymer-grafted CNCs with varying graft lengths and polymer type in order to incorporate hydrophobic CNCs into the core of acrylate polymer latex particles. Polymer-grafted CNCs were dispersed in the monomer phase of the miniemulsion polymerization of methyl methacrylate (MMA) along with an oil soluble initiator, and anionic sodium dodecyl sulfate (SDS) was used as the stabilizing agent in order to prepare PMMA latexes where polymer-grafted CNCs were incorporated inside the PMMA particles.

Experimental Section

Materials

α-Bromoisobutyryl Bromide (BiB), ethyl α-Bromoisobutyrate (EBiB), *N*,*N*,*N*′,*N*′′,*N*′′-Pentamethyldiethylenetriamine (PMDETA), copper (I) bromide ($CuBr_2$), 4-(dimethylamino)pyridine (DMAP), trimethylamine (TEA), aluminum oxide, ethylenediaminetetraacetic acid (EDTA), sodium dodecyl sulfate (SDS), and benzoyl peroxide (Luperox A98, BPO) were purchased from Sigma Aldrich and used as received. Dimethylformamide (DMF), toluene, and ethanol (95%) were purchased from Caledon Labs. Poly(allylamine hydrochloride) (PAH, M_w = 120 000 – 200 000 Da) was purchased from Polysciences. Methyl methacrylate (MMA) and butyl acrylate (BA) were purchased from Sigma Aldrich and passed through a column of basic aluminum oxide prior to use. All water used was purified using a Barnstead GenPure Pro water purification system from ThermoFisher Scientific. Unmodified cellulose nanocrystals were provided as a spray dried powder (sodium form) by CelluForce Inc.

Methods

Initiator modified CNCs were prepared by redispersing dried CelluForce CNCs in DMF at a concentration of 1 wt.%. The suspension was sonicated in a sonicator bath for 60-120 min in order to promote proper dispersion of the CNCs. In a typical reaction, 2 g of CNCs were dispersed in 200 mL of DMF. After sonication, the suspension was transferred to a round bottom flask, and 4.6 mL of TEA and a catalytic amount of DMAP were added. The suspension was degassed by bubbling Ar for 15 min, after which 3.0 mL of BiB was added dropwise. The suspension was degassed for 5 additional minutes and then added to a 70°C oil bath for 18 h, after which the reaction was stopped by opening the flask to air. The BiB-CNCs were purified by centrifugation at 5000 rpm for 5 min at 15°C in order to remove DMF and unreacted reagents. The resulting CNCs, denoted BiB-CNCs, were then redispersed in ethanol and centrifuged and washed three additional times at 7000 rpm, then redispersed in water, dialyzed against purified water for 10 rinses, and freeze dried.

Polymer-grafted CNCs were prepared by redispersing dried BiB-CNCs in toluene. BiB-CNCs were grafted with either BA or MMA. In a typical reaction to graft BA, 1 g of BiB-CNCs was dispersed in 100 mL toluene, resulting in a 1 wt.% suspension that was stirred via magnetic stirring for 24 h and sonicated for 120 min in a sonicator bath in order to ensure proper dispersion. The suspension was then transferred to a round bottom flask, where 101.8 mL of purified butyl acrylate was added, along with 1.47 mL PMDETA and 1.0 mL EBiB as a sacrificial initiator. Sacrifical initiator was added to provide free polymer not grafted from CNCs in order to determine grafted polymer molecular weight. The reaction was degassed for 30 min, after which 1.0 g CuBr was added and the reaction was degassed for 15 additional min. The degree of polymerization (DP, or polymer graft length) was controlled based on the molar ratio of monomer:initiator, and a target DP of 200 was chosen for both PBA and PMMA modified CNCs, and DP 50 for PBA in order to evaluate the effect of graft length. After degassing, the flask was sealed and added to an oil bath at 90°C for 6 h. The reaction was stopped by opening the flask to air. The reaction mixture was centrifuged at 11 000 rpm for 10 min, and the first supernatant was collected and contained free polymer dissolved in toluene. The free polymer was purified using an aluminum oxide column, precipitated in cold methanol, and collected for analysis. The CNC-*g*-PBA_{200} were then purified by excessive washing and centrifugation first in methanol then in acetone until the supernatants were no longer coloured (assuming the Cu catalyst was fully removed). In order to remove any remaining Cu, the CNC-*g*-PBA_{200} were redispersed in toluene and added to a separation funnel. A 0.5 wt.% solution of EDTA in water was also added to the separation funnel in order to selectively bind any remaining copper. After several EDTA solution changes, the CNC-*g*-PBA_{200} were collected and dried under vacuum. CNC-*g*-$PMMA_{200}$ were prepared and purified using a similar procedure but with MMA monomer.

Poly(methyl methacrylate) latexes were prepared via miniemulsion polymerization. The miniemulsion water phase was prepared by dissolving SDS in purified water to a final concentration of 4.2 mM. The miniemulsion oil phase was prepared by dispersing polymer-grafted CNCs into purified MMA (resulting in either a 0.5 wt.% or 2.5 wt.% polymer-grafted CNC suspension in MMA) using a bath sonicator for 120 min in an ice bath. After proper dispersion was ensured, BPO was dissolved in the MMA. For each reaction, 7 mL SDS solution was used as the water phase, and 3 mL of the monomer suspension was used, resulting in a 30:70 monomer:water ratio by volume. The two phases were mixed and sonicated using a probe sonicator (Sonifier 450, Branson Ultrasonics, Danbury, DT) at 60% output for 1 min in an ice bath. The emulsion was then transferred to a round bottom flask with a stir bar, sealed, and degassed by bubbling Ar while stirring in an ice bath for 15 min. The emulsion was then added to a 60°C oil bath and allowed to react for 6 h, after which the reaction was ended by opening the flask to air. Samples were collected and stored at room temperature for characterization.

Zeta potential was measured using a Zeta Potential ZetaPlus Analyser (Brookhaven, USA). All samples were measured at 0.1 wt.% CNC or latex, with 10 mM NaCl at 25°C. Zeta potential was calculated from the electrophoretic mobility assuming Smoluchowski behaviour. Reported data is an average of three measurements with the standard deviation reported as the error.

Dynamic light scattering was used to measure the apparent size of CNC samples as well as the diameter of PMMA latexes. Unmodified CNCs, BiB-CNCs, and PMMA latexes were measured at a concentration of 0.025 wt.% in water. All samples were measured using a ZEN3600 – Zetasizer Nano ZS at 20°C. Reported data is an average of three measurements with the standard deviation reported as the error.

Elemental analysis was performed on BiB-CNCs in order to determine the Br content. Bromine content was determined via Schoniger Combustion and was carried out by Midwest MicroLab (Indianapolis, IN) on freeze dried BiB-CNCs.

Attenuated total reflectance Fourier transform infrared spectroscopy (ATR-FTIR) was performed on dry polymer-grafted CNC samples using a Bruker Vertex 70 FTIR with a background of 32 scans and 64 sample scans.

Contact angle samples were prepared by drop casting a 1 wt.% suspension of polymer-grafted CNCs in toluene on Piranha cleaned Si wafers until a full and complete film was observed. Measurements were obtained using the sessile drop method on a Future Digital Scientific OCA 20 High Speed Contact Angle Measurer (USA). Water contact angles were measured 2-3 seconds after placing the drop on the CNC film.

Gel permeation chromatography (GPC) samples were prepared by dissolving a small amount of free PBA or PMMA in THF, resulting in a 1 mg/mL solution. Molecular weight and polydispersity index (PDI) were analyzed using a Waters 2695 separations module, equipped with a Waters 2414 refractive index detector, and a Jordi Fluorinated DVB mixed-bed column. Polystyrene standards were used for calibration, with THF as the eluent at a flow rate of 3.0 mL/min.

Differential scanning calorimetry (DSC) samples were prepared by weighing 3-5 mg of dried latex samples into TZero hermetic sealed aluminum pans. DSC measurements were conducted using a Q200 differential scanning calorimeter (TA Instruments, New Castle, DE) under a nitrogen gas purge of 50 mL/min following a heat/cool/heat cycle with a heating rate of 10°C/min, cooling rate of 5°C/min, maximum temperature of 250°C and minimum temperature of -20°C. The glass transition temperature (T_g) was calculated using the software provided.

Transmission electron microscopy (TEM) samples were prepared by drop casting dilute latex suspensions (0.025 wt.%) onto Formvar-coated copper TEM grids and air drying for ~18 h. TEM images were acquired using a JOEL 1200 EX TEMSCAN microscope operating at 80 kV. No staining was used.

Results and Discussion

Polymer-grafted CNCs

Unmodified CNCs were first modified with ATRP initiator groups to prepare BiB-CNCs (Figure 1). The reaction was carried out in DMF, which has been shown to be a relatively good polar organic solvent for the dispersion of CNCs.[59] Upon extensive purification in order to remove unreacted reagents, the BiB-CNCs were freeze dried. The SI-ATRP reactions were performed in toluene, and therefore proper dispersion of BiB-CNCs was critical in order to ensure individual BiB-CNCs were grafted with polymer. BiB-CNCs were redispersed via bath sonication until no aggregates or sedimentation was observed by eye. The SI-ATRP was then performed in the presence of sacrificial initiator (schematic shown in Figure 1) in order to collect free homopolymer for GPC analysis.

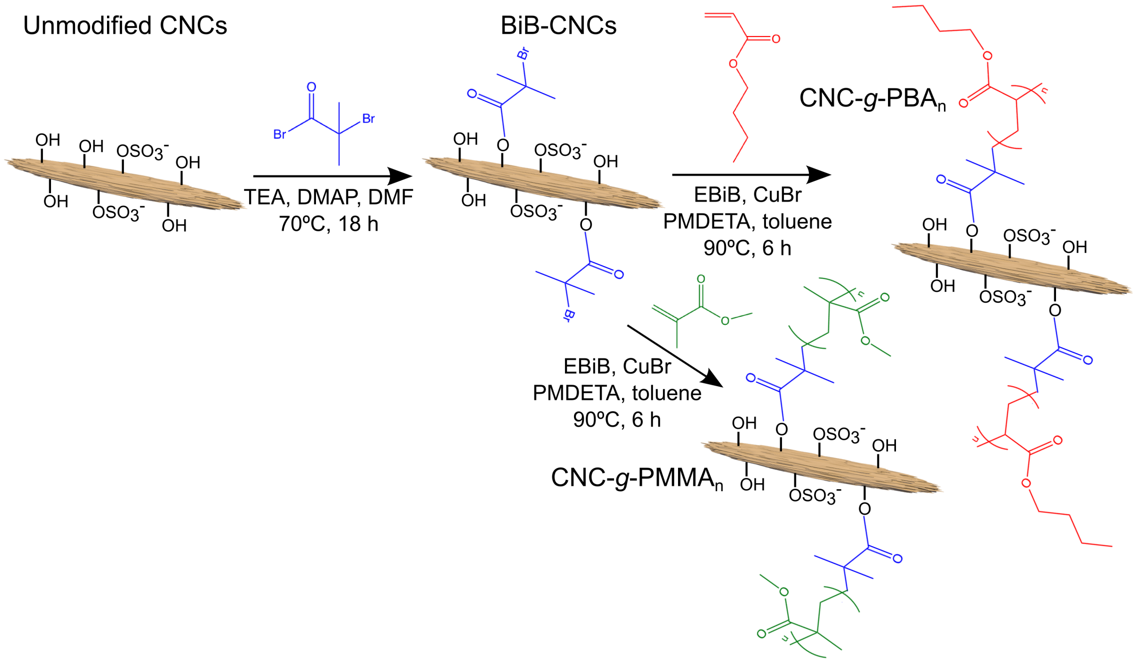

Figure 1. Schematic showing the modification of unmodified CNCs (left), to prepare BiB-CNCs (center) in DMF using TEA and DMAP which were then polymerized using SI-ATRP to prepare CNC-*g*-PBA$_n$ (top right) or CNC-*g*-PMMA$_n$ (bottom right).

Unmodified CNCs and BiB-CNCs were characterized in order to ensure that the BiB modification did not effect the CNC size and surface charge (Table 1). The apparent size of the CNCs was measured in an aqueous suspension by DLS and is denoted "apparent size" as DLS measures the radius of spherical particles, while CNCs are rod-shaped. However, DLS remains an important tool in order to perform an internal comparison. DLS shows that after BiB modification, BiB-CNCs show some aggregation which is attributed to the fact that during the modification CNCs are extensively centrifuged, likely resulting in some irreversible aggregation. Nonetheless, BiB-CNCs retain their nanoscale dimensions. The zeta potential of unmodified and BiB-CNCs is within error, implying that the BiB modification does not effect the sulfate half ester groups on the CNC surface, or their colloidal stability. Furthermore, elemental analysis showed that the BiB-CNCs used to graft PBA had a Br content of 3.5% (by mass), and BiB-CNCs used to graft PMMA had a Br content of 2.3% (by mass). Using average CNC dimensions of 120 nm in length and 15 nm in width,[4] and an approximate molar mass of CNCs of 6.9×10^6 g/mol (calculated using CNC and cellulose unit cell dimensions[60]), the grafting density (chains/nm^2) can be calculated. BiB-CNCs for PBA had a grafting density of 0.5 chains/nm^2, meaning that if all reactive sites were grafted from, there would be 0.5 polymer chains/nm^2, while BiB-CNCs for PMMA had a grafting density of 0.33 chains/nm^2. The difference in grafting density was not anticipated to provide significant differences in the hydrophobicity of the polymer-grafted CNCs, and in fact we performed SI-ATRP from BiB-CNCs with a grafting density of 1 chain/nm^2 and found that the polymer-grafted CNCs had similar properties to those with a grafting density of 0.5 chains/nm^2 (data not shown).

Table 1. Characterization of unmodified and initiator modified CNCs.

	Apparent size[a] (nm)	Zeta potential (mV)	%Br	Grafting density
Unmodified CNCs	65 ± 1	-36 ± 5	--	--
BiB-CNCs (for PBA modification)	123 ± 7	-39 ± 5	3.5	0.5 chains/nm^2
BiB-CNCs (for PMMA modification)	166 ± 7	-37 ± 3	2.4	0.33 chains/nm^2

[a]Measured by DLS under the assumption of spherical particles.

BiB-CNCs were then grafted with butyl acrylate at two different graft lengths, DP 50 and DP 200, and with methyl methacrylate at DP 200, resulting in three different polymer grafted samples: CNC-*g*-PBA$_{50}$, CNC-*g*-PBA$_{200}$, and CNC-*g*-PMMA$_{200}$, respectively. The modified CNCs were characterized using ATR-FTIR in order to determine the presence of polymer on the CNC surface (Figure 2). All modified CNCs showed a carbonyl peak at 1730 cm^{-1}, indicating the carbonyl in the polymer backbone (PBA and PMMA), which is not present in unmodified CNCs and is also present to a lesser degree in BiB-CNCs.

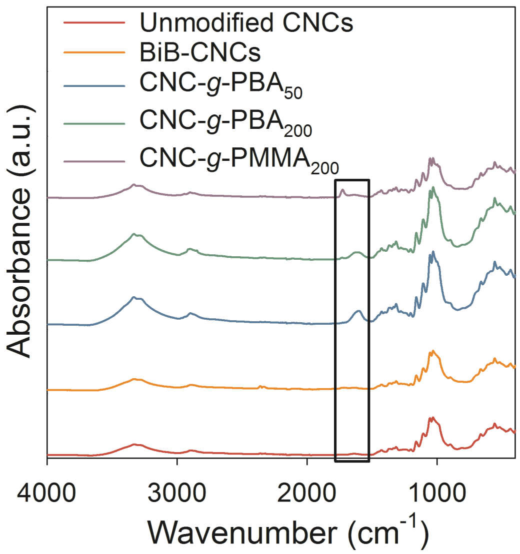

Figure 2. ATR-FTIR spectra showing the carbonyl peak (1730 cm^{-1}, highlighted with the black box) present in BiB-CNCs (orange) and in all polymer-grafted CNCs: CNC-*g*-PBA$_{50}$ (blue), CNC-*g*-PBA$_{200}$ (green), and CNC-*g*-PMMA$_{200}$ (purple), while the carbonyl peak is not present in unmodified CNCs (red).

The polymer grafted CNCs were further characterized by water contact angle measurements. Films were prepared by drop casting CNCs from toluene. Unmodified CNCs have a reported contact angle < 20°,[19] while BiB-CNCs prepared using the same protocol reported here have been shown to have a contact angle of 36°, with the increase being attributed to the grafting of more hydrophobic moieties on the CNC surface.[36] CNC-*g*-PBA$_{50}$ had a contact angle of 53°, while CNC-*g*-PBA$_{200}$ had a contact angle of 121°, and CNC-*g*-PMMA$_{200}$ had a contact angle of 131° (Table 2). This suggests that at a lower DP, the CNC-*g*-PBA$_{50}$ are hydrophobically modified, but with longer polymer chains (DP 200) the polymer-grafted CNCs become significantly more hydrophobic.

The free polymer produced in the SI-ATRP reactions was characterized in order to determine the polymer graft length and polydispersity (PDI) (Table 2). For DP 200 samples, the free polymer showed low PDI, implying that good control was maintained over the course of the reaction, with either PBA or PMMA grafting. For the PBA prepared at DP 50, a slightly higher PDI was measured in the free polymer MW but relatively good control was maintained and the target DP was reached. As the initiator group used here is not cleavable we rely on sacrificial initiator as shown in the literature[32,34,36,38,43,46,48] to quantify DP and PDI, however previous work has shown that this is a reasonable assumption in CNC grafting-from using SI-ATRP.[33]

Table 2. Characterization of free polymer prepared during the SI-ATRP reactions of BiB-CNCs to prepare three different polymer-grafted CNCs.

	Free polymer M_n (Da)	Free polymer M_w (Da)	Free polymer PDI	Target DP	Actual DP_n[b]	Contact angle of polymer-grafted CNC films
CNC-*g*-PBA_{50}	6833	7994	1.17	50	53	53°
CNC-*g*-PBA_{200}	21 647	22 995	1.06	200	170	121°
CNC-*g*-$PMMA_{200}$	19 686	22 585	1.16	200	196	131°

[b]Number average degree of polymerization determined using M_n measured by GPC.

Nanocomposite Latexes

Nanocomposite latexes of PMMA were prepared by miniemulsion polymerization, whereby the polymer-grafted CNCs were dispersed in the MMA monomer phase in order to promote their incorporation inside the latex particles. In order to determine if the polymer-grafted CNCs would remain in the monomer phase during the reaction, a monomer suspension of 0.5 wt.% CNC-*g*-PBA_{200} was prepared via bath sonication and is shown in Figure 3a. The polymer grafted CNCs are colloidally stable in MMA monomer and impart a slight yellow cloudy appearance to the normally transparent liquid. After the CNC-*g*-PBA_{200} MMA suspension shown in Figure 3a was prepared, 7 mL of water was added giving a 30:70 monomer:water (vol.) mixture, which is the same ratio used in the miniemulsion polymerization. For this test, the water phase did not contain surfactant and the mixture was heavily vortexed and then allowed to phase separate over 5-10 minutes. Figure 3b shows that the polymer-grafted CNCs remained in the monomer phase after intense mixing and contact with both phases, as indicated by the colored cloudy monomer top phase and transparent lower water phase. This suggests that during sonication, the polymer-grafted CNCs remain in the monomer phase as they are more compatible in monomer than in water.

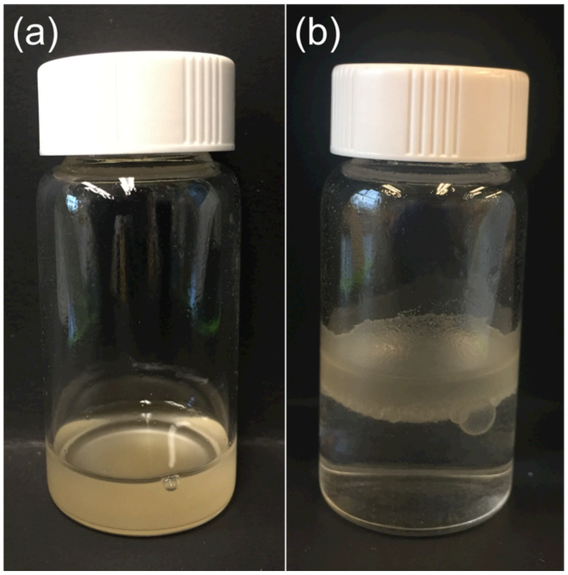

Figure 3. Photographs of (a) a suspension of 0.5 wt.% CNC-*g*-PBA$_{200}$ in MMA, and (b) after the water phase was added (without surfactant) and the monomer and water phase were allowed to separate, showing that the CNCs remain in the monomer phase.

PMMA latexes were prepared via miniemulsion polymerization with four different loadings/types of CNCs in the monomer phase: 0.5 wt.% CNC-*g*-PBA$_{50}$, 0.5 wt.% CNC-*g*-PBA$_{200}$, 0.5 wt.% CNC-*g*-PMMA$_{200}$, and 2.5 wt.% CNC-*g*-PBA$_{200}$. The effect of graft length, polymer graft type, and CNC loading could then be studied. In this work we chose to omit the hydrophobe which is typically used in miniemulsion polymerization in order to compartmentalize the monomer droplets such that the number of monomer droplets is the same as the number of polymer particles. The hydrophobe was omitted in order to provide a simple system where the effect of polymer-grafted CNC properties could be studied. Furthermore, the concentration of anionic SDS surfactant was chosen below the critical micelle concentration (CMC) of SDS in order to form larger monomer droplets to incorporate the relatively large polymer-grafted CNCs.

Table 3 shows the size and zeta potential of the resulting PMMA latexes with each type/loading of polymer-grafted CNC. Without the addition of polymer-grafted CNCs, the latex diameter is around 200 nm, and with the addition of either PMMA or PBA grafted CNCs, the size by DLS remains similar. However, it is of note that the PMMA latex with CNC-*g*-PBA$_{50}$ appears larger by DLS, with a diameter of 248 nm, indicating the possibility of latex particles that contain polymer-grafted CNCs. An increase in latex diameter is anticipated if the polymer-grafted CNCs are incorporated into the latex particles, since the polymer-grafted CNCs themselves are on the order of several hundred nm in length (including grafted polymer chains). The zeta potential of the PMMA latex is negative for all PMMA latexes (with or without polymer-grafted CNCs), implying that the anionic surfactant is present at the polymer/water interface and that good colloidal stability of the PMMA particles is maintained throughout the reaction.

DSC was used to measure the glass transition temperature (T_g) of the PMMA nanocomposite latexes. A shift in T_g implies a change in the polymer mobility, and tethering of PMMA polymer within the latex to or from the polymer-grafted CNCs. However, no observable difference in T_g was observed, indicating that the polymer-grafted CNCs are not necessarily tethered to the PMMA latex, or that polymer-grafted CNCs are not added in high enough quantities to detect a change.

Table 3. Characterization of PMMA nanocomposite latex properties with polymer-grafted CNCs in the monomer phase. The wt.% of CNCs added was 0.5 wt.% of the monomer unless otherwise stated.

	Average Latex Size (nm)	Latex Zeta Potential (mV)	Latex T_g (°C)	Wt.% Micro	Wt.% Nano
PMMA	204 ± 16	-30 ± 8	100°C	65%	35%
PMMA + CNC-*g*-PBA_{50}	248 ± 9	-15 ± 6	103°C	81%	19%
PMMA + CNC-*g*-PBA_{200}	162 ± 7	-36 ± 6	103°C	65%	35%
PMMA + CNC-*g*-$PMMA_{200}$	172 ± 42	-29 ± 6	102°C	48%	52%
PMMA + 2.5 wt.% CNC-*g*-PBA_{200}	189 ± 28	-21 ± 2	101°C	20%	80%

Since the CNCs are hundreds of nanometers long, we anticipate that if the CNCs were to be incorporated inside the PMMA latex core that the diameter should be in the micron range. In order to determine if any latex particles were above 1 μm in diameter, the latexes were diluted and passed through a 1 μm filter. The difference in the starting wt.% and the filtered wt.% was used to determine mass percent of micro and nanoparticles. We anticipate that the particles > 1 μm are more likely to contain CNCs (which is supported by TEM imaging below). Table 3 shows that the nanocomposite latex containing CNC-*g*-PBA_{50} has the most microparticles compared to the other nanocomposite latexes and the PMMA base case latex (without CNCs). The other nanocomposite latexes contained 20-65% microparticles by mass meaning that they may also have a fraction of latex particles that contain CNCs in their core. The nanocomposite latex with the highest CNC loading (2.5 wt.% CNC-*g*-PBA_{200}) had the lowest number of microparticles, suggesting that higher loadings of CNCs does not encourage incorporation and potentially leads to more CNC aggregation/phase segregation. Furthermore, the microparticles measured in the PMMA base case latex are attributed to the fact that the miniemulsion polymerization is carried out below the critical micelle concentration of SDS, therefore some aggregation was expected.

The PMMA latexes were imaged using TEM in order to determine their size and morphology and to locate the polymer-grafted CNCs within the latex (either inside or outside of the particles). In the PMMA latex without CNCs, only nanoparticles with some aggregation were observed (Figure 4a). However, in the case of nanocomposite latexes with CNC-*g*-PBA_{200} and CNC-*g*-$PMMA_{200}$, large latex particles were observed, but the polymer-grafted CNCs could not be seen inside the latex as it appeared too dark and lacked any contrast (Figure 4c and 4d). In the nanocomposite latex where 2.5 wt.% CNC-*g*-PBA_{200} was added (i.e., higher CNC loading), the latex nanoparticles are small enough such that it is highly unlikely that the polymer-grafted CNCs would be included in the core of the particles (Figure 4e). However, the miniemulsion polymerization carried out with CNC-*g*-PBA_{50} showed larger latex particles (500 nm – 1.5 μm) and polymer-grafted

CNCs inside the polymer particles (Figure 4b). This is further shown in Figure 5, where several larger latex particles were imaged with TEM and appear to contain rod-like polymer-grafted CNCs inside the particles. It has been reported that highly crystalline particles cause a distinct diffraction of the electron beam in TEM,[61] and interestingly, when the CNCs were uniformly dispersed throughout the latex suspension, such diffraction was undetectable; however, the opposite was observed when the CNCs were clustered within the individual latex particles as in the latex containing CNC-*g*-PBA$_{50}$.

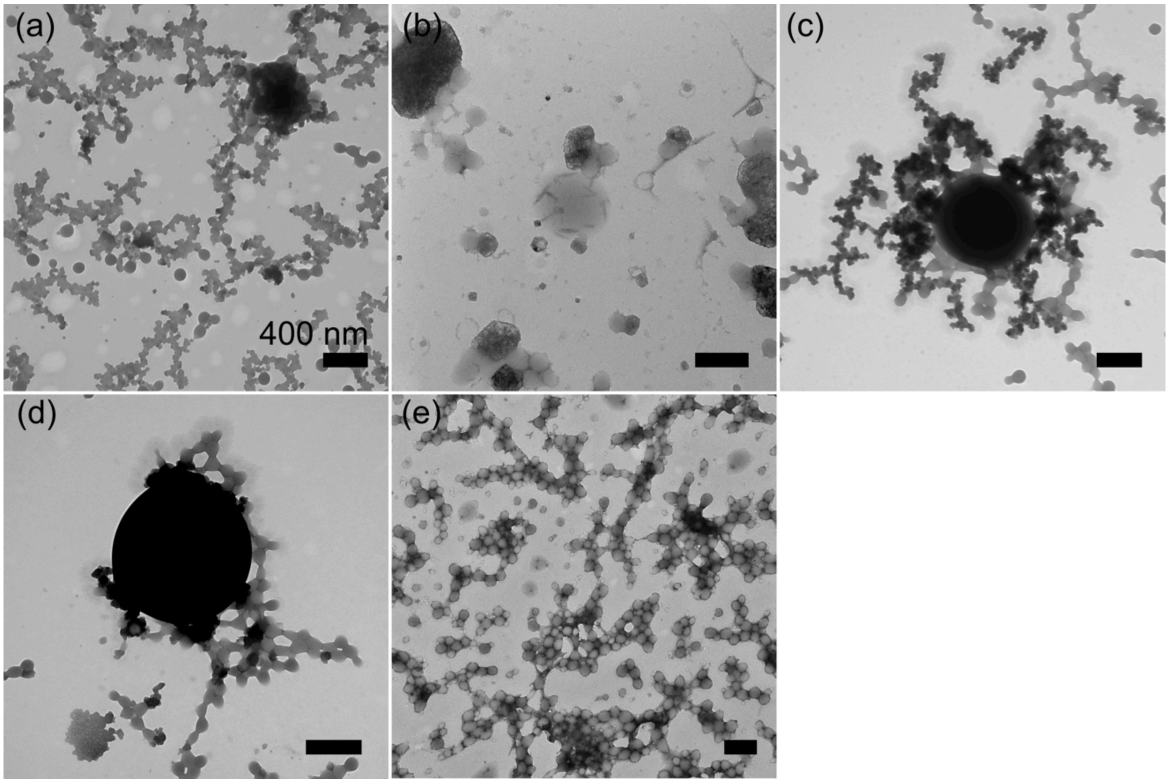

Figure 4. TEM images of PMMA latexes prepared (a) without CNCs, (b) with 0.5 wt.% CNC-*g*-PBA$_{50}$ in the MMA phase, (c) with 0.5 wt.% CNC-*g*-PBA$_{200}$ in the MMA phase, (d) with 0.5 wt. % CNC-*g*-PMMA$_{200}$ in the MMA phase, and (e) with 2.5 wt.% CNC-*g*-PBA$_{200}$ in the MMA phase. All scale bars are 400 nm.

While sample preparation and the drying of latexes for TEM imaging may change the appearance and degree of aggregation of the samples, we believe that the combination of DLS/zeta results and TEM give us a reasonable picture of the nanocomposite latexes. Overall they are colloidally stable, well dispersed and mostly nano and we have strong indication that in the case of CNC-*g*-PBA$_{50}$ the CNCs were inside the PMMA latex particles. To the contrary, CNC-*g*-PBA$_{200}$ were not observable inside the latex, perhaps due to their size or degree of aggregation. By rough calculation, PBA chains with DP 50 have an end to end distance (for a fully extended chain) of 15 nm, while PBA chains with DP 200 have an end to end distance of 62 nm. This increase could result in entanglement of polymer chains on neighbouring CNCs, which likely leads to loose CNC-*g*-PBA$_{200}$ agglomerates that are too large to be incorporated into the monomer droplets. We anticipate that shorter polymer chains (DP 50) allow for a sufficiently hydrophobic polymer-grafted CNC without the tendency to entangle or form a separate CNC rich phase and therefore the DP 50 polymer-grafted CNCs are small enough to be incorporated inside the polymer latex (Figure 5).

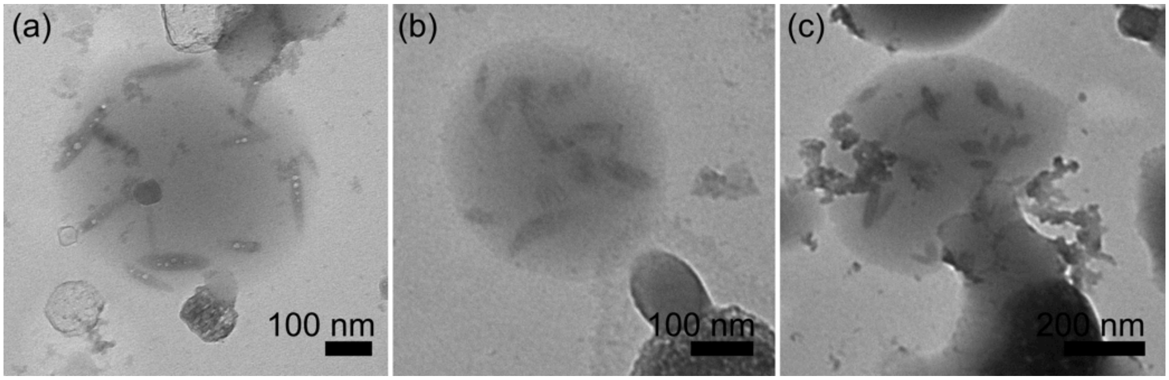

Figure 5. TEM images showing CNC-*g*-PBA_{50} inside the PMMA nanocomposite latex in three different particles from the same sample.

In order to determine if the CNCs could be located in the latex that was able to pass through the 1 μm filter (since free polymer-grafted CNCs should also be able to pass through the 1 μm filter), the filtered latex was imaged via TEM (Figure 6). For the nanocomposite latex with 0.5 wt.% CNC-*g*-PBA_{50}, no CNCs were observed in the filtered water phase (Figure 6a), indicating that they are indeed incorporated in the PMMA latex as implied in Figures 4 and 5. However, for the nanocomposite latexes containing CNC-*g*-PBA_{200} and CNC-*g*-$PMMA_{200}$ (Figure 6b and 6c, respectively), rod-shaped polymer-grafted CNCs were observed among the filtered latex nanoparticles, implying that not all polymer-grafted CNCs were incorporated inside the latex particles. A fraction of the polymer-grafted CNCs may be present in the large dark latex particles observed in Figure 4, but a fraction remain at the interface/water phase. In the latex containing CNC-*g*-$PMMA_{200}$, the CNCs appear aggregated amongst the nanoscale latex, suggesting they may be located at the interface as opposed to fully incorporated in the core of the particle. For the 2.5 wt.% loading of CNC-*g*-PBA_{200}, many CNCs are visible in both the filtered (Figure 6d) and unfiltered (Figure 4e) samples, suggesting that CNC-*g*-PBA_{200} are not incorporated at either loading, likely due to their long polymer chains resulting in CNC aggregation.

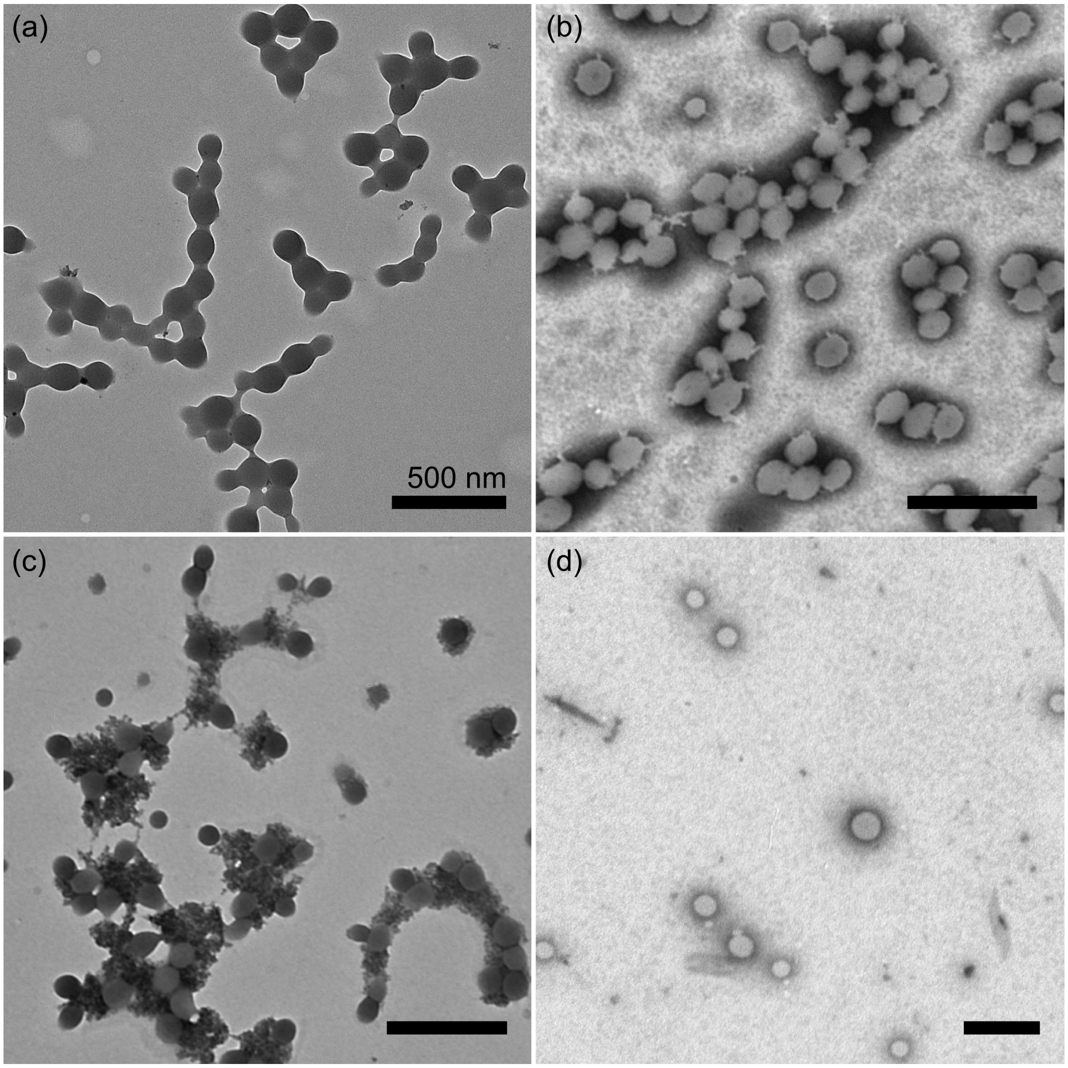

Figure 6. TEM of latexes after filtering through a 1 μm filter for PMMA latex containing (a) 0.5 wt.% CNC-*g*-PBA_{50}, (b) 0.5 wt.% CNC-*g*-PBA_{200}, (c) 0.5 wt.% CNC-*g*-$PMMA_{200}$, and (d) 2.5 wt.% CNC-*g*-PBA_{200}. All scale bars are 500 nm.

The grafted polymer type did not have an observable role on the incorporation of polymer-grafted CNCs, as no difference between CNC-*g*-PBA_{200} and CNC-*g*-$PMMA_{200}$ was seen by TEM and other physical properties (Table 3) were similar. This is likely due to the higher DP used in both samples, which may result in polymer-grafted CNC aggregation, making them unable to be incorporated into the monomer droplets. Furthermore, this shows that the type of polymer grafted from the CNCs does not play a critical role in incorporation but simply changes the CNC hydrophobicity, and in this case with a contact angle of 53° the PBA-grafted CNCs at DP 50 were sufficiently hydrophobic and small enough to be successfully incorporated into a PMMA latex.

Conclusions

SI-ATRP was used to prepare polymer-grafted CNCs with varying graft lengths and polymer type. The polymer-grafted CNCs were added to a miniemulsion polymerization of MMA to prepare PMMA nanocomposite latexes. Shorter grafted polymer chains resulted in CNCs being incorporated inside the polymer particles as imaged via TEM. While the polymer-grafted CNCs with longer chains were not directly shown to be inside the polymer particles, other characterization implied that a fraction may be inside the large latex particles, while the remaining fraction remained aggregated at the surface of the PMMA particles or was not incorporated. No observable difference in grafted polymer type were seen via the characterization methods used, suggesting that a variety of hydrophobic polymers may be used to allow for the incorporation of CNCs into hydrophobic polymer latexes. This work provides a new mechanism for the incorporation of CNCs into latex nanocomposites and is expected to result in products with improved mechanical properties.

Acknowledgements

The authors are grateful to CelluForce Inc. for providing the unmodified CNC starting material, and to Drs. Pelton and Adronov for equipment use. The Biointerfaces Institute at McMaster is acknowledged for equipment use and training. Special thanks to Marcia Reid and the Electron Microscopy Facility in the Health Science Center at McMaster University for training and equipment use.

References

(1) Habibi, Y.; Lucia, L. A.; Rojas, O. J. Cellulose Nanocrystals: Chemistry, Self-Assembly, and Applications. *Chem. Rev.* **2010**, *110* (6), 3479–3500.
(2) Klemm, D.; Kramer, F.; Moritz, S.; Lindström, T.; Ankerfors, M.; Gray, D.; Dorris, A. Nanocelluloses: A New Family of Nature-Based Materials. *Angew. Chemie Int. Ed.* **2011**, *50* (24), 5438–5466.
(3) Dufresne, A. Cellulose Nanomaterial Reinforced Polymer Nanocomposites. *Curr. Opin. Colloid Interface Sci.* **2017**, *29*, 1–8.
(4) Reid, M. S.; Villalobos, M.; Cranston, E. D. Benchmarking Cellulose Nanocrystals: From the Laboratory to Industrial Production. *Langmuir* **2017**, *33* (7), 1583–1598.
(5) Habibi, Y. Key Advances in the Chemical Modification of Nanocelluloses. *Chem. Soc. Rev.* **2014**, *43* (5), 1519–1542.
(6) Eyley, S.; Thielemans, W. Surface Modification of Cellulose Nanocrystals. *Nanoscale* **2014**, *6*, 7764–7779.
(7) Salajkova, M.; Berglund, L. A.; Zhou, Q. Hydrophobic Cellulose Nanocrystals Modified with Quaternary Ammonium Salts. *J. Mater. Chem.* **2012**, *22* (37), 19798.
(8) Ansari, F.; Salajková, M.; Zhou, Q.; Berglund, L. A. Strong Surface Treatment Effects on Reinforcement Efficiency in Biocomposites Based on Cellulose Nanocrystals in Poly(vinyl acetate) Matrix. *Biomacromolecules* **2015**, *16* (12), 3916–3924.
(9) Abitbol, T.; Marway, H.; Cranston, E. D. Surface Modification of Cellulose Nanocrystals with Cetyltrimethylammonium Bromide. *Nord. Pulp Pap. Res. J.*

2014, *29* (1), 46–57.

(10) Abraham, E.; Nevo, Y.; Slattegard, R.; Attias, N.; Sharon, S.; Lapidot, S.; Shoseyov, O. Highly Hydrophobic Thermally Stable Liquid Crystalline Cellulosic Nanomaterials. *ACS Sustain. Chem. Eng.* **2016**, *4* (3), 1338–1346.

(11) Fumagalli, M.; Sanchez, F.; Boisseau, S. M.; Heux, L. Gas-Phase Esterification of Cellulose Nanocrystal Aerogels for Colloidal Dispersion in Apolar Solvents. *Soft Matter* **2013**, *9* (47), 11309.

(12) Girouard, N. M.; Xu, S.; Schueneman, G. T.; Shofner, M. L.; Meredith, J. C. Site-Selective Modification of Cellulose Nanocrystals with Isophorone Diisocyanate and Formation of Polyurethane-CNC Composites. *ACS Appl. Mater. Interfaces* **2016**, *8* (2), 1458–1467.

(13) Shang, W.; Huang, J.; Luo, H.; Chang, P. R.; Feng, J.; Xie, G. Hydrophobic Modification of Cellulose Nanocrystal via Covalently Grafting of Castor Oil. *Cellulose* **2013**, *20* (1), 179–190.

(14) Dash, R.; Elder, T.; Ragauskas, A. J. Grafting of Model Primary Amine Compounds to Cellulose Nanowhiskers Through Periodate Oxidation. *Cellulose* **2012**, *19* (6), 2069–2079.

(15) Lin, N.; Huang, J.; Chang, P. R.; Feng, J.; Yu, J. Surface Acetylation of Cellulose Nanocrystal and its Reinforcing Function in Poly(lactic acid). *Carbohydr. Polym.* **2011**, *83* (4), 1834–1842.

(16) de Oliveira Taipina, M.; Ferrarezi, M. M. F.; Yoshida, I. V. P.; Gonçalves, M. do C. Surface Modification of Cotton Nanocrystals with a Silane Agent. *Cellulose* **2013**, *20* (1), 217–226.

(17) Hu, Z.; Berry, R. M.; Pelton, R.; Cranston, E. D. One-Pot Water-Based Hydrophobic Surface Modification of Cellulose Nanocrystals Using Plant Polyphenols. *ACS Sustain. Chem. Eng.* **2017**, *5* (6), 5018–5026.

(18) Kan, K. H. M.; Li, J.; Wijesekera, K.; Cranston, E. D. Polymer-Grafted Cellulose Nanocrystals as pH-Responsive Reversible Flocculants. *Biomacromolecules* **2013**, *14* (9), 3130–3139.

(19) Kedzior, S. A.; Graham, L.; Moorlag, C.; Dooley, B. M.; Cranston, E. D. Poly(methyl methacrylate)-Grafted Cellulose Nanocrystals: One-step Synthesis, Nanocomposite Preparation, and Characterization. *Can. J. Chem. Eng.* **2016**, *94* (5), 811–822.

(20) Zhou, C.; Wu, Q.; Yue, Y.; Zhang, Q. Application of Rod-Shaped Cellulose Nanocrystals in Polyacrylamide Hydrogels. *J. Colloid Interface Sci.* **2011**, *353* (1), 116–123.

(21) Zhou, C.; Wu, Q.; Zhang, Q. Dynamic Rheology Studies of in situ Polymerization Process of Polyacrylamide-Cellulose Nanocrystal Composite Hydrogels. *Colloid Polym. Sci.* **2011**, *289* (3), 247–255.

(22) Yang, J.; Han, C.-R.; Duan, J.-F.; Ma, M.-G.; Zhang, X.-M.; Xu, F.; Sun, R.-C.; Xie, X.-M. Studies on the Properties and Formation Mechanism of Flexible Nanocomposite Hydrogels from Cellulose Nanocrystals and Poly(acrylic acid). *J. Mater. Chem.* **2012**, *22* (42), 22467–22480.

(23) Habibi, Y.; Goffin, A.-L.; Schiltz, N.; Duquesne, E.; Dubois, P.; Dufresne, A. Bionanocomposites Based on Poly(ε-caprolactone)-Grafted Cellulose Nanocrystals by Ring-Opening Polymerization. *J. Mater. Chem.* **2008**, *18* (41), 5002.

(24) Goffin, A.-L.; Raquez, J.-M.; Duquesne, E.; Siqueira, G.; Habibi, Y.; Dufresne, A.; Dubois, P. Poly(ε-caprolactone) Based Nanocomposites Reinforced by Surface-Grafted Cellulose Nanowhiskers via Extrusion Processing: Morphology, Rheology, and Thermo-Mechanical Properties. *Polymer (Guildf).* **2011**, *52* (7), 1532–1538.

(25) Chen, G.; Dufresne, A.; Huang, J.; Chang, P. R. A Novel Thermoformable Bionanocomposite Based on Cellulose Nanocrystal-graft-Poly(ε -caprolactone). *Macromol. Mater. Eng.* **2009**, *294* (1), 59–67.

(26) Lin, N.; Chen, G.; Huang, J.; Dufresne, A.; Chang, P. R. Effects of Polymer-Grafted Natural Nanocrystals on the Structure and Mechanical Properties of Poly(lactic acid): A Case of Cellulose Whisker-Graft-Polycaprolactone. *J. Appl. Polym. Sci.* **2009**, *113* (5), 3417–3425.

(27) Labet, M.; Thielemans, W. Improving the Reproducibility of Chemical Reactions on the Surface of Cellulose Nanocrystals: ROP of ε-caprolactone as a Case Study. *Cellulose* **2011**, *18* (3), 607–617.

(28) Labet, M.; Thielemans, W. Citric Acid as a Benign Alternative to Metal Catalysts for the Production of Cellulose-Grafted-Polycaprolactone Copolymers. *Polym. Chem.* **2012**, *3* (3), 679.

(29) Braun, B.; Dorgan, J. R.; Hollingsworth, L. O. Supra-Molecular EcoBioNanocomposites Based on Polylactide and Cellulosic Nanowhiskers: Synthesis and Properties. *Biomacromolecules* **2012**, *13* (7), 2013–2019.

(30) Roeder, R. D.; Garcia-Valdez, O.; Whitney, R. A.; Champagne, P.; Cunningham, M. F. Graft Modification of Cellulose Nanocrystals via Nitroxide-Mediated Polymerisation. *Polym. Chem.* **2016**, *7* (41), 6383–6390.

(31) Yi, J.; Xu, Q.; Zhang, X.; Zhang, H. Chiral-Nematic Self-Ordering of Rodlike Cellulose Nanocrystals Grafted with Poly(styrene) in Both Thermotropic and Lyotropic States. *Polymer (Guildf).* **2008**, *49* (20), 4406–4412.

(32) Morandi, G.; Heath, L.; Thielemans, W. Cellulose Nanocrystals Grafted with Polystyrene Chains Through Surface-Initiated Atom Transfer Radical Polymerization (SI-ATRP). *Langmuir* **2009**, *25* (14), 8280–8286.

(33) Morandi, G.; Thielemans, W. Synthesis of Cellulose Nanocrystals Bearing Photocleavable Grafts by ATRP. *Polym. Chem.* **2012**, *3* (6), 1402–1407.

(34) Yin, Y.; Tian, X.; Jiang, X.; Wang, H.; Gao, W. Modification of Cellulose Nanocrystal via SI-ATRP of Styrene and the Mechanism of its Reinforcement of Polymethylmethacrylate. *Carbohydr. Polym.* **2016**, *142*, 206–212.

(35) Wang, H.-D.; Roeder, R. D.; Whitney, R. A.; Champagne, P.; Cunningham, M. F. Graft Modification of Crystalline Nanocellulose by Cu(0)-mediated SET Living Radical Polymerization. *J. Polym. Sci. Part A Polym. Chem.* **2015**, *53* (24), 2800–2808.

(36) Hatton, F. L.; Kedzior, S. A.; Cranston, E. D.; Carlmark, A. Grafting-from Cellulose Nanocrystals via Photoinduced Cu-mediated Reversible-deactivation Radical Polymerization. *Carbohydr. Polym.* **2017**, *157*, 1033–1040.

(37) Boujemaoui, A.; Mongkhontreerat, S.; Malmström, E.; Carlmark, A. Preparation and Characterization of Functionalized Cellulose Nanocrystals. *Carbohydr. Polym.* **2015**, *115*, 457–464.

(38) Rosilo, H.; McKee, J. R.; Kontturi, E.; Koho, T.; Hytönen, V. P.; Ikkala, O.;

Kostiainen, M. A. Cationic Polymer Brush-Modified Cellulose Nanocrystals for High-Affinity Virus Binding. *Nanoscale* **2014**, *6* (20), 11871–11881.
(39) Yi, J.; Xu, Q.; Zhang, X.; Zhang, H. Temperature-Induced Chiral Nematic Phase Changes of Suspensions of Poly(N,N-dimethylaminoethyl methacrylate)-Grafted Cellulose Nanocrystals. *Cellulose* **2009**, *16* (6), 989–997.
(40) Zoppe, J. O.; Habibi, Y.; Rojas, O. J.; Venditti, R. A.; Johansson, L. S.; Efimenko, K.; Österberg, M.; Laine, J. Poly(N-isopropylacrylamide) Brushes Grafted from Cellulose Nanocrystals via Surface-Initiated Single-Electron Transfer Living Radical Polymerization. *Biomacromolecules* **2010**, *11* (10), 2683–2691.
(41) Hemraz, U. D.; Lu, A.; Sunasee, R.; Boluk, Y. Structure of Poly(N-isopropylacrylamide) Brushes and Steric Stability of Their Grafted Cellulose Nanocrystal Dispersions. *J. Colloid Interface Sci.* **2014**, *430*, 157–165.
(42) Zoppe, J. O.; Dupire, A. V. M.; Lachat, T. G. G.; Lemal, P.; Rodriguez-Lorenzo, L.; Petri-Fink, A.; Weder, C.; Klok, H. Cellulose Nanocrystals with Tethered Polymer Chains: Chemically Patchy versus Uniform Decoration. *ACS Macro Lett.* **2017**, 892–897.
(43) Wu, W.; Huang, F.; Pan, S.; Mu, W.; Meng, X.; Yang, H.; Xu, Z.; Ragauskas, A. J.; Deng, Y. Thermo-Responsive and Fluorescent Cellulose Nanocrystals Grafted with Polymer Brushes. *J. Mater. Chem. A* **2015**, *3* (5), 1995–2005.
(44) Zoppe, J. O.; Xu, X.; Känel, C.; Orsolini, P.; Siqueira, G.; Tingaut, P.; Zimmermann, T.; Klok, H.-A. Effect of Surface Charge on Surface-Initiated Atom Transfer Radical Polymerization from Cellulose Nanocrystals in Aqueous Media. *Biomacromolecules* **2016**, *17*, 1404–1413.
(45) Hemraz, U. D.; Campbell, K. A.; Burdick, J. S.; Ckless, K.; Boluk, Y.; Sunasee, R. Cationic Poly(2-aminoethylmethacrylate) and Poly(N-(2-aminoethylmethacrylamide) Modified Cellulose Nanocrystals: Synthesis, Characterization, and Cytotoxicity. *Biomacromolecules* **2015**, *16*, 319–325.
(46) Majoinen, J.; Walther, A.; McKee, J. R.; Kontturi, E.; Aseyev, V.; Malho, J. M.; Ruokolainen, J.; Ikkala, O. Polyelectrolyte Brushes Grafted from Cellulose Nanocrystals using Cu-mediated Surface-Initiated Controlled Radical Polymerization. *Biomacromolecules* **2011**, *12* (8), 2997–3006.
(47) Xu, Q.; Yi, J.; Zhang, X.; Zhang, H. A Novel Amphotropic Polymer Based on Cellulose Nanocrystals Grafted with Azo Polymers. *Eur. Polym. J.* **2008**, *44* (9), 2830–2837.
(48) Yu, J.; Wang, C.; Wang, J.; Chu, F. In Situ Development of Self-reinforced Cellulose Nanocrystals Based Thermoplastic Elastomers by Atom Transfer Radical Polymerization. *Carbohydr. Polym.* **2016**, *141*, 143–150.
(49) Arredondo, J.; Jessop, P. G.; Champagne, P.; Bouchard, J.; Cunningham, M. F. Synthesis of Carbon Dioxide Responsive Cellulose Nanocrystals by Surface-Initiated Cu(0)-Mediated Polymerisation. *Green Chem.* **2017**.
(50) Zhang, X.; Zhang, J.; Dong, L.; Ren, S.; Wu, Q.; Lei, T. Thermoresponsive poly(poly(ethylene glycol) methylacrylate)s grafted cellulose nanocrystals through SI-ATRP polymerization. *Cellulose* **2017**.
(51) Favier, V.; Chanzy, H.; Cavaillé, J. Y. Polymer Nanocomposites Reinforced by Cellulose Whiskers. *Macromolecules* **1995**, *28* (18), 6365–6367.
(52) Favier, V.; Canova, G. R.; Cavaillé, J. Y.; Chanzy, H.; Dufresne, A.; Gauthier, C.

Nanocomposite materials from latex and cellulose whiskers. *Polym. Adv. Technol.* **1995**, *6* (5), 351–355.

(53) Vatansever, A.; Dogan, H.; Inan, T.; Sezer, S.; Sirkecioglu, A. Properties of Na-Montmorillonite and Cellulose Nanocrystal Reinforced Poly(butyl acrylate-co-methyl methacrylate) Nanocomposites. *Polym. Eng. Sci.* **2015**, *55* (12), 2922–2928.

(54) Elmabrouk, A. Ben; Thielemans, W.; Dufresne, A.; Boufi, S. Preparation of Poly(styrene-co-hexylacrylate)/Cellulose Whiskers Nanocomposites via Miniemulsion Polymerization. *J. Appl. Polym. Sci.* **2009**, *114* (5), 2946–2955.

(55) Mabrouk, A. Ben; Vilar, M. R.; Magnin, A.; Belgacem, M. N.; Boufi, S. Synthesis and Characterization of Cellulose Whiskers/Polymer Nanocomposite Dispersion by Mini-Emulsion Polymerization. *J. Colloid Interface Sci.* **2011**, *363* (1), 129–136.

(56) Dastjerdi, Z.; Cranston, E. D.; Dubé, M. A. Synthesis of Poly(n-butyl acrylate/methyl methacrylate)/CNC Latex Nanocomposites via In Situ Emulsion Polymerization. *Macromol. React. Eng.* **2017**, *201700013*, 1700013.

(57) Kedzior, S. A.; Marway, H. S.; Cranston, E. D. Tailoring Cellulose Nanocrystal and Surfactant Behavior in Miniemulsion Polymerization. *Macromolecules* **2017**, *50* (7), 2645–2655.

(58) Kedzior, S. A.; Dubé, M. A.; Cranston, E. D. Cellulose Nanocrystals and Methyl Cellulose as Co-stabilizers for Nanocomposite Latexes with Double Morphology. *Submitt. to ACS Sustain. Chem. Eng.* **2017**.

(59) Viet, D.; Beck-Candanedo, S.; Gray, D. G. Dispersion of Cellulose Nanocrystals in Polar Organic Solvents. *Cellulose* **2007**, *14* (2), 109–113.

(60) Nishiyama, Y.; Sugiyama, J.; Chanzy, H.; Langan, P. Crystal structure and hydrogen bonding system in cellulose Iα from synchrotron x-ray and neutron fiber diffraction. *J. Am. Chem. Soc.* **2003**, *125* (47), 14300–14306.

(61) Wang, Z. L. Transmission Electron Microscopy of Shape-Controlled Nanocrystals and Their Assemblies. *J. Phys. Chem. B* **2000**, *104* (6), 1153–1175.

Chapter 9 Concluding Remarks

This thesis provides a range of methods to incorporate CNCs into polymer latexes. The specific interactions between CNCs and polymer latex components were studied in order to prepare novel nanocomposite latexes whereby CNCs either played an active or passive role as emulsion stabilizers or as reinforcing agents. The ability to surface modify CNCs through polymer grafting or adsorption was key to controlling their role during latex synthesis. The results of this thesis will help to extend the use of CNCs in emulsion-based systems such as adhesives, cosmetics, and coatings. The information presented here, along with our collaborative work with the University of Ottawa, will hopefully facilitate transfer of knowledge to industry and show the versatility of CNCs and the ease with which they can be incorporated into commercial latex products. The research objectives proposed in Chapter 1 were fully achieved and the major contributions to knowledge are described below.

1. Investigation of novel surface modification routes yielded two different methods of polymer grafting. The first method, presented in Chapter 3, was a water-based free radical polymerization method whereby CNCs were grafted with hydrophobic PMMA. This work was one of the first comprehensive reports to include polymer grafting, characterization, and nanocomposite preparation and testing. The method provides a water-based "green" protocol for compatibilizing CNCs for use in polymer nanocomposites.

In Chapter 4 we used a photoinduced Cu-mediated RDRP method to prepare CNCs grafted with PMA. This method overcame the setbacks associated with free radical polymer grafting and allowed for control over graft density and graft length. While other RDRP methods from CNCs have been reported, the novelty of this method was the short reaction times and simple purification compared to traditional Cu-mediated RDRP. This method is anticipated to allow for facile modification of CNCs for their incorporation into new products containing hydrophobic polymer matrices.

Chapter 5 presented a new method for characterizing modified CNCs which was a collaborative project with NMR experts at the University of Helsinki. This method is expected to be used widely by other nanocellulose researchers and addresses the difficulties in characterizing CNCs modified by free radical polymerization or other non-specific modification routes.

2. Control of the location and function of CNCs in latex polymer systems was achieved by modifying the CNC surface either non-covalently via surfactant or polymer adsorption or covalently by grafting polymers from the CNC surface.

a. The work presented in Chapter 6 describes the role of CNCs in surfactant-based systems, and uses the miniemulsion polymerization of MMA as a model system. We showed that oppositely charged CNCs and surfactants were able to co-stabilize PMMA latexes and that like charged CNCs and surfactants resulted in PMMA latexes stabilized by surfactant alone, while the CNCs remained passive in the water phase. This work will extend the use of CNCs in existing emulsion formulations where surfactants are required, and provides design rules for controlling the location of CNCs within these systems. This was the first report of a systematic study regarding the use of CNCs and surfactants as co-stabilizers in miniemulsion polymerization.

b. CNCs were surface modified by the adsorption of methyl cellulose in Chapter 7, where they were shown to stabilize the microsuspension polymerization of MMA to produce PMMA latexes with a hierarchical double morphology. The latex could be tailored based on the ratio of CNC and methyl cellulose used as co-stabilizers, and on the drying conditions. This work provides a new route to produce latexes with an “in between” size of ~10 µm, which is large for emulsion but small for suspension polymerization. Importantly this polymerization method may be considered overall “greener” since it avoids the use of synthetic surfactants.

c. With the goal of incorporating CNCs into the core of polymer latex particles, Chapter 8 described polymer grafting from CNCs using traditional Cu-mediated RDRP and the incorporation of polymer-grafted CNCs into PMMA nanocomposite latexes. Polymer-grafted CNCs were successfully incorporated into the core of the PMMA latex particles, providing an entirely novel way of preparing CNC nanocomposite latexes that has not been reported previously in literature.

The work presented in this thesis provides novel methods to functionalize and incorporate CNCs into latex systems which should extend the use of CNCs in emulsion-based products. The results are expected to be used by researchers in the adhesive, coating, paint, and cosmetic industries, to name just a few. We have shown that CNCs have the potential to replace potentially toxic surfactants, with the ability to impart new properties and morphologies to latex particles. The three approaches for incorporating CNCs provide a wide range of properties which may be used to tailor new or existing formulations.

Currently, we are collaborating with pressure sensitive adhesive experts at the University of Ottawa to explore the role of CNCs in adhesive latexes. Our goal is to use the knowledge gained in this thesis to impart new properties to PSAs. Modified CNCs will be added to the large scale production of PSA latexes and their mechanical and adhesive properties will be tested. We have preliminary evidence for improved latex properties and believe that emulsion polymerization with CNCs may be able to replace some traditional solvent polymerization methods, giving comparable or better performance. Emulsion polymerization routes are favourable from an environmental perspective because the bulk phase is water, no solvents are needed and separation/purification is straightforward. CNCs show promise to provide new properties in polymer systems and overall “greener” materials.